INFORMATION TO USERS

This dissertation was produced from a microfilm copy of the original document. While the most advanced technological means to photograph and reproduce this document have been used, the quality is heavily dependent upon the quality of the original submitted.

The following explanation of techniques is provided to help you understand markings or patterns which may appear on this reproduction.

1. The sign or "target" for pages apparently lacking from the document photographed is "Missing Page(s)". If it was possible to obtain the missing page(s) or section, they are spliced into the film along with adjacent pages. This may have necessitated cutting thru an image and duplicating adjacent pages to insure you complete continuity.

2. When an image on the film is obliterated with a large round black mark, it is an indication that the photographer suspected that the copy may have moved during exposure and thus cause a blurred image. You will find a good image of the page in the adjacent frame.

3. When a map, drawing or chart, etc., was part of the material being photographed the photographer followed a definite method in "sectioning" the material. It is customary to begin photoing at the upper left hand corner of a large sheet and to continue photoing from left to right in equal sections with a small overlap. If necessary, sectioning is continued again — beginning below the first row and continuing on until complete.

4. The majority of users indicate that the textual content is of greatest value, however, a somewhat higher quality reproduction could be made from "photographs" if essential to the understanding of the dissertation. Silver prints of "photographs" may be ordered at additional charge by writing the Order Department, giving the catalog number, title, author and specific pages you wish reproduced.

73-6472

BELL, William Alvin, 1944-
EXPERIMENTAL DETERMINATION OF THREE-DIMENSIONAL
LIQUID ROCKET NOZZLE ADMITTANCES.

Georgia Institute of Technology, Ph.D., 1972
Engineering, aeronautical

University Microfilms, A XEROX Company, Ann Arbor, Michigan

EXPERIMENTAL DETERMINATION OF THREE-DIMENSIONAL

LIQUID ROCKET NOZZLE ADMITTANCES

A THESIS

Presented to

The Faculty of the Division of Graduate

Studies and Research

By

William Alvin Bell

In Partial Fulfillment

of the Requirements for the Degree

Doctor of Philosophy in the School of Aerospace Engineering

Georgia Institute of Technology

July, 1972

EXPERIMENTAL DETERMINATION OF THREE-DIMENSIONAL

LIQUID ROCKET NOZZLE ADMITTANCES

Approved:

_____

/ Ben T. Zinn, Chairman

_____

/James E. Hubbartt

_____

Warren C. Strahle

PLEASE NOTE:

Some pages may have

indistinct print.

Filmed as received.

University Microfilms, A Xerox Education Company

In presenting the dissertation as a partial fulfillment of
the requirements for an advanced degree from the Georgia
Institute of Technology, I agree that the Library of the
Institute shall make it available for inspection and
circulation in accordance with its regulations governing
materials of this type. I agree that permission to copy
from, or to publish from, this dissertation may be granted
by the professor under whose direction it was written, or,
in his absence, by the Dean of the Graduate Division when
such copying or publication is solely for scholarly purposes
and does not involve potential financial gain. It is under-
stood that any copying from, or publication of, this dis-
sertation which involves potential financial gain will not
be allowed without written permission.

7/25/68

ACKNOWLEDGMENTS

I would like to express my appreciation to Dr. Ben T. Zinn for his suggestion of the thesis topic and for his help and guidance while this research was being conducted. I would also like to thank Dr. Warren C. Strahle and Professor James E. Hubbartt for their careful examination and constructive criticism of the manuscript.

The numerous discussions with my colleagues have provided me with valuable insight into the various aspects of the problem from time to time. I especially appreciate the assistance given by Mr. B. R. Daniel. The many hours we spent in discussing this problem and the assistance he gave were invaluable. In addition, I would like to thank the staff of the Rich Electronics Computer Center for the use of the UNIVAC 1108 and the School of Aerospace Engineering who paid for the use of the UNIVAC 1108.

The finanical support of the National Aeronautics and Space Administration under NASA Grant NGR-11-002-085, the National Science Foundation, NDEA, and the Georgia Institute of Technology is gratefully acknowledged.

I also thank Ms. Mary Ann Owen for the excellent job done in typing and correcting the manuscript.

I wish to thank my parents, Mr. and Mrs. William H. Bell, for their moral support and assistance during the years of my education. I also greatly appreciate the support given me by my brother, Mr. Thomas F. Bell, and my sister, Ms. Bonnie Rose Chase.

Finally, I wish to thank my wife, Melody, whose moral support give me strength and whose strength gave me moral support.

TABLE OF CONTENTS

Chapter

Background
Nozzle Admittance Theories
Experimental Techniques
Objectives

Governing Equations
Admittance Relation
Theoretical Predictions

Governing Equations
Standing Wave Analysis
Experimental Technique for Computing the
    Admittance
Nonlinear Regression

Air Supply System
Test Facility
Tested Nozzles
Instrumentation
Data Reduction
Experimental Procedure

TABLE OF CONTENTS (Concluded)

LIST OF TABLES

LIST OF TABLES (Concluded)

LIST OF ILLUSTRATIONS

LIST OF ILLUSTRATIONS (Continued)

LIST OF ILLUSTRATIONS (Continued)

LIST OF ILLUSTRATIONS (Concluded)

GLOSSARY OF SYMBOLS

Symbol	Definition
a	quantity defined after equation (3-13)
a_{jk}	scaled correlation coefficient
A	constant defined by equation (3-14) or variable coefficient in equation (2-15)
A_{db}	A_{mn} in decibels
A_{mn}	$AJ_m(S_{mn})$
A_{nl}	parameter defined after equation (3-26)
A_+	complex amplitude of the incident wave
A_-	complex amplitude of the reflected wave
b_n^k	coefficient used in the nonlinear regression method defined after equation (3-32)
B	variable coefficient in equation (2-15)
B_{nl}	quantity defined after equation (3-26)
c	speed of sound
c_p	specific heat at constant pressure
C	variable coefficient in equation (2-15)
C_θ	integration constant
e	constant equal to 2.71828...
$\vec{e}_r,\ \vec{e}_\theta,\ \vec{e}_z$	unit vectors in the radial, tangential, and axial directions, respectively
E_i	experimentally measured pressure amplitude or phase at the i-th axial location along the impedance tube
F	measure of the rms deviation between the theoretical equations and the experimental data

GLOSSARY OF SYMBOLS(Continued)

Symbol	Definition
i	$\sqrt{-1}$
J_m	Bessel function of the first kind of order m
k	wave number
$K(\psi,\theta,t)$	lumped parameter defined as $J_m\left[S_{mn}\left(\dfrac{\psi}{\psi_w}\right)^{\frac{1}{2}}\right]e^{im\theta}e^{i\omega t}$
k_{mn}	quantity defined after equation (3-13)
L	tube length or sound pressure level in decibels
m	number of diametral nodal lines
M	Mach number
n	number of azimuthal nodal lines
N(z)	function describing the axial dependence of the density oscillation
p	pressure
P(z)	function describing the axial dependence of the pressure oscillation
q	velocity
r	radial coordinate
R(z)	radial dependence of a perturbation quantity
s	nondimensional frequency
S_{mn}	the n-th root of the equation $\dfrac{dJ_m(x)}{dx} = 0$
t	time coordinate
T_i	theoretical expression for the pressure amplitude or phase

GLOSSARY OF SYMBOLS (Continued)

Symbol	Definition
u	axial velocity component
$U(z)$	function describing the axial dependence of the axial velocity perturbation
v	radial velocity component
$V(z)$	function describing the axial dependence of the radial velocity perturbation
w	tangential velocity component
$W(z)$	function describing the axial dependence of the tangential velocity perturbation
x	parameter defined after equation (3-26)
x_i	independent variable used in the nonlinear regression method
y	irrotational specific nozzle admittance or parameter defined after equation (3-26)
z	axial coordinate

Greek Symbol	Definition
α	$\left. \dfrac{\text{reflected wave amplitude}}{\text{incident wave amplitude}} \right|_{\substack{\text{Nozzle} \\ \text{Entrance}}} = e^{-2\pi\alpha}$
β	$\left\{ \begin{array}{l}\text{phase shift of the incident wave} \\ \text{upon reflection from the nozzle entrance}\end{array}\right\} = \pi(2\beta+1)$
γ	ratio of specific heats
Δ	difference between two quantities
δ	phase

GLOSSARY OF SYMBOLS (Continued)

Greek Symbol	Definition
ϵ	denotes a small quantity
ζ	irrotational admittance parameter defined after equation (2-14)
θ	tangential coordinate
θ_1	nozzle half-angle
$\Theta(\theta)$	function describing the tangential dependence of a perturbation quantity
λ	wavelength
λ_n	convergence parameter
λ_1	amplification coefficient
π	constant given as 3.14159...
ρ	density
τ	admittance parameter defined before equation (2-16)
φ	steady state velocity potential
Φ	φ-dependence of the radial velocity perturbation
ψ	steady state stream function
Ψ	ψ-dependence of the oscillations
ω	angular frequency

Subscripts	Definition
c	at the chamber wall
e	evaluated at the nozzle entrance

GLOSSARY OF SYMBOLS (Concluded)

Subscripts	Definition
i	imaginary part of a complex quantity or axial station
n	at the n-th iteration
o	stagnation or initial value
r	real part of a complex quantity
w	at the wall
+	incident wave
-	reflected wave

Superscripts	Definition
-	steady state value
'	perturbation quantity
*	in Chapter II, a dimensional quantity

SUMMARY

The nozzle admittance is an important parameter in determining the stability characteristics of rocket motors. In theoretical high frequency combustion instability analyses, the three-dimensional nozzle admittance theory developed by Crocco is used to obtain values of the nozzle admittance although these values have not been checked experimentally. The present investigation was undertaken to experimentally determine the admittance of various liquid rocket engine nozzles subjected to three-dimensional oscillations and to compare the experimental results with the theoretical predictions.

The theoretical predictions are calculated using Crocco's theory for the nozzles under investigation. The values of the real and imaginary parts of the admittance are tabulated over a range of nondimensional frequencies which includes longitudinal and mixed first tangential-longitudinal modes.

To obtain experimental data for comparison with the theoretical predictions, a technique based on the classical impedance tube method is developed. The classical impedance tube theory is extended to account for the presence of a one-dimensional mean flow and three-dimensional oscillations. In this analysis expressions are developed which describe the dependence of the pressure amplitude and phase of the standing wave pattern in the tube upon the spacial coordinates, the magnitude of the mean flow Mach number, and the conditions at the nozzle entrance. By measuring the standing wave pattern, the

interaction between the incident and reflected waves at the nozzle entrance is determined and used to calculate the nozzle admittance. Three techniques were developed which can be used to determine the nozzle admittance. Two were eliminated from consideration for the present study because of practical limitations. The technique which is used consists of measuring the pressure amplitude at several predetermined locations along the length of the tube. The numerical technique for determining the admittance from the pressure amplitude measurements is then presented.

The experimental facility consists of an aluminum tube 10 feet in length. The nozzles under consideration are mounted at one end and a multi-orifice injector is attached to the other end. To acoustically isolate the system, sonic conditions are maintained across the injector and at the nozzle throat. Two electropneumatic drivers located near the injector are used to generate longitudinal and mixed first tangential-longitudinal waves in the tube.

The experimental admittance results are obtained in the form of graphs of the real and imaginary parts of the nozzle admittance versus nondimensional frequency. Data are obtained for nozzles with half-angles of 15, 30, and 45 degrees and entrance Mach numbers of 0.08, 0.16, and 0.20. These data are compared with the theoretical predictions. For longitudinal oscillations, the theoretical and experimental results were in agreement to within experimental error. However, for mixed first tangential-longitudinal modes, the agreement was satisfactory for entrance Mach numbers 0.16 or above.

CHAPTER I

INTRODUCTION

Background

Combustion instability is an important consideration in the design of rocket engines. This phenomenon is characterized by organized pressure oscillations in the rocket engine which are driven by a nonsteady combustion process. These oscillations can cause mechanical failure, high heat transfer rates to the chamber walls, and interference with the control and guidance systems. Any of these effects can result in engine or mission failure.

Two types of instability are generally observed and are categorized according to the frequency of the oscillations. Low frequency instability[1], or "chugging", occurs at frequencies ranging from ten to several hundred Hertz. Characterized by spacially uniform oscillations, this type of instability is generally caused by coupling between the feed system and the fluid dynamics in the chamber. Since low frequency instability is sufficiently understood[2], it can usually be avoided or eliminated. A second type of instability, known as high frequency or acoustic instability, is much more difficult to analyze and control. Driven by the combustion processes, oscillations with frequencies of several thousand Hertz have been observed. The oscillations are no longer spacially uniform but can vary in either the transverse or axial direction. Of the two types of combustion

instability, high frequency instability is more detrimental and less understood.

The wave system inside the converging section of the nozzle can significantly affect the oscillations in the combustor, and thus the stability characteristics of the rocket motor. Therefore, the nozzle wave system is an important consideration in combustion instability studies.

The nozzle admittance is an essential parameter in determining the interaction between the nozzle and combustor wave systems. For irrotational oscillations, which are assumed in the present investigation, this parameter is defined as the ratio of the axial component of the velocity perturbation to the pressure perturbation, evaluated at the nozzle entrance. A more general definition of the admittance parameter is given in Reference 3. Once the nozzle admittance is known, the interaction between the wave systems in the nozzle and the combustion chamber can be determined.

The nozzle admittance can also be related to the stability of a rocket motor. In linear stability analyses, the pressure oscillation in the combustor is described by the following equation:

$$p' = p'(\underset{\rightarrow}{r}) \, e^{(\lambda_1 + i\omega)t} \tag{1-1}$$

where $\underset{\rightarrow}{r}$ is the spacial coordinate, t is the time, λ_1 is the amplification coefficient, and ω is the angular frequency. If $\lambda_1 > 0$ the oscillations will grow with time and the motor will be linearly

unstable. Crocco[3] has derived the following expression for λ_1:

$$\lambda_1 z_e = - (y_r + \gamma \bar{u}_e) + \left(\frac{\gamma}{\pi P_0}\right) \int_0^{z_e} \frac{dq_r'}{dz} \cos \omega z \, dz \qquad (1\text{-}2)$$

$$+ (2 - \gamma)\omega \int_0^{z_e} \bar{u}(z) \sin 2 \omega z \, dz$$

where y is the nozzle admittance, z is the axial distance from the injector, γ is the ratio of specific heats, $\bar{u}$ is the nondimensional mean flow velocity, P_0 is the amplitude of the pressure perturbations, and q' is the unsteady perturbation in the energy released by the combustion process. The subscript e denotes a quantity evaluated at the nozzle entrance and the subscript r denotes the real part of a quantity. For many combustion distributions, the term involving q' is destabilizing, and the terms involving $\bar{u}$ are stabilizing. The effect of the nozzle admittance can now be ascertained from equation (1-2). Positive values of the real part of the admittance decrease λ_1 which means that the presence of a nozzle has a stabilizing influence on the rocket motor in this case. However, negative values of y_r tend to increase λ_1 and thus destabilize the motor.

Nozzle Admittance Theories

Calculation of the nozzle admittance has been the subject of several theoretical analyses. In these investigations the mean flow

in the nozzle is assumed to be one-dimensional, and the gas is assumed to be ideal and non-reacting.

Tsien[4] was the first to study the response of a choked nozzle under the influence of axial pressure and velocity perturbations superimposed upon the steady mean flow. In order to account for the effect of the nozzle, he introduced a "transfer function" defined as the ratio of the mass flow oscillation to the chamber pressure oscillation at the nozzle entrance. Assuming isothermal perturbations and a linear velocity distribution in the nozzle, Tsien restricted his studies to the limiting cases of very high and very low frequency oscillations.

Later, Crocco[1,5] removed the assumption of isothermal oscillations, extended Tsien's work to include the entire frequency range, and introduced the concept of admittance to study the influence of the nozzle on the flow oscillations. By assuming a linear velocity profile and isentropic perturbations in the nozzle, Crocco obtained a hypergeometric equation which he then solved for the admittance. Both Tsien and Crocco showed that the nozzle has a damping effect on the chamber oscillations for axial perturbations; that is, the real part cf the admittance was positive.

In 1967, Crocco extended his earlier analysis to consider the admittances of choked nozzles with three-dimensional flow oscillations; this analysis is given in Reference 6. This reference includes the numerical solutions for the admittances of various nozzle configurations over the frequency range of interest in combustion instability studies.

It was found that the admittance values could become negative in the case of three-dimensional oscillations. This means that the nozzle has a destabilizing influence on the oscillations in the chamber.

Crocco's three-dimensional nozzle admittance theory has never been checked experimentally, although it has been widely used in theoretical combustion instability studies.[7] Therefore, it is important that an experimental investigation be undertaken which yields quantitative admittance data for use in rocket motor design and for comparison with the theoretical results.

Experimental Techniques

To date, two techniques have been used to measure the one-dimensional nozzle admittance. In 1961, Crocco, Monti, and Grey[8] determined the real and imaginary parts of the admittance from direct measurements of the pressure and velocity perturbations at the nozzle entrance. They showed that the experimental values of the real part of the admittance were consistently greater than the corresponding theoretical predictions. This discrepancy was attributed to non-isentropic conditions and was eliminated by assuming a polytropic process with an appropriate exponent. The accuracy of the data was limited by wave distortion at higher frequencies, a low signal to noise ratio, and difficulties in measuring the velocity perturbations with hotwire anemometers.

Later, Buffum, Dehority, Slates, and Price[9] measured the amplification factor λ_1, which can be related back to the admittance of the nozzle, by use of the half-power bandwidth technique. With

this method the frequency of the oscillations is varied from a value below a resonant frequency of the chamber to a value above this resonant frequency. If the amplitude of the pressure oscillation is then plotted as a function of the driven frequency, a resonance curve is obtained. From the shape of this curve, the amplification factor of the system can be determined. In this investigation the wave attenuation caused by the presence of the nozzle was determined for several contraction ratios. Testing a family of short nozzles, they found the attenuation to be as much as twice the value obtained from the theoretical predictions. However, losses associated with the rest of the system also contributed to the measured attenuation, thus causing inaccuracies in the results. Culick and Dehority[10] have shown that this method is valid only when the nozzle admittance is not a function of frequency which may not be true for liquid rocket nozzles. Therefore, the half-power bandwidth technique may not be applicable to liquid rocket nozzle admittance studies.

In principle, the methods used to measure the one-dimensional nozzle admittances could be extended to the three-dimensional case. However, to obtain more accurate admittance data a different method is used in this investigation. This method is based on the classical impedance tube technique[11,12,13] which is known to yield accurate admittance data. Widely used, this method consists of a smooth-walled tube with a sound source at one end and the sample for which the admittance is to be measured at the other end. By measurements of the standing wave pattern in the tube, the admittance of the sample

can be obtained. However, the classical impedance tube method is only valid for one-dimensional oscillations with no mean flow present. For use in the nozzle admittance studies the classical impedance tube method must be modified to include the effects of three-dimensional waves and mean flow.

Objectives

The objectives of this investigation are to determine the nozzle admittances for longitudinal and mixed first tangential-longitudinal modes of typical liquid propellant rocket nozzle configurations used in theoretical combustion instability studies and to compare these data with theoretical predictions. To achieve these objectives, Crocco's theory is used to obtain theoretical admittance values. This theory is discussed in Chapter II, and the admittance values for the nozzles studied in this investigation are computed and tabulated. To obtain experimental nozzle admittance data, the classical impedance tube theory is extended in Chapter III to account for three-dimensional oscillations and mean flow. Various techniques for determining the nozzle admittance are discussed. Based on this theory, an experimental facility is presented in Chapter IV which is used to obtain the necessary data for determination of the nozzle admittance. The results of the preliminary testing conducted with this facility are presented in Chapter V. The experimental admittance data obtained from the experiment are given in Chapter VI and compared with the theoretical predictions. The effects of the nozzle shape and entrance Mach number on the admittance values are then discussed.

CHAPTER II

THREE-DIMENSIONAL NOZZLE ADMITTANCE THEORY

The equations necessary for the computation of the nozzle admittance values are presented in Reference 6. This reference provides tables from which theoretical admittances can be computed for a family of nozzles. However, more complete tables were desired in order to obtain more information about the behavior of the real and imaginary parts of the nozzle admittances for the nozzle geometries, Mach numbers, and frequency ranges of interest in this study. Therefore, a computer program was written which uses the equations developed by Crocco[6] to calculate the admittances for the nozzles under investigation in this study.

Governing Equations

The expressions used to compute the nozzle admittance are derived in detail in References 6 and 14, and only the salient points of this derivation are included here. These expressions are obtained from the equations describing the three-dimensional oscillatory flow in the nozzle. If the nozzle is assumed to contain the flow of an inviscid, irrotational, adiabatic, perfect gas, the equations of motion are

Continuity:

$$\frac{\partial \rho^*}{\partial t^*} + \nabla^* \cdot (\rho^* \; \vec{q}^*) = 0 \qquad\qquad (2\text{-}1)$$

Momentum:

$$\frac{\partial \vec{q}^*}{\partial t^*} + \frac{1}{2} \nabla^*(q^{*2}) = - \frac{1}{\rho^*} \nabla^* p^* \qquad\qquad (2\text{-}2)$$

where the superscript * denotes a dimensional quantity, t^* the time, ρ^* the density, p^* the pressure, and q^* the velocity vector. Also, for isentropic conditions, the following relations hold:

$$c^{*2} = \frac{\gamma p^*}{\rho^*} \text{ and } \frac{p^*}{p_o^*} = \left(\frac{\rho^*}{\rho_o^*}\right)^\gamma \qquad\qquad (2\text{-}3)$$

where c^* is the speed of sound and γ is the ratio of specific heats. The subscript o denotes a stagnation quantity.

Equations (2-1) through (2-3) are now expressed in terms of nondimensional variables. Since the steady state stagnation quantities remain constant throughout the flow, they serve as convenient parameters for nondimensionalizing the equations. The following non-dimensional quantities are introduced:

$$\vec{q} = \frac{\vec{q}^*}{c_o^*} \; , \quad p = \frac{p^*}{p_o^*} \; , \quad \rho = \frac{\rho^*}{\rho_o^*}$$

where steady state quantities are indicated by a bar over the symbol. Lengths are nondimensionalized by the chamber radius r_c^* and t is the nondimensional time defined as

$$t = \frac{\bar{c}_o^*}{r_c^*} t^*$$

The equations of motion in nondimensional form become

$$\frac{\partial \rho}{\partial t} + \nabla \cdot (\rho \vec{q}) = 0 \qquad (2\text{-}4)$$

$$\frac{\partial \vec{q}}{\partial t} + \frac{1}{2} \nabla q^2 = -\frac{1}{\rho} \nabla p \qquad (2\text{-}5)$$

where $c^2 = p/\rho$ and $p = \rho^\gamma$.

In order to linearize these equations, the unsteady perturbations about the steady state quantities are assumed to be infinitesimal so that only linear terms in the perturbations need be retained in the conservation equations. Let

$$\vec{q} = \bar{\vec{q}} + \vec{q}', \quad p = \bar{p} + p', \quad \rho = \bar{\rho} + \rho' \qquad (2\text{-}6)$$

where the primed quantities represent the flow perturbations. Substituting these expressions into equations (2-4) and (2-5) and neglecting all nonlinear terms yield one set of equations governing

the steady state flow field and another set describing the behavior of the perturbations. The steady state equations are

$$\nabla \cdot (\bar{\rho}\vec{\bar{q}}) = 0; \quad \bar{c}^2 = 1 - \frac{\gamma-1}{2}\,\bar{q}^2; \quad \bar{p} = \bar{\rho}^\gamma \tag{2-7}$$

The equations describing the behavior of the perturbations are

$$\frac{\partial \rho'}{\partial t} + \nabla \cdot (\vec{\bar{q}}\rho' + \bar{\rho}\vec{q}') = 0 \tag{2-8a}$$

$$\frac{\partial \vec{q}'}{\partial t} + \nabla(\vec{\bar{q}}\cdot\vec{q}') = - \nabla\left(\frac{p'}{\gamma\bar{p}}\right) \tag{2-8b}$$

where $p' = \bar{c}^2\rho'$.

In order to simplify the boundary conditions at the nozzle walls, a (φ,ψ,θ) coordinate system is chosen where φ represents the steady state velocity potential function, ψ denotes the steady state stream function, and θ is the azimuthal variable. Assuming one-dimensional mean flow, the velocity vector is written as

$$\vec{\bar{q}} = \vec{e}_\varphi\, \bar{q}(\varphi)$$

$$\vec{q}' = u'\vec{e}_\varphi + v'\vec{e}_\psi + w'\vec{e}_\theta$$

It is shown in Reference 6 that

$$\psi = \frac{1}{2}\,\bar{\rho}(\varphi)\bar{q}(\varphi)r^2$$

$$\bar{q}(\varphi) = \frac{d\varphi}{dz}$$

where r is the local radius and dz an infinitesimal displacement along a constant ψ surface. In this coordinate system the equations of motion become

Continuity

$$\frac{\partial}{\partial t}\left(\frac{\rho'}{\bar{\rho}}\right) + \bar{q}^2\,\frac{\partial}{\partial\varphi}\left(\frac{\rho'}{\bar{\rho}} + \frac{u'}{\bar{q}}\right) + 2\bar{\rho}\bar{q}\,\frac{\partial}{\partial\psi}\left(\frac{v'}{r\bar{\rho}\bar{q}}\right) + \frac{\bar{\rho}\bar{q}}{2\psi}\,\frac{\partial}{\partial\theta}(rw') = 0 \qquad (2\text{-}9)$$

Momentum

φ - component

$$\frac{\partial(\frac{u'}{\bar{q}})}{\partial t} + \frac{\partial}{\partial\varphi}\left(\bar{q}^2\,\frac{u'}{\bar{q}}\right) + \frac{\partial}{\partial\varphi}\left(\frac{p'}{\gamma\bar{p}}\right) = 0 \qquad (2\text{-}10)$$

ψ - component

$$\frac{\partial}{\partial t}\left(\frac{v'}{r\bar{\rho}\bar{q}}\right) + \bar{q}^2\,\frac{\partial}{\partial\varphi}\left(\frac{v'}{r\bar{\rho}\bar{q}}\right) + \frac{\partial}{\partial\psi}\left(\frac{p'}{\gamma\bar{p}}\right) = 0 \qquad (2\text{-}11)$$

θ - component

$$\frac{\partial}{\partial t}(rw') + \bar{q}^2 \frac{\partial}{\partial \varphi}(rw') + \frac{\partial}{\partial \theta}\left(\frac{p'}{\gamma\bar{p}}\right) = 0 \qquad (2\text{-}12)$$

Equations (2-9) through (2-12) are now solved by using the method of separation of variables. The solutions are written in the form

$$\frac{u'}{\bar{q}} = \frac{d\Phi(\varphi)}{d\varphi} K(\psi,\theta,t)$$

$$\frac{v'}{r\bar{\rho}\bar{q}} = \Phi(\varphi) \frac{\partial}{\partial\psi} K(\psi,\theta,t)$$

$$rw' = \Phi(\varphi) \frac{\partial}{\partial\theta} K(\psi,\theta,t)$$

$$\frac{p'}{\bar{p}} = - [i\omega\Phi(\varphi) + \bar{q}^{-2}(\varphi) \frac{d\Phi(\varphi)}{d\varphi}]K(\psi,\theta,t)$$

$$\frac{\rho'}{\bar{\rho}} = - \left(\frac{1}{\bar{c}^2}\right)[i\omega\Phi(\varphi) + \bar{q}^{-2}(\varphi) \frac{d\Phi(\varphi)}{d\varphi}]K(\psi,\theta,t)$$

where

$$K(\psi,\theta,t) = J_m \left[S_{mn}\left(\frac{\psi}{\psi_w}\right)^{\frac{1}{2}} \right] \cos m\theta \; e^{i\omega t}$$

for standing waves and

$$K(\psi,\theta,t) = J_m \left[S_{mn}\left(\frac{\psi}{\psi_w}\right)^{\frac{1}{2}} \right] e^{\pm im\theta} \; e^{i\omega t}$$

for spinning waves. In these expressions the nondimensional frequency ω is defined as

$$\omega = \frac{r_c^* \omega^*}{\bar{c}_o^*}$$

where ω^* is the dimensional angular frequency. Also, S_{mn} is the nth root of the equation

$$\frac{d}{dx} J_m(x) = 0,$$

m is the number of diametral nodal lines and n is the number of azimuthal nodal lines in the transverse wave pattern. For longitudinal modes, $m = n = 0$ and $S_{00} = 0$; for the first tangential modes $m = 1$, $n = 0$, and $S_{10} = 1.8413$. Substituting the given solutions into the

conservation equations and eliminating variables yield the following

differential equation for Φ:

$$\bar{q}^2 \left(\bar{c}^2 - \bar{q}^2 \right) \frac{d^2\Phi}{d\varphi^2} - \bar{q}^2 \left(\frac{1}{\bar{c}^2} \frac{d\bar{q}^2}{d\varphi} + 2i\omega \right) \frac{d\Phi}{d\varphi} \qquad (2\text{-}13)$$

$$+ \left[\omega^2 - \frac{\gamma-1}{2} i\omega \frac{\bar{q}^2}{\bar{c}^2} \frac{d\bar{q}^2}{d\varphi} - \frac{s_{mn}^2 \bar{c}^2}{r_w^2} \right] \Phi = 0$$

Admittance Relation

The function Φ can be related to the specific acoustic admittance by the formula[6]

$$y = \bar{\rho}\bar{c} \frac{u'}{p'} = - \frac{\bar{\rho}\bar{c}\zeta}{\bar{q}^2 \zeta + i\omega} \qquad (2\text{-}14)$$

where

$$\zeta = \frac{1}{\Phi} \frac{d\Phi}{d\varphi}$$

The differential equation for ζ is derived from equation (2-13) and

the definition of ζ. The resulting differential equation is a complex

Riccati equation given as

$$\frac{d\zeta}{d\varphi} - \frac{B}{A}\zeta + \zeta^2 = \frac{C}{A} \qquad (2\text{-}15)$$

where

$$A = \bar{q}^2(\bar{c}^2 - \bar{q}^2)$$

$$B = \bar{q}^2\left(\frac{1}{\bar{c}^2}\frac{d\bar{q}^2}{d\varphi} + 2i\omega\right)$$

$$C = -\left[\omega^2 - \frac{S_{mn}^2}{r_w^2}\bar{c}^2 - i\left(\frac{\gamma-1}{2}\omega\frac{\bar{q}^2}{\bar{c}^2}\frac{d\bar{q}^2}{d\varphi}\right)\right]$$

To determine the nozzle admittance for irrotational perturbations, equation (2-15) is solved to find the value of ζ at the nozzle entrance; this value is then used to determine the admittance directly from equation (2-14). From equation (2-15), the value of ζ depends upon the values of A, B, and C. These coefficients are functions of the acoustical properties of the oscillations and the mean flow field characteristics in the nozzle. In the expressions for A, B, and C, the acoustical properties contribute the terms involving ω and S_{mn}. For this study the values of ω cover the frequency range of the longitudinal modes, for which S_{mn} is zero, and the mixed first tangential-longitudinal modes, for which S_{mn} equals 1.8413. Mixed first tangential-longitudinal

modes are those modes of oscillation which occur between the cutoff
frequencies of the first tangential mode and the second tangential
mode. The terms involving $\bar{q}$ and $\bar{c}$ in the relations for A, B, and C
represent the effects of the mean flow. The values of $\bar{q}$ and $\bar{c}$ in the
nozzle can be computed once γ and the nozzle contour are specified.
The equations used for this computation are given in Reference 14.

To determine ζ for given values of ω and S_{mn} and a
specific nozzle contour, equation (2-15) must be numerically inte-
grated. The major difficulty in this integration is that ζ can
become unbounded whenever Φ approaches zero, which causes numerical
difficulties in the integration scheme. Crocco and Sirignano[6] noted
that this phenomenon occurred for low chamber Mach numbers and high
values of ω/S_{mn}. At these Mach numbers and frequencies they developed
asymptotic solutions for ζ .

Instead of using the asymptotic theory, a different approach is
employed in this study. The problem appears to be resolved by defining
a new independent variable

$$\tau = \frac{1}{\zeta} = \frac{\Phi}{\frac{d\Phi}{d\varphi}}$$

Thus, as Φ approaches zero and the magnitude of ζ becomes large,
τ becomes small. Introducing the definition of τ into equation
(2-15) gives the following Riccati equation for τ:

$$\frac{d\tau}{d\varphi} + \frac{B}{A}\tau + \frac{C}{A}\tau^2 = 1 \qquad (2\text{-}16)$$

At those points in the nozzle where ζ becomes unbounded, equation (2-16) is integrated instead of equation (2-15).

Values of ζ or τ are obtained by numerically integrating equation (2-15) or (2-16). The numerical integration must start at the throat because at this point

$$\bar{q}^2 = \bar{c}^2 = \frac{2}{\gamma+1}$$

and equations (2-15) and (2-16) are singular. The procedure used to evaluate the mean flow variables, ζ, and the coefficients A, B, and C at the throat is presented in References 6 and 14. These values are used to start the integration. Equation (2-15) and the equations governing the mean flow[14] are then integrated by a modified Adams predictor-corrector scheme using a Runge-Kutta of order four to start the integration. During the integration the magnitude of ζ is monitored. If ζ exceeds a value at which instabilities can occur in the integration scheme, then the integration of equation (2-15) is terminated at that point. Here the value of τ is computed and the integration proceeds using equation (2-16) for τ. Similarly, should the magnitude of τ become large, then the value of ζ is determined at that point and equation (2-15) is integrated from that point on. This process is repeated until the nozzle entrance is reached. A computer program

which employs this procedure has been written in FORTRAN V for use on the UNIVAC 1108 and is given in Appendix A. From this computer program admittance values are calculated for given nozzle geometries and entrance Mach numbers.

Theoretical Predictions

Theoretical admittance values have been obtained for the nozzles under investigation in this program. The nozzles are axisymmetric, and the geometries consist of three sections as shown in Figure 1. The first section starts at the combustion chamber and is generated by a circular arc of radius r_{cc} which is turned through an angle θ_1, the nozzle half-angle. This section connects smoothly to the next which is a conical nozzle of angle θ_1. The conical nozzle then joins with the third section, which ends at the throat, and is generated by a circular arc of radius r_{cc} turned through an angle θ_1.

The nozzles under investigation are presented in Table 1 where the ratio of the radius of curvature r_{cc} to the chamber radius r_c is given for each nozzle half-angle and Mach number considered. By studying these nozzles the dependence of the nozzle admittance upon the entrance Mach number, nozzle half-angle, and radius of curvature can be determined.

The theoretical values of the admittance for these nozzles are given in the tables included in Appendix B for longitudinal and mixed first tangential-longitudinal modes. The real and imaginary parts of the admittance are tabulated over a range of the nondimensional

frequency S, where

$$S = \frac{\omega^* r_c^*}{\bar{c}^*}$$

For the longitudinal modes the theoretical results show that the values of the real part of the admittance are positive, which means that the presence of a nozzle has a stabilizing influence on the oscillations inside a rocket motor. This result is predicted by all existing nozzle admittance theories[1,4,5,6] for longitudinal oscillations. For the nozzles under investigation in this study, increasing θ_1 decreases the value of the real part of the admittance for an entrance Mach number $\bar{M}$ of 0.08 as shown in Figure 2. In Figure 3, for a half-angle of 45 degrees, increasing $\bar{M}$ has little effect on the real and imaginary parts of the admittance. Changing r_{cc}, the ratio of the radius of curvature to the chamber radius, also has little effect as shown in Figure 4 for a half-angle of 15 degrees and an entrance Mach number of 0.08.

The theoretical results for the mixed first tangential-longitudinal modes show that the real part of the admittance can be nagative over the range of frequencies applicable to this investigation. Thus, the nozzle can have a destabilizing influence on the oscillations inside the rocket motor. Increasing θ_1 at an entrance Mach number of 0.08 tends to increase the value of the real part of the admittance as shown in Figure 5. Increasing $\bar{M}$ for half-angle of 45 degrees decreases the values of the real part of the admittance close to the

frequency of the first tangential mode, but increases the values at the higher frequencies as presented in Figure 6 . From Figure 7, changing r_{cc} has little effect on the admittance values for a nozzle half-angle of 15 degrees and an entrance Mach number of 0.08.

These results will be compared with experimental data in Chapter V. The experimental technique used to obtain these data will now be presented.

CHAPTER III

EXPERIMENTAL TECHNIQUE

Crocco's nozzle admittance theory[6] has been used in theoretical combustion instability analyses of rocket motors[7] although the predicted admittance values for three-dimensional waves have never been confirmed experimentally. To check the theoretical predictions, an accurate method of obtaining experimental nozzle admittance data is needed. Based on the results of Culick and Dehority[10], the impedance tube technique[11,12,13] would be most suitable for this purpose. The choice of an appropriate experimental technique for the measurement of the nozzle admittance was investigated independently by Bell[15], who concluded that the impedance tube method should be used in the experimental determination of nozzle admittances.

Based on the conclusions of References 10 and 15, a modification of the classical impedance tube method was developed for this investigation. The apparatus used in the classical impedance tube technique consists of a smooth-walled cylindrical tube with a sound source at one end and the sample, the admittance of which is to be measured, at the other end as shown in Figure 8. A standing wave pattern is established in the tube by the incident wave transmitted from the sound source and the wave reflected from the tested sample. The structure of the standing wave depends upon the admittance of the tested sample. By measuring the structure of the standing wave pattern

in the tube, the admittance of the sample is determined. However, the classical impedance tube method is limited to one-dimensional oscillations with no mean flow present. Because the nozzle admittance studies deal with both one- and three-dimensional waves superimposed upon a steady, axial mean flow, the classical impedance tube theory had to be extended in order to account for these effects. The development of the modified impedance tube theory is described in the following sections.

Governing Equations

The conservation equations which are needed to describe the behavior of the standing wave pattern in the impedance tube have been developed in Chapter II, and they are given by equations (2-9) to (2-12). These equations are simplified by the fact that the steady state flow properties are constant throughout the tube. Since the tube is cylindrical in shape, it is convenient to rewrite these equations in cylindrical coordinates using the relations

$$dz = \frac{d\varphi}{q} \quad \text{and} \quad dr = \frac{d\psi}{\rho q}$$

Also, since the experimentally measured quantities are dimensional, these equations are rewritten in dimensional form. In this chapter only dimensional quantities are used, and the superscript $*$ which denoted such quantities in Chapter II will not be employed here.

Equations (2-9) to (2-12) become

$$\frac{1}{\bar{\rho}} \frac{\partial \rho'}{\partial t} + \frac{1}{r} \frac{\partial(rv')}{\partial r} + \frac{1}{r} \frac{\partial w'}{\partial \theta} + \frac{\partial}{\partial z}\left[u' + \bar{q}\left(\frac{\rho'}{\bar{\rho}}\right)\right] = 0 \qquad (3\text{-}1)$$

$$\frac{\partial u'}{\partial t} + \bar{q} \frac{\partial u'}{\partial z} + \frac{1}{\bar{\rho}} \frac{\partial p'}{\partial z} = 0 \qquad (3\text{-}2)$$

$$\frac{\partial v'}{\partial t} + \bar{q} \frac{\partial v'}{\partial z} + \frac{1}{\bar{\rho}} \frac{\partial p'}{\partial r} = 0 \qquad (3\text{-}3)$$

$$\frac{\partial w'}{\partial t} + \bar{q} \frac{\partial w'}{\partial z} + \frac{1}{\bar{\rho}r} \frac{\partial p'}{\partial \theta} = 0 \qquad (3\text{-}4)$$

where the dimensional velocities are defined as

$$\vec{\bar{q}} = \bar{q}\ \vec{e}_z$$

$$\vec{q}' = u'\vec{e}_z + v'\vec{e}_r + w'\vec{e}_\theta$$

and $\vec{e}_z$, $\vec{e}_r$, and $\vec{e}_\theta$, are unit vectors in the axial, radial, and

tangential directions, respectively.

The method of separation of variables is employed to solve equations (3-1) to (3-4) for the dependent variables u', v', w', p', and ρ'. The simple harmonic solutions are:

$$u' = U(z)R(r)\Theta(\theta)e^{i\omega t}$$

$$v' = V(z) \frac{dR(r)}{dr} \Theta(\theta)e^{i\omega t}$$

$$rw' = W(z)R(r) \frac{d\Theta(\theta)}{d\theta} e^{i\omega t}$$

$$p' = P(z)R(r)\Theta(\theta)e^{i\omega t}$$

$$\rho' = N(z)R(r)\Theta(\theta)e^{i\omega t}$$

where

$$R(r) = J_m(S_{mn} \frac{r}{r_c})$$

$$\Theta(\theta) = \cos m(\theta - C_\theta)$$

for standing waves and

$$\Theta(\theta) = e^{\pm i(m\theta - C_\theta)}$$

for spinning waves; C_θ is a complex integration constant. Substituting these solutions into equations (3-1) to (3-4) and simplifying gives

$$\left(\frac{i\omega}{\bar{\rho}}\right)N + \frac{\bar{q}}{\bar{\rho}}\frac{dN}{dz} + \frac{dU}{dz} - \left(\frac{S_{mn}}{r_c}\right)^2 V = 0 \qquad (3\text{-}5)$$

$$i\omega U + \bar{q}\frac{dU}{dz} + \frac{1}{\bar{\rho}}\frac{dP}{dz} = 0 \qquad (3\text{-}6)$$

$$i\omega V + \bar{q}\frac{dV}{dz} + \frac{1}{\bar{\rho}}P = 0 \qquad (3\text{-}7)$$

$$i\omega W + \bar{q}\frac{dW}{dz} + \frac{1}{\bar{\rho}}P = 0 \qquad (3\text{-}8)$$

For isentropic flow

$$N = \frac{P}{\bar{c}^2} \tag{3-9}$$

Making the usual assumption in impedance tube analyses of irrotational perturbations, it can be shown that[6]

$$U = \frac{dV}{dz}; \quad V = W \tag{3-10}$$

Equation (3-5) can now be rewritten in terms of V by using equations (3-7), (3-9), and (3-10) to eliminate N and U. Thus, equation (3-5) gives

$$(1 - \bar{M}^2) \frac{d^2V}{dz^2} - 2i\bar{M}k \frac{dV}{dz} + \left[k^2 - \left(\frac{S_{mn}}{r_c} \right)^2 \right] V = 0$$

where the chamber Mach number $\bar{M}$ is given as

$$\bar{M} = \frac{\bar{q}}{\bar{c}}$$

and the wave number k is defined as

$$k = \frac{\omega}{\bar{c}}$$

Solving for V from this expression and using equations (3-7) and (3-10) to obtain P and U gives

$$P = A_+ e^{i(a - k_{mn})z} + A_- e^{i(a + k_{mn})z}$$ (3-11)

$$\bar{\rho c}U = - \frac{A_+(a - k_{mn})e^{i(a - k_{mn})z}}{k + \bar{M}(a - k_{mn})} - \frac{A_-(a + k_{mn})e^{i(a + k_{mn})z}}{k + \bar{M}(a + k_{mn})}$$ (3-12)

$$\bar{\rho c}V = \frac{iA_+ e^{i(a - k_{mn})z}}{k + \bar{M}(a - k_{mn})} + \frac{iA_- e^{i(a - k_{mn})z}}{k + \bar{M}(a + k_{mn})}$$ (3-13)

where

$$a = \frac{k\bar{M}}{1-\bar{M}^2}$$

and

$$k_{mn} = \frac{\sqrt{k^2 - \left(\frac{S_{mn}}{r_c}\right)^2 (1 - \bar{M}^2)}}{1 - \bar{M}^2}$$

In a cylindrical chamber with mean flow, the axial dependence of the standing waves are given by equations (3-11), (3-12), and (3-13).

The standing waves are formed by the superposition of two simple harmonic waves traveling along the tube. The wave with amplitude A_+ travels in the positive z direction, while the one with amplitude A_- propagates in the negative z direction. Because of the Doppler effect, the two traveling waves have different wavelengths. The structures of the standing waves are determined by the relationships between A_+ and A_- which is governed by the admittance at the nozzle entrance. The impedance tube method consists of measuring the standing wave pattern in order to determine the relationship between A_+ and A_- which is then used to compute the admittance.

Standing Wave Analysis

To be consistent with the analyses in References 11, 12, and 13, equations (3-11) through (3-13) are written in terms of hyperbolic functions by introducing the following definitions:

$$A_+ = \frac{1}{2} A e^{\pi\alpha - i\pi(\beta + \frac{1}{2})} \qquad (3\text{-}14)$$

$$A_- = \frac{1}{2} A e^{-\pi\alpha + i\pi(\beta + \frac{1}{2})}$$

where A is determined by the pressure amplitude at the driven end where $z = -L$. Using equation (3-14) it can easily be shown that the ratio of the reflected to incident wave amplitudes at the nozzle entrance is $e^{-2\pi\alpha}$ and the phase between the incident and reflected pressure waves at the nozzle entrance is $\pi(2\beta + 1)$. Introducing

equation (3-14) into equations (3-11) through (3-13) gives

$$P = -iAe^{iaz}\sinh[\pi\alpha - i(\pi\beta + k_{mn}z)] \qquad (3-15)$$

$$U = \frac{-i\,Ae^{iaz}}{\bar{\rho}\bar{c}\left[k^2 + \left(\frac{S_{mn}}{r_c}\bar{M}\right)^2\right]}\{kk_{mn}(1 - \bar{M}^2)\cosh[\pi\alpha-i(\pi\beta + k_{mn}z)] \qquad (3-16)$$

$$- \left(\frac{S_{mn}}{r_c}\right)^2 \bar{M}\sinh[\pi\alpha - i(\pi\beta + k_{mn}z)]\}$$

$$V = \frac{Ae^{iaz}}{\bar{\rho}\bar{c}\left[k^2 + \left(\frac{S_{mn}}{r_c}\bar{M}\right)^2\right]}\{k\,\sinh[\pi\alpha - i(\pi\beta + k_{mn}z)] \qquad (3-17)$$

$$+ \bar{M}k_{mn}(1 - \bar{M}^2)\cosh[\pi\alpha - i(\pi\beta + k_{mn}z)]\}$$

where z is zero at the nozzle entrance and the positive z direction is toward the nozzle throat. The specific admittance y at the nozzle entrance can now be obtained from equations (3-15) and (3-16). By definition,

$$y = \bar{\rho}\bar{c}\left.\frac{u'}{p'}\right|_{z=0} = \bar{\rho}\bar{c}\left.\frac{U}{P}\right|_{z=0}$$

Substituting for P and U from equations (3-15) and (3-16) respectively gives

$$y = \frac{s\sqrt{s^2 - s_{mn}^2(1-\bar{M}^2)} \ \coth \pi(\alpha - i\beta) - s_{mn}^2\bar{M}}{s^2 + (s_{mn}\bar{M})^2} \tag{3-18}$$

Separating the admittance into its real and imaginary components gives

$$y_r = \frac{\left[\dfrac{s\sqrt{s^2 - s_{mn}^2(1-\bar{M}^2)} \ \tanh \pi\alpha \ \sec^2 \pi\beta}{\tanh^2 \pi\alpha + \tan^2 \pi\beta} - s_{mn}^2\bar{M}\right]}{s^2 + (s_{mn}\bar{M})^2} \tag{3-19}$$

$$y_i = \frac{s\sqrt{s^2 - s_{mn}^2(1 - \bar{M}^2)} \ \tan \pi\beta \ \mathrm{sech}^2 \pi\alpha}{\left[s^2 + (s_{mn}\bar{M})^2\right](\tanh^2\pi\alpha + \tan^2 \pi\beta)} \tag{3-20}$$

Equation (3-18) differs from the classical admittance relation through the addition of the terms involving S_{mn} and $\bar{M}$, which account for the effects of three-dimensional waves and mean flow, respectively. For longitudinal waves ($S_{mn} = 0$) and no mean flow ($\bar{M} = 0$), this equation

reduces to the classical result given in Reference 13.

For three-dimensional oscillations, the real part of the admittance consists of two terms as given in equation (3-19). The first term,

$$\frac{S\sqrt{S^2 - S_{mn}^2(1 - \bar{M}^2)}}{S^2 + (S_{mn}\bar{M})^2} \quad \frac{\tanh\pi\alpha \, \sec^2\pi\beta}{\tanh^2\pi\alpha + \tan^2\pi\beta} \, ,$$

results from the interaction between the incident and reflected waves at the nozzle entrance. The sign of α determines whether this term is positive or negative. From the definition of α, when the amplitude of the incident wave is greater than the amplitude of the reflected wave, α is positive, which means that this term has a stabilizing effect on the rocket motor. The second term, given by

$$\frac{-S_{mn}^2 \bar{M}}{S^2 + (S_{mn}\bar{M})^2}$$

results from the interaction between the axial mean flow and the transverse velocity wave. Since this term is always negative, it represents a destabilizing effect upon the oscillations in the tube.

According to theoretical predictions, negative values of the real part of the admittance can occur for transverse waves with axial mean flow present. At the entrance Mach numbers for the nozzles under

investigation, the negative values can arise because of the second term of equation (3-19) even though α is positive. These negative values result when the value of α is a small positive number and the value of β is close to 1/2. However, over the entire frequency range of mixed first tangential-longitudinal modes at an entrance Mach number of 0.08 and over part of this frequency range at entrance Mach numbers of 0.16 and 0.20, the negative values of the real part of the admittance predicted from theory can be obtained from equation (3-19) only if both the first and second terms are negative. This suggests that α is negative which implies that the nozzle wave system supplies acoustic energy to the wave system in the chamber.

Experimental Technique for Computing the Admittance

Equation (3-19) can be used to determine the values of the nozzle admittance once α and β are known for a given frequency, a given mean flow Mach number, and a given acoustic mode. Several methods are available for determining α and β experimentally which involve measurements of the standing wave pattern in the impedance tube. The dependence of the standing wave pattern for the pressure oscillations on the location in the chamber is obtained from equation (3-15) and the assumed solutions to equations (3-1) through (3-4). These pressure oscillations are described by

$$p' = |p'| \; e^{i(\delta + \omega t)}$$

where the pressure amplitude $|p'|$ is given by

$$|p'| = AJ_m(S_{mn} \frac{r}{r_c})\cos(m\theta+C_\theta)[\cosh^2\pi\alpha-\cos^2\pi(\beta + \frac{2z}{\lambda})]^{\frac{1}{2}} \tag{3-22}$$

and the phase δ is

$$\delta = az + \text{Arctan}\,[\tanh \pi\alpha \cot \pi(\beta + \frac{2z}{\lambda})] \tag{3-23}$$

The axial wavelength λ is

$$\lambda = \frac{2\pi}{k_{mn}}$$

Because C_θ is not involved in the admittance calculations, it is assumed to be zero. For pressure measurements taken at the chamber wall where $r = r_c$ and the $\theta = 0$ position, equation (3-22) becomes

$$|p'| = A_{mn}[\cosh^2\pi\alpha - \cos^2\pi(\beta + \frac{2z}{\lambda})]^{\frac{1}{2}} \tag{3-24}$$

where

$$A_{mn} = AJ_m(S_{mn})$$

In this experiment, pressure amplitudes are measured in decibels. The sound pressure level in decibels, L, is defined as

$$L = 20 \log_{10} \left[\frac{p'}{p_{ref}}\right]$$

where p_{ref} is the reference pressure level, the value of which is 2×10^{-4} dynes per square cm. For pressures measured in decibels, equation (3-24) and the definition of L give

$$L = A_{db} + 10 \log_{10}[\cosh^2 \pi\alpha - \cos^2 \pi(\beta + \frac{2z}{\lambda})] \qquad (3\text{-}24a)$$

where A_{db} is in decibels.

The most widely used method for finding α and β is the traversing microphone technique which is discussed in References 11, 12, and 13. It consists of a microphone probe which is used to traverse the impedance tube in the axial direction in order to measure the standing wave pattern. By measuring the distance between two successive minima, the half-wavelength $\lambda/2$ is determined. The value of β is then computed by measuring the distance, $-z_{min}$, from the sample to the first minimum. From equation (3-24) this minimum occurs when

$$\cos^2 \pi(\beta - \frac{2z_{min}}{\lambda}) = 1$$

or when

$$\beta - \frac{2z_{min}}{\lambda} = 0$$

Thus

$$\beta = \frac{2z_{min}}{\lambda}$$

Then α is obtained by measuring a maximum pressure amplitude where

$$\left| P_{max} \right| = A_{mn} \cosh \pi\alpha$$

and a minimum pressure amplitude where

$$\left| P_{min} \right| = A_{mn} \sinh \pi\alpha$$

The expression for α is then

$$\tanh \pi\alpha = \left| \frac{P_{min}}{P_{max}} \right|$$

or

$$\alpha = \frac{1}{2\pi} \ln \left[\frac{1 + \left| \frac{p_{min}}{p_{max}} \right|}{1 - \left| \frac{p_{min}}{p_{max}} \right|} \right]$$

Since the wavelength is known, the nondimensional frequency S can be found from the following expression:

$$S = \sqrt{\left[\frac{2\pi}{\lambda} (1 - \bar{M}^2) r_g \right]^2 + (S_{mn})^2 (1 - \bar{M}^2)}$$

If the frequency and speed of sound are known, S can also be determined from the expression, $S = \omega r_c / \bar{c}$. The admittance can now be determined from equations (3-19) and (3-20) for a given Mach number and S_{mn}.

In principle, the traversing technique can be employed in the nozzle admittance studies. However, for the experimental facility available for this study, the run time allowed by the air supply system is significantly shorter than the time required for a microphone to traverse the tube. Also, the air is stored in high pressure tanks at 3000 psig. When the air passes from the tanks through the impedance tube, the pressure in the tanks decreases causing a corresponding decrease in temperature, which changes the acoustical properties of the air in the tube. The change in acoustical properties will cause variations in the wave pattern in the tube as it is being traversed. Leakage problems and uncertainties in the flow interaction

with the microphone probe must also be considered. Because of these problems, the traversing technique was not employed in this study.

Instead, the discrete point method is used. With this method, pressure amplitude measurements are taken at different axial locations along the tube, and the wavelength λ is computed from frequency and temperature measurements by using the following relation:

$$\lambda = \frac{2\pi}{k_{mn}} = \frac{2\pi(1 - \bar{M}^2)}{\sqrt{\left(\frac{2\pi f}{\bar{c}}\right)^2 - \left(\frac{S_{mn}}{r_c}\right)^2(1-\bar{M}^2)}}$$

where f is the measured frequency in Hertz, $\bar{c}$ is determined from temperature measurements, S_{mn} is known for a given frequency, speed of sound, and chamber radius, and $\bar{M}$ is determined from the nozzle contraction ratio. These data are then used to compute α, β, and A_{mn} from equation (3-24). In principle, three pressure amplitude measurements - $|p_1'|$, $|p_2'|$, $|p_3'|$ - at different axial locations - z_1, z_2, z_3 - are required to determine α, β, and A_{mn}. Explicit relations for α and β are derived in Appendix C from equation (3-24) and are given by

$$\alpha = \frac{1}{2\pi} \ln (x + \sqrt{x^2 - 1}) \qquad (3-25)$$

$$\beta = \frac{1}{2\pi} \text{Arctan } y \qquad (3-26)$$

where

$$x = \frac{\left| A_{31}B_{21} - A_{21}B_{31} \right|}{\left\{ \left[B_{21}(1-P_{31}) - B_{31}(1-P_{21}) \right]^2 + \left[A_{21}(1-P_{31}) - A_{31}(1-P_{21}) \right]^2 \right\}^{\frac{1}{2}}}$$

$$y = \frac{A_{21}(1 - P_{31}) - A_{31}(1 - P_{21})}{B_{21}(1 - P_{31}) - B_{31}(1 - P_{21})}$$

$$A_{n1} = \cos \frac{4\pi}{\lambda} z_n - P_{n1} \cos \frac{4\pi}{\lambda} z_1, \qquad n = 2,3$$

$$B_{n1} = \sin \frac{4\pi}{\lambda} z_n - P_{n1} \sin \frac{4\pi}{\lambda} z_1, \qquad n = 2,3$$

$$P_{n1} = \left| \frac{p'_n}{p'_1} \right|^2 \quad \text{for pressure amplitudes in psi, } n = 2,3$$

$$P_{n1} = 10^{\left(\frac{L_n - L_1}{20} \right)} \quad \text{for pressure amplitudes in decibels, } n = 2,3$$

Gately and Cohen[16] investigated the accuracy of the results for α and β using three pressure measurements. In some cases they found that a 0.3 percent error in pressure resulted in a 16 percent error in α. This

inaccuracy was considered unacceptable, and these results were substantiated in the present study as shown in Table 2. In this table 10 different values of α were obtained experimentally for the same standing wave pattern by using five pressure measurements at different axial locations which yields 10 combinations of three pressure measurements. These data show variations in α of from 0.01 to 0.11, depending upon the positions at which data are taken. Since a value of 0.01 for α means that 96 percent of the incident wave is reflected from the nozzle whereas 0.11 means that 71 percent of the incident wave is reflected, no reliable information regarding the effect of the nozzle can be obtained. Also, in some cases the parameter x in equation (3-25) for α is less than one because of experimental errors, and a value of α cannot be computed.

The reason for these large variations in α is that three pressure measurements do not yield enough accurate information about the shape of the standing wave pattern from which α and β are determined. For example, if the three pressures are measured at distances $\lambda/2$ apart, then the amplitudes are the same, and a value of α cannot be computed. To avoid such results, it is necessary to take as many pressure measurements as possible at different axial locations. In this manner, enough information about the standing wave pattern can be obtained so that α and β can be accurately determined. In the experiments conducted in this investigation, up to 10 pressure amplitude measurements have been taken.

In addition to pressure amplitude measurements, phase measure-

ments can also be used to calculate α and β. However, no reliable phase data were obtained in this study for reasons discussed in the next chapter. The analysis using phase data is included for completeness. From equation (3-23) the phase difference between pressures at two axial locations, z_1 and z_2, is

$$\Delta\delta = \delta_2 - \delta_1 = a(z_2 - z_1).$$
(3-27)

$$+ \text{Arctan} \left\{ \frac{\tanh\pi\alpha[\cot\pi(\beta + \frac{2z_2}{\lambda}) - \cot\pi(\beta + \frac{2z_1}{\lambda})]}{1 + \tanh^2\pi\alpha\cot\pi(\beta + \frac{2z_2}{\lambda})\cot\pi(\beta + \frac{2z_1}{\lambda})} \right\}$$

In order to compute α and β a minimum of three phase measurements are required - one is used as a reference, and the other two are used to generate two equations in the two unknowns, α and β. Explicit relations for these parameters are derived in Appendix C; however, as with three pressure amplitude measurements, inaccurate values of α and β are obtained with only three phase measurements. Therefore, as many phase measurements as possible need to be taken at different axial locations along the tube.

Nonlinear Regression

To compute α and β from the measured pressure amplitude or phase data, the method of nonlinear regression[17] is used. The procedure for obtaining α and β from pressure amplitude data will first

be discussed. In this experiment the pressure amplitudes are measured at up to 10 axial locations along the tube, and the wavelength is determined from the frequency and temperature measurements. Nonlinear regression consists of finding the values of α, β, and A_{mn} which give the best fit between the theoretical curve described by equation (3-24) and the experimental points. This is accomplished by computing the values of α, β, and A_{mn} which minimize the root-mean-square deviation between the theoretical curve and the experimental points. To find the minimum root-mean-square deviation, the following function F is minimized:

$$F = \sum_{i=1}^{M} [E_i - T_i(\alpha,\beta,A_{mn})]^2 \tag{3-28}$$

for pressure amplitudes measured in psi and

$$F = \sum_{i=1}^{M} [E_i - T_i(\alpha,\beta,A_{db})]^2 \tag{3-28a}$$

for pressure amplitudes in decibels. In these expressions M is the number of pressure amplitude measurements and $3 \leq M \leq 10$ for the present experiment. The parameter E_i represents the pressure amplitude measured a distance z_i from the nozzle entrance where $i = 1, 2, \ldots, M$. The corresponding theoretical prediction T_i is given as

$$T_i(\alpha,\beta,A_{mn}) = A_{mn}[\cosh^2\pi\alpha - \cos^2\pi(\beta + \frac{2z_i}{\lambda})]^{\frac{1}{2}} \qquad (3\text{-}29)$$

for pressure amplitudes in psi and

$$T_i(\alpha,\beta,A_{db}) = A_{db} + 10\log_{10}[\cosh^2\pi\alpha-\cos^2\pi(\beta + \frac{2z_i}{\lambda})] \qquad (3\text{-}29a)$$

for amplitudes measured in decibels. If a minimum for F exists, then

$$\frac{\partial F}{\partial \alpha} = \frac{\partial F}{\partial \beta} = \frac{\partial F}{\partial A_{mn}} = \frac{\partial F}{\partial A_{db}} = 0 \qquad (3\text{-}20)$$

Equation (3-30) provides three equations in the three unknowns - α, β, and A_{db} or A_{mn}. Substituting equations (3-28), (3-29), and (3-29a) into equation (3-30) gives

$$\sum_{i=1}^{M}(E_i - T_i)\frac{\partial T_i}{\partial \alpha} = 0 \qquad (3\text{-}31)$$

$$\sum_{i=1}^{M}(E_i - T_i)\frac{\partial T_i}{\partial \beta} = 0$$

$$\sum_{i=1}^{M}(E_i - T_i)\frac{\partial T_i}{\partial A_{mn}} = 0$$

or

$$\sum_{i=1}^{M} (E_i - T_i) \frac{\partial T_i}{\partial A_{db}} = 0$$

where, for pressures measured in psi

$$\frac{\partial T_i}{\partial \alpha} = \frac{\pi A_{mn} \cosh \pi \alpha \sinh \pi \alpha}{\left[\cosh^2 \pi \alpha - \cos^2 \pi (\beta + \frac{2z_i}{\lambda}) \right]^{\frac{1}{2}}}$$

$$\frac{\partial T_i}{\partial \beta} = \frac{\pi A_{mn} \cos \pi (\beta + \frac{2z_i}{\lambda}) \sin (\beta + \frac{2z_i}{\lambda})}{\left[\cosh^2 \pi \alpha - \cos^2 \pi (\beta + \frac{2z_i}{\lambda}) \right]^{\frac{1}{2}}}$$

$$\frac{\partial T_i}{\partial A_{mn}} = \left[\cosh^2 \pi \alpha - \cos^2 \pi (\beta + \frac{2z_i}{\lambda}) \right]^{\frac{1}{2}}$$

and, for pressure amplitudes in decibels,

$$\frac{\partial T_i}{\partial \alpha} = (20 \pi \log_{10} e) \left[\frac{\sinh \pi \alpha \cosh \pi \alpha}{\cosh^2 \pi \alpha - \cos^2 \pi (\beta + \frac{2z_i}{\lambda})} \right]$$

$$\frac{\partial T_i}{\partial \beta} = (20 \pi \log_{10} e) \left[\frac{-\sin \pi (\beta + \frac{2z_i}{\lambda}) \cos \pi (\beta + \frac{2z_i}{\lambda})}{\cosh^2 \pi \alpha - \cos^2 \pi (\beta + \frac{2z_i}{\lambda})} \right]$$

$$\frac{\partial T_i}{\partial A_{db}} = 1$$

Once equation (3-31) is solved, the values of α, β, and A_{mn} or A_{db} are obtained which provide the best fit between the theoretical curve described by equation (3-29) or (3-29a) and the experimental data. Since equation (3-31) is nonlinear, an explicit solution for α, β, and A_{mn} or A_{db} cannot be derived and the equations must be solved numerically.

Marquardt's algorithm[18] is used to solve equation (3-31). This algorithm is an extension of the Newton-Raphson iteration scheme. It keeps the rapid convergence properties of the Newton-Raphson method, and at the same time it improves the stability characteristics. To start the iteration, equation (3-24) or (3-24a) is solved explicitly for α, β, and A_{mn} or A_{db} using various combinations of three amplitude measurements and equations (3-25) and (3-26). For 10 amplitude measurements taken at different axial locations along the tube, 120 combinations of three pressure amplitudes are obtained. The values of α, β, A_{mn} or A_{db} obtained from the combination which gives the minimum value of F from equation (3-28) are then used to start the iteration. Using the notation of Reference 17, the equation to be solved after the nth iteration is

$$\begin{bmatrix} 1 + \lambda_n & a^n_{12} & a^n_{13} \\ a^n_{12} & 1 + \lambda_n & a^n_{23} \\ a^n_{13} & a^n_{23} & 1 + \lambda_n \end{bmatrix} \begin{bmatrix} y^{n+1}_1 - y^n_1 \\ y^{n+1}_2 - y^n_2 \\ y^{n+1}_3 - y^n_3 \end{bmatrix} = \begin{bmatrix} b^n_1 \\ b^n_2 \\ b^n_3 \end{bmatrix}$$

(3-32)

where

$$b^n_k = \frac{\sum\limits_{i=1}^{M} (E_i - T^n_i)\left(\frac{\partial T_i}{\partial x_k}\Big|_n\right)}{\sum\limits_{i=1}^{M} \left(\frac{\partial T_i}{\partial x_k}\Big|_n\right)^2}$$

$$a^n_{jk} = \frac{\sum\limits_{i=1}^{M} \left(\frac{\partial T_i}{\partial x_k}\Big|_n\right)\left(\frac{\partial T_i}{\partial x_i}\Big|_n\right)}{\left[\sum\limits_{i=1}^{M} \left(\frac{\partial T_i}{\partial x_j}\Big|_n\right)^2 \sum\limits_{i=1}^{M} \left(\frac{\partial T_i}{\partial x_k}\Big|_n\right)^2\right]^{\frac{1}{2}}}$$

$$y^n_k = \left[\sum\limits_{i=1}^{M} \left(\frac{\partial T_i}{\partial x_k}\Big|_n\right)^2\right]^{\frac{1}{2}} x^n_k$$

$$j,k = 1,2,3$$

$$x_1 = \alpha, \quad x_2 = \beta, \quad x_3 = A_{mn} \text{ or } A_{db}$$

and λ_n is a convergence parameter which can be changed at each iteration to improve the convergence characteristics.

In practice, when α is on the order of 10^{-4} or less, equation (3-32) does not converge to a value of α when F approaches a minimum because of roundoff errors. Instead, values of α oscillate about zero with an amplitude of 10^{-5} or less. In such cases, in order to avoid these numerical difficulties, α is assumed to be zero. Then from equations (3-29) and (3-29a),

$$T_i(\alpha, \beta, A_{mn}) = A_{mn} \mid \sin\pi(\beta + \frac{2z_i}{\lambda}) \mid$$

or

$$T_i(\alpha, \beta, A_{db}) = A_{db} + 20 \log_{10}\left[\mid \sin\pi(\beta + \frac{2z_i}{\lambda}) \mid \right]$$

and the appropriate equation is solved for β and A_{mn} or A_{db}. A computer program has been written in FORTRAN V for use on a UNIVAC 1108 computer which calculates α and β from pressure amplitude measurements in decibels and is included in Appendix D.

Values of α and β can also be computed from phase measurements using the nonlinear regression method. For this case

$$T_i(\alpha,\beta) = a(z_i - z_{ref}) +$$

(3-33)

$$\text{Arctan} \left\{ \frac{\tanh\pi\alpha[\cot\pi(\beta + \frac{2z_i}{\lambda}) - \cot\pi(\beta + \frac{2z_{ref}}{\lambda})]}{1 + \tanh^2\pi\alpha\cot\pi(\beta + \frac{2z_i}{\lambda})\cot\pi(\beta + \frac{2z_{ref}}{\lambda})} \right\}$$

where one of the phase measurements at the axial location z_{ref} is used as a reference. The equations to be solved for the values of α and β which give the minimum root-mean-square deviation between the theoretical and experimental phase values are

$$\frac{\partial F}{\partial \alpha} = \sum_{i=1}^{M} [E_i - T_i(\alpha,\beta)] \frac{\partial T_i}{\partial \alpha} = 0$$

(3-34)

$$\frac{\partial F}{\partial \beta} = \sum_{i=1}^{M} [E_i - T_i(\alpha,\beta)] \frac{\partial T_i}{\partial \beta} = 0$$

(3-35)

where now E_i is the experimental phase value measured at position z_i, and T_i is the theoretical phase value obtained from equation (3-33). Using equation (3-33),

$$\frac{\partial T_i}{\partial \alpha} = \pi(1 - \tanh^2 \pi\alpha)\left[\frac{\cot\pi(\beta + \frac{2z_i}{\lambda})}{1 + \tanh^2\pi\alpha\cot^2\pi(\beta + \frac{2z_i}{\lambda})} - \right.$$

$$\left. - \frac{\cot\pi(\beta + \frac{2z_{ref}}{\lambda})}{1 + \tanh^2\pi\alpha\cot^2\pi(\beta + \frac{2z_{ref}}{\lambda})}\right]$$

$$\frac{\partial T_i}{\partial \beta} = -\pi\tanh\pi\alpha\left[\frac{1 + \cot^2\pi(\beta + \frac{2z_i}{\lambda})}{1 + \tanh^2\pi\alpha\cot^2\pi(\beta + \frac{2z_i}{\lambda})} - \right.$$

$$\left. - \frac{1 + \cot^2\pi(\beta + \frac{2z_{ref}}{\lambda})}{1 + \tanh^2\pi\alpha\cot^2\pi(\beta + \frac{2z_{ref}}{\lambda})}\right]$$

As with the pressure amplitude measurements, Marquardt's algorithm is then employed to obtain values of α and β from equations (3-34) and (3-35). One advantage in using phase measurements is that one unknown, A_{mn} or A_{db}, is eliminated, thus simplifying the computations. A listing of the computer program used to determine α and β from phase data is included in Appendix D.

Once α and β are known, the real and imaginary parts of the admittance are determined by use of equations (3-19) and (3-20). In the nozzle admittance studies conducted in this investigation, only

admittance data obtained from pressure amplitude measurements are presented because of inaccuracies associated with the phase measurements. The cause of these inaccuracies will be discussed in the next chapter.

CHAPTER IV

IMPEDANCE TUBE EXPERIMENT

To measure the nozzle admittance, the classical impedance tube experiment has been modified to include mean flow and three-dimensional waves. To maintain flow in the tube, an air supply system is used. The three-dimensional pressure oscillations are generated by two electropneumatic drivers.

Air Supply System

The air supply for the impedance tube experiment is stored in 14 tanks having a total volume of 500 cubic feet and a maximum pressure of 3,000 psia. With a nominal 12-inch diameter tube, the air supply provides approximately four minutes of continuous testing at a tube Mach number of 0.08 and a static pressure of 25 psig. A schematic of the flow system is presented in Figure 9.

Three parallel pressure regulators maintain a constant pressure air supply upstream of the main and driver air supply control valves for all tube test condition requirements. The main air supply control valve maintains a constant pressure in the tube, and the driver air supply control valve maintains a constant pressure differential across the acoustic drivers. The chamber flow, which includes the main and driver flows, is exhausted through the tested nozzle into a silencer tunnel that is open to atmosphere.

Test Facility

The modified impedance tube is specifically designed to investigate the admittance characteristics of rocket engine exhaust nozzles. The components of the facility are presented in Figure 10.

Two Ling EPT-94B electropneumatic drivers, each capable of developing 4,000 watts of acoustic power, are close-coupled to the tube wall four inches downstream of the injector. The frequency and waveform output of the acoustic drivers are controlled by a Spectral Dynamics, Model SD104A-5 sweep oscillator. For this investigation the waveforms of the oscillations are sinusoidal. During a test, the frequencies of the generated waves are varied linearly over the range from 40 Hertz to 640 Hertz for longitudinal modes and from 600 Hertz to 1100 Hertz for mixed first tangential-longitudinal modes at a rate of from two to eight Hertz per second. In the frequency range of this investigation, the two drivers can develop resonant sound pressure levels greater than 165 decibels (referenced to 2.2×10^{-4}, dynes per cm^2) in the tube. For the sound pressure levels attained, linear acoustic theory was applicable. Based on the tests discussed in Chapter V, to minimize wave distortion and to obtain high sound pressure levels, the drivers oscillate in phase for longitudinal modes and 180 degrees out of phase for mixed first tangential-longitudinal modes. The flow from the main air supply control valve enters a muffler which attenuates the flow noise and provides a uniform pressure distribution across the injector. The injector is a one-inch thick plate with 1,627 holes spaced to provide a uniform flow distribution

at the entrance to the tube. A supercritical pressure ratio is maintained across the injector during test operations to ensure sonic velocity at the exit of the injector orifices. This minimizes acoustic feedback by isolating the flow system upstream of the injector from the pressure oscillations in the tube.

The impedance tube is a cylindrical aluminum pipe 120 inches long with an inside diameter of 11-3/8 inches. The test nozzle is coupled directly to the downstream or exhaust end of the tube by a flange attachment. Provisions have been made along the length of the tube for the installation of acoustic drivers, dynamic pressure transducers, thermocouples, and static pressure orifices. The positions of the acoustic drivers and the locations of the instrumentation ports utilized for this investigation are shown in Figure 11.

Tested Nozzles

Initial tests were conducted with two nozzles made of fiber glass as shown in Figure 12. To fabricate these nozzles, two wooden mandrils were machined to the desired nozzle contour. Layers of fiber glass were then placed on the mandrils and allowed to harden. This method was not used to fabricate the other nozzles because it was found to require excessive amounts of time and expense.

Instead, the other nozzles were machined from three aluminum cylinders. The inside of each cylinder was cast in the shape of a conical nozzle to minimize machining time. The conical nozzles had half-angles of 15, 30, and 45 degrees, respectively. To produce the nozzles in Table 1, the conical nozzles were then machined to have a

radius of curvature of 2.5 inches at the nozzle throat and entrance and an entrance Mach number of 0.08. Upon completion of the testing of the nozzle with a half-angle of 45 degrees, this nozzle was re-machined for an entrance Mach number of 0.16. This sequence of re-machining and testing, illustrated in Figure 13, was repeated until a Mach number of 0.20 was attained.

Instrumentation

A diagram of the instrumentation system used to monitor, control, measure, and record the test conditions in the tube is shown in Figure 14. The location and orientation of the instrumentation along the length of the tube is presented in Figure 11.

The steady state pressures in the tube and at the inlets to the driver are controlled by monitoring two 12-inch Heise gauges and manually setting the desired pressure levels to be maintained by the respective control valves.

The chamber air temperature is measured by two copper-constantan thermocouples and recorded at discrete frequencies during the test run on a strip chart recorder.

The pressure oscillation generated in the tube during a test run are measured by ten Photocon, Model 403, pressure transducers, amplified, and recorded on an Ampex, FR-1300, 14-channel tape recorder. The transducers have a dynamic range of from 110 decibels to approximately 180 decibels and exhibit a flat frequency response over the frequency range from 10 to 3,000 Hertz. A calibration of the transducer system using a Whittaker Corporation, Model PC-125,

acoustic calibrator is recorded prior to each test. In addition to the 10 dynamic transducers, the signal from the frequency generator to the acoustic drivers is recorded during the tests to be used in the data reduction procedures as a reference frequency for signal analysis.

Data Reduction

A diagram of the instrumentation used to determine the sound pressure level as a function of driver frequency is shown in Figure 15. The data are recorded on a tape recorder and then played back at a reduced speed. The data are passed through a Spectral Dynamics System, Model 101A, dynamic analyzer. The analyzer is a frequency-tuned band-pass filter in which the center frequency of a narrow band pass is continuously tuned to track the reference driver frequency. The filtered signal is passed through a Hewlett-Packard, Model 7560A, logarithmic converter which transforms the A-C input signal to a D-C voltage proportional to the peak or average amplitude of the input signal. The frequency signal is converted to a D-C output voltage proportional to the frequency. The sound pressure level output of the logarithmic converter is plotted as a function of driver frequency on a Hewlett-Packard Model ZFRA, X-Y recorder.

Phase data can also be obtained by replacing the logarithmic converter with a phase meter and recording the output on the X-Y plotter. However, experience has shown that the tape recorder can introduce phase errors of up to 60 degrees because of the gap scatter, gap azimuth, and interspacing between the individual record

and playback heads. Therefore, accurate phase data cannot be obtained with this instrumentation and no reliable admittance data have been computed using phase measurements.

Experimental Procedure

Before testing, all components of each dynamic pressure data channel are calibrated simultaneously by imposing a calibrated, sinusoidal pressure signal from the acoustic calibrator on the pressure transducer. This signal is recorded on the analog tape recorder to be used in data reduction as the reference pressure to account for the sensitivity of the pressure transducer and the amplification factors of the system components. The chamber air temperature thermocouple is calibrated by recording reference temperature voltage outputs on the strip chart recorder.

To initiate the test run three parallel high pressure regulator valves are set to maintain 300 psig pressure upstream of the main and driver control valves. The sweep generator, which controls the driver output waveform and frequency, is set for a sinusoidal signal at the low frequency limit of the frequency range. The driver flow control valve is then set to maintain 40 psi pressure differential across the drivers. Next the main flow control valve is set to provide a pressure level of 20 psig in the chamber. The main flow control valve automatically maintains the desired pressure throughout the test.

After test conditions are established in the chamber the recording of pressure and temperature data is initiated simultaneously

with the start of the frequency sweep. The sweep oscillator maintains an eight Hertz per second rate of change of the driver frequency from the initiation of the sweep until the upper limit of the test frequency range is reached. The pressure oscillations in the chamber are continuously recorded during the test run on the analog tape recorder. Chamber air temperature is periodically recorded on the strip chart recorder every four or five seconds during the test. To correlate the pressure and temperature data the output frequency of the sweep oscillator is manually recorded on the strip chart recorder for each chamber temperature record made during the frequency sweep. The temperature of the intermediate data points are determined by interpolation. When the upper limit of the frequency sweep is reached the test is concluded.

Once the pressure amplitude and frequency data are recorded on analog tape, plots of sound pressure level versus frequency are obtained. From these plots pressure amplitudes are taken at selected frequencies for each of the transducers located along the length of the tube. For a given frequency, up to 10 pressure amplitudes are obtained; and these data, together with the steady state temperature data used to compute the speed of sound, are input into a computer program which employs the nonlinear regression method to obtain nozzle admittance values over a range of the nondimensional frequency S.

To evaluate the experimental facility and the supporting impedance tube theory, preliminary tests were conducted before nozzle testing was initiated, and the results are presented in Chapter V.

CHAPTER V

PRELIMINARY TESTING

To obtain reliable nozzle admittance data using pressure amplitude measurements, equation (3-22) must adequately predict the spacial dependence of the pressure amplitude in the impedance tube. Preliminary tests were conducted to evaluate the mathematical model and to ensure that the standing wave pattern in the tube under test conditions could be described by the mathematical model.

Assumption of No Attenuation

In the development of the impedance tube theory, wave attenuation in the tube was assumed to be negligible. To investigate the validity of this assumption, two tests were conducted with a fiber glass nozzle for which the nozzle half-angle was 15 degrees, the entrance Mach number was 0.08, and the ratio of the radius of curvature to chamber radius was 1.0. This nozzle is shown in Figure 12. In one test the microphones were placed from 24 to 49 inches from the nozzle entrance plane, and in the other test the microphones were positioned from one to 33 inches from the nozzle entrance. If the assumption of no attenuation of the wave is invalid, a discrepancy should exist in the data between the two tests. From Figure 16, the admittance values agree within experimental error. This result indicates that the assumption of no attenuation is justifiable.

Frequency Sweep Rate

In the preliminary tests the frequency was varied at a rate of three Hertz per second over a range from 600 to 1,000 Hertz. It was assumed that this sweep rate was sufficiently slow to allow the tracking filter enough time to react to the change in frequency so that no wave distortion resulted. In order to verify this assumption, nozzle admittance data were obtained keeping the frequency constant during testing. These data are compared with the frequency sweep data from Figure 16 and Figure 17. The data agree to experimental error.

Tests With No Flow

According to the theory developed in Chapter III, the form of the mixed first tangential-longitudinal mode in the transverse plane is described by the expression

$$p'(r,\theta) = J_1(S_{10} \frac{r}{r_w}) \cos (\theta)$$

and is shown in Figure 18. A nodal line extends from the 12:00 position to the 6:00 position along the diameter of the tube when the drivers are placed at the 3:00 and 9:00 positions. However, based on pressure amplitude data taken under test conditions, a nodal line is not present at the 12:00 position at certain values of the frequency. This is shown in Figure 19 which is a typical plot of sound pressure level versus frequency for the mixed first tangential-longitudinal

modes at a distance 49 inches from the nozzle entrance with the two

drivers oscillating 180 degrees out of phase. In order to investigate

this behavior and determine the shape of the three-dimensional standing

wave pattern for the mixed first tangential-longitudinal modes, a

microphone probe was used. Since it was impractical to probe the tube

with flow present, tests without flow were conducted.

A schematic of the experimental facility used in the tests

without flow is presented in Figure 20. The aluminum tube used in the

impedance tube studies was terminated at the driven end by a blind

flange of aluminum 3/4 of an inch in thickness. The opposite end

of the tube was left open for probing.

Two University drivers, an ID-75 75 watt and a PA-HF 50 watt,

were utilized to generate a standing wave pattern in the tube.

Amplitudes of over 150 decibels could be obtained at resonant

frequencies. The driver frequency was controlled by a Hewlett-

Packard, Model 202C, low frequency oscillator which was used to estab-

lish standing wave patterns at from 55 to 1300 Hertz. The output of the

individual drivers was varied by two Krohn-hite, DCA-50R, wide-band,

50 watt amplifiers. The signal from the amplifiers was passed

through two Krohn-hite, 50 watt, MT-56, matching transformers into the

drivers.

In order to measure the pressure oscillation in the tube, a

Bruel and Kjaer 1/4-inch microphone was mounted to a 1/2-inch plexi-

glass bar four feet in length. This probe was used to determine the

shape of the standing wave. The signal from the microphone was

passed through a Bruel and Kjaer, Model 2604, microphone amplifier and displayed on a Model 502A, Tektronix, dual-beam oscilloscope. The dependence of the standing wave pattern on driver configuration and phasing was investigated by first using only one driver located at the 9:00 position and then using two drivers located at the 9:00 and 3:00 positions. The amplitude and phase of the two drivers were varied independently over a range of frequencies from 600 to 1200 Hertz. The tube was probed axially, circumferentially, and radially to determine the standing wave pattern.

The experimental results offered explanations as to the difference between the predicted and measured pressure amplitude versus frequency plots at the 12:00 position shown in Figure 19.

Skewing was detected and is illustrated in Figure 21. For mixed first tangential-longitudinal modes, this phenomenon was characterized by a constant rotation of the transverse nodal line about the axis of the tube. The angle of skew was invariant with respect to driver configuration, phasing, and amplitude. However, the skew angle varied with frequency and depended upon the conditions at the driven end.

In the frequency range near the cutoff frequency for the first tangential mode of the tube - 700 Hertz at $76.5^{\circ}F$ - , skew angles of up to 36 degrees from the 12:00 position were measured. From 700 to 710 Hertz the skew angle varied 66 degrees. Throughout the range of frequencies from 710 to 970 Hertz at $78^{\circ}F$, the skew angle was less than 10 degrees and no detectable skew was present above 750 Hertz.

From 970 to 1200 Hertz no skew angle was detected for two drivers oscillating 180 degrees out of phase at approximately the same amplitude. However, wave distortion occurred in this frequency range when only one driver was used.

Besides being frequency dependent, the skew angle was dependent upon the conditions at the driven end. When one of the driver ports was left open, the skew angle shifted as much as 60 degrees for a given frequency in the range from 700 to 710 Hertz.

A phenomenon which was given the name "cusping" also occurred and is illustrated in Figure 22. Two types were detected. With the first type, the nodal line in the radial direction was curved into roughly the shape of the letter "c". When the curve opened toward the 3:00 position, the sound pressure level at 3:00 was less than the sound pressure level at 9:00, and there was a node at the tube center. As the tube was traversed in the axial direction toward the driver, the curvature became less pronounced until a straight nodal line extended from the 6:00 to 12:00 positions, and the pressure amplitudes were equal at the 3:00 and 9:00 positions. Further axial traversing toward the driven end showed that the nodal line again becomes curved but opened toward the 9:00 position. Here, the pressure amplitude was less at the 9:00 position than at the 3:00 location, and a node exists at the tube center.

During the second type of cusping, the nodal line was straight but displaced to one side of the tube center. When the line was displaced toward the 3:00 position, the pressure amplitude at 3:00 was

less than the amplitude at 9:00. As the tube was traversed axially

toward the driver, the displacement of the nodal line from the tube

center became less until the nodal line extended from the 6:00 to

the 12:00 positions, and the pressure amplitudes at the 9:00 and

3:00 positions were the same. Further traversing showed that the

nodal line was displaced toward the 9:00 position.

Both types of cusping occurred when one driver was used.

Cusping was independent of amplitude and is noticeable only above

970 Hertz at 79.8°F. When two drivers were used and driven 180

degrees out of phase at approximately the same amplitude, this

phenomenon was eliminated. The mathematical model of the standing

wave pattern in the tube could not account for cusping; so in the tests

conducted to obtain nozzle admittance data, the drivers were

oscillated 180 degrees out of phase to avoid this phenomenon.

Near resonant conditions in the tube, it was discovered that the

nodal line predicted by classical acoustic theory for the transverse

wave pattern of mixed first tangential-longitudinal modes was not a

true nodal line. Instead, the pressure amplitude near the tube wall

was appreciable; and, as the line was traversed radially, the pressure

amplitude decreased to zero at the tube center. This phenomenon is

shown in Figure 23 and was encountered near resonant frequencies

for both skewed and unskewed transverse wave patterns. It was not

detectable at nonresonant conditions in the tube.

Based on the results of the no flow experiment, it was decided

to use two drivers producing approximately the same pressure amplitude

and driven 180 degrees out of phase in order to eliminate cusping.

High sound pressure levels of 160 decibels or above are also obtained by driving in this manner. Skewing and the variation of the pressure amplitude along the classically predicted nodal line can be accounted for in the mathematical model by the complex integration constant C_θ appearing in equation (3-22). From this equation the form of the transverse wave pattern is described by the following expression:

$$| \, p'(r,\theta) \, | \; = J_1(\frac{S_{10}}{r_w}r)| \; \cos(\theta + C_\theta) \, |$$

for the mixed first tangential-longitudinal modes. This pattern is formed by the superposition of two transverse waves - one rotating in the clockwise direction and the other rotating in the counter-clockwise direction. Based on this model, skewing is caused by a difference in phase between these two waves and is accounted for by the real part of C_θ. The variation of the pressure amplitude along the transverse nodal line predicted by classical acoustic theory can be attributed to a difference in amplitude between the clockwise and counterclockwise rotating waves and is accounted for by the imaginary part of C_θ. As mentioned in Chapter III, C_θ does not enter into the admittance computations. Therefore, skewing and pressure amplitude variations along the classically predicted nodal line do not affect the measured nozzle admittance values.

CHAPTER VI

RESULTS

Longitudinal Modes

For the longitudinal modes the experimental values of the real and imaginary parts of the admittance are compared with the theoretical predictions in Figures 24 through 30. The nozzle designations are explained in Table 1.

The reliability and repeatability of the experimental procedure is demonstrated in Figures 24 to 26. In each of these figures the admittance data from two tests conducted at different times for a given nozzle are compared. The mean square deviation in the values of the real and imaginary parts of the admittance between the two tests is 0.1.

The mean square deviation between the theoretical predictions and the experimental data is also 0.1. Therefore, the theoretical and experimental admittance results agree to within the precision of the experiment. The disagreement which occurs at the higher frequencies, when S is greater than 1.6, is attributed to experimental errors. For a fixed number of pressure amplitudes taken along the standing wave, the number of points per wavelength decreases with increasing frequency, and it becomes more difficult to accurately determine the standing wave pattern and, consequently, the admittance.

These data indicate that the assumption of one-dimensional .

mean flow in the nozzle used in Crocco's theory[6] appears valid. Even for the nozzles with half-angles of 45 degrees, where theoretical and experimental studies[19] show that the one-dimensional assumption is invalid, the experimental admittance values agree to within experimental error as shown in Figures 26 through 28.

The effect of changing the nozzle radius of curvature on the admittance values is presented in Figure 31. In this figure, data are compared for ratios of the radius of curvature to chamber radius of 0.44 and 1.0 when θ_1 = 15 degrees and $\bar{M}$ = 0.08. For these nozzles changing the radius of curvature has little effect. This result is in agreement with the theoretical predictions presented in Figure 4.

The result of changing the nozzle half-angle is shown in Figure 32 for $\bar{M}$ = 0.08 and r_{cc}/r_c = 0.44. The data indicate that increasing the nozzle half-angle apparently increases the frequency at which the real part of the admittance is a maximum.

The consequences of varying the Mach number at the nozzle entrance is shown in Figure 33 for θ_1 = 45 degrees and r_{cc}/r_c = 0.44. At this nozzle half-angle and radius of curvature, increasing the Mach number has little effect on the admittance values.

Mixed First-Tangential Longitudinal Modes

For the mixed first tangential-longitudinal modes, the experimental nozzle admittance data are compared with the theoretical predictions in Figures 34 through 40. The data from two different tests are compared in Figures 34 to 36; and in general the repeatability of the experimental admittance data is the same as the repeatability

for the longitudinal modes. Two exceptions are shown in Figures 36 and 37 for nozzles 15-08-5.7 and 15-08-2.5, respectively. At S values above 2.6, considerable data scatter is evident. For example, in Figure 36 the value of the real part of the admittance can vary from zero to four over an interval of 0.02 of S. This behavior is caused by computational difficulties and not by a physical phenomenon. In this range of S, α and β are approaching zero; and small experimental errors in these parameters can result in large errors in the admittance values. To illustrate this point, consider equations (3-19) and (3-20) for the real and imaginary parts of the admittance, respectively.

$$y_r = \frac{\left[\dfrac{s\sqrt{s^2 - s_{mn}^2(1 - \bar{M}^2)}\ \tanh\pi\alpha\sec^2\pi\beta}{\tan^2\pi\alpha + \tan^2\pi\beta}\right] - s_{mn}^2\bar{M}}{s^2 + (s_{mn}\bar{M})^2} \quad (3-19)$$

$$y_i = \frac{s\sqrt{s^2 - s_{mn}^2(1 - \bar{M}^2)}\ \tan\pi\beta\mathrm{sech}^2\pi\alpha}{[s^2\ s\sqrt{s^2 - s_{mn}^2(1 - \bar{M}^2)}\ \tan\pi\beta\mathrm{sech}^2\pi\alpha} \quad (3-20)$$

First, assume that α is identically zero and β is a very small number ϵ; then

$$y_r = - \frac{(S_{mn})^2 \bar{M}}{s^2 + (S_{mn}\bar{M})^2} \sim O(\bar{M})$$

and

$$y_i = \frac{s\sqrt{s^2 - (S_{mn})^2(1 - \bar{M}^2)}}{s^2 + (S_{mn}\bar{M})^2} \cot \pi\epsilon$$

It follows from the above relationship that $y_i \to \infty$ as $\epsilon \to 0^+$ and $y_i \to -\infty$ as $\epsilon \to 0^-$. Now assume that β is identically zero and α is a very small number equal to ϵ. Then

$$y_r = \frac{s\sqrt{s^2 - s_{mn}^2(1 - \bar{M}^2)}}{s^2 + (S_{mn}\bar{M})^2} \coth \pi\epsilon - O(\bar{M})$$

and $y_r \to \infty$ as $\epsilon \to 0$. Since β is assumed to be identically zero, then $y_i \equiv 0$. Thus, when the magnitude of α and β are small, in practice less than 0.01, small experimental errors in these parameters produce large errors in the computed admittance values. Physically, this situation corresponds to a nozzle which absorbs little acoustic energy and for which the standing wave pattern has a pressure minimum at the nozzle entrance.

Figures 35, 39, and 40 show that the theoretical admittance

values agree with the experimental data for entrance Mach numbers of

0.16 or greater at the half-angles and radii of curvature tested.

However, as shown in Figures 36 and 37, the theoretical and experi-

mental values of the real part of the admittance do not agree for an

entrance Mach number of 0.08 and a nozzle half-angle of 15 degrees

although values of the imaginary part of the admittance are in good

agreement.

From equation (3-19), the real part of the admittance is shown

to consist of two terms. The term

$$- \frac{S_{mn}^2 \bar{M}}{S^2 + (S_{mn}\bar{M})^2}$$

contributes a negative component to the real part of the admittance.

However, the magnitude of this term for mixed first tangential-

longitudinal modes is smaller than or equal to the Mach number $\bar{M}$.

Since Figures 36 and 37 indicate that the theoretical predictions for

the real part of the admittance are smaller than -0.08, it follows

from equation (3-19) that the term involving α and β must be negative.

This means that α is negative which implies that the wave reflected

back from the nozzle is greater in amplitude than the incident wave.

This conjecture cannot be verified using pressure amplitude measure-

ments. According to equation (3-24), the axial variation in the

pressure amplitude of the standing wave pattern is the same regardless

of the sign of α. Since only the magnitude of α can be determined from pressure amplitude measurements, the sign of α was taken to be positive which is consistent with previous impedance tube studies[11,12,13]. When α is assumed to be negative, the resulting experimental admittance data agrees with the theoretical predictions as shown in Figure 41 for nozzle 15-08-2.5.

In general, both the magnitude and sign of α need to be determined in order to assure the accuracy of the measured admittance data. The magnitude and sign of α can be determined from phase measurements, and Bell[15] recommended that phases be used to determine the admittances for mixed first tangential-longitudinal modes. However, because of experimental difficulties in measuring the phase accurately, no reliable admittance results have been obtained from phase data.

The effects of changing the nozzle geometry and entrance Mach number on the admittance values are shown in Figures 42, 43, and 44. The effect of changing the nozzle half-angle θ_1 is presented in Figure 42 for $\bar{M} = 0.08$ and $r_{cc}/r_c = 0.44$. Increasing θ_1 tends to decrease the dependence of the nozzle admittance on frequency in the investigated frequency range. The effect of varying the entrance Mach number is shown in Figure 43 for $\theta_1 = 45$ degrees and $r_{cc}/r_c = 0.44$. At this half-angle and radius of curvature, increasing the Mach number has little effect on the admittance values. Changing the ratio of the radius of curvature to the tube radius from 1.0 to 0.44 also has little effect as shown in Figure 44, where $\theta_1 = 15$ degrees and $\bar{M} =$

0.08. This result is in agreement with the available theoretical predictions.

CHAPTER VII

SUMMARY AND CONCLUSIONS

A new impedance tube technique was developed which accounts for three-dimensional waves and a one-dimensional mean flow. With this technique pressure amplitude measurements were used to determine the admittances of nozzles for longitudinal and mixed first tangential modes. The admittances of a family of nozzles were measured to determine the effects of nozzle geometry.

The results are summarized as follows. Increasing the nozzle half-angle increases the value of the frequency at which the maximum value of the real part of the admittance occurs. Increasing Mach number at a nozzle half-angle of 45 degrees and at a radius of curvature to chamber radius ratio of .44 has little effect. Changing the ratio of the radius of curvature to chamber radius from .44 to 1.0 also has little effect at a nozzle half-angle of 15 degrees and a chamber Mach number of 0.08. For longitudinal modes the theoretical values obtained from Crocco's theory compare with the experimental data to within experimental error. For mixed first tangential-longitudinal modes the theoretical and experimental values for the imaginary part of the nozzle admittance were in agreement; however, the values of the real part of the admittance differ by a minus sign. Phase measurements are necessary to determine the sign of the real part of the admittance.

TABLES

Table 1. Matrix of Nozzles Under Investigation*

Entrance Mach Number

		0.08	0.16	0.20
Nozzle Half-Angle	15	15-08-5.7** 15-08-2.5		
	30	30-08-2.5	30-16-5.7**	
	45	45-08-2.5	45-08-2.5	45-20-2.5

* The first two numbers give the nozzle half-angle, the
    next two represent the Mach number to two decimal
    places, and the last two numbers denote the radius of
    curvature in inches to one decimal place

** Fiber glass nozzle

Table 2. Effect of Errors in Pressure Amplitude
Measurements on the Computed Values of
α and β

Frequency (Hertz)	Transducer Number	Distance From the Nozzle Entrance (in)	Pressure Amplitude (Decibels)
735	1	49	147.0
	2	40	166.0
	3	35	164.2
	4	33	160.1
	5	24	163.8

Transducer Combination	α	β
1,2,3	.0532	.4854
1,2,4	.0150	.4575
1,2,5	.0130	.4566
1,3,4	x < 1	x < 1
1,3,5	.0297	.4727
1,4,5	.0145	.4573
2,3,4	x < 1	x < 1
2,3,5	.1112	.4744
2,4,5	.0206	.4570
3,4,5	x < 1	x < 1

FIGURES
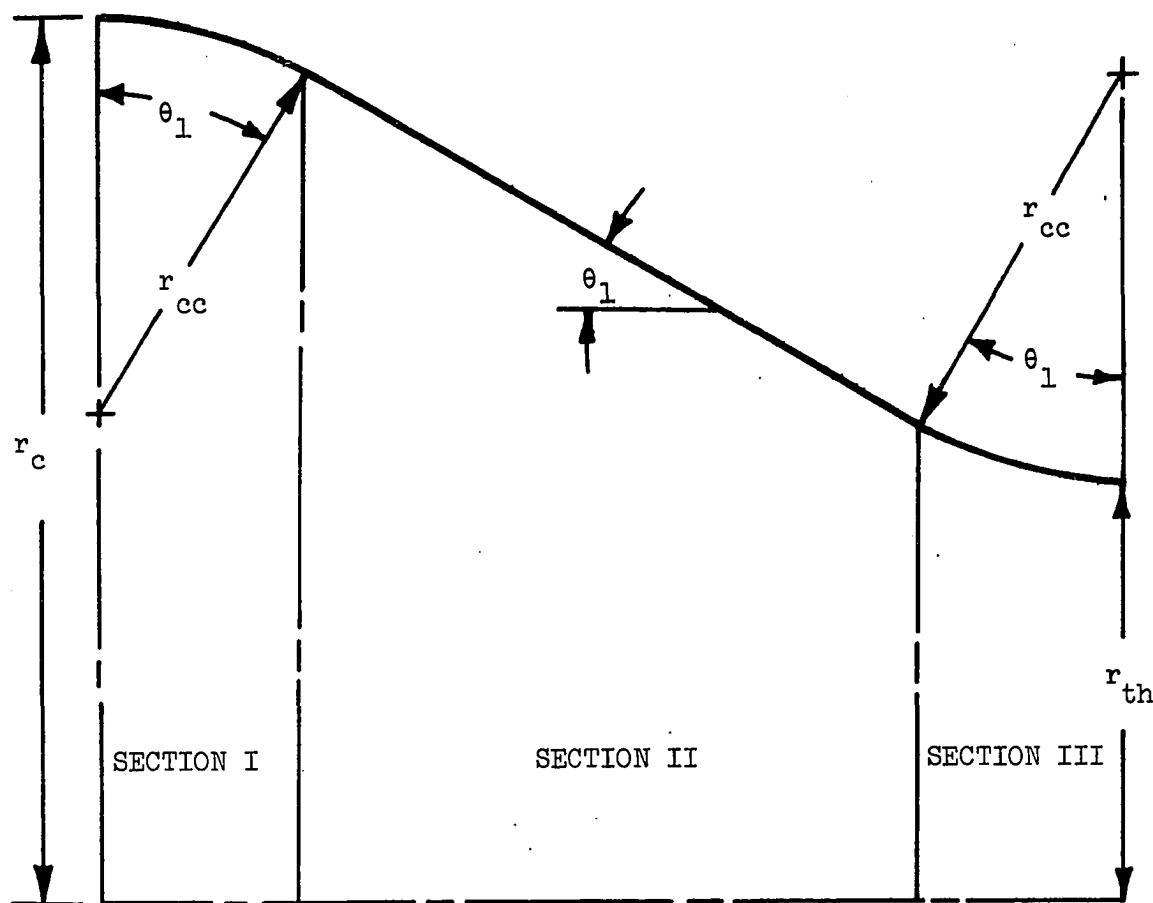
Figure 1. Geometry of the Convergent Portion of the Nozzle.
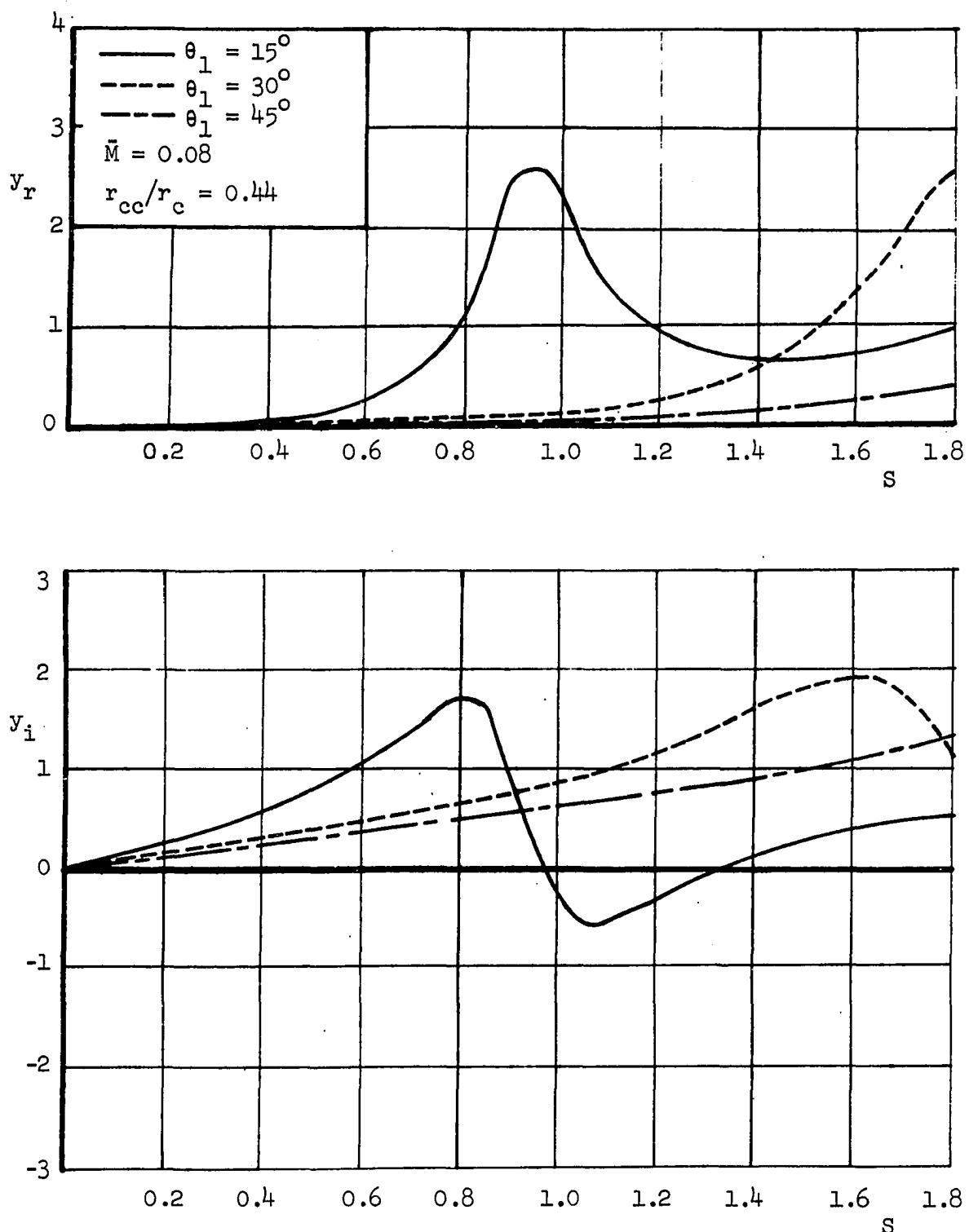
Figure 2. Effect of Nozzle Half-Angle on the Admittance
Values Predicted by Theory; Longitudinal Modes.
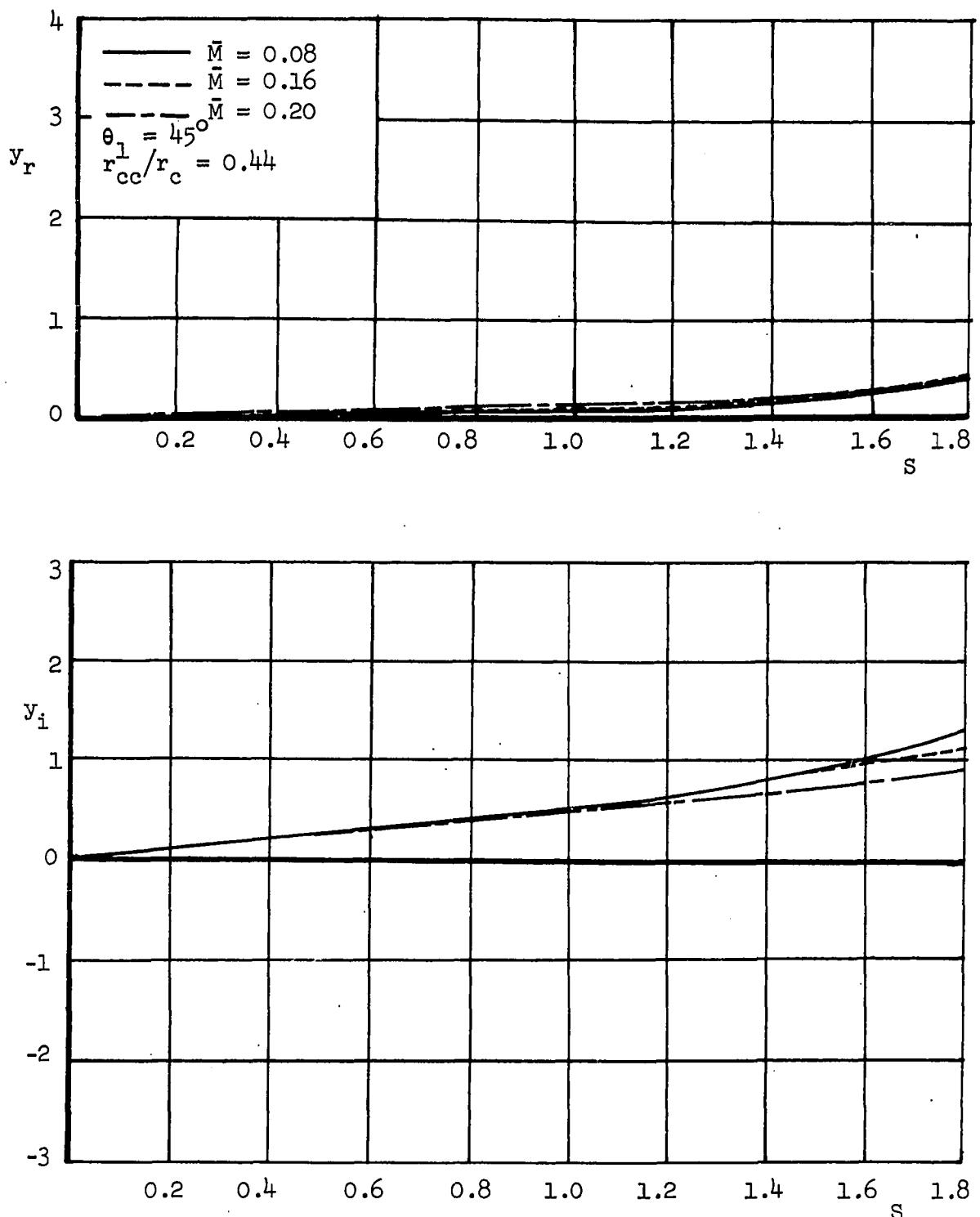
Figure 3. Effect of Entrance Mach Number on the Admittance Values
Predicted by Theory for Longitudinal Modes.
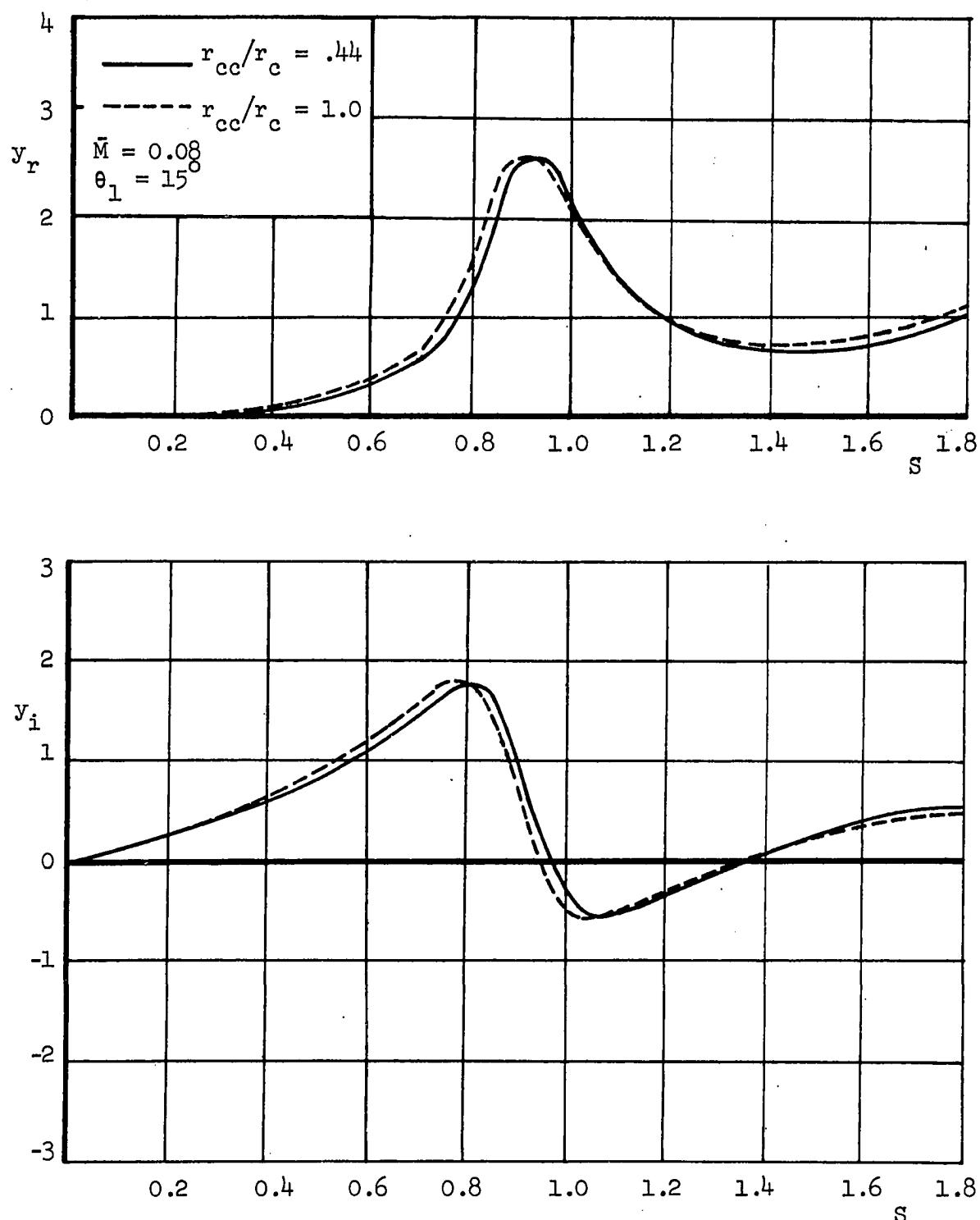
Figure 4. Effect of Radius of Curvature on the Admittance Values
Predicted by Theory for Longitudinal Modes.
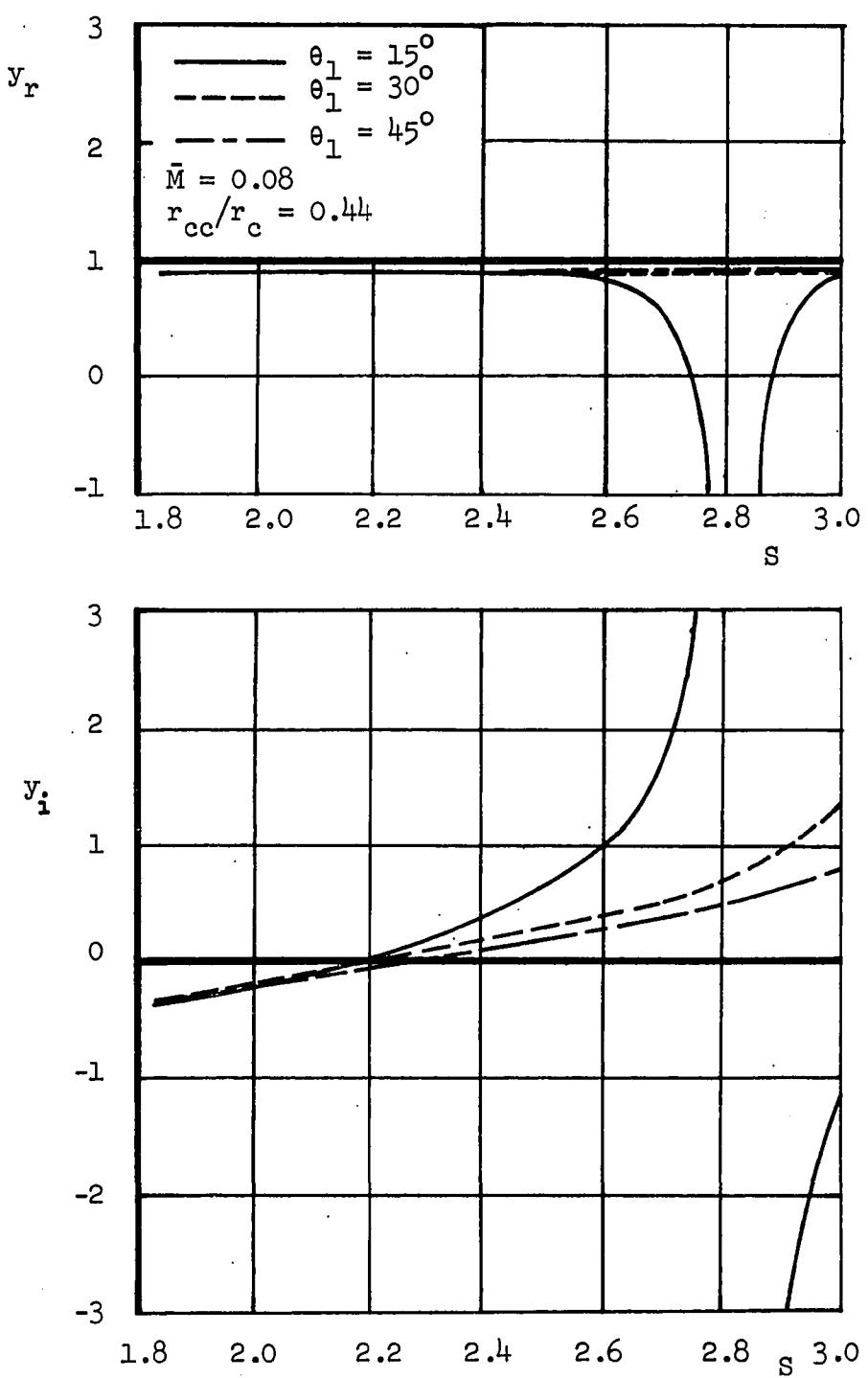
Figure 5. Effect of Nozzle Half-Angle on the Admittance Values Predicted by Theory for Mixed First Tangential-Longitudinal Modes.
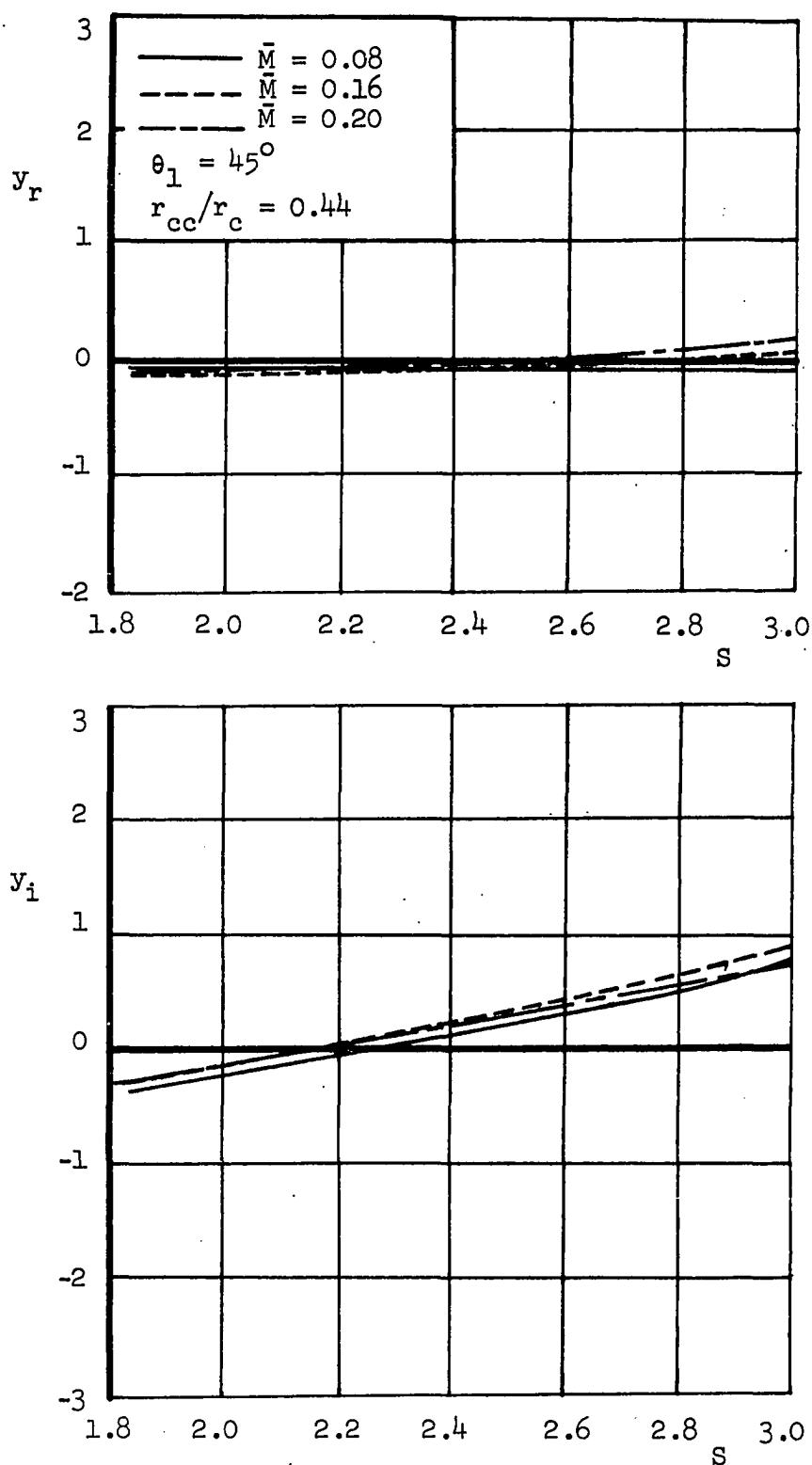
Figure 6. Effect of Entrance Mach Number on the Admittance Values Predicted by Theory for Mixed First Tangential-Longitudinal Modes.
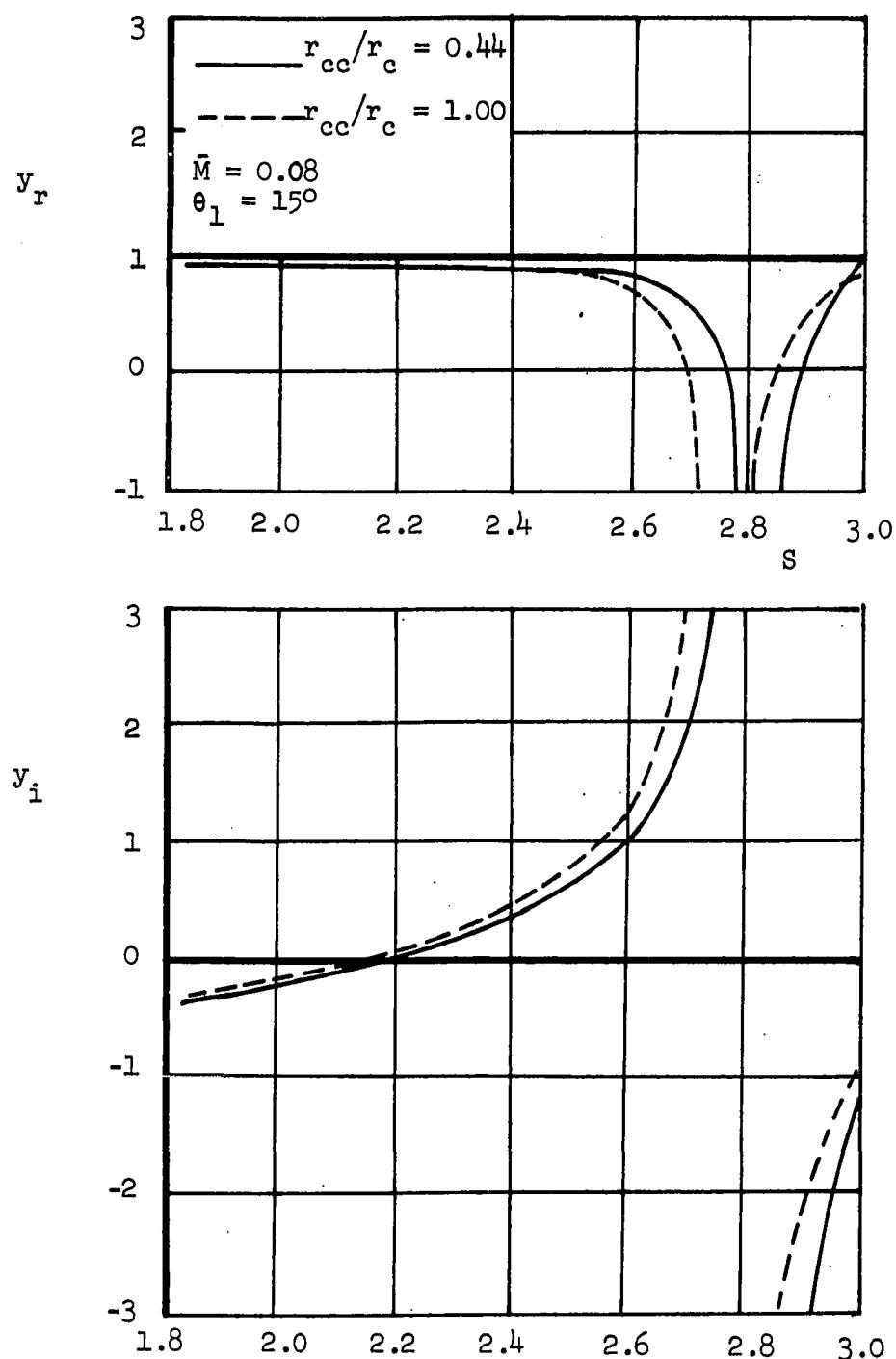
Figure 7. Effect of Radius of Curvature on the Admittance
Values Predicted by Theory for Mixed First
Tangential-Longitudinal Modes.
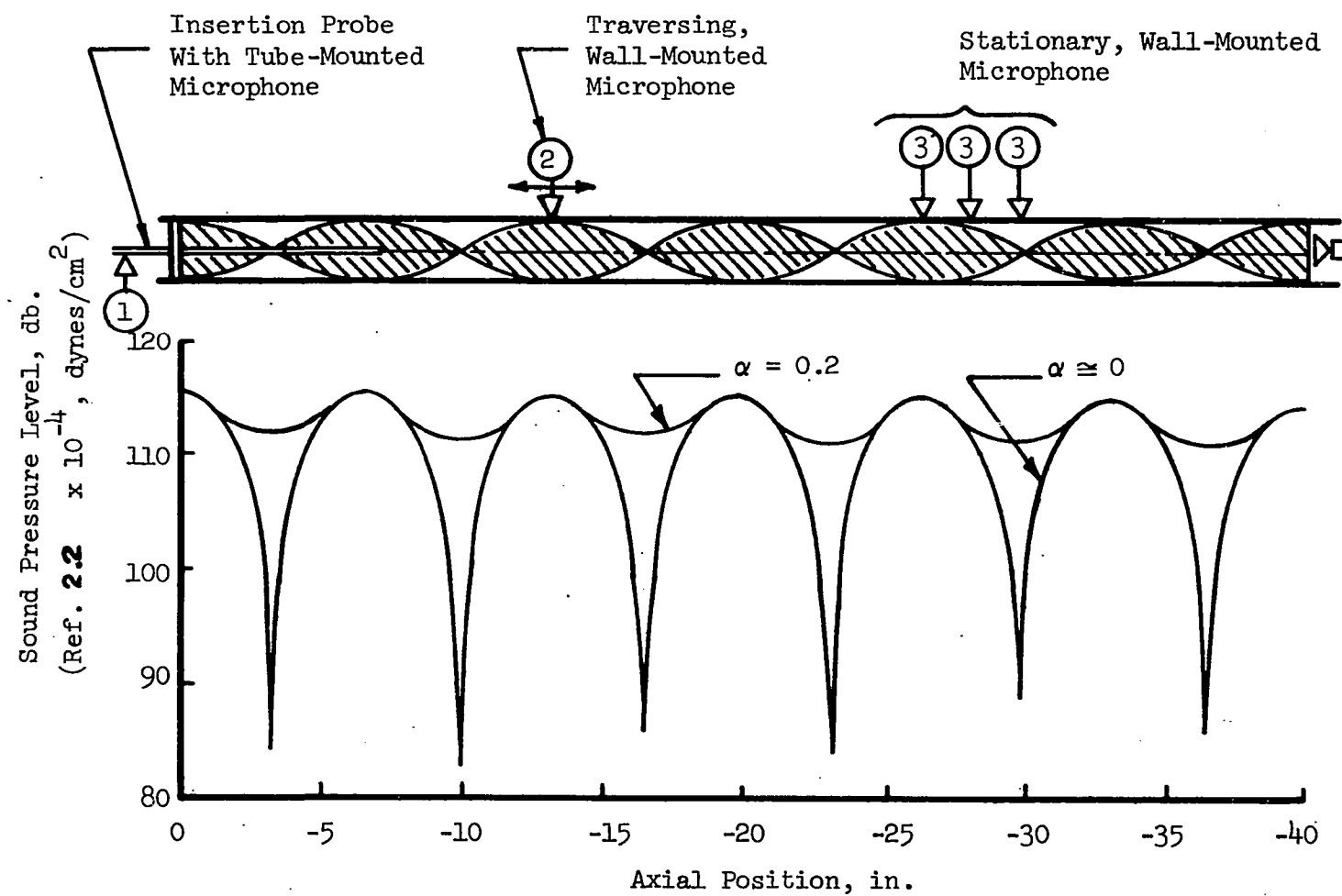
Figure 8. Standing Wave Measurement Techniques.
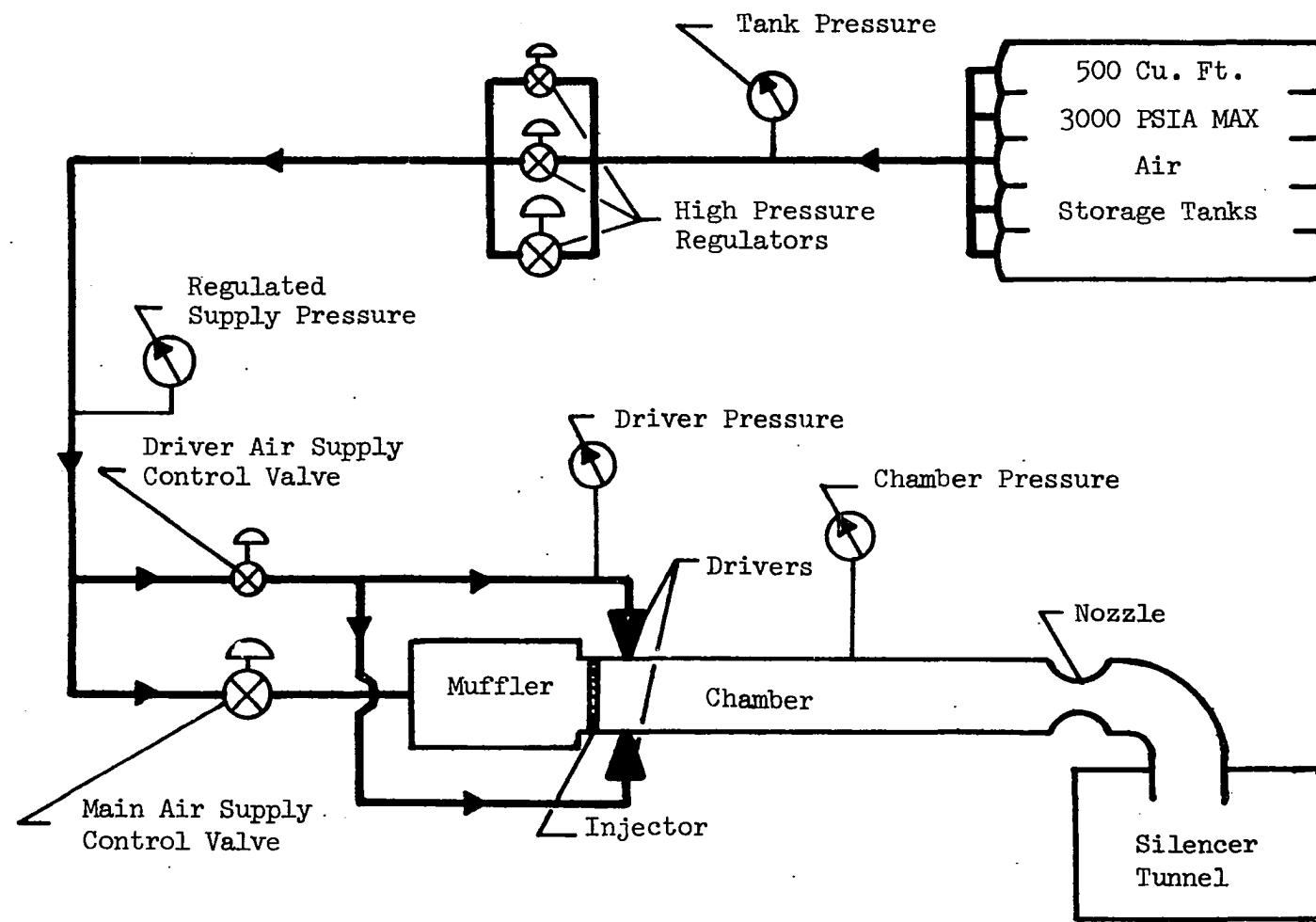
Figure 9. Schematic Diagram of the Acoustic Test Facility Flow System.

Control Valve
(Driver Air
Supply)

Injector

Acoustic
Driver

Chamber

Nozzle

Control Valve
(Main Air Supply)

PLAN VIEW

Muffler

Filter

Exhaust

ELEVATION VIEW

Silencer
Tunnel

Figure 10. Test Facility

86

SIDE VIEW

(Inches, Ref to Nozzle Entrance Plane)

Section A-A
Driver
Locations

Section B-B
Static
Pressure
Orifice
Locations

Section C-C
Dynamic
Pressure
Transducer
Locations

Section D-D
Thermocouple
Locations
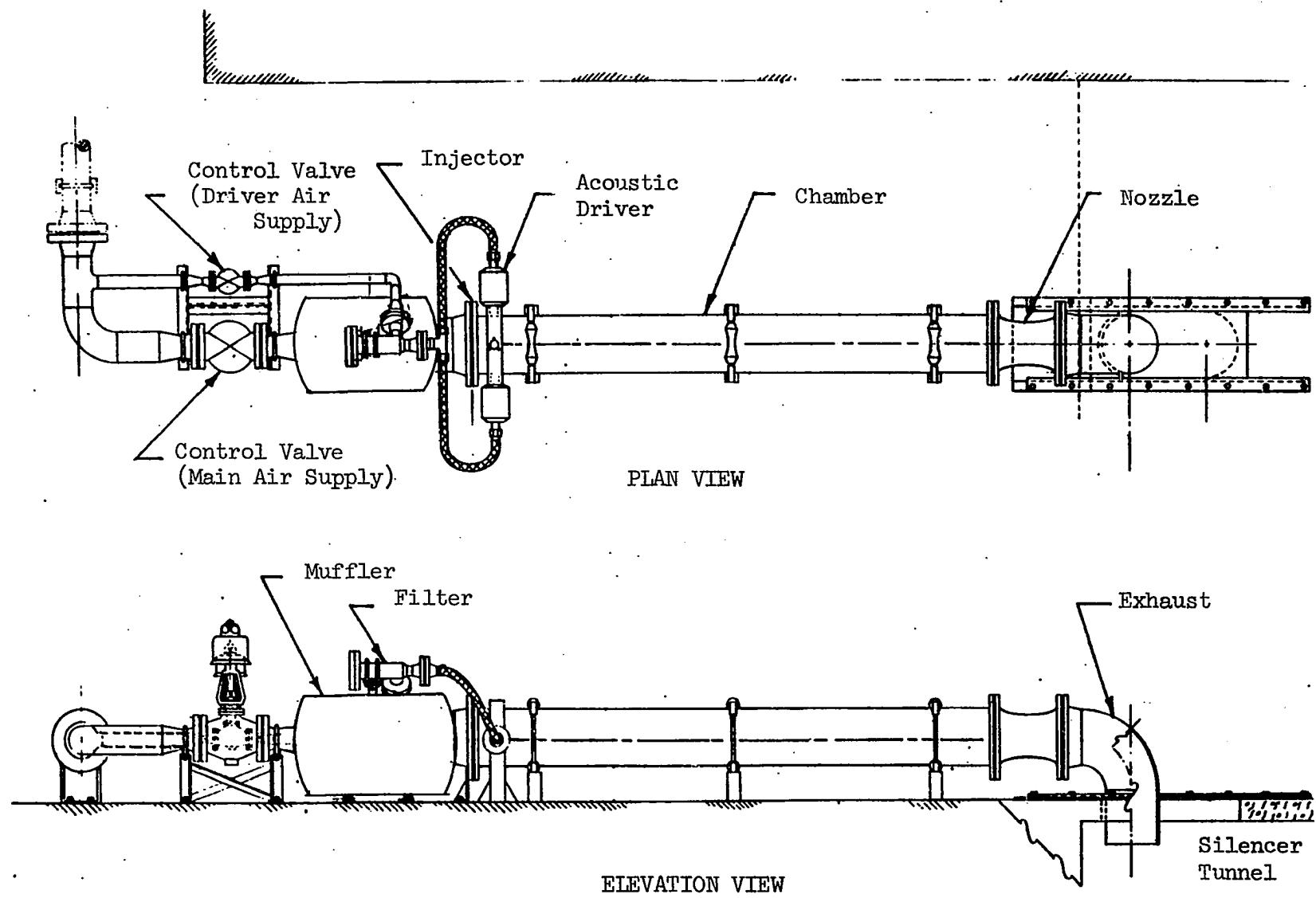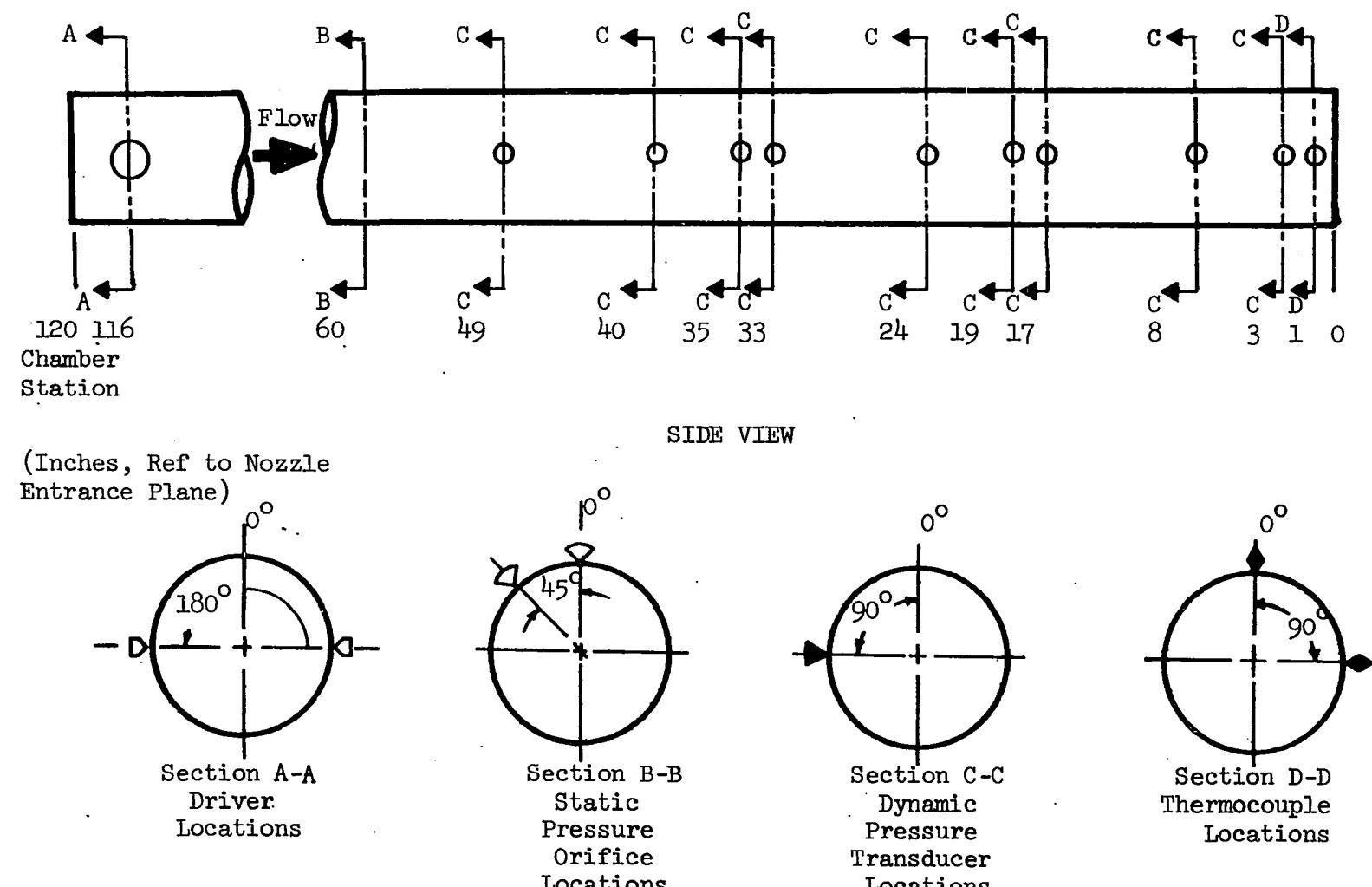
Figure 11. Driver and Instrumentation Ports Utilized
for This Investigation.

87

88
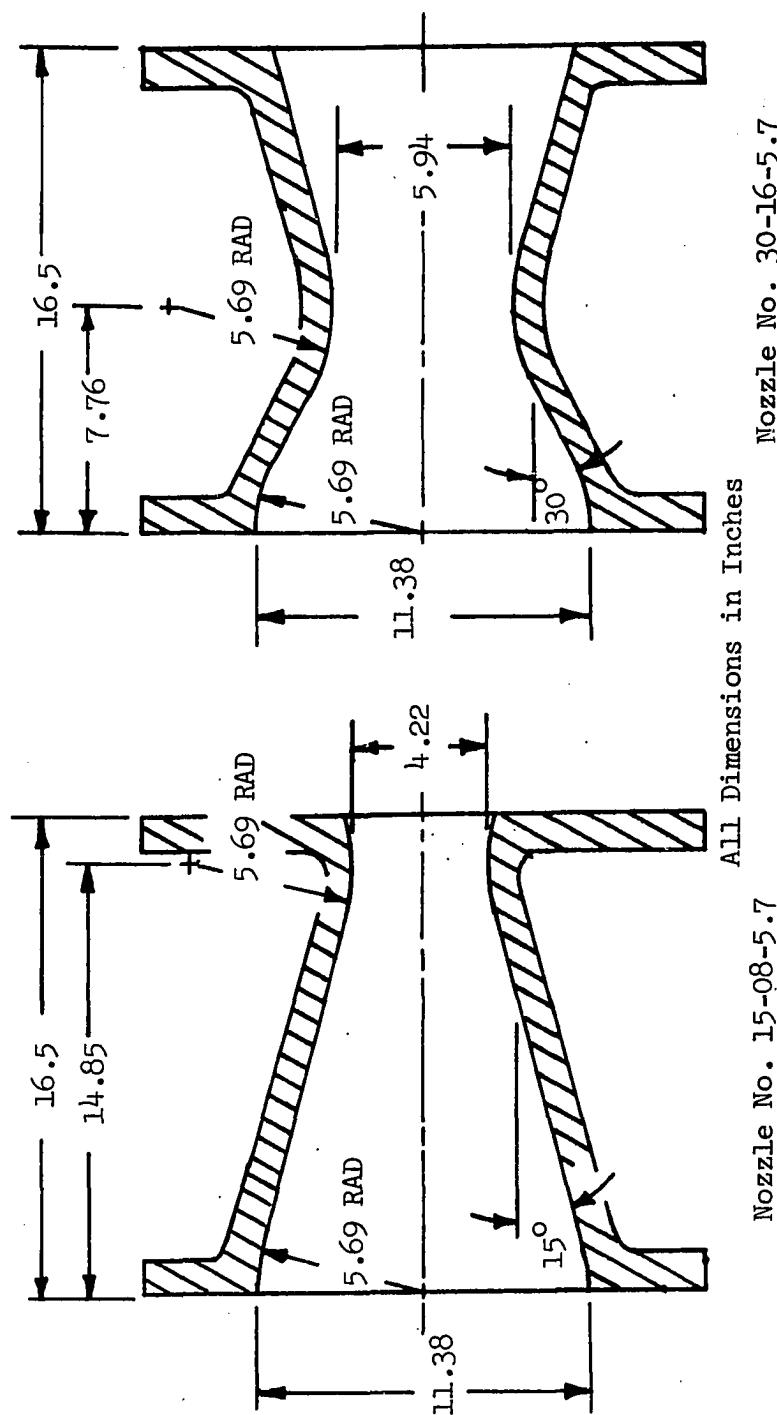
Figure 12. Fiber Glass Nozzle Details.

All Dimensions in Inches

Nozzle No. 30-16-5.7

Nozzle No. 15-08-5.7
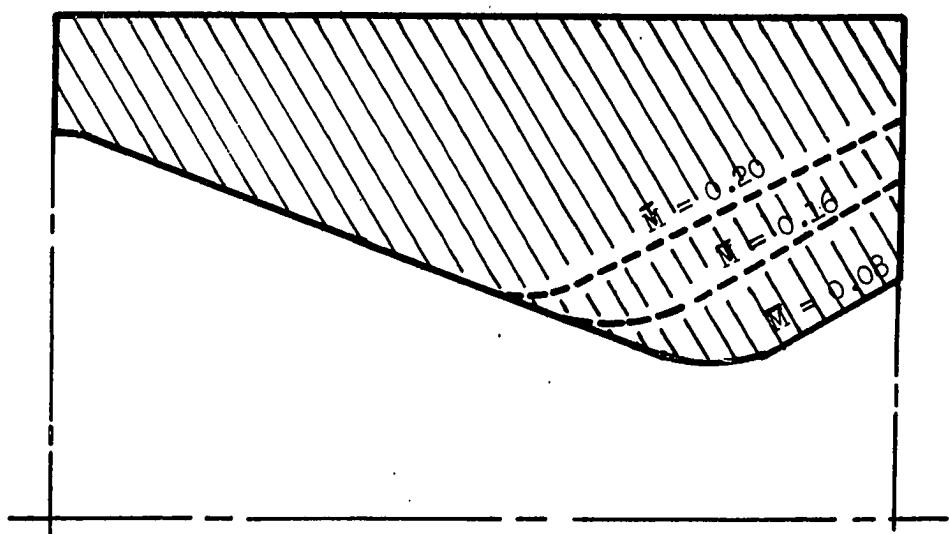
Figure 13. The Technique Used to Obtain Nozzles
From a Given Aluminum Cylinder.
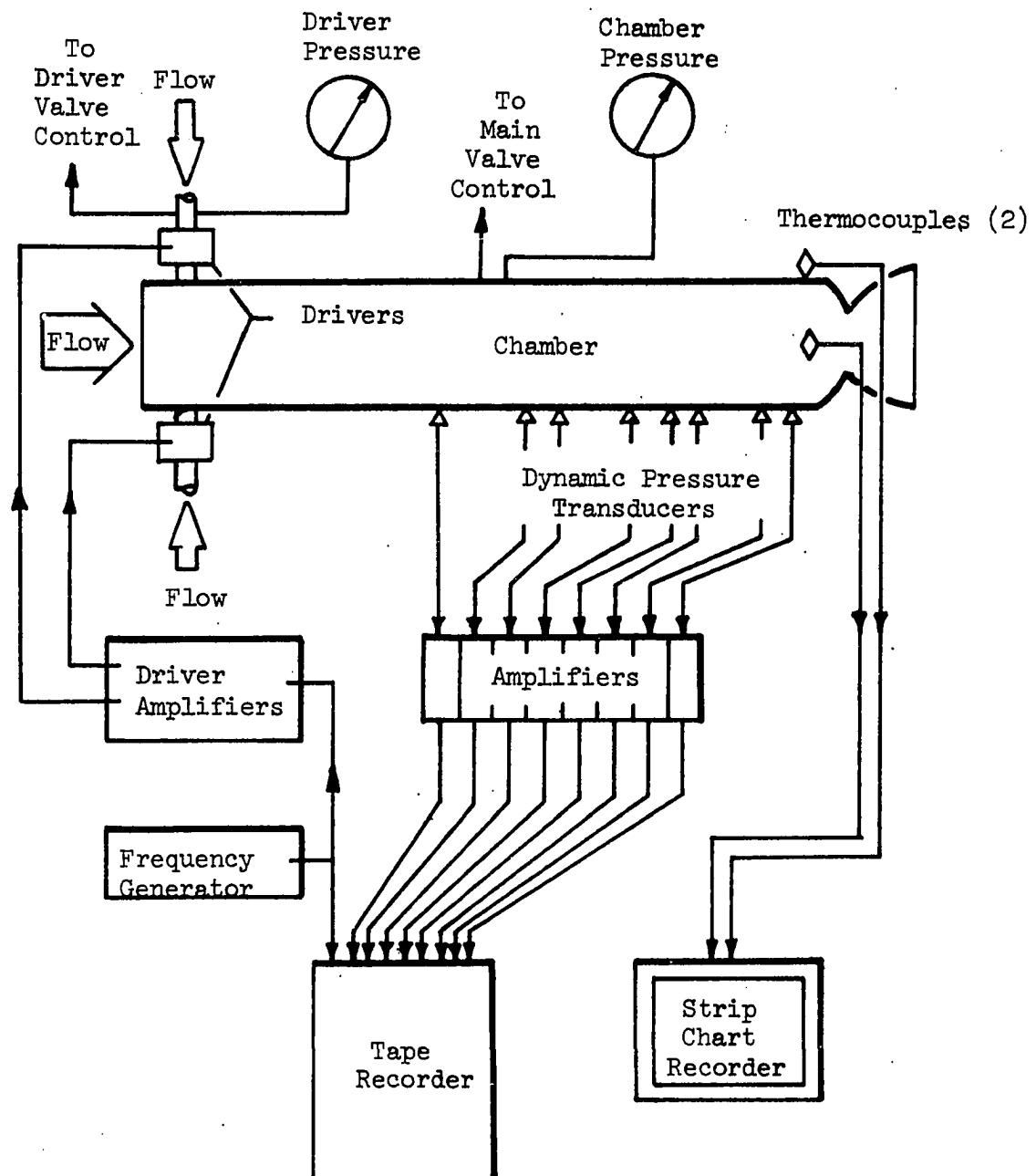
Figure 14. Instrumentation Diagram.

Dynamic Pressure Signal

Frequency

```
            ┌─────────────┐              ┌─────────────┐
            │             │              │   Dynamic   │
            │    Tape     │              │  Analyzer   │
            │  Recorder   │              │             │
            │             │              │             │
            └─────────────┘              └─────────────┘

        ┌─────────────┐          ┌─────────────┐
        │  AC  to  DC │          │ Logarithmic │
        │  Converter  │          │  Converter  │
        └─────────────┘          └─────────────┘

                    ┌─────────────────────┐
                    │  ┌───────────────┐  │
                    │  │   X-Y Plotter │  │
                    │  └───────────────┘  │
                    └─────────────────────┘
```
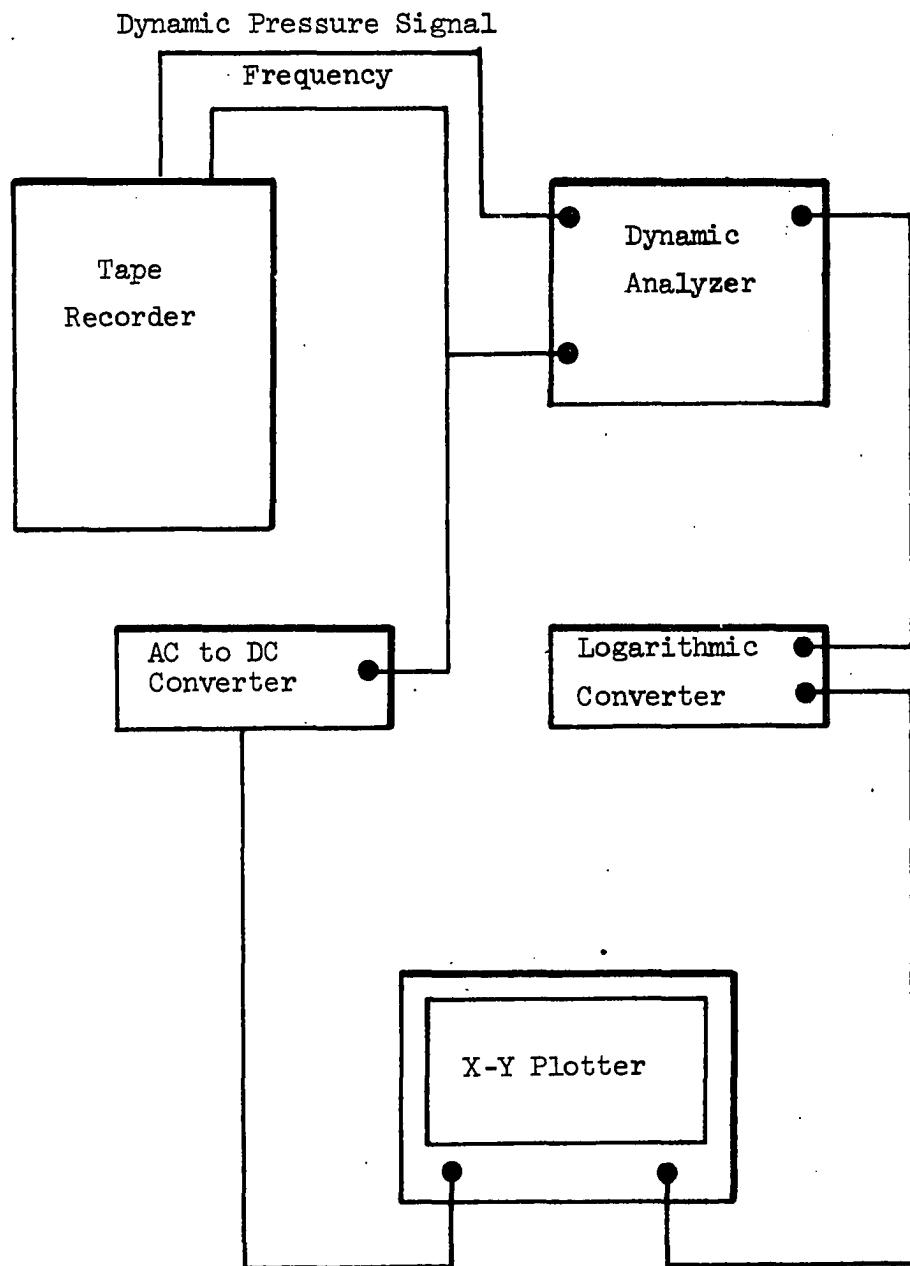
Figure 15. Diagram of Data Reduction Instrumentation.
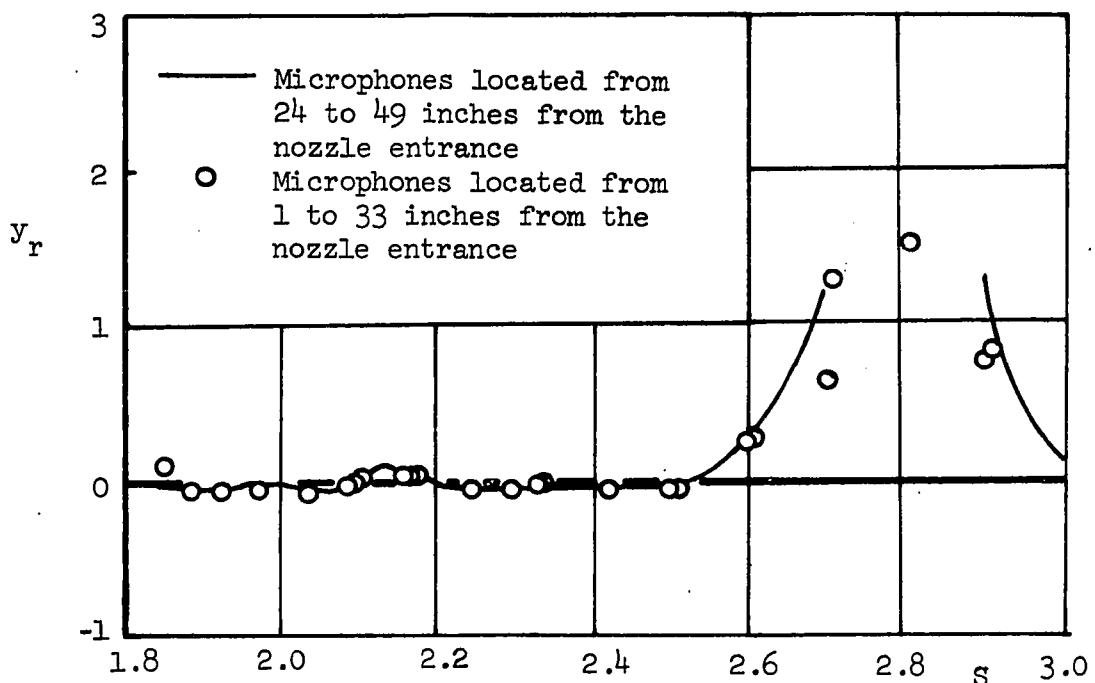
Figure 16. Comparison of Admittance Values Measured at Different Locations along the Tube.
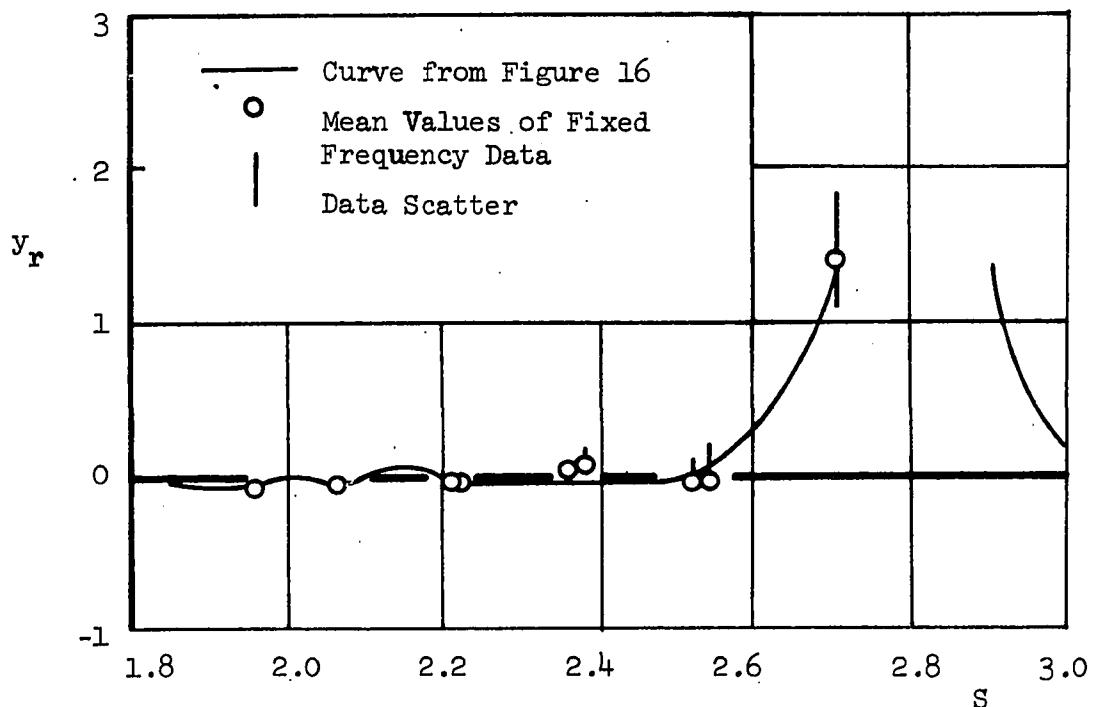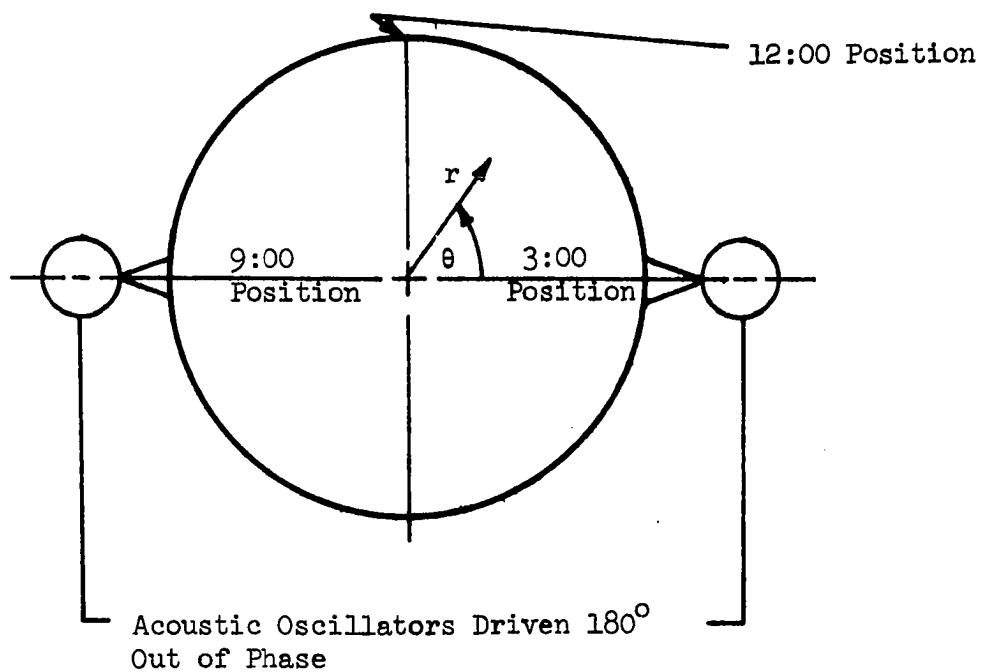
Figure 17. Comparison of the Admittance Data Obtained From Discrete Frequency and Frequency Sweep Data.

12:00 Position

r

9:00
Position

θ

3:00
Position

Acoustic Oscillators Driven 180°
Out of Phase

· First Tangential Mode Pattern
From Classical Acoustic Theory
at the θ = 0 Position

Pressure Amplitude

P_{max}

t = 0

$t = \dfrac{Period}{2}$

$t = \dfrac{Period}{4}$

0

$r=r_w$

$r=0$

$r=r_w$
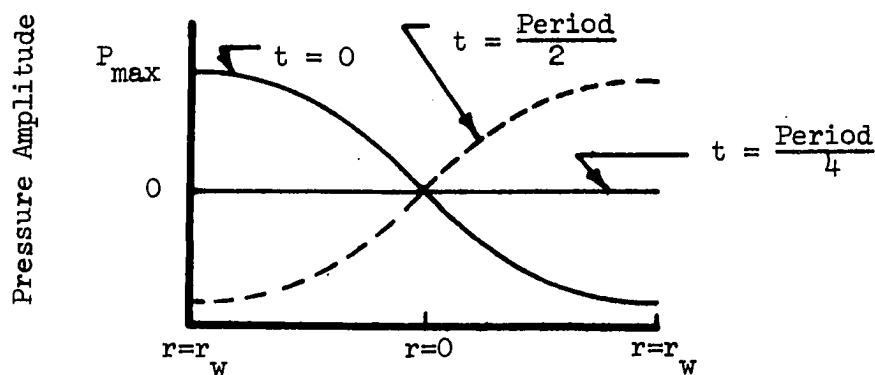
Figure 18. Technique Used to Obtain Mixed First
Tangential-Longitudinal Wave Patterns
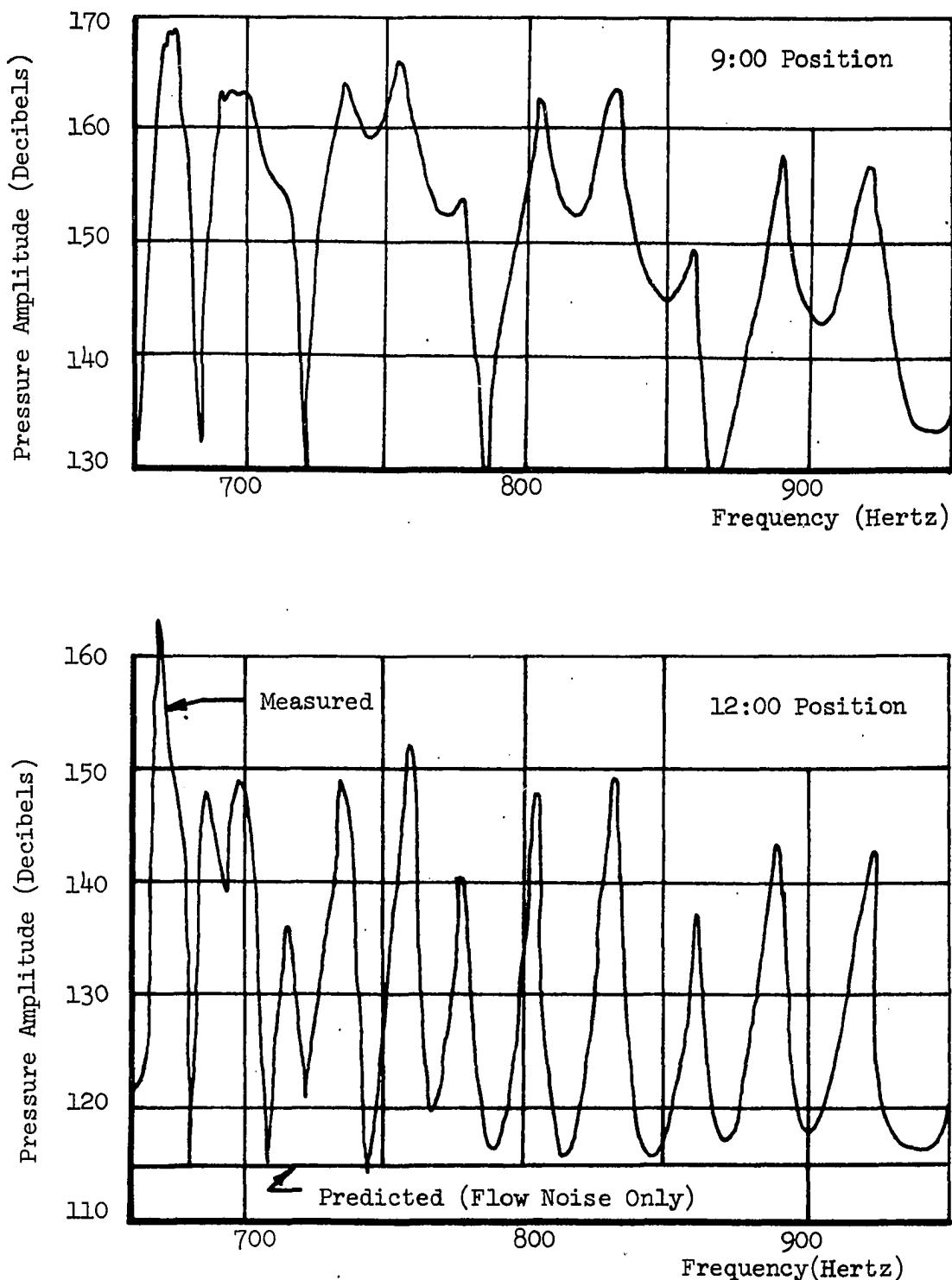
Figure 19. Sound Pressure Amplitude Versus Frequency at the 9:00 and
12:00 Positions 49 Inches From the Nozzle Entrance for a
Nozzle with $\theta_1 = 15^\circ$, $\bar{M} = 0.08$, and $r_{cc}/r_c = 1.0$.
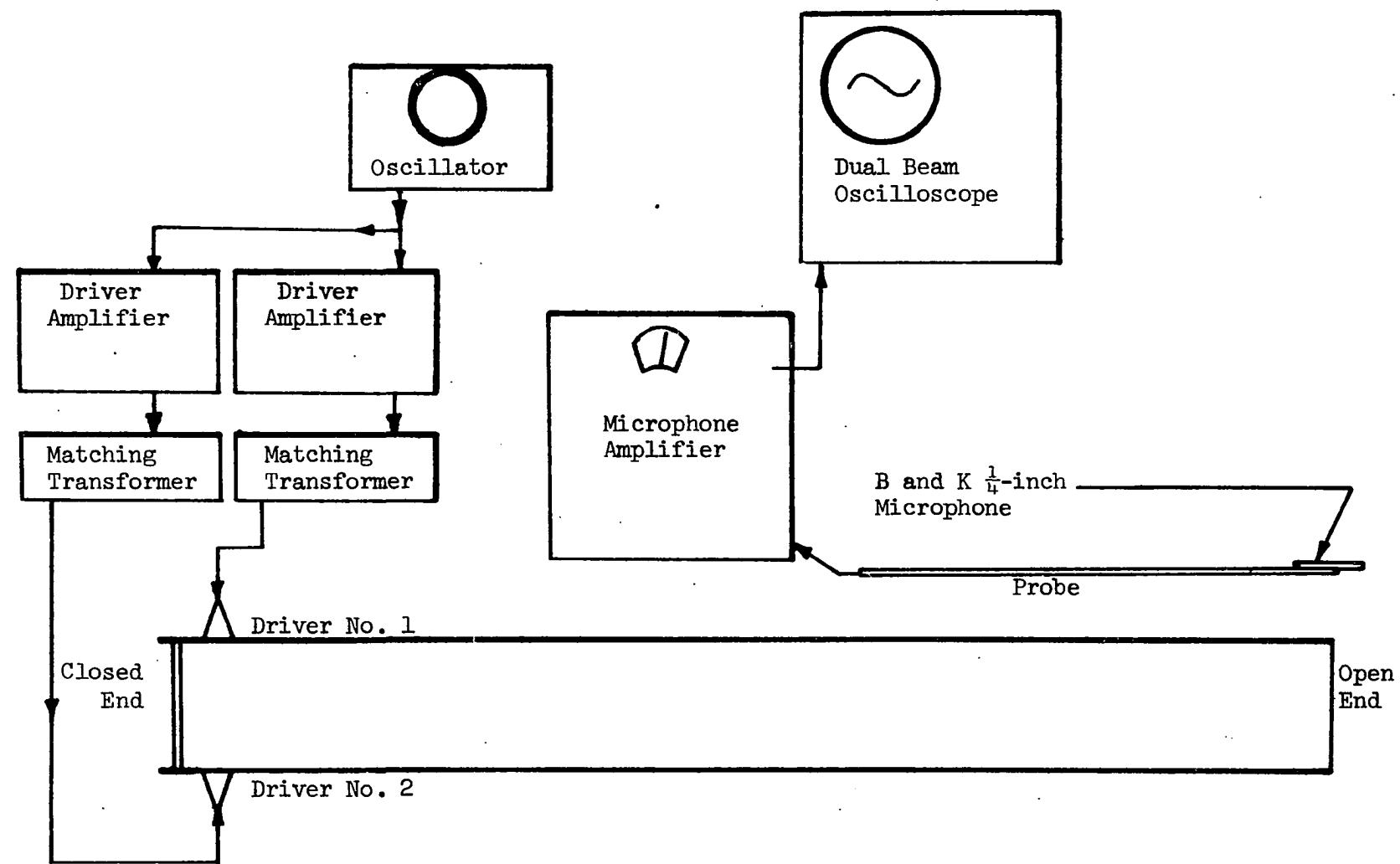
Figure 20. Schematic of Experimental Apparatus for
Preliminary Tests Conducted Without Flow.

TOP VIEWS

Driver
Positions

Classical 1-T

A-A

DRIVEN
END

Skewed

B-B

Cusping

C-C
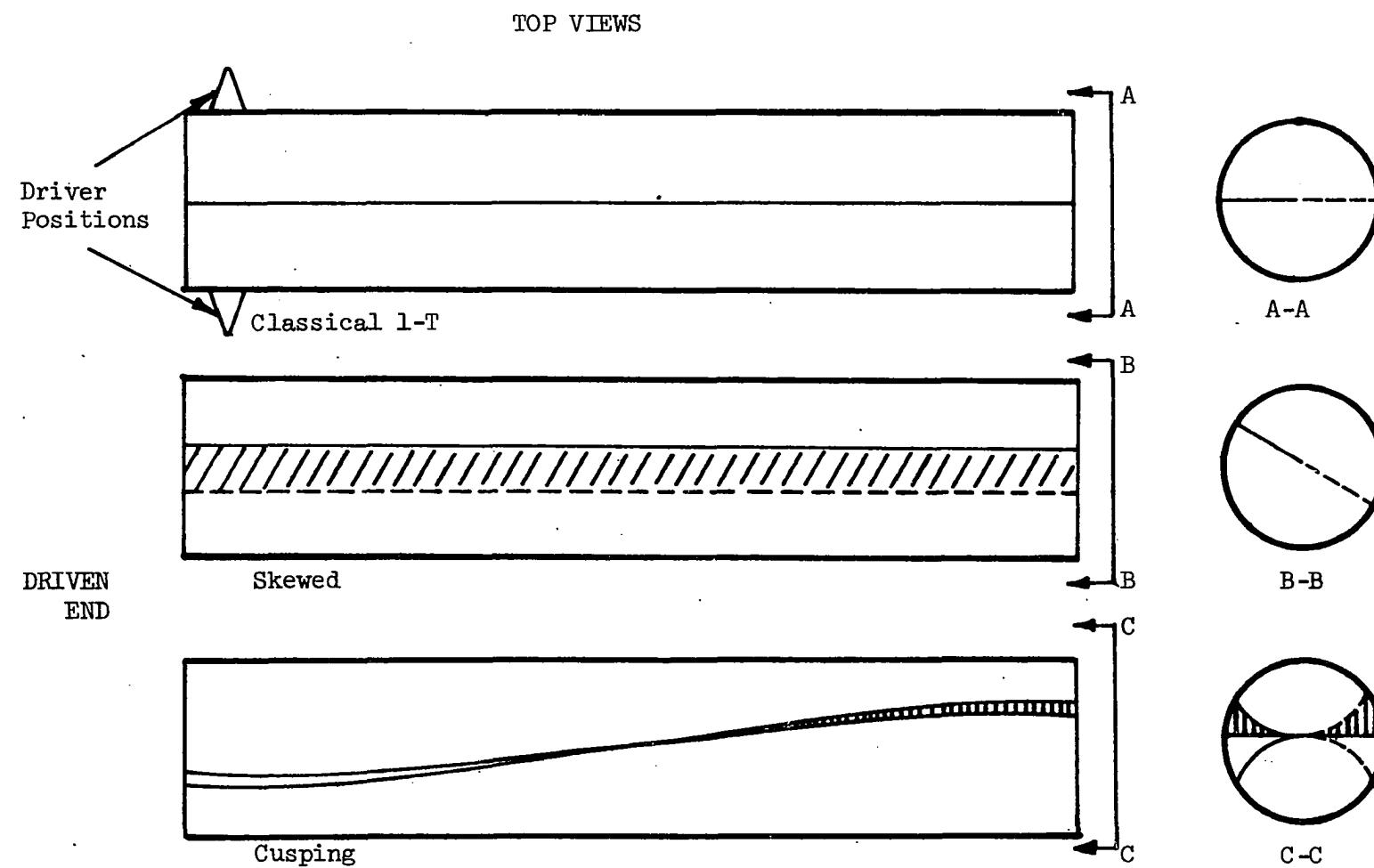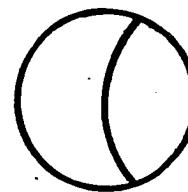
Figure 21.   Wave Patterns Measured in the Preliminary Tests
Without Flow.

96

Z = Distance From Open End
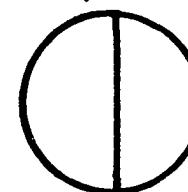
SPL_3 = Sound Pressure Level at 3:00 Position

SPL_9 = Sound Pressure Level at 9:00 Position
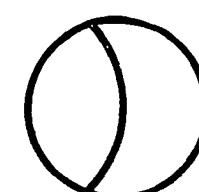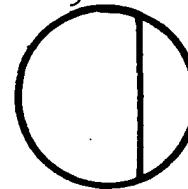
$SPL_9 = 2SPL_3$ $SPL_9 = SPL_3$ $2SPL_9 = SPL_3$
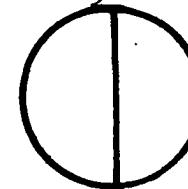
Curved Nodal Line

$SPL_9 = 2SPL_3$ $SPL_9 = SPL_3$ $2SPL_9 = SPL_3$
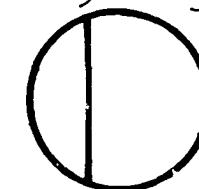
Z = 1 ft. $Z = 2\frac{1}{2}$ ft. Z = 4 ft.

Displaced Nodal Line

Figure 22. Nodal Line Shapes During Cusping.
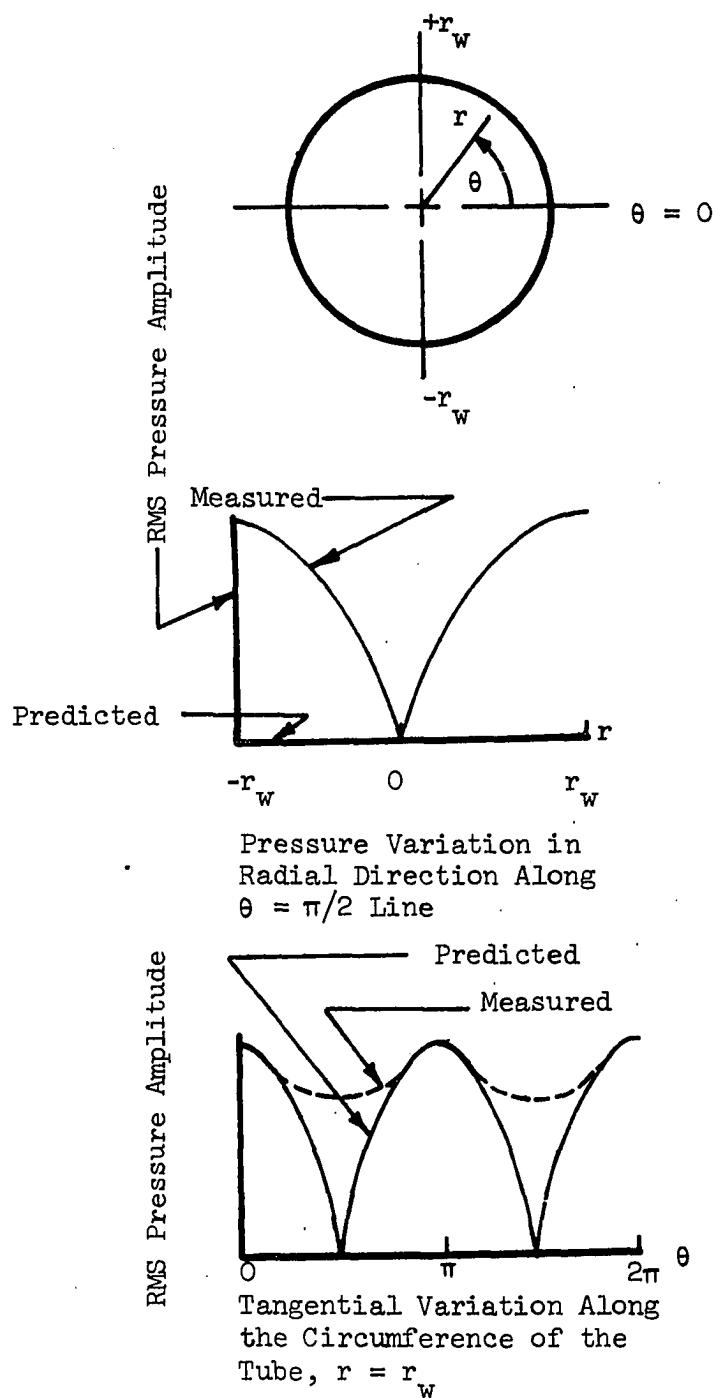
Figure 23. Mixed First Tangential-Longitudinal Wave
Patterns for the Tests Conducted
Without Flow.
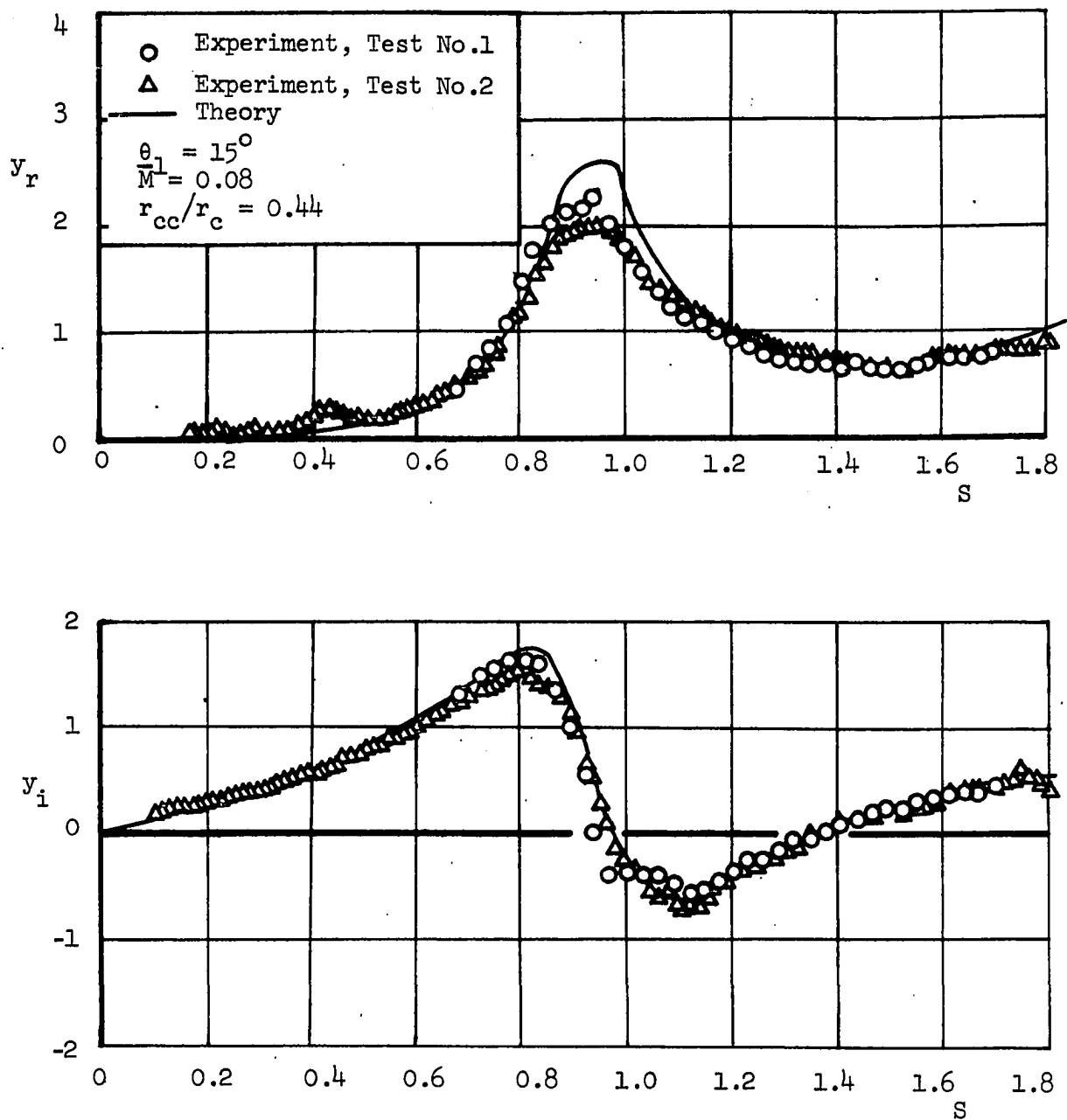
Figure 24. Comparison of the Theoretical and Experimental Admittance Results for Nozzle 15-08-2.5 for Longitudinal Modes.
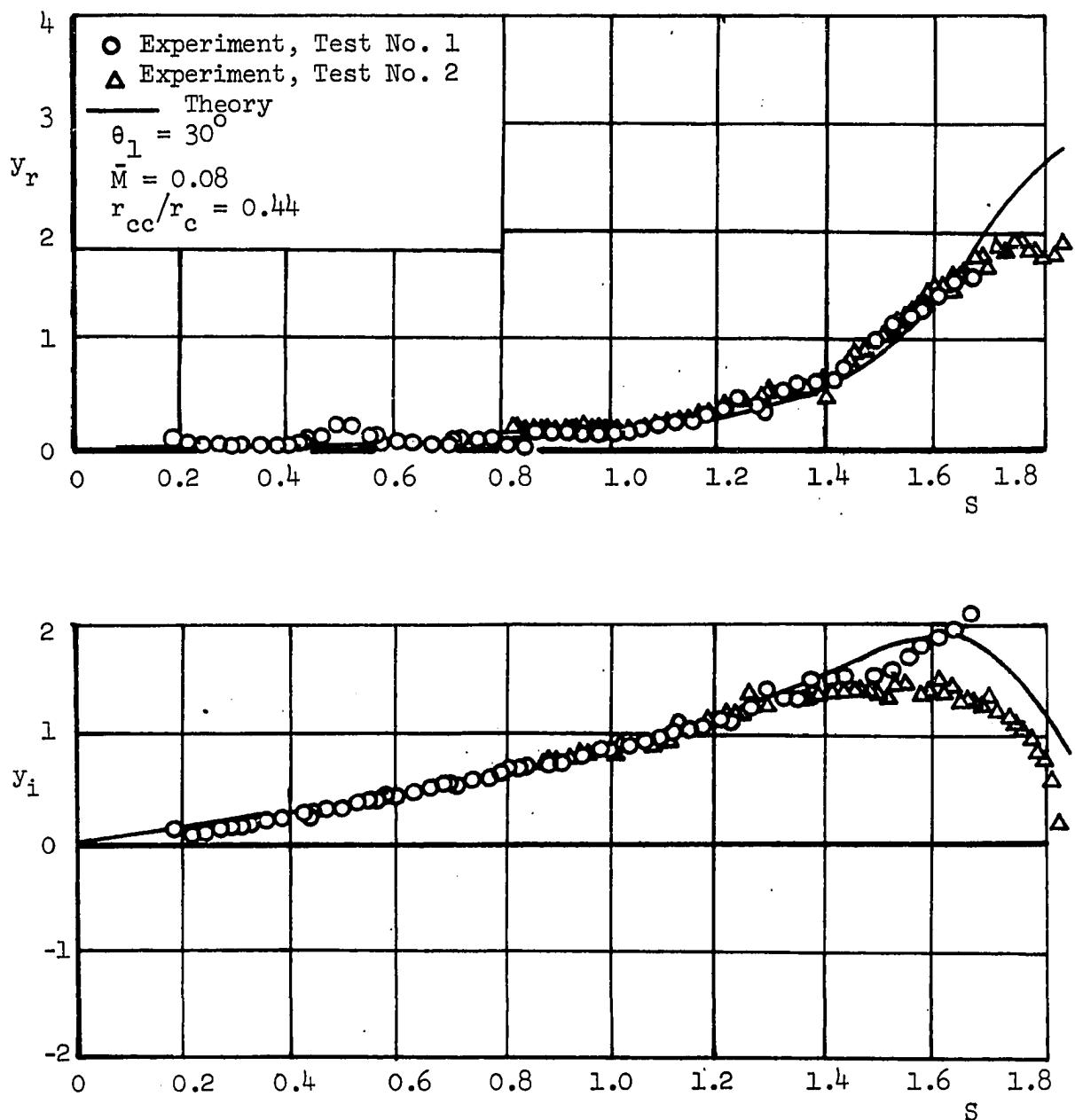
Figure 25. Comparison of the Theoretical and Experimental
Admittance Results for Nozzle 30-08-2.5 for
Longitudinal Modes.
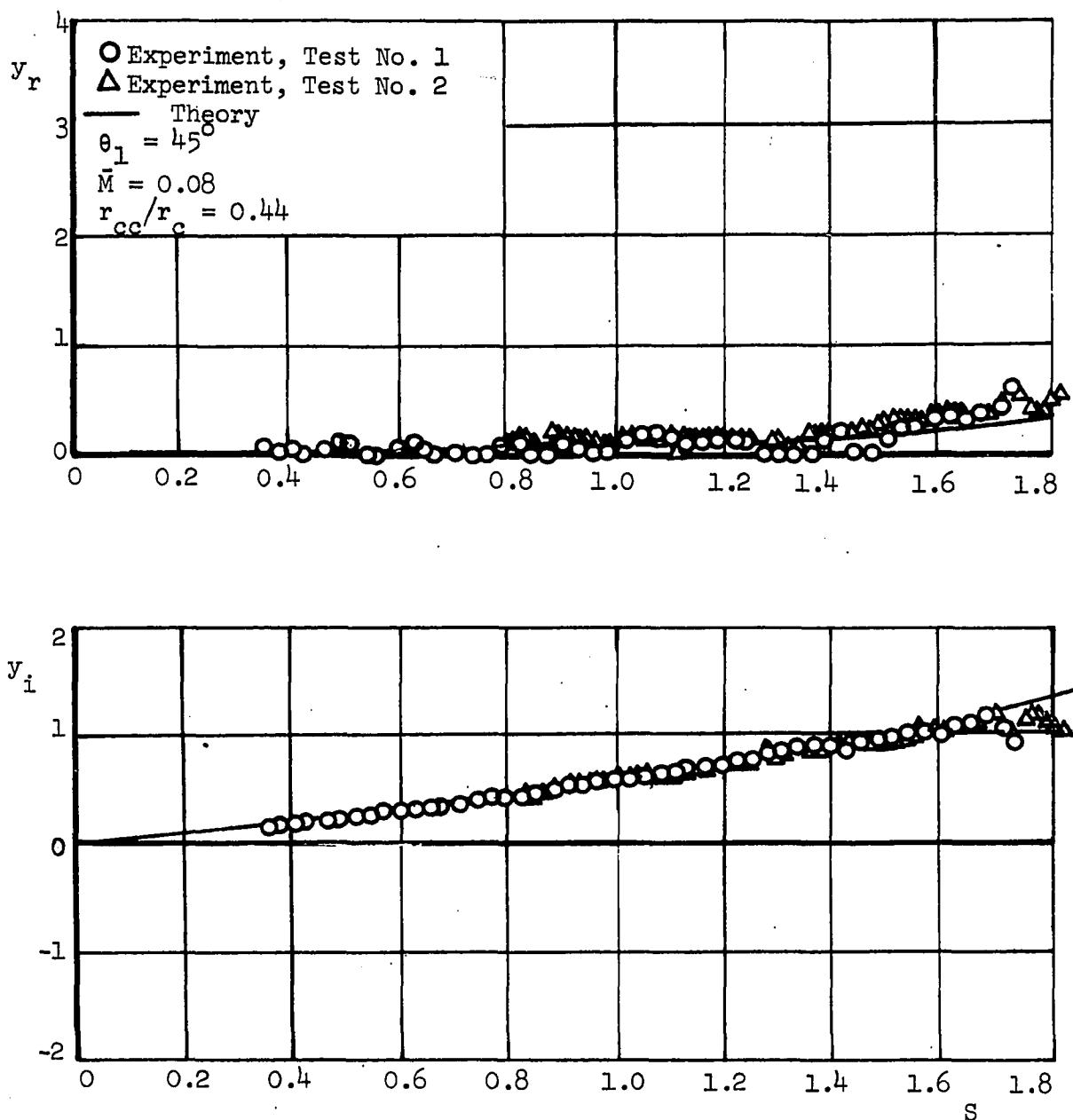
Figure 26. Comparison of the Experimental and Theoretical
Admittance Results for Nozzle 45-08-2.5 for
Longitudinal Modes.
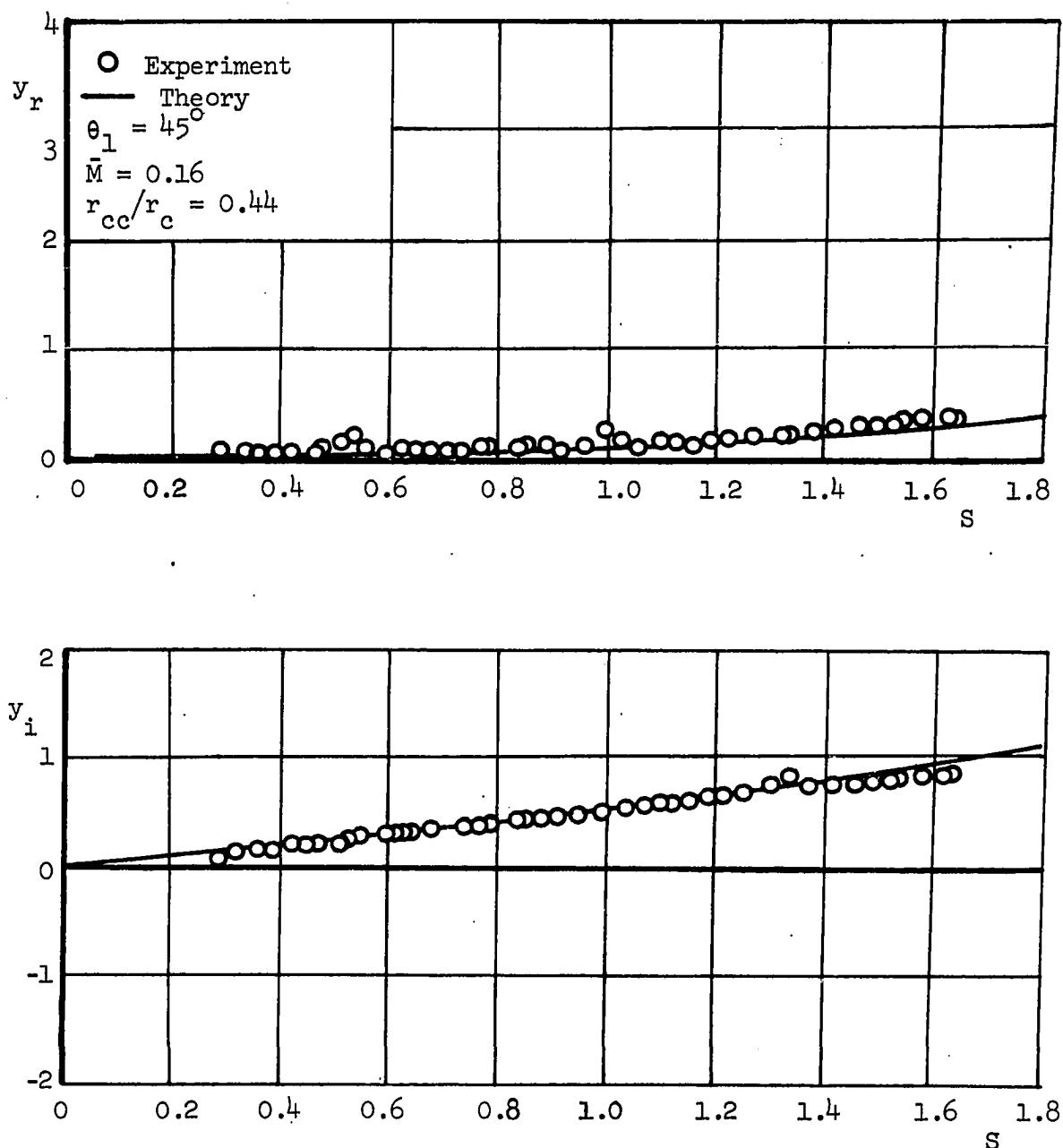
Figure 27. Comparison of the Experimental and Theoretical
Admittance Results for Nozzle 45-16-2.5 for
Longitudinal Modes.
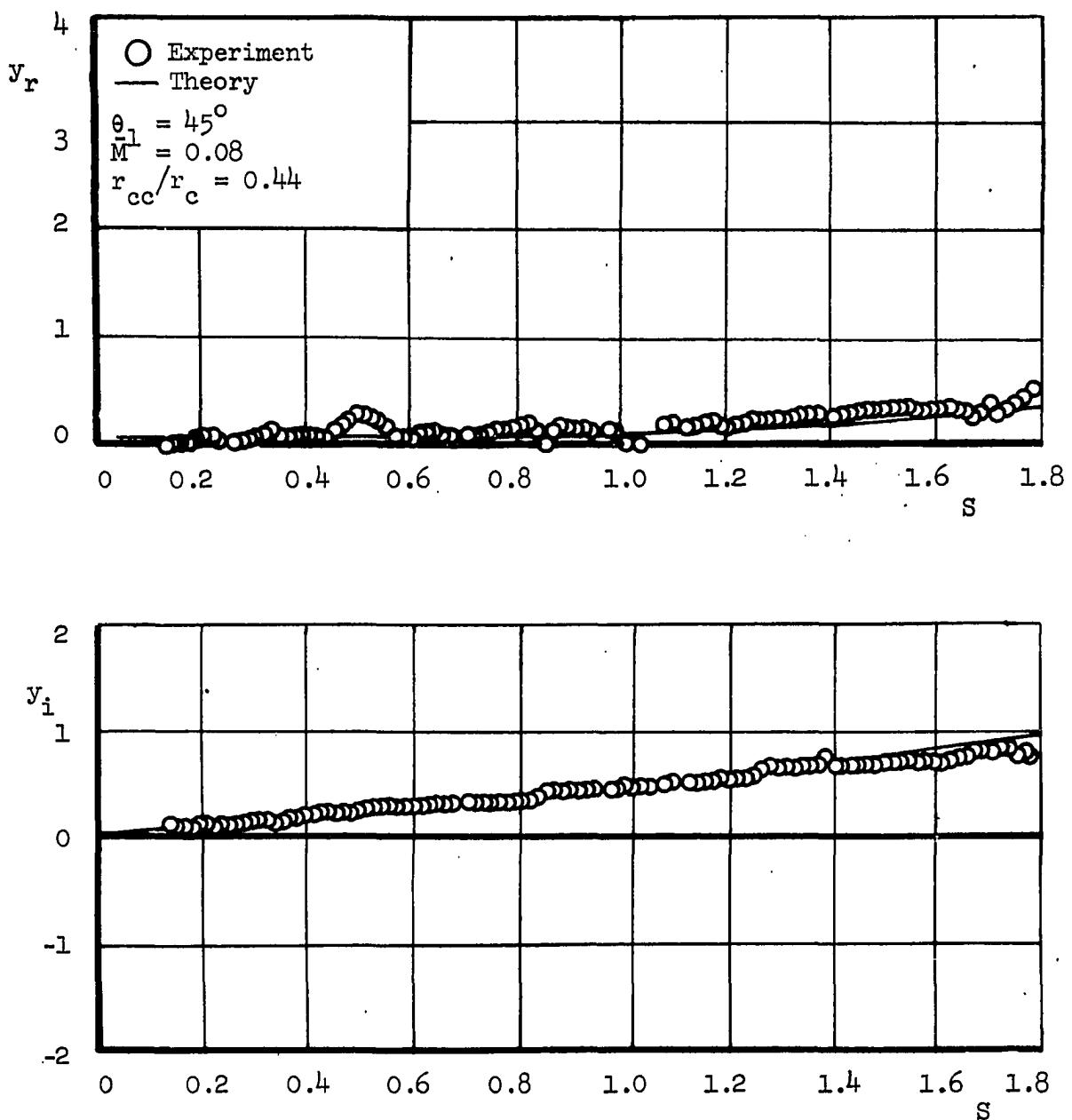
Figure 28. Comparison of the Theoretical and Experimental Results for Nozzle 45-20-2.5 for Longitudinal Modes.
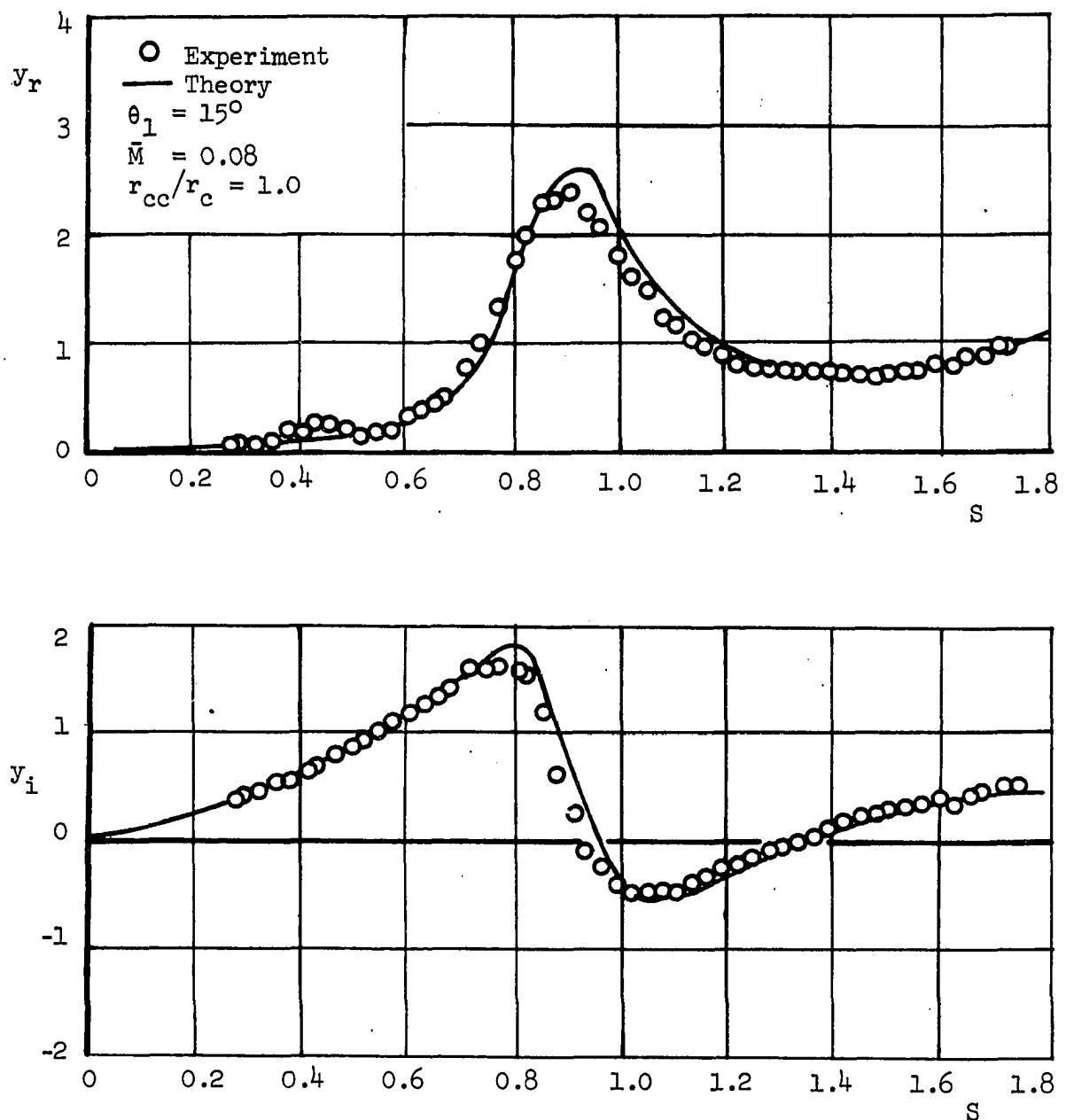
Figure 29. Comparison of the Theoretical and Experimental
Admittance Results for Nozzle 15-08-5.7 for
Longitudinal Modes.
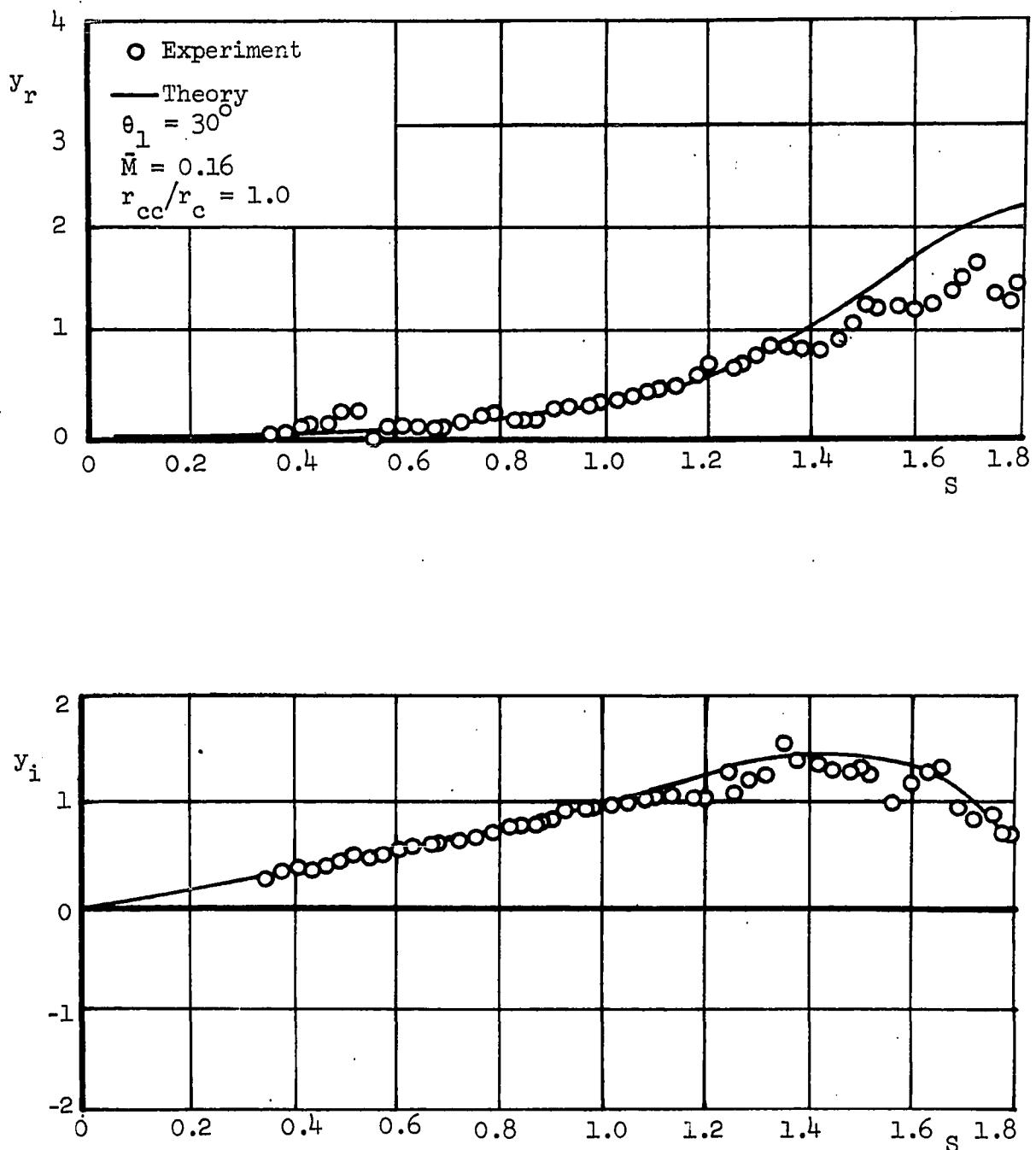
Figure 30. Comparison of the Theoretical and Experimental Admittance Values for Nozzle 30-16-5.7 for Longitudinal Modes.
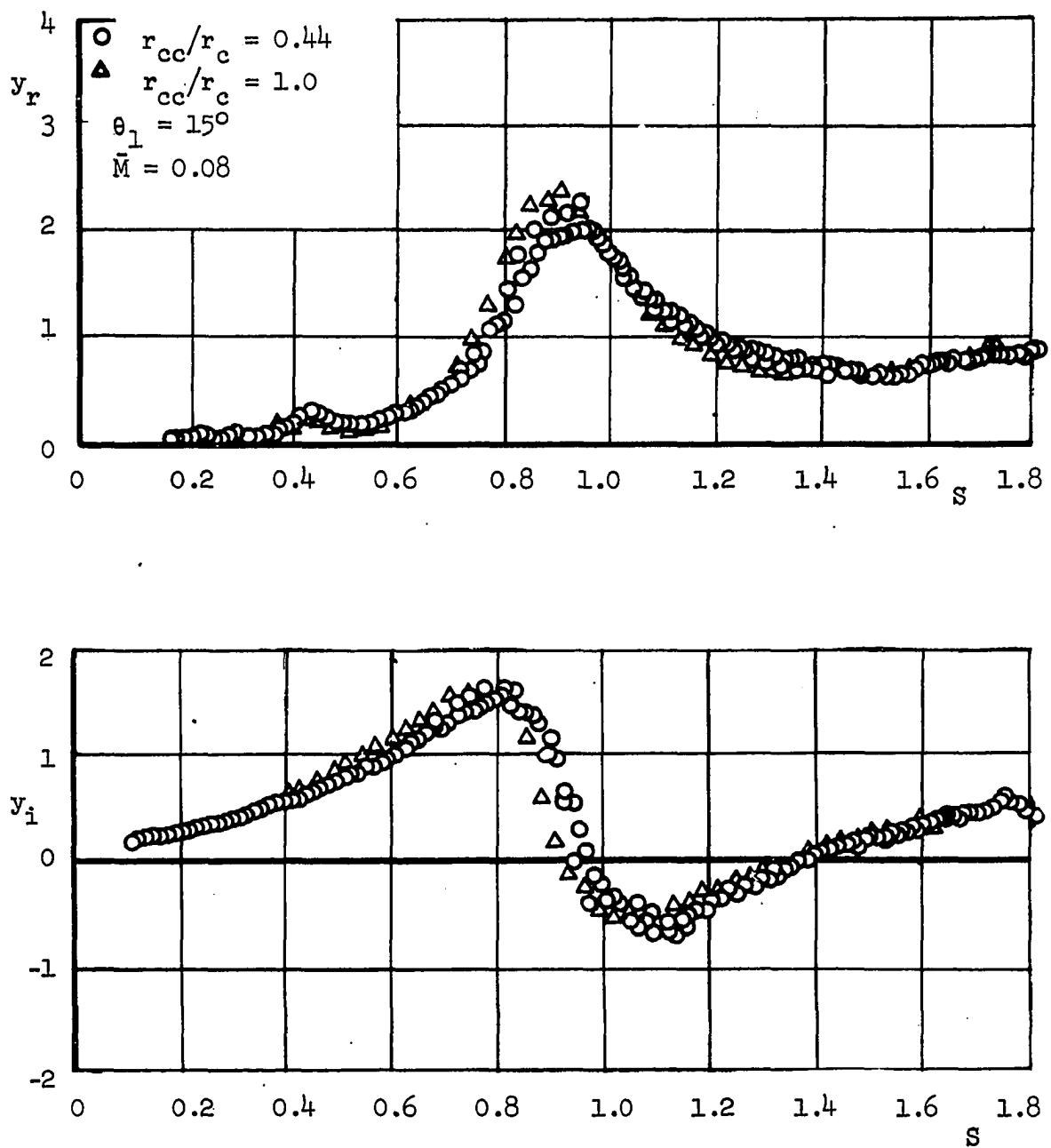
Figure 31. Effect of the Radius of Curvature on the Admittance Values.
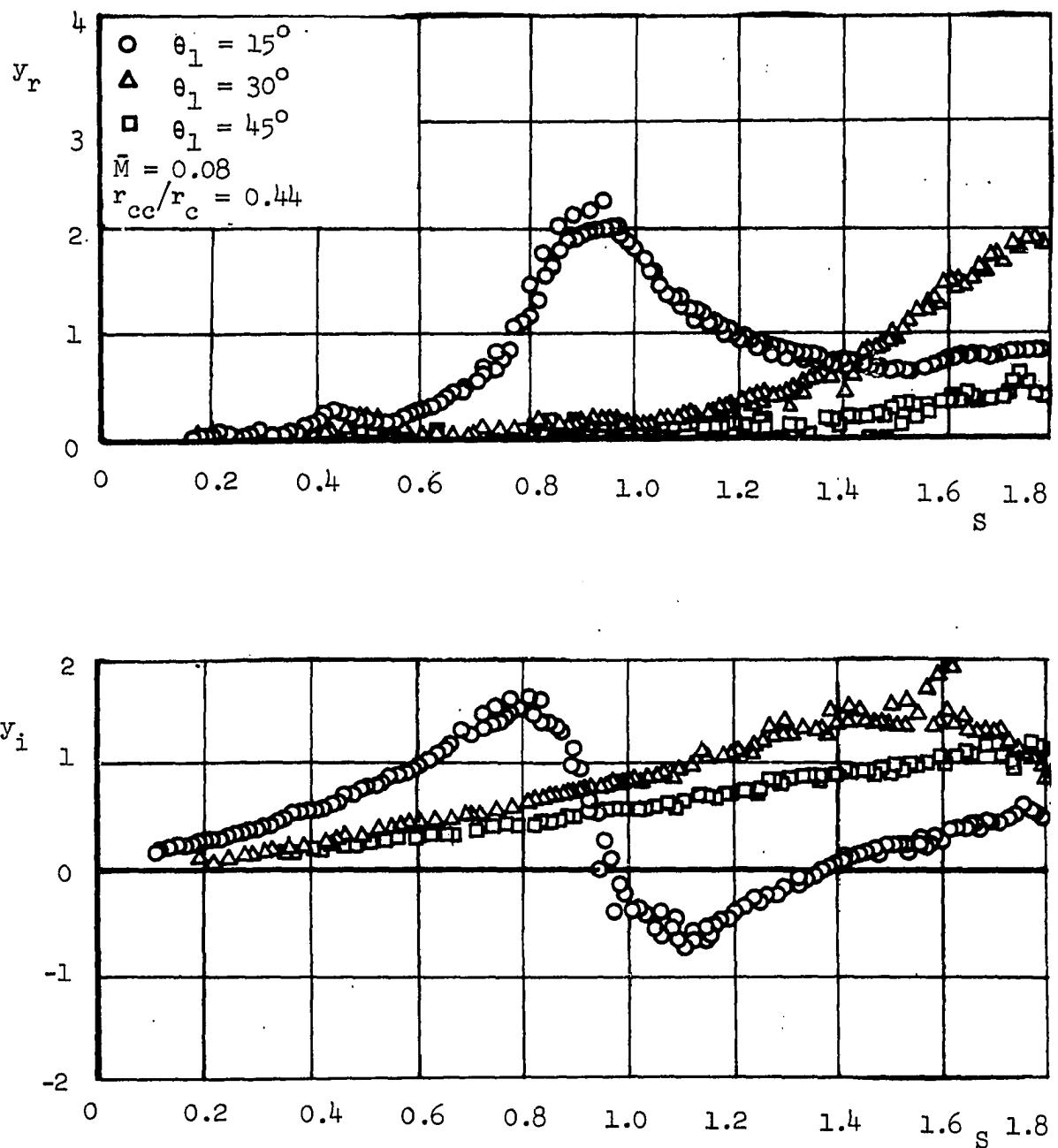
Figure 32. Effect of Nozzle Half-Angle on the Values of the Admittance
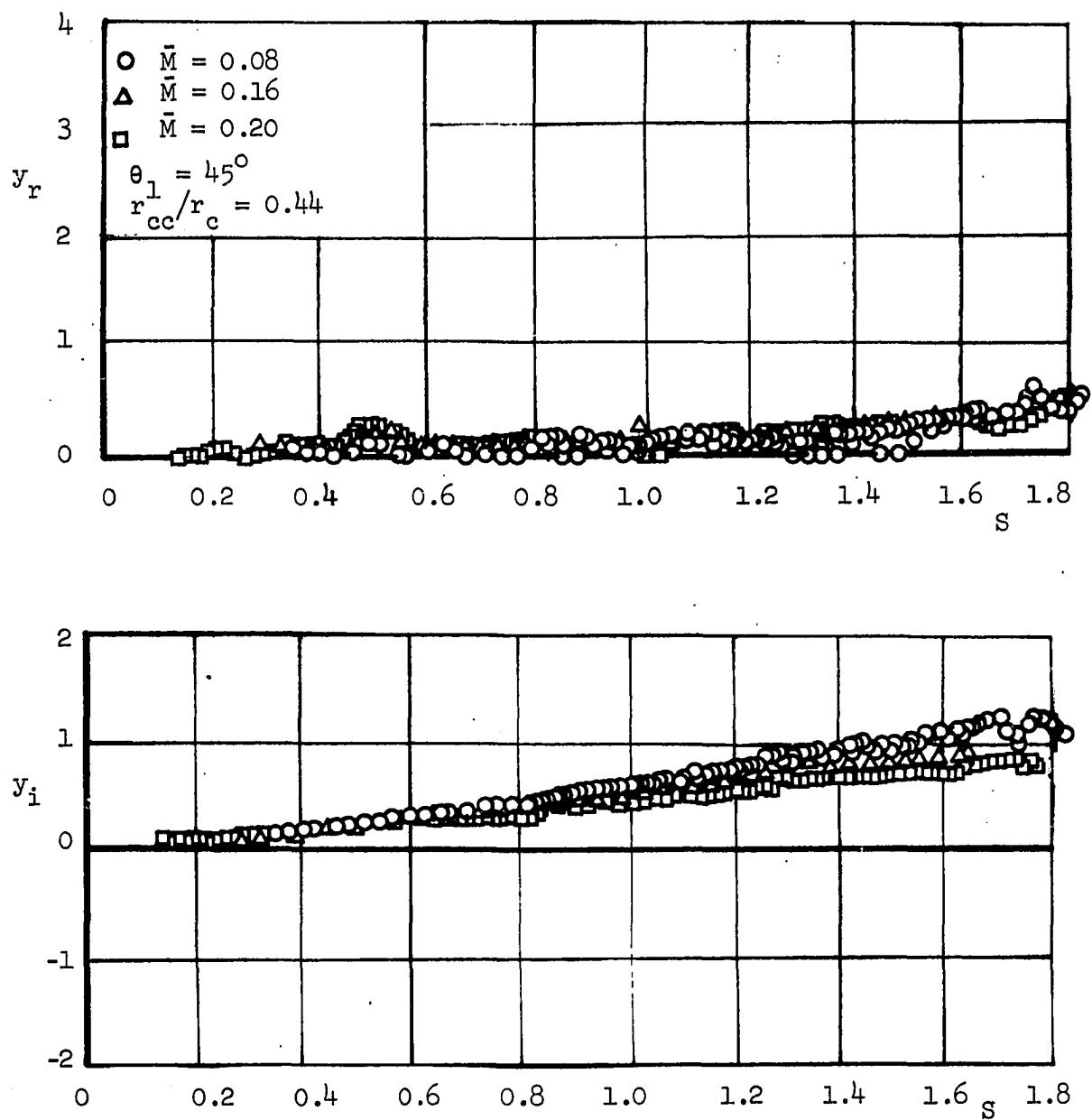
Figure 33. Effect of Entrance Mach Number on the Values of the Admittance.
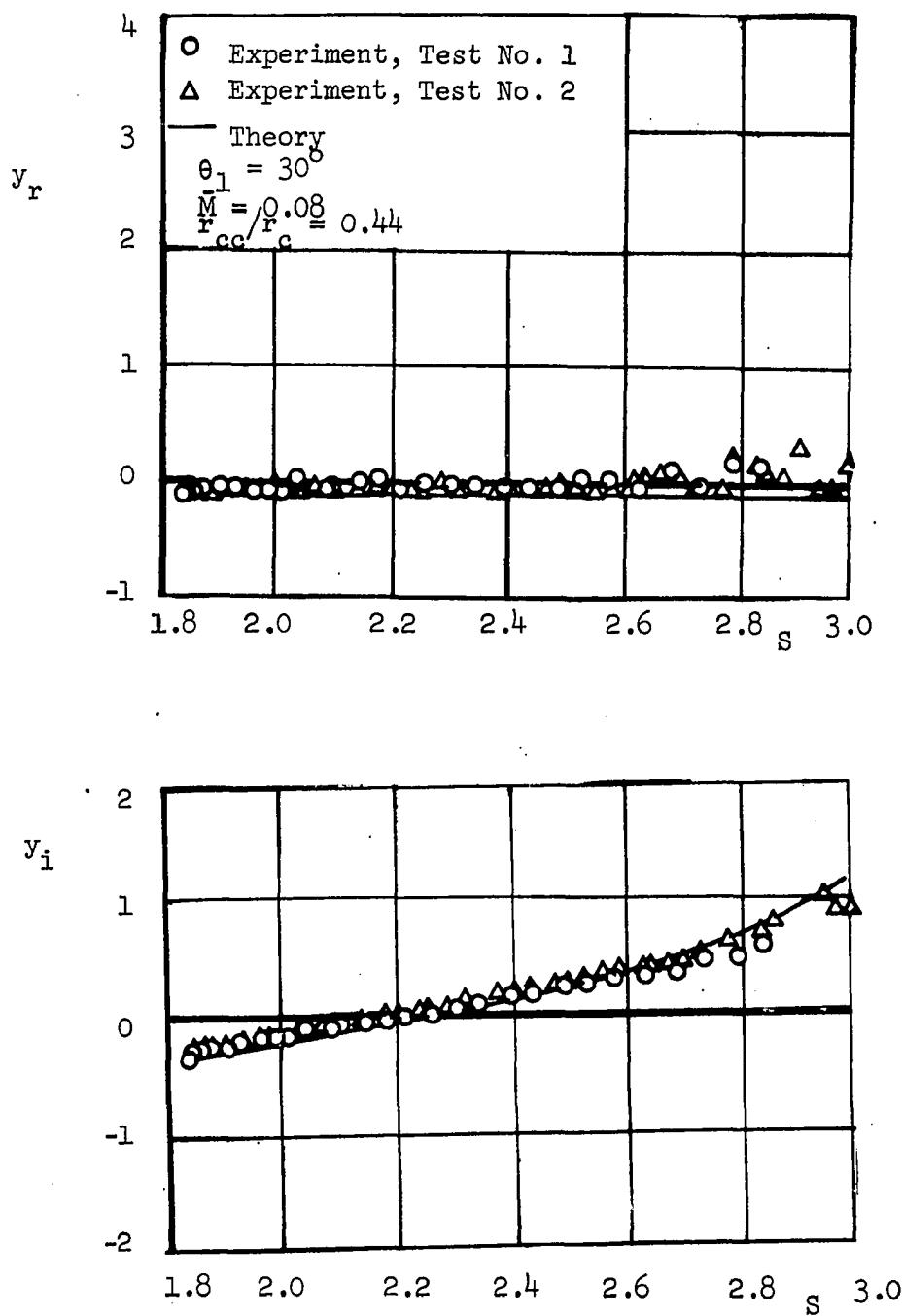
Figure 34. Comparison of the Theoretical and Experimental
Nozzle Admittance Results for Nozzle 30-08-2.5
for Mixed First Tangential-Longitudinal Modes.
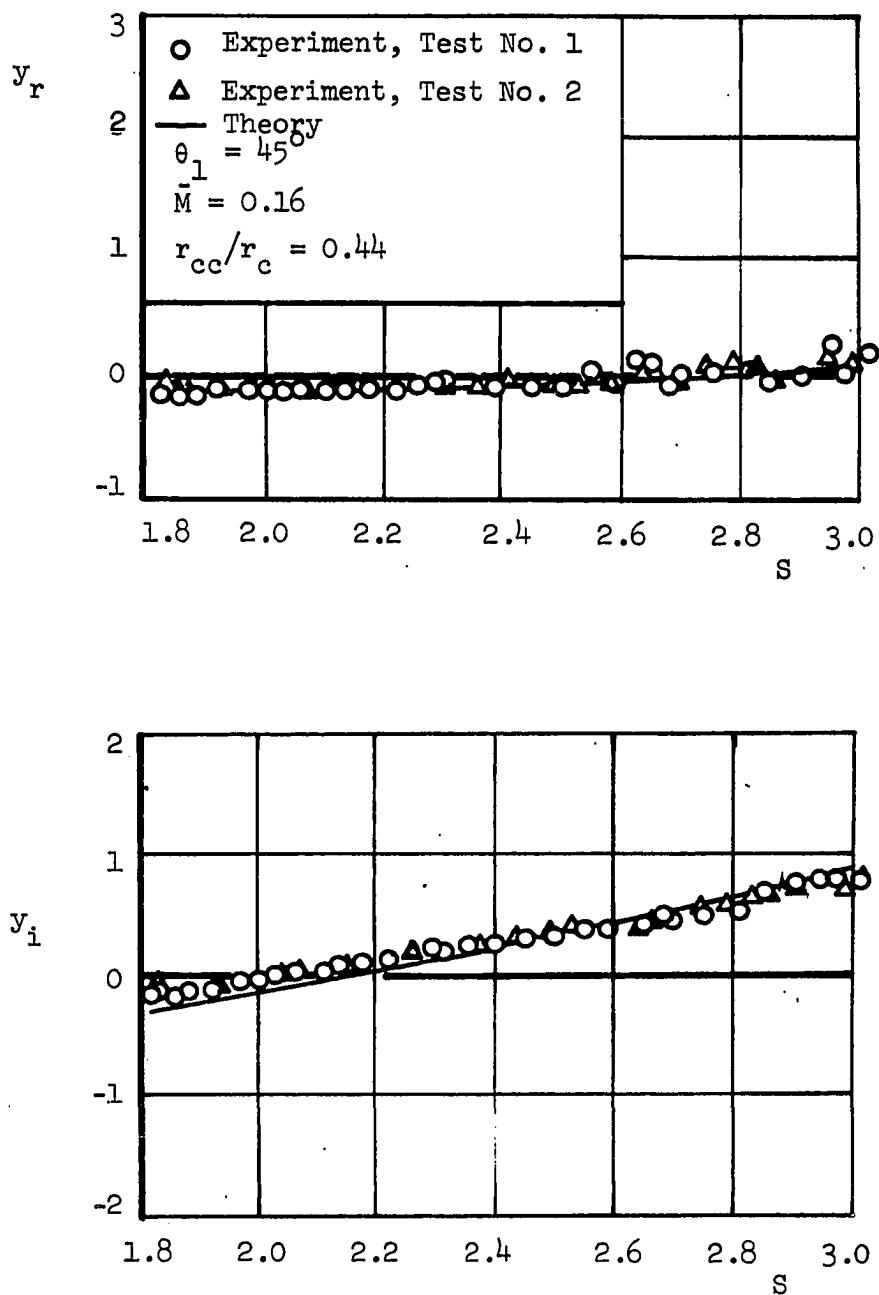
Figure 35. Comparison of the Theoretical and Experimental
Nozzle Admittance Results for Nozzle 45-16-2.5
for Mixed First Tangential-Longitudinal Modes.
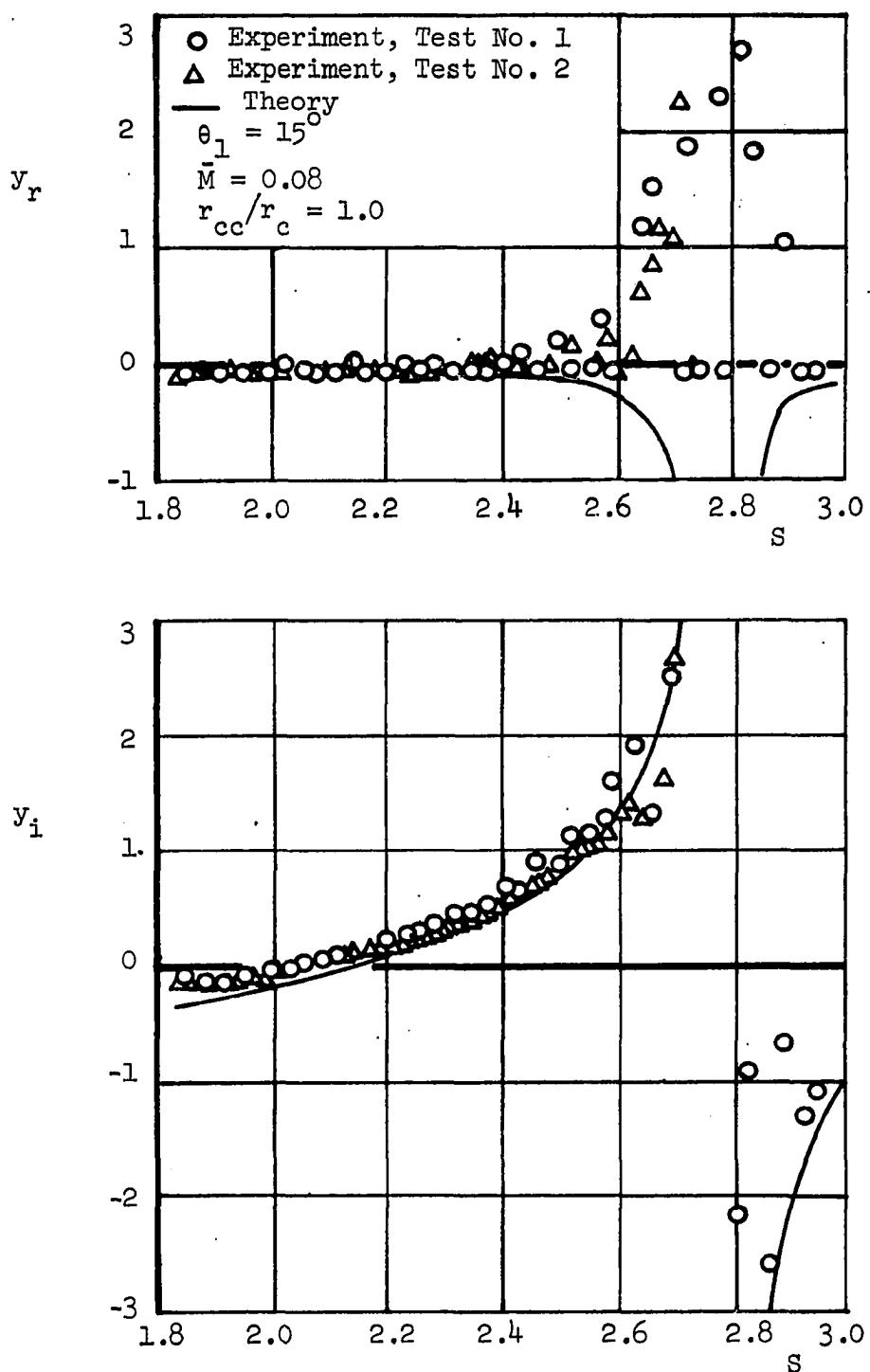
Figure 36. Comparison of the Theoretical and Experimental
Nozzle Admittance Results for Nozzle 15-08-5.7
for Mixed First Tangential-Longitudinal Modes.
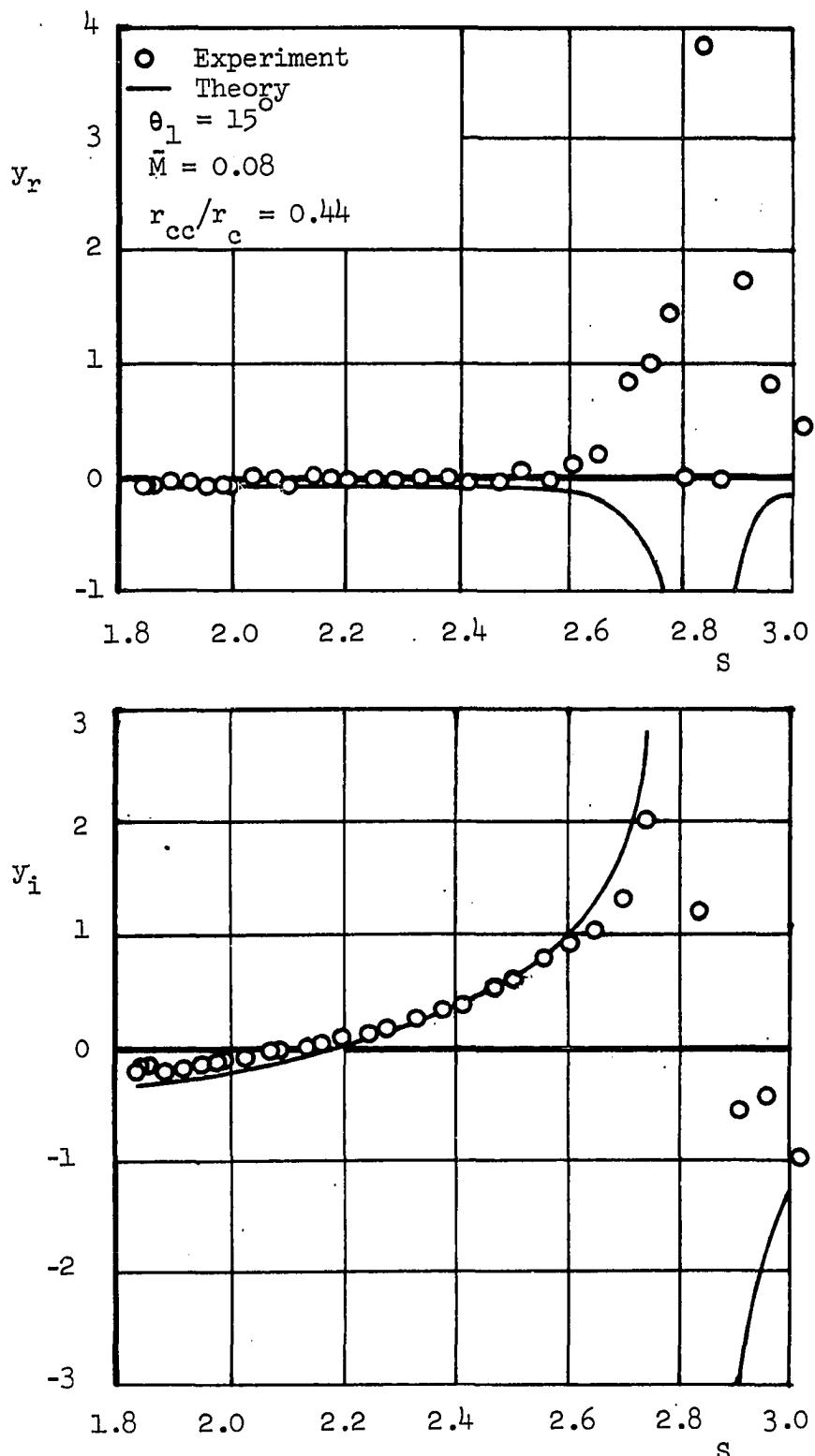
Figure 37. Comparison of the Theoretical and Experimental Nozzle
Admittance Results for Nozzle 15-08-2.5 for Mixed
First Tangential-Longitudinal Modes.
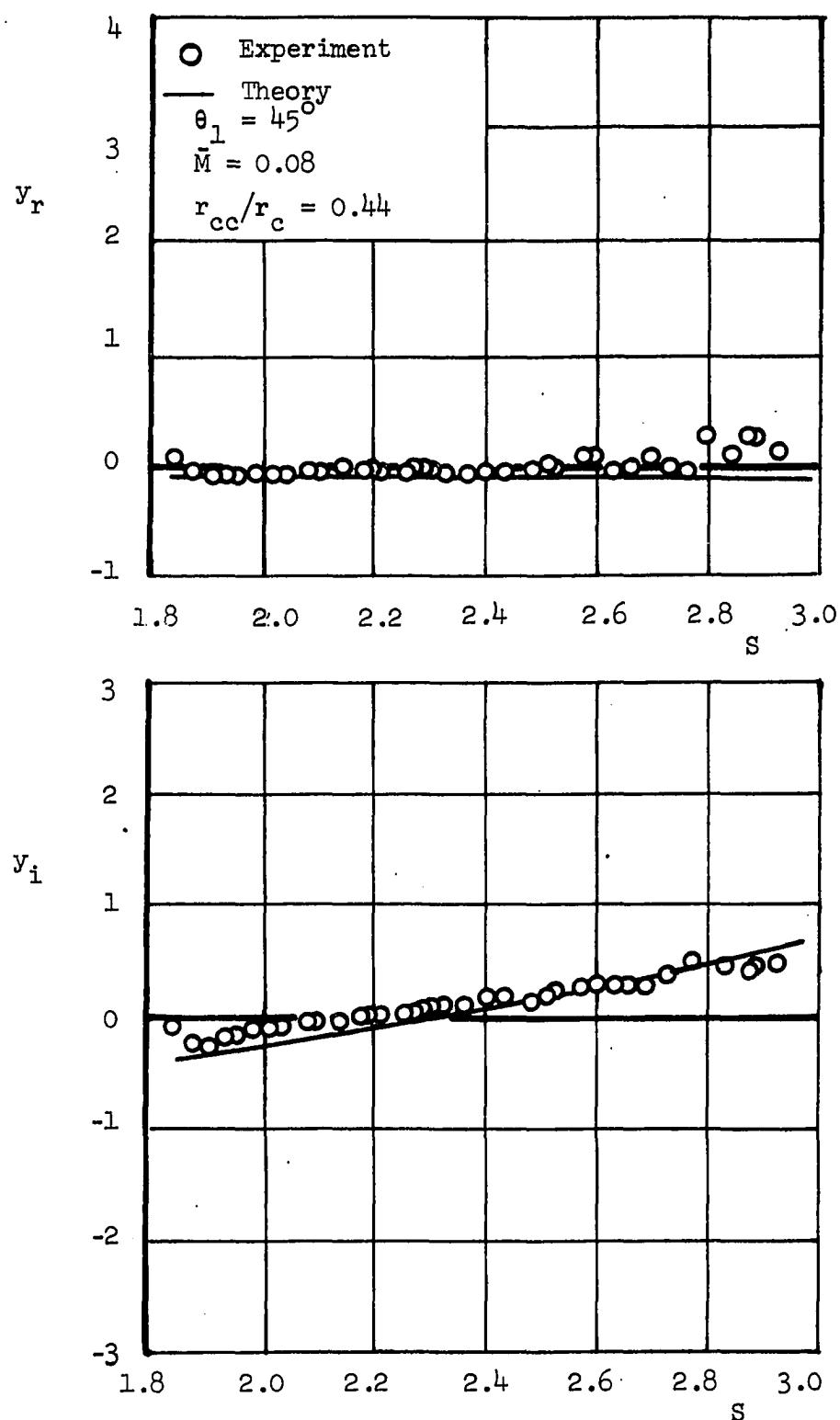
Figure 38. Comparison of the Theoretical and Experimental
Nozzle Admittance Results for Nozzle 45-08-2.5
for Mixed First Tangential-Longitudinal Modes.
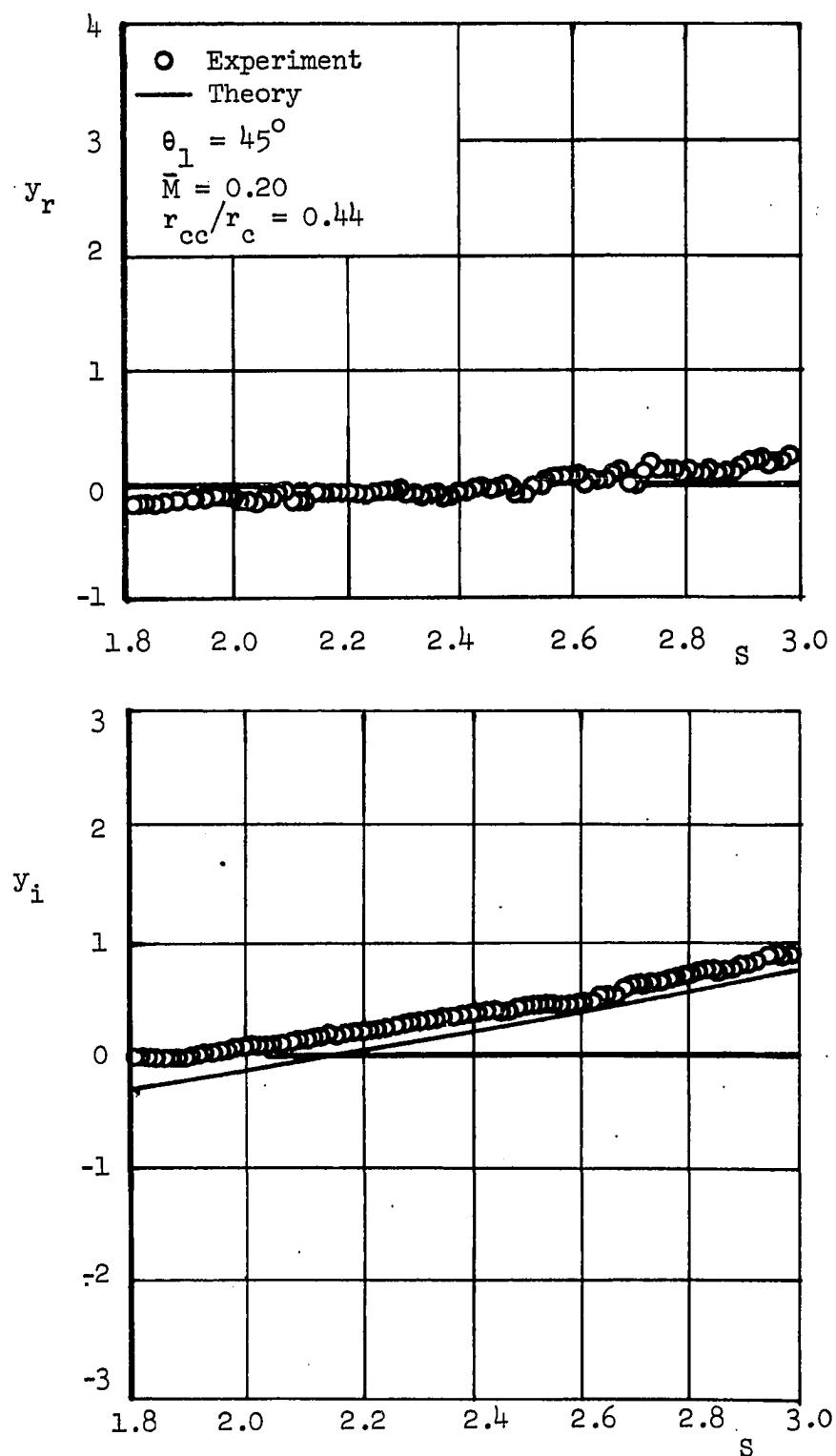
Figure 39. Comparison of the Theoretical and Experimental
Nozzle Admittance Results for Nozzle 45-20-2.5
for Mixed First Tangential-Longitudinal Modes.
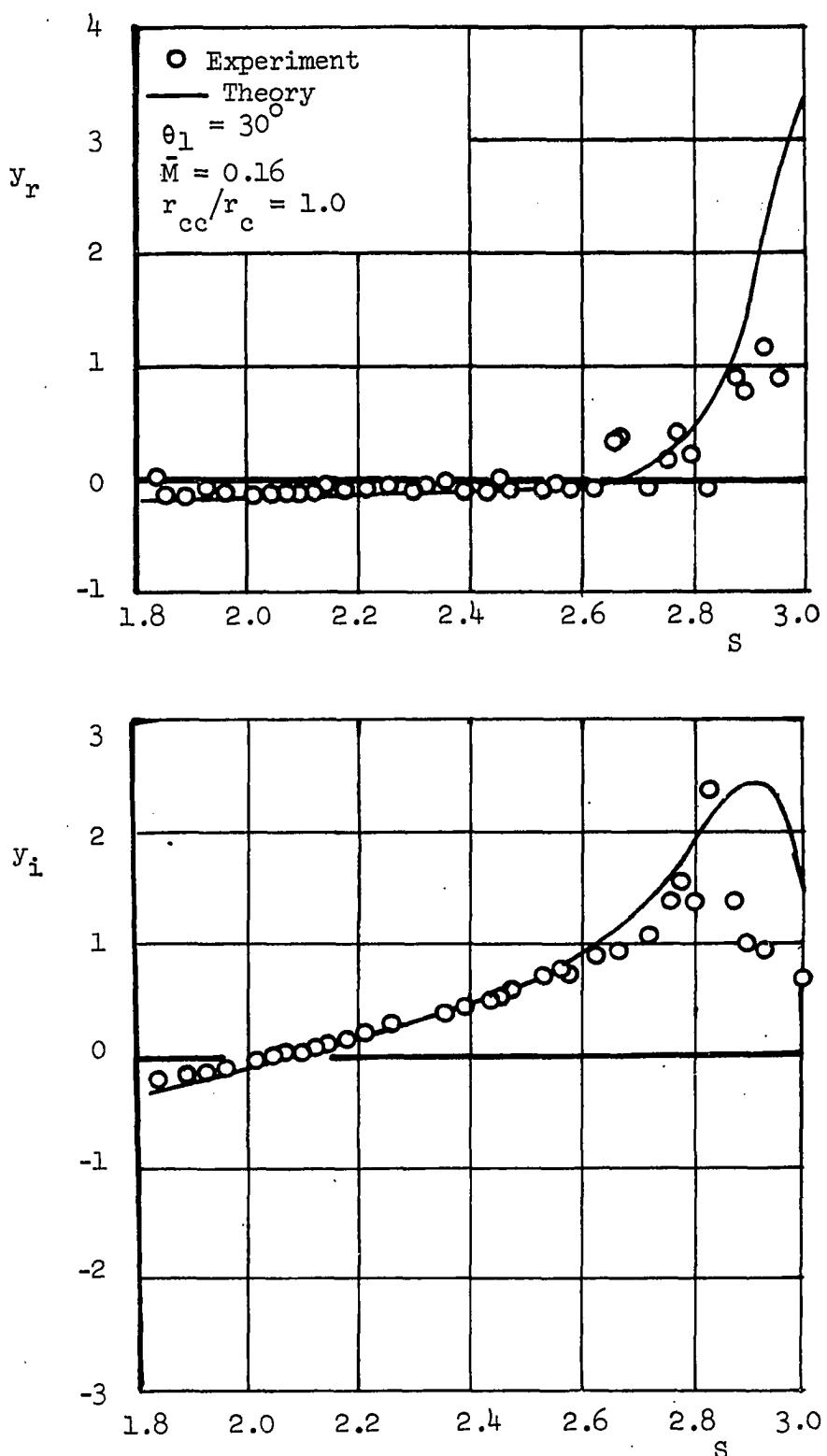
Figure 40. Comparison of the Theoretical and Experimental
Nozzle Admittance Results for Nozzle 30-16-5.7
for Mixed First Tangential-Longitudinal Modes.
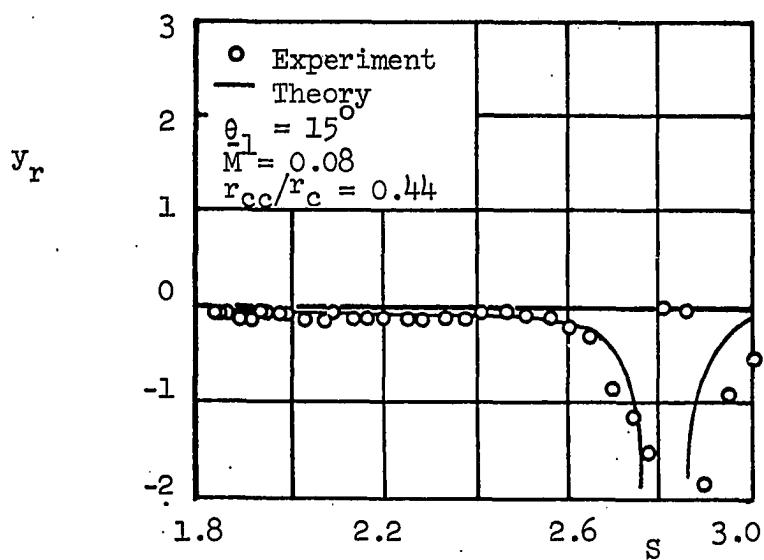
Figure 41. Experimental Values of the Real Part of the Admittance from Figure 37 Recomputed Assuming Negative Values of α.
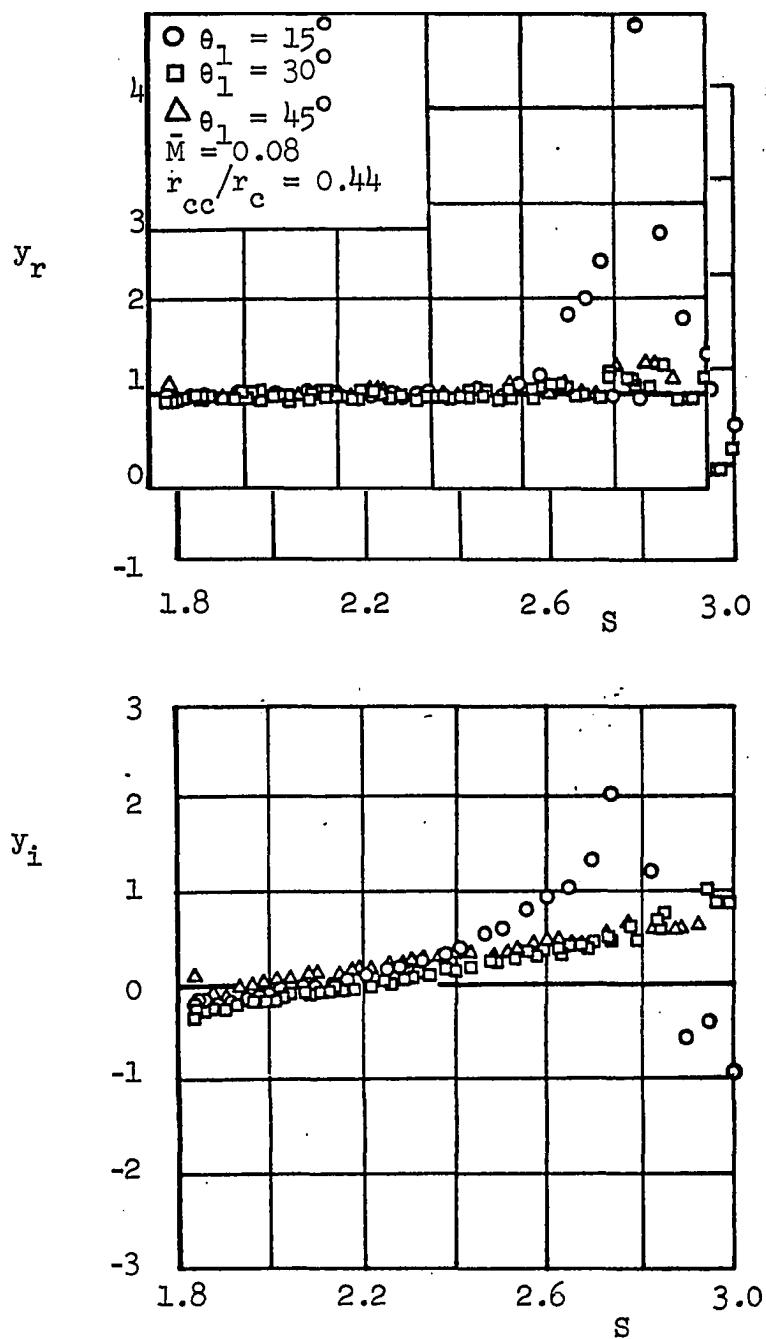
Figure 42. Effect of the Nozzle Half-Angle on the Experimental Values of the Admittance.
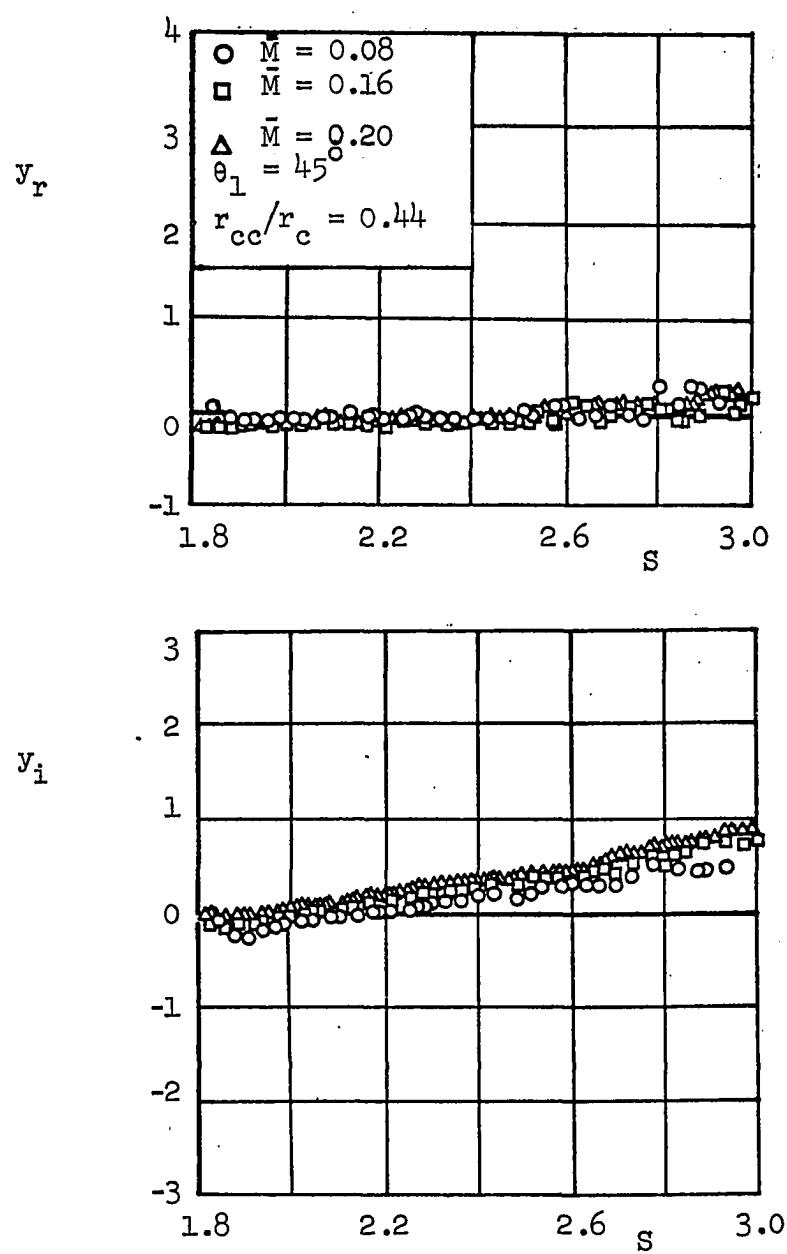
Figure 43. Effect of Entrance Mach Number on the Experimental Values of the Admittance.
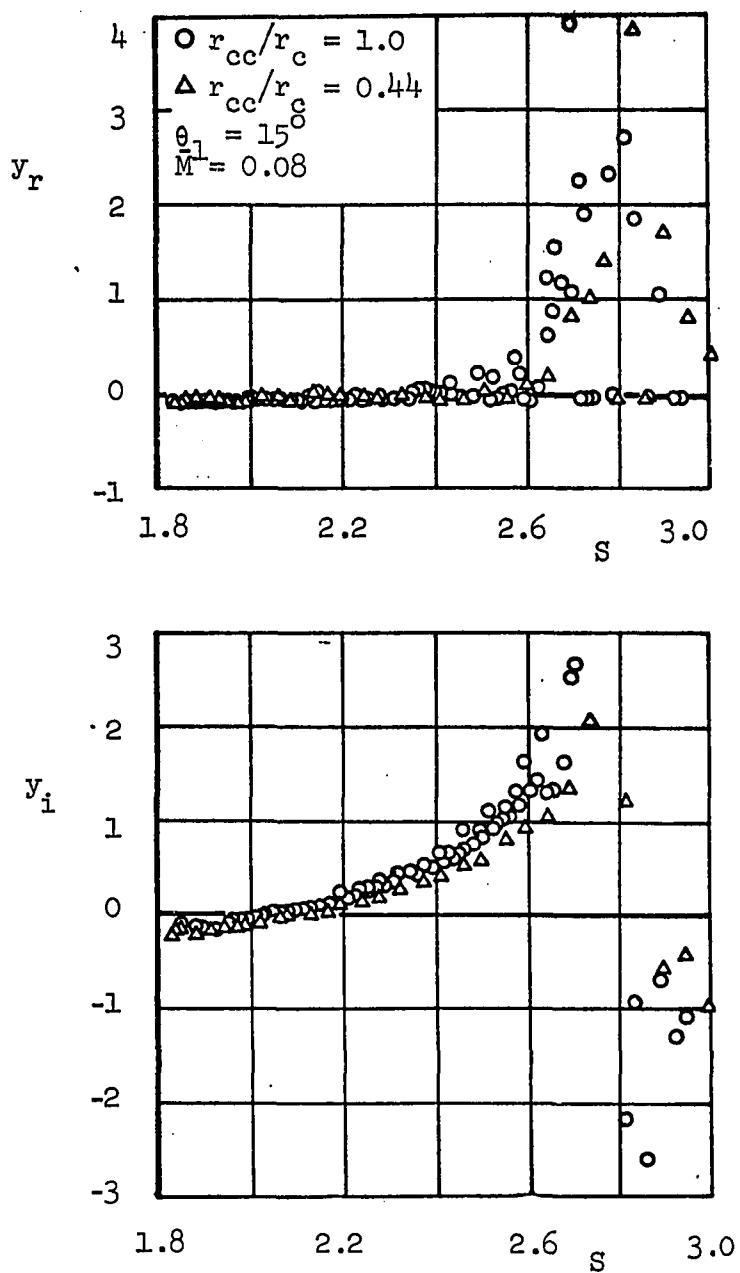
Figure 44. Effect of the Radius of Curvature on the Experimental Values of the Admittance.

APPENDIX A

COMPUTER PROGRAM USED TO DETERMINE THE IRROTATIONAL

NOZZLE ADMITTANCE FROM CROCCO'S THEORY

The computer program for calculating the irrotational nozzle admittance from Crocco's theory[6] is written in FORTRAN V interpretive language compatible with the UNIVAC 1108 machine language compiler. This program consists of seven routines - the main or control program and six subroutines. The names of the routines are listed in Table 3 in sequential order. The FORTRAN symbols used in these routines and their definitions are presented in Table 4 in alphabetical order. The input parameters necessary for the admittance computations must be specified in the main program and are listed in Table 5. The output parameters and their definitions are listed in Table 6. A detailed flow chart of the computer program is shown in Figure 45; and the program listing and sample output are presented in Tables 7 and 8, respectively.

Table 3. List of Subroutines in the Computer Program Used
to Determine the Irrotational Nozzle Admittance
from Crocco's Theory

Subroutine	Description
MAIN	Specifies the nozzle geometry and operating conditions in the converging section of the nozzle
NOZADM	Specifies initial conditions at the throat, computes the final nozzle admittance values, and contains all output formats
RKTZ	Uses the Runge-Kutta of order four to obtain initial values for the modified Adams integration routine
RKZDIF	Computes the differential element in the converging section of the nozzle used to solve equation (2-15)
RKTDIF	Computes the differential element in the converging section of the nozzle used to solve equation (2-16)
ZADAMS	Numerically integrates equation (2-15) using the modified Adams numerical integration scheme
TADAMS	Numerically integrates equation (2-16) using the modified Adams numerical integration scheme

Table 4. Definition of FORTRAN Variables

Variable	Definition
A	Real coefficient A of equation (2-15)
A(5)	Coefficients of the Runge-Kutta formulas of order four
ANGLE	Nozzle half-angle, degrees
A1R	Derivative of the coefficient A evaluated at the throat
BI	Imaginary part of the coefficient B in equation (2-15)
BR	Real part of the coefficient B in equation (2-15)
BOI	Value of BI at the throat
BOR	Value of BR at the throat
B1I	Derivative of BI evaluated at the throat
B1R	Derivative of BR evaluated at the throat
C	Nondimensional speed of sound defined after equation (2-5)
CI	Imaginary part of the coefficient C in equation (2-15)
CM	Mach number at the nozzle entrance
COR(5)	Formula for the corrector in the Modified Adams integration routine
CR	Real part of the coefficient C in equation (2-15)
COI	Value of CI at the throat
COR	Value of CR at the throat
C1I	Derivative of CI evaluated at the throat
C1R	Derivative of CR evaluated at the throat

123

Table 4. Continued

Variable	Definition
DP	Integration stepsize
DP(5)	Derivative used in the corrector formula in the modified Adams integration routine
DR	Derivative of the local wall radius with respect to axial distance
DU	Derivative of the nondimensional velocity $\bar{q}^2$ with respect to the wall radius r
DWC	Increment of the nondimensional frequency ω defined in Chapter II
DY(5,4)	Derivative used in the modified Adams integration scheme
F	Constant given as $\bar{q}/\gamma\bar{p}$
FZ(4,5)	Derivative used in the Runge-Kutta method
F1	Lumped parameter determined by the conditions at the throat
F2	Lumped parameter determined by the conditions at the throat
GAM	Ratio of specific heats
G(5)	Dependent variable in the Runge-Kutta integration routine
GP(5)	Derivative of the dependent variable G(5)
H	Integration stepsize
I	Integer counter
IP	Integer constant. If IP = 0 the nozzle admittance is output. If IP $\neq$ 0 the amplitude and phase of the pressure oscillation are output

Table 4. Continued

Variable	Definition
IQ	If IQ = 2, the integration of equation (2-16) for τ is complete
IQZ	=1: equation (2-16) for τ is integrated =2: equation (2-15) for ζ is integrated
IWC	Integer constant used in determining the initial value of ω
J	Integer variable
JOPT	=1: equation (2-16) for τ is integrated =2: equation (2-15) for ζ is integrated
K	Integer variable
N	Integer variable
NU	Number of differential equations to be solved by the Runge-Kutta or the modified Adams integration routine
NWC	Number of frequency points
P	Value of the steady state velocity potential
PARG	Phase of the pressure oscillation in the nozzle
PHII	Imaginary part of Φ defined in equation (2-13)
PHIR	Real part of Φ defined in equation (2-13)
PI	Imaginary part of the pressure
PMAG	Magnitude of the pressure oscillation
PR	Real part of the pressure oscillation
PRED(5)	Predictor formula for the modified Adams integration routine

Table 4. Continued

Variable	Definition
Q	Constant given as $(r_{th}/4) \left(\frac{2}{\gamma+1}\right)^{\frac{\gamma+1}{4(\gamma-1)}}$
QBAR	Nondimensional steady state velocity $\bar{q}$
R	Local wall radius r
RCC	Radius of curvature at the nozzle entrance
RCT	Radius of curvature at the throat
RHO	Nondimensional, steady state density $\bar{\rho}$
RT	Nondimensional throat radius
R1	Nondimensional radius at the entrance to Section 2 of the converging portion of the nozzle
R2	Nondimensional radius at the entrance to Section 3 of the converging portion of the nozzle
SRTR	Constant given as $\sqrt{r_{th} r_{cc}}$
SVN	S_{mn}
SVNR	S_{mn}/r_{th}
SYI	Imaginary part of the specific admittance
SYR	Real part of the specific admittance
T	Nozzle half-angle, in radians
TDN	Inverse of the square of the magnitude of ζ
TI	Imaginary part of τ
TMAG	Magnitude of τ

Table 4. Continued

Variable	Definition
TPI	Derivative of TI with respect to φ
TPR	Derivative of TR with respect to φ
TR	Real part of τ
TZ	Value of φ at the n-th integration point
T2	Square of the magnitude of τ
U	Steady state velocity squared, $\bar{q}^2$
UZ	Dependent variable in the Runge-Kutta integration scheme
W	Nondimensional frequency S defined in Chapter III
WC	Nondimensional frequency ω defined in Chapter II
X	Value of φ at the n-th integration point
Y(5)	Dependent variable used in the modified Adams integration scheme
YI	Imaginary part of the nozzle admittance defined by equation (2-14)
YR	Real part of the nozzle admittance defined by equation (2-14)
ZDN	Inverse of the square of the magnitude of ζ
ZI	Imaginary part of ζ
ZMAG	Magnitude of ζ
ZPI	Derivative of ZI with respect to φ
ZPR	Derivative of ZR with respect to φ
ZR	Real part of ζ

Table 4. Concluded

Variable	Definition
ZOI	Value of ZI at the throat
ZOR	Value of ZR at the throat
Z1I	Value of ZPI at the throat
Z1R	Value of ZPR at the throat
Z2	Square of the magnitude of ζ

Table 5. Input Parameters

Variable	Definition
GAM	Ratio of specific heats
CM	Chamber Mach number
SVN	N-th root of the equation $\dfrac{dJ_V(x)}{dx} = 0$ = 0 for longitudinal modes = 1.84129 for mixed first tangential-longitudinal modes
WC	Initial frequency. If WC is not specified, the value is taken to be the first tangential cutoff frequency $WC = \dfrac{\text{frequency(radians/second)}r_c(\text{feet})}{\text{stagnation speed of sound (f/s)}}$
DWC	Increment of frequency
NWC	Number of frequency points desired
ANGLE	Nozzle half-angle, degrees
RCT	Radius of curvature at the throat nondimensionalized with respect to the chamber radius
RCC	Radius of curvature at the nozzle entrance non-dimensionalized with respect to the chamber radius
IP	= 0: nozzle admittances are printed $\neq$ 0: pressure magnitude and phase are printed at each point along the nozzle

Table 6. Output Parameters

Variable	Definition
WC	$$\dfrac{\text{frequency(radians per second)}r_c(\text{feet})}{\text{stagnation speed of sound (feet/second)}}$$
YR	Real part of the admittance as defined by equation (2-14)
YI	Imaginary part of the admittance as defined by equation (2-14)
W	Nondimensional frequency defined in Chapter III as $$W = WC \frac{\text{stagnation speed of sound}}{\text{steady state speed of sound}}$$
SYR	Real part of the specific admittance
SYI	Imaginary part of the specific admittance
W, SYR, SYI	Correspond to experimental values

Table 7. Listing of the Computer Program Used to
Determine the Irrotational Nozzle Admittance
from Crocco's Theory

```
 1*          COMMON/X1/GAM, SVN, ANGLE, RCT, RCC /X2/T,RT, Q, R1, R2, IP, WC
 2*          COMMON/X3/Z1R, Z1I
 3*          COMMON/X4/ CM
 4*          GAM = 1.4
 5*          DWC=0.05
 6*          IP=0
 7*          RCC = 1
 8*          RCT = 1
 9*          RCC=2.5/5.6875
10*          RCT=2.5/5.6875
11*          DO 300 I = 1,2
12*          IF( I.EQ. 2) GO TO 20
13*          SVN = 0
14*          NWC = 38
15*          GO TO 30
16*      20  NWC = 26
17*          SVN = 1.84129
18*      30  CONTINUE
19*          DO 200 J=1,3
20*          ANGLE = 15.0*J
21*          DO 100 K=1,4
22*          CM = 0.08*K
23*          WC = SVN*SQRT(1-CM*CM)*SQRT(1/(1+(GAM-1)*CM*CM*.5))
24*          IF(IP .EQ. 0) GO TO 10
25*          WRITE(6, 1000) CM, SVN, GAM, ANGLE, RCT, RCC
26*      10  CALL NOZADM(CM, NWC, DWC)
27*     100  CONTINUE
28*     200  CONTINUE
29*     300  CONTINUE
30*    1000  FORMAT(46X, 28HPRESSURE MAGNITUDE AND PHASE, //, 38X,
31*     1        14HMACH NUMBER = , F3.2, 7H SVN = , F6.4, 9H GAMMA = , F3.1
32*     2      , /, 22X, 15HNOZZLE ANGLE = , F4.1, 21H RADII OF CURVATURE:
33*     3      , 9HTHROAT = , F6.4, 12H ENTRANCE = , F6.4, //, 46X,
34*     4      2H X, 7X, 4HPMAG, 10X, 4HPARG, /)
35*          STOP
36*          END
```

Table 7. Continued

```
 1*          SUBROUTINE NOZADM(CM,      NWC, DWC)
 2*          DIMENSION DY(5,4), G(5), GP(5), Y(5)
 3*          COMMON/X1/GAM,SVN,ANGLE,RCT,RCC/X2/T,RT,Q,R1,R2,IP,WC/X3/Z1R,Z1I
 4*          DP = -0.001
 5*          T = 3.1415927 * ANGLE / 180
 6*          WRITE(6,1000) CM, SVN, GAM, ANGLE, RCT, RCC
 7*          DO 10 N = 1, NWC
 8*          IF(N .GT. 1) GO TO 15
 9*          GO TO 25
10*      15  IF(N .GT. 2) GO TO 20
11*          IWC = 10 * WC
12*          WC = IWC/10.0 + DWC
13*          GO TO 25
14*      20  WC = WC + DWC
15*      25  RT =(CM**0.5)*((1+ (GAM-1)*CM*CM/2)**((-GAM-1)/(4*(GAM-1)))
16*       1      )*((2/(GAM+1))**((-GAM-1)/(4*(GAM-1))))
17*          Q = (0.25*RT)*((2/(GAM+1))**((GAM+1)/(4*(GAM-1))))
18*          PHIR = 1
19*          PHII = 0
20*          R1 = RT + RCT*(1 - COS(T))
21*          R2 = 1 - RCC*(1 - COS(T))
22*          R = RT
23*          P = 0
24*          U = 2 / (GAM+1)
25*          SRTR = (RT * RCT)**0.5
26*          A1R = -4 /((GAM+1)*SRTR)
27*          BOR = -A1R
28*          BOI = 4 * WC /(GAM+1)
29*          SVNR = SVN/RT
30*          COR = WC * WC -((SVNR*SVNR) * 2 / (GAM+1))
31*          COI = -2 * WC * (GAM-1) / ((GAM+1)*SRIR)
32*          B1R = (24 + 4*GAM)/(3*RCT*RT*(GAM+1))
33*          B1I = -8 * WC / (SRTR*(GAM+1))
34*          C1R = 2 * (GAM - 1) * SVNR * SVNR /(SRTR * (GAM+1))
35*          C1I = -B1R * WC * (GAM - 1) * 0.5
36*          ZOR = (BOR*COR + BOI*COI) / (BOR*BOR + BOI*BOI)
37*          ZOI = (BOR*COI - BOI*COR) / (BOR*BOR + BOI*BOI)
38*          F1 = B1R*ZOR - B1I*ZOI - ZOR*ZOR*A1R + A1R*ZOI*ZOI - C1R
39*          F2 = B1I*ZOR + B1R*ZOI - 2*A1R*ZOI*ZOR - C1I
40*          Z1R = (F1*(A1R - BOR) - F2*BOI) / ((A1R-BOR)*(A1R-BOR) +
41*       1              BOI*BOI)
42*          Z1I = (F2*(A1R - BOR) + F1*BOI) / ((A1R-BOR)*(A1R-BOR) +
43*       1              BOI*BOI)
44*          C = U
45*          G(1) = U
46*          G(2) = ZOR
47*          G(3) = ZOI
48*          G(4) = PHIR * ZOR - PHII * ZOI
49*          G(5) = PHII * ZOR + ZOI * PHIR
50*          DY(1,1) = -A1R
51*          DY(2,1) = Z1R
52*          DY(3,1) = Z1I
53*          DY(4,1) = PHIR
54*          DY(5,1) = PHII
55*          IQZ = 2
56*          DO 30 I = 2,4
57*          CALL RKTZ(5,DP,P,G,GP,IQZ)
```

Table 7. Continued

```
58*                          P = P + DP
59*                          U = G(1)
60*                        ZR = G(2)
61*                        ZI = G(3)
62*                      PHIR = G(4)
63*                      PHII = G(5)
64*                    DY(1,I) = GP(1)
65*                    DY(2,I) = GP(2)
66*                    DY(3,I) = GP(3)
67*                    DY(4,I) = GP(4)
68*        30          DY(5,I) = GP(5)
69*                 Y(1) = U
70*                 Y(2) = ZR
71*                 Y(3) = ZI
72*                 Y(4) = PHIR
73*                 Y(5) = PHII
74*                 CALL ZADAMS(5,DP,P,Y,DY,IQZ)
75*                 IF(IP .EQ. 1) GO TO 10
76*                 U = Y(1)
77*                 ZR = Y(2)
78*                 ZI = Y(3)
79*        PHIR = Y(4)
80*        PHII = Y(5)
81*                 QBAR = U**0.5
82*                 C = 1 - U*0.5*(GAM-1)
83*                 RHO = C**(2/(GAM-1))
84*                 F = QBAR / (GAM*RHO)
85*                 IF(IQZ .EQ. 1) GO TO 35
86*                 ZDN = (U*U*ZR*ZR) + (WC+U*ZI)*(WC+U*ZI)
87*                 YR = -(U*(ZR*ZR + ZI*ZI) + WC*ZI) * F / ZDN
88*                 YI = F * WC * ZR / ZDN
89*                 GO TO 40
90*        35       TR = Y(2)
91*                 TI = Y(3)
92*                 TDN = (U - WC*TI)*(U - WC*TI) + (WC*TR)*(WC*TR)
93*                 YR = -F * (U - WC*TI) / TDN
94*                 YI = F * WC * TR / TDN
95*        40       SYR = GAM*((1+(GAM-1)*CM*CM*0.5)**((-GAM-1)/(2*(GAM-1))))*YR
96*                 SYI = GAM*((1+(GAM-1)*CM*CM*0.5)**((-GAM-1)/(2*(GAM-1))))*YI
97*                 W = WC *(C**-.5)
98*                 WRITE(6,1005) WC, YR, YI, W, SYR, SYI
99*        10 CONTINUE
100*        1000 FORMAT(1H1, 45X, 30HTHEORETICAL NOZZLE ADMITTANCES, //, 38X,
101*        1            14HMACH NUMBER = , F3.2, 7H SVN = , F6.4, 9H GAMMA = , F3.1
102*        2 , //, 22X, 15HNOZZLE ANGLE = , F4.1, 2X, 21HRADII OF CURVATURE:
103*        3            , 9HTHROAT = , F6.4, 12H ENTRANCE = , F6.4, //, 34X, 2HWC,
104*        4            7X, 2HYR, 8X, 2HYI, 8X, 1HW, 8X, 3HSYR, 8X, 3HSYI, /)
105*        1005 FORMAT(31X, F6.4, 5F10.5)
106*             RETURN
107*             END
```

Table 7. Continued

```
1*        SUBROUTINE RKTZ(NU, H, T1, U, DUM, JOPT)
2*        COMMON/X2/T,RT,G,R1,R2,IP,WC
3*        DIMENSION U(5), A(5), UZ(5), FZ(4,5),DUM(5)
4*        A(1) = 0
5*        A(2) = 0
6*        A(3) = 0.5
7*        A(4) = 0.5
8*        A(5) = 1.0
9*        TZ = T1
10*       DO 10 J = 1, NU
11*          UZ(J) = U(J)
12*   10     DUM(J) = FZ(1,J)
13*       IF(JOPT .EQ. 2) GO TO 15
14*       CALL RKTDIF(TZ,UZ,DUM)
15*       GO TO 20
16*   15 CALL RKZDIF(TZ,UZ,DUM)
17*   20 DO 25 J = 1, NU
18*   25    FZ(1,J) = DUM(J)
19*       DO 30 I = 2,4
20*          TZ = T1 + A(I+1)*H
21*          DO 35 J = 1, NU
22*             UZ(J) = U(J) + A(I+1)*H*FZ(I-1,J)
23*   35        DUM(J) = FZ(I,J)
24*          IF(JOPT .EQ. 2) GO TO 40
25*          CALL RKTDIF(TZ,UZ,DUM)
26*          GO TO 45
27*   40     CALL RKZDIF(TZ,UZ,DUM)
28*   45     DO 50 J = 1, NU
29*   50        FZ(I,J) = DUM(J)
30*   30 CONTINUE
31*       DO 55 J = 1, NU
32*   55     U(J) = U(J) + H*(FZ(1,J)+2*(FZ(2,J)+FZ(3,J))+FZ(4,J)) / 6.0
33*       GO TO (60,65),JOPT
34*   60 CALL RKTDIF(TZ,U ,DUM)
35*       GO TO 70
36*   65 CALL RKZDIF(TZ,U ,DUM)
37*   70 IF(IP.EQ.0) GO TO 75
38*       PR = WC*U(5)- U(1)*DUM(4)
39*       PI = -WC*U(4) - U(1)*DUM(5)
40*       PMAG = SQRT(PR*PR + PI*PI)
41*       PARG = ATAN(PI/PR)
42*       WRITE(6,1000) TZ, PMAG, PARG
43* 1000 FORMAT(46X, F6.4, 1X, F10.5, 3X, F10.5)
44*   75 RETURN
45*       END
```

Table 7. Continued

```
 1*       SUBROUTINE RKZDIF(P,G,GP)
 2*       COMMON/X1/GAM,SVN,ANGLE,RCT,RCC/X2/T,RT,Q,R1,R2,IP,WC/X3/Z1R,Z1I
 3*       DIMENSION G(5), GP(5)
 4*          U = G(1)
 5*          ZR = G(2)
 6*          ZI = G(3)
 7*       PHIR = G(4)
 8*       PHII = G(5)
 9*       IF(P) 15, 10, 15
10*   10  GP(1) = 4/((GAM+1)*((RCT*RT)**0.5))
11*       GP(2) = Z1R
12*       GP(3) = Z1I
13*       GP(4) = Z1R
14*       GP(5) = Z1I
15*       GO TO 20
16*   15     C = 1 - (GAM - 1) * U * 0.5
17*          R = Q * ((C)**(-1/(2*(GAM-1)))) * (U**-0.25) *4.0
18*       IF(R-1) 22, 22, 50
19*   22  IF(R - R1) 25, 30, 30
20*   25     DR = -((2*RCT*(R-RT) - (R-RT)*(R-RT))**0.5)/(RT+RCT-R)
21*       GO TO 45
22*   30  IF(R-R2) 35, 40, 40
23*   35     DR = -TAN(T)
24*       GO TO 45
25*   40     DR = ((2*RCC*(1-R) - (R-1)*(R-1))**0.5)/(1-R-RCC)
26*   45     DU = -(U**0.75)*(C**((2*GAM-1)/(2*(GAM-1))))/(Q*(1-(GAM+1)*U*.5)
27*          )
28*       GP(1)= DU*DR
29*       GO TO 55
30*   50  GP(1) = 0
31*   55     A = U*(C-U)
32*       BR = U*GP(1)/C
33*       BI = 2*WC*U
34*       CR = WC*WC - SVN*SVN*C/(R*R)
35*       CI = -(GAM-1)*WC*U*GP(1)*0.5*(1/C)
36*       GP(2)= ((BR*ZR - BI*ZI - CR) / A) - ZR*ZR + ZI*ZI
37*       GP(3)= ((BI*ZR + BR*ZI - CI) / A) - 2*ZR*ZI
38*       GP(4)= ZR*PHIR - ZI*PHII
39*       GP(5)= ZR*PHII + ZI*PHIR
40*   20  RETURN
41*       END
```

Table 7. Continued

```
1*          SUBROUTINE RKTDIF(P,G,GP)
2*          COMMON/X1/GAM,SVN,ANGLE,RCT,RCC/X2/T,RT,Q,R1,R2,IP,WC
3*          DIMENSION G(5), GP(5)
4*              U = G(1)
5*              TR = G(2)
6*              TI = G(3)
7*          PHIR = G(4)
8*          PHII = G(5)
9*              C = 1 - (GAM-1)*U*0.5
10*             R = Q * ((C)**(-1/(2*(GAM-1)))) * (U**-0.25) *4.0
11*         IF(R-1) 22,22,50
12*      22 IF(R-R1) 25, 30, 30
13*      25    DR = -((2*RCT*(R-RT) - (R-RT)*(R-RT))**0.5)/(RT+RCT-R)
14*             GO TO 45
15*      30 IF(R-R2) 35,40,40
16*      35    DR = -TAN(T)
17*          GO TO 45
18*      40    DR = ((2*RCC*(1-R) - (R-1)*(R-1))**0.5)/(1-R-RCC)
19*      45    DU = -(U**0.75)*(C**((2*GAM-1)/(2*(GAM-1)))) / (Q*(1-(GAM+1)*U*
20*      1        0.5))
21*          GP(1)= DU*DR
22*          GO TO 55
23*      50 GP(1) = 0
24*      55    A = U*(C-U)
25*             BR = U*GP(1)/C
26*          BI = 2*WC*U
27*          CR = WC*WC - (SVN*SVN*C)/(R*R)
28*          CI = -(GAM-1)*WC*U*GP(1)*0.5/C
29*          GP(2)= 1 - ((BR*TR-BI*TI) - (CR*(TR*TR-TI*TI)-2*CI*TR*TI))/ A
30*          GP(3)= (-BR*TI - BI*TR + CI*(TR*TR-TI*TI) + 2*CR*TR*TI) /A
31*             T2 = TR*TR + TI*TI
32*          GP(4)= (TR*PHIR - TI*PHII)/T2
33*          GP(5)= (TR*PHII + TI*PHIR)/T2
34*          RETURN
35*          END
```

Table 7. Continued

```
 1*           SUBROUTINE ZADAMS(N,H,X,Y,DY,IQZ)
 2*           COMMON/X1/GAM,SVN,ANGLE,RCT,RCC/X2/T,RT,Q,R1,R2,IP,WC
 3*           COMMON/X4/ CM
 4*           DIMENSION COR(5), DP(5), DY(5,4), PRED(5), Y(5), G(5), GP(5)
 5*       10  CONTINUE
 6*           DO 15 I = 1,N
 7*               PRED(I) = Y(I)+H*(55.*DY(I,4)-59.*DY(I,3)+37.*DY(I,2)-9.*DY(I,1)
 8*          1                         )/24.0
 9*       15  CONTINUE
10*               X = X+H
11*               U = PRED(1)
12*               ZR = PRED(2)
13*               ZI = PRED(3)
14*           PHIR = PRED(4)
15*           PHII = PRED(5)
16*               C = 1 - (GAM-1)*U*0.5
17*               R = Q * ((C)**(-1/(2*(GAM-1)))) * (U**-0.25) **4.0
18*           IF(R-1) 17,17,100
19*       17  IF(R-R1) 20, 25, 25
20*       20  DR = -((2*RCT*(R-RT)-(R-RT)*(R-RT))**0.5) / (RT+RCT-R)
21*           GO TO 40
22*       25  IF(R-R2) 30, 35, 35
23*       30  DR = -TAN(T)
24*           GO TO 40
25*       35  DR = ((2*RCC*(1-R) - (1-R)*(1-R))**0.5) / (1-R-RCC)
26*       40  DU = -(U**0.75)*(C**((2*GAM-1)/(2*(GAM-1))))/(Q*(1-(GAM+1)*U*0.5
27*          1                  ))
28*           DP(1)= DR*DU
29*               A = U*(C-U)
30*           BR = U*DP(1)/C
31*           BI = 2*WC*U
32*           CR = WC*WC - (SVN*SVN*C)/(R*R)
33*           CI = -(GAM-1)*WC*U*DP(1)*0.5/C
34*           DP(2)= ((BR*ZR - BI*ZI - CR)/A) - ZR*ZR + ZI*ZI
35*           DP(3)= ((BI*ZR + BR*ZI - CI)/A) - 2*ZR*ZI
36*           DP(4)= ZR*PHIR - ZI*PHII
37*           DP(5)= ZR*PHII + ZI*PHIR
38*           DO 45 I = 1,N
39*               COR(I) = Y(I)+H*(DY(I,2)-5.*DY(I,3)+19.*DY(I,4)+9.*DP(I))/24.0
40*       45      Y(I) = (251.*COR(I) + 19.*PRED(I)) / 270.
41*               U = Y(1)
42*               ZR = Y(2)
43*               ZI = Y(3)
44*           PHIR = Y(4)
45*           PHII = Y(5)
46*               C = 1 - (GAM-1)*U*0.5
47*       52  DO 55 I = 1,N
48*               DY(I,1) = DY(I,2)
49*               DY(I,2) = DY(I,3)
50*       55      DY(I,3) = DY(I,4)
51*               ZMAG = (ZR*ZR + ZI*ZI)**0.5
52*           IF(ZMAG - 10 ) 60, 90, 90
53*       60      R = Q * ((C)**(-1/(2*(GAM-1)))) * (U**-0.25) **4.0
54*           IF(R-1) 62, 62, 100
55*       62  IF(R-R1) 65,70,70
56*       65  DR = -((2*RCT*(R-RT) - (R-RT)*(R-RT))**0.5)/(RT+RCT-R)
57*           GO TO 85
```

Table 7. Continued

```
 58*          7o IF(R-R2) 75,80,80
 59*          75    DR = -TAN(T)
 60*             GO TO 85
 61*          80    DR = ((2*RCC*(1-R) - (1-R)*(1-R))**0.5)/(1-R-RCC)
 62*          85    DU = -(U**0.75)*(C**((2*GAM-1)/(2*(GAM-1)))))/(Q*(1-(GAM+1)*U/2))
 63*                DY(1,4)= DR*DU
 64*                A = U*(C-U)
 65*                BR = U*DY(1,4)/C
 66*                BI = 2*WC*U
 67*                CR = WC*WC - (SVN*SVN*C)/(R*R)
 68*                CI = -(GAM-1)*WC*U*DY(1,4)*0.5/C
 69*          DY(2,4)= (BR*ZR - BI*ZI -CR)/A - ZR*ZR + ZI*ZI
 70*          DY(3,4)= (BI*ZR + BR*ZI -CI)/A - 2*ZR*ZI
 71*          DY(4,4)= ZR*PHIR - ZI*PHII
 72*          DY(5,4)= ZR*PHII + ZI*PHIR
 73*             IF(IP .EQ. 0) GO TO 87
 74*                PR = WC*PHII - U*DY(4,4)
 75*                PI = -WC*PHIR -U*DY(5,4)
 76*                PMAG = (PR*PR + PI*PI)**.5
 77*             PARG = ATAN(PI/PR)
 78*             WRITE(6,1000) X, PMAG, PARG
 79*          87 GO TO 10
 80*          9o IQZ = 1
 81*                Z2 = ZMAG*ZMAG
 82*                Y(2) = ZR/Z2
 83*                Y(3) = -ZI/Z2
 84*                ZPR = DY(2,4)
 85*                ZPI = DY(3,4)
 86*                DY(2,4)= -(ZPR*(ZR*ZR - ZI*ZI) + 2*ZR*ZI*ZPI)/(Z2*Z2)
 87*             DY(3,4)= (2*ZPR*ZR*ZI - ZPI*(ZR*ZR - ZI*ZI))/(Z2*Z2)
 88*                G(1) = U
 89*             G(2) = Y(2)
 90*             G(3) = Y(3)
 91*             G(4) = PHIR
 92*             G(5) = PHII
 93*          DY(1,1)= DY(1,4)
 94*          DY(2,1)= DY(2,4)
 95*          DY(3,1)= DY(3,4)
 96*          DY(4,1)= PHIR*ZR - PHII*ZI
 97*          DY(5,1)= PHII*ZR + PHIR*ZI
 98*          DO 95 I = 2,4
 99*             CALL RKTZ(5,H,X,G,GP,IQZ)
100*                X = X+H
101*                U = G(1)
102*                TR = G(2)
103*                TI = G(3)
104*                PHIR = G(4)
105*                PHII = G(5)
106*                DY(1,I) = GP(1)
107*                DY(2,I) = GP(2)
108*                DY(3,I) = GP(3)
109*                DY(4,I) = GP(4)
110*          95    DY(5,I) = GP(5)
111*                Y(1) = U
112*                Y(2) = TR
113*                Y(3) = TI
114*                Y(4) = PHIR
```

Table 7. Continued

```
115*             Y(5) = PHII
116*_____CALL TADAMS(N,H,X,Y,DY,IGZ,IQ)_____
117*             GO TO (10, 100),IQ
118*_____1000 FORMAT(46X,F6.4,1X,F10.5,3X,F10.5)_____
119*        100 RETURN
120*_____END_____
```

Table 7. Continued

```
1*        SUBROUTINE TADAMS(N,H,X,Y,DY,IQZ,IQ)
2*        COMMON/X1/GAM,SVN,ANGLE,RCT,RCC/X2/T,RT,Q,R1,R2,IP,WC
3*        COMMON/X4/ CM
4*        DIMENSION COR(5),DP(5),DY(5,4),PRED(5),Y(5),G(5),GP(5)
5*     10 CONTINUE
6*        DO 15 I = 1,N
7*        PRED(I) = Y(I)+H*(55*DY(I,4)-59.*DY(I,3)+37.*DY(I,2)-9*DY(I,1))/
8*     1            24.0
9*     15 CONTINUE
10*       X = X+H
11*       U = PRED(1)
12*       TR = PRED(2)
13*       TI = PRED(3)
14*       PHIR = PRED(4)
15*       PHII = PRED(5)
16*       C = 1 - (GAM-1)*U*.5
17*       R = Q * ((C)**(-1/(2*(GAM-1)))) * (U**-0.25) *4.0
18*       IF(R-1) 17,17,100
19*    17 IF(R-R1) 20, 25, 25
20*    20 DR = -((2*RCT*(R-RT) - (R-RT)*(R-RT))**.5)/(RT+RCT-R)
21*       GO TO 40
22*    25 IF(R-R2) 30, 35, 35
23*    30 DR = -TAN(T)
24*       GO TO 40
25*    35 DR = ((2*RCC*(1-R) - (1-R)*(1-R))**.5)/(1-R-RCC)
26*    40 DU =-(U**.75)*(C**((2*GAM-1)/(2*(GAM-1))))/(Q*(1-(GAM+1)*U*.5))
27*       DP(1)= DR*DU
28*       A = U*(C-U)
29*       BR = U*DP(1)/C
30*       BI = 2*WC*U
31*       CR = WC*WC - (SVN*SVN*C)/(R*R)
32*       CI = -(GAM-1)*WC*U*DP(1)*.5/C
33*       DP(2)= 1 + (-BR*TR+BI*TI+CR*(TR*TR-TI*TI)-2*CI*TR*TI)/A
34*       DP(3)= (-BR*TI - BI*TR + CI*(TR*TR - TI*TI) + 2*CR*TR*TI)/A
35*       T2 = TR*TR + TI*TI
36*       DP(4)= (TR*PHIR - TI*PHII)/T2
37*       DP(5)= (TR*PHII + TI*PHIR)/T2
38*       DO 45 I = 1,N
39*       COR(I) = Y(I)+H*(DY(I,2)-5.*DY(I,3)+19.*DY(I,4)+9.*DP(I))/24.0
40*    45 Y(I) = (251.*COR(I) + 19.*PRED(I))/270.
41*       U = Y(1)
42*       TR = Y(2)
43*       TI = Y(3)
44*       PHIR = Y(4)
45*       PHII = Y(5)
46*       C = 1 - (GAM-1)*U*.5
47*    52 DO 55 I = 1,N
48*       DY(I,1) = DY(I,2)
49*       DY(I,2) = DY(I,3)
50*    55 DY(I,3) = DY(I,4)
51*       T2 = TR*TR + TI*TI
52*       TMAG = T2**.5
53*       IF(TMAG - 10.) 60, 90, 90
54*    60 R = Q * ((C)**(-1/(2*(GAM-1)))) * (U**-0.25) *4.0
55*       IF(R-1) 62, 62, 100
56*    62 IF(R-R1) 65,70,70
57*    65 DR = -((2*RCT*(R-RT)-(R-RT)*(R-RT))**.5)/(RT+RCT-R)
```

Table 7. Continued

```
58*          GO TO 85
59*      70  IF(R-R2) 75,80,80
60*      75  DR = -TAN(T)
61*          GO TO 85
62*      80  DR = ((2*RCC*(1-R) - (1-R)*(1-R))**.5)/(1-R-RCC)
63*      85  DU = -(U**.75)*(C**((2*GAM-1)/(2*(GAM-1))))/(Q*(1-(GAM+1)*U**.5))
64*          DY(1,4)= DR*DU
65*          A = U*(C-U)
66*          BR = U*DY(1,4)/C
67*          BI = 2*WC*U
68*          CR = WC*WC - (SVM*SVN*C)/(R*R)
69*          CI = -(GAM-1)*WC*U*DY(1,4)*0.5/C
70*          DY(2,4)= 1 + (-BR*TR + BI*TI + CR*(TR*TR - TI*TI) - 2*CI*TR*TI)/A
71*          DY(3,4)= (-BR*TI - BI*TR + CI*(TR*TR - TI*TI) + 2*CR*TR*TI)/A
72*          DY(4,4)= (TR*PHIR - PHII*TI)/T2
73*          DY(5,4)= (TR*PHII + PHIR*TI)/T2
74*          IF(IP .EQ. 0) GO TO 87
75*          PR = WC*PHII - U*DY(4,4)
76*          PI = -WC*PHIR- U*DY(5,4)
77*          PMAG = (PR*PR + PI*PI)**.5
78*          PARG = ATAN(PI/PR)
79*          WRITE(6,1000) X, PMAG, PARG
80*      87  GO TO 10
81*      90  IQZ = 2
82*          Y(2) = TR/T2
83*          Y(3) = -TI/T2
84*          TPR = DY(2,4)
85*          TPI = DY(3,4)
86*          DY(2,4)= -(TPR*(TR*TR - TI*TI) + 2*TR*TI*TPI)/(T2*T2)
87*          DY(3,4)= (2*TPR*TR*TI - TPI*(TR*TR - TI*TI))/(T2*T2)
88*          G(1) = U
89*          G(2) = Y(2)
90*          G(3) = Y(3)
91*          G(4) = PHIR
92*          G(5) = PHII
93*          DY(1,1)= DY(1,4)
94*          DY(2,1)= DY(2,4)
95*          DY(3,1)= DY(3,4)
96*          DY(4,1)= (PHIR*TR - PHII*TI)/T2
97*          DY(5,1)= (PHII*TR - PHIR*TI)/T2
98*          DO 95 I = 2,4
99*          CALL RKTZ(5,H,X,G,GP,IQZ)
100*          X = X+H
101*          U = G(1)
102*          ZR = G(2)
103*          ZI = G(3)
104*          PHIR = G(4)
105*          PHII = G(5)
106*          DY(1,I) = GP(1)
107*          DY(2,I) = GP(2)
108*          DY(3,I) = GP(3)
109*          DY(4,I) = GP(4)
110*      95  DY(5,I) = GP(5)
111*          Y(1) = U
112*          Y(2) = ZR
113*          Y(3) = ZI
114*          Y(4) = PHIR
```

Table 7. Concluded

```
115*          Y(5) = PHII
116*             IO  = 1
117*          GO TO 105
118*      10n   IO = 2
119*      100g FORMAT(46X, F6.4, 1X, F10.5, 3X, F10.5)
120*      105 RETURN
121*          END
```

Table 8. Sample Output

THEORETICAL NOZZLE ADMITTANCES					
MACH NUMBER = .08 SVN = 1.8413 GAMMA = 1.4					
NOZZLE ANGLE = 15.0 RADII OF CURVATURE: THROAT = 1.0000 ENTRANCE = 1.0000					
WC	YR	YI	W	SYR	SYI
1.8342	-.06449	-.24904	1.83539	-.08994	-.34732
1.8500	-.06382	-.23679	1.85118	-.08901	-.33023
1.9000	-.06192	-.19768	1.90122	-.08635	-.27569
1.9500	-.06033	-.15789	1.95125	-.08414	-.22020
2.0000	-.05907	-.11708	2.00128	-.08238	-.16329
2.0500	-.05816	-.07486	2.05131	-.08111	-.10440
2.1000	-.05764	-.03072	2.10134	-.08038	-.04285
2.1500	-.05755	.01594	2.15138	-.08027	.02224
2.2000	-.05800	.06595	2.20141	-.08089	.09198
2.2500	-.05913	.12037	2.25144	-.08246	.16787
2.3000	-.06114	.18070	2.30147	-.08527	.25201
2.3500	-.06639	.28256	2.35150	-.09258	.39407
2.4000	-.06951	.32969	2.40154	-.09694	.45840
2.4500	-.07752	.42460	2.45157	-.10812	.59216
2.5000	-.09052	.54529	2.50160	-.12624	.76049
2.5500	-.11291	.70627	2.55163	-.15747	.98499
2.6000	-.15565	.93913	2.60166	-.21707	1.30974
2.6500	-.25250	1.31936	2.65170	-.35214	1.84003
2.7000	-.55404	2.07611	2.70173	-.77269	2.89542
2.7500	-2.48186	4.07119	2.75176	-3.46130	5.67783
2.8000	-5.34227	-4.66059	2.80179	-7.45054	-6.49983
2.8500	-.71330	-2.42480	2.85182	-.99480	-3.38172
2.9000	-.25175	-1.38285	2.90185	-.35111	-1.92857
2.9500	-.13284	-.90379	2.95189	-.18527	-1.26046
3.0000	-.08644	-.61995	3.00192	-.12065	-.86461
3.0500	-.06388	-.42272	3.05195	-.08909	-.58954
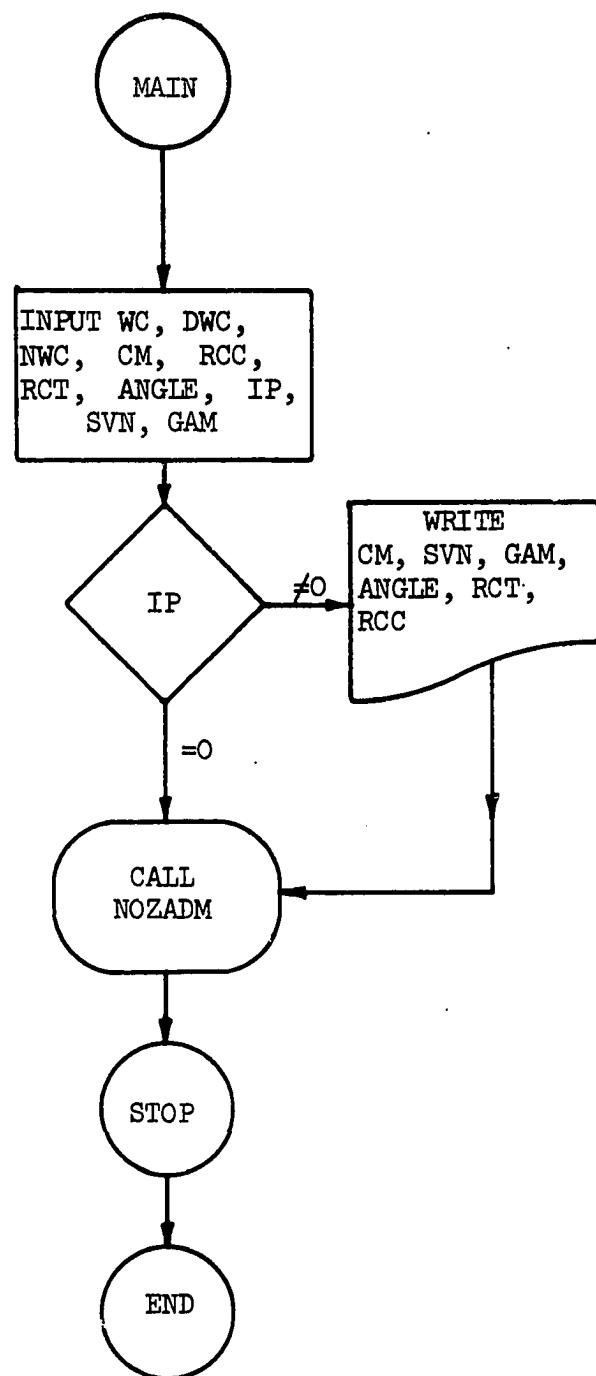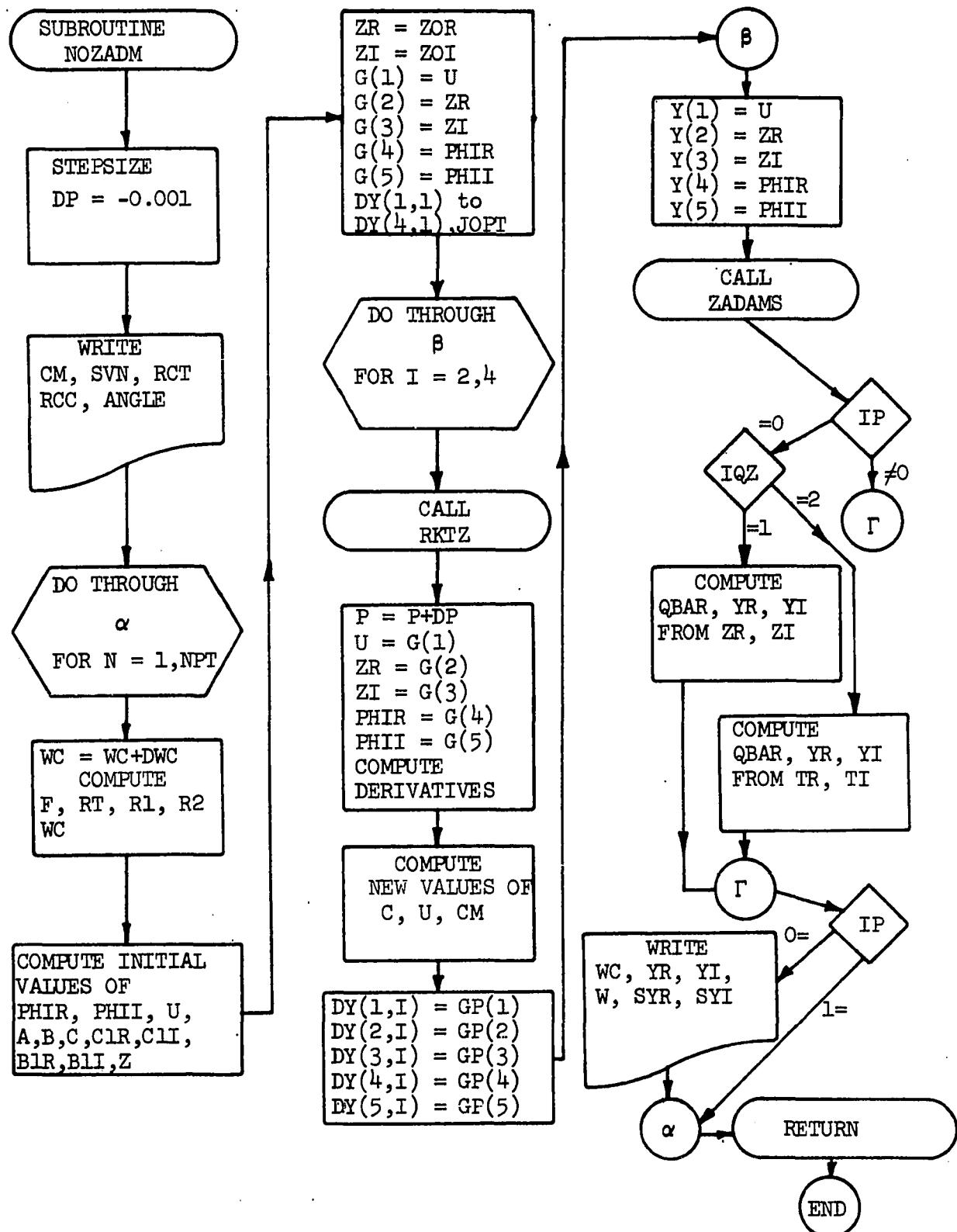
Figure 45. Flow Chart for the Nozzle Admittance Program.

Figure 45. Continued

SUBROUTINE
NOZADM

STEPSIZE
DP = -0.001

WRITE
CM, SVN, RCT
RCC, ANGLE

DO THROUGH
α
FOR N = 1,NPT

WC = WC+DWC
COMPUTE
F, RT, R1, R2
WC

COMPUTE INITIAL
VALUES OF
PHIR, PHII, U,
A,B,C,C1R,C1I,
B1R,B1I,Z

ZR = ZOR
ZI = ZOI
G(1) = U
G(2) = ZR
G(3) = ZI
G(4) = PHIR
G(5) = PHII
DY(1,1) to
DY(4,1).JOPT

DO THROUGH
β
FOR I = 2,4

CALL
RKTZ

P = P+DP
U = G(1)
ZR = G(2)
ZI = G(3)
PHIR = G(4)
PHII = G(5)
COMPUTE
DERIVATIVES

COMPUTE
NEW VALUES OF
C, U, CM

DY(1,I) = GP(1)
DY(2,I) = GP(2)
DY(3,I) = GP(3)
DY(4,I) = GP(4)
DY(5,I) = GP(5)

β

Y(1) = U
Y(2) = ZR
Y(3) = ZI
Y(4) = PHIR
Y(5) = PHII

CALL
ZADAMS

IP

IQZ

=0

≠0

Γ

=1

=2

COMPUTE
QBAR, YR, YI
FROM ZR, ZI

COMPUTE
QBAR, YR, YI
FROM TR, TI

Γ

WRITE
WC, YR, YI,
W, SYR, SYI

IP

0=

1=

α

RETURN

END

Figure 45. Continued

Figure 45. Continued

Figure 45. Continued

Figure 45. Continued

Figure 45. Sontinued
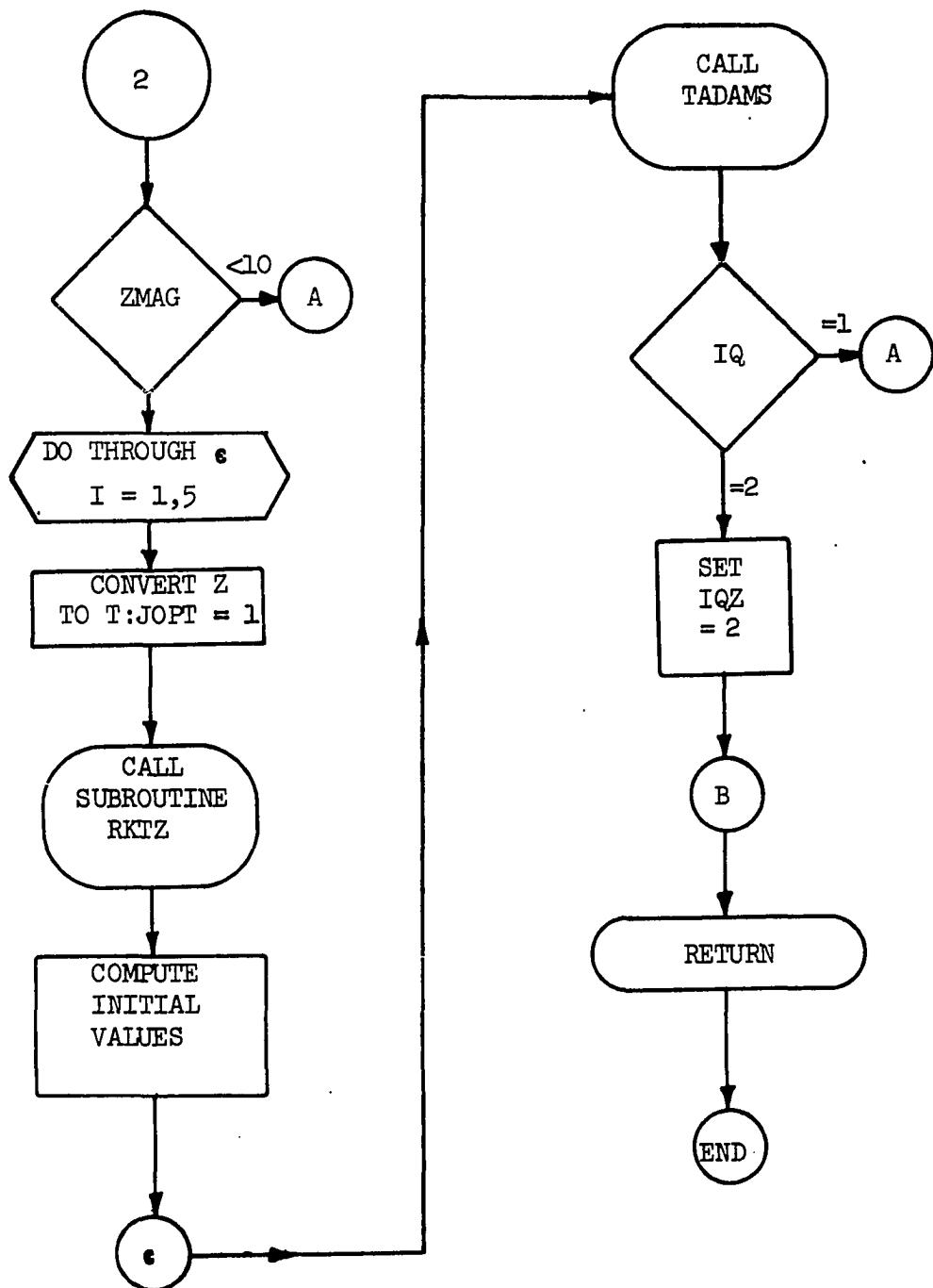
Figure 45. Continued
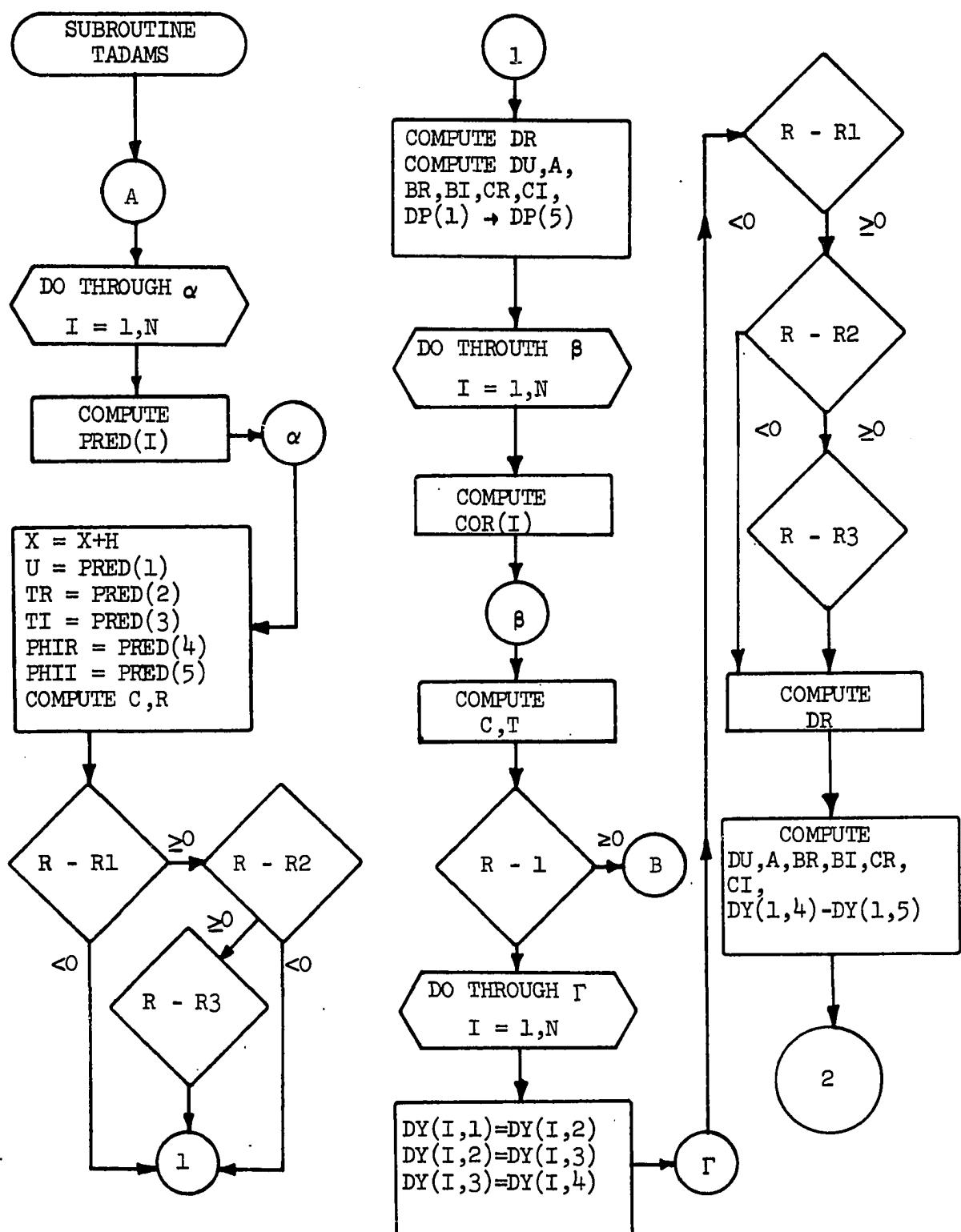
Figure 45. Continued
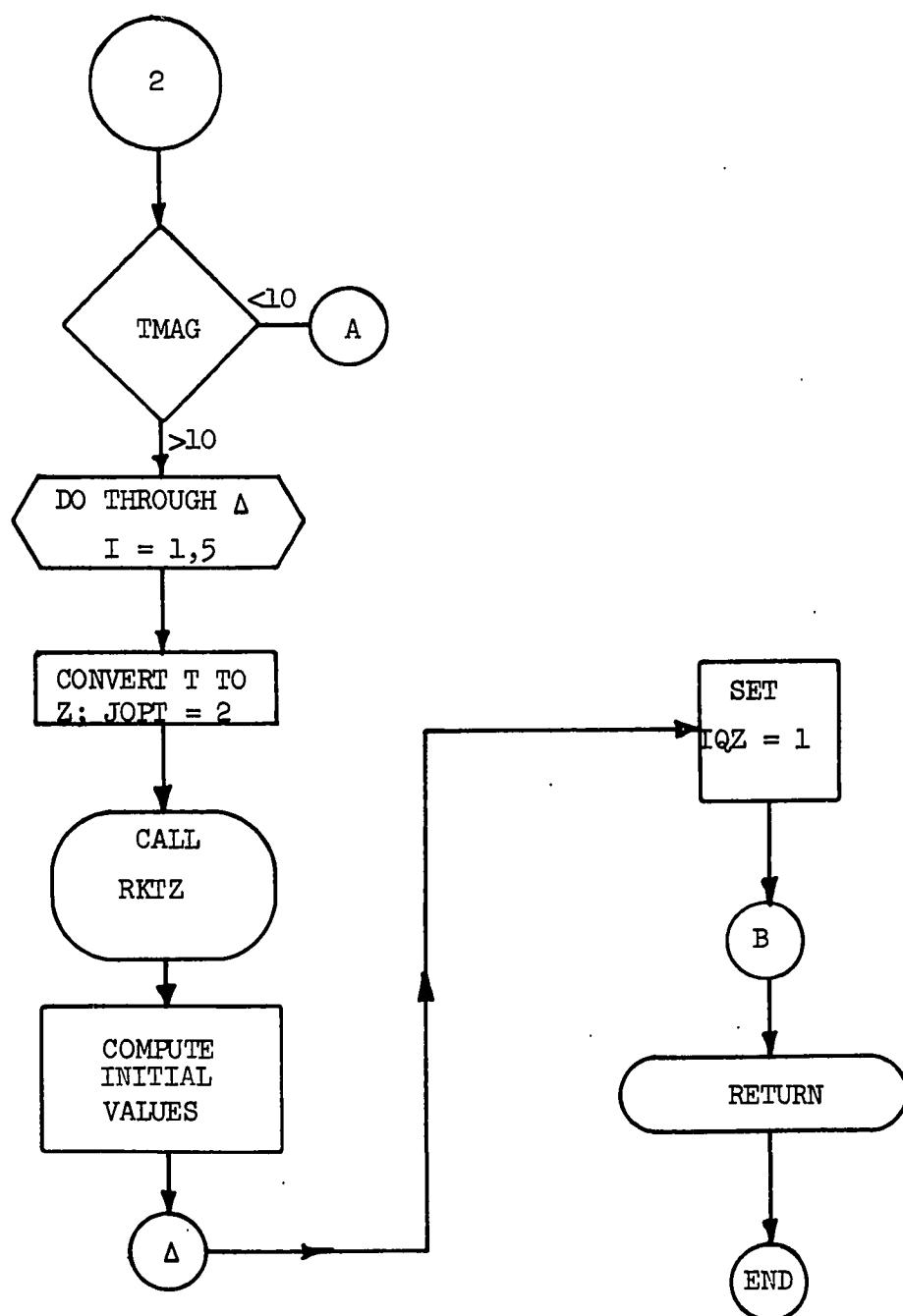
Figure 45. Concluded

APPENDIX B

THEORETICAL NOZZLE ADMITTANCE VALUES

Table 9. Theoretical Nozzle Admittances

Chamber Mach Number = 0.08, S_{mn} = 0, γ = 1.4, θ_1 = 15°

Radii of Curvature: Throat = 1.0, Entrance = 1.0

.00000	.00000	.00000
.05003	.01662	.06567
.10006	.01836	.13213
.15010	.02142	.20024
.20013	.02605	.27091
.25016	.03266	.34520
.30019	.04185	.42438
.35022	.05460	.50999
.40026	.07235	.60396
.45029	.09741	.70874
.50032	.13350	.82745
.55035	.18677	.96390
.60038	.26777	1.12237
.65042	.39497	1.30583
.70045	.60071	1.51057
.75048	.93749	1.70719
.80051	1.46357	1.79598
.85054	2.13195	1.56123
.90058	2.59206	.86614
.95061	2.49517	.07147
1.00064	2.05852	-.39064
1.05067	1.62237	-.53231
1.10070	1.29620	-.51180
1.15074	1.07163	-.42841
1.20077	.92033	-.32563
1.25080	.81966	-.22026
1.30083	.75471	-.11821
1.35086	.71623	-.02123
1.40090	.69861	.07042
1.45093	.69864	.15676
1.50096	.71468	.23759
1.55099	.74607	.31215
1.60102	.79274	.37886
1.65106	.85465	.43504
1.70109	.93120	.47681
1.75112	1.02027	.49912
1.80115	1.11715	.49649
1.85118	1.21379	.46454

Table 10. Theoretical Nozzle Admittances

Chamber Mach Number = 0.16, S_{mn} = 0, γ = 1.4, θ_1 = 30°

Radii of Curvature: Throat = 1.0, Entrance = 1.0

.00000	.00000	.00000
.05013	.03276	.04082
.10026	.03380	.08176
.15038	.03556	.12295
.20051	.03807	.16453
.25064	.04139	.20661
.30077	.04558	.24934
.35089	.05072	.29285
.40102	.05692	.33728
.45115	.06431	.38278
.50128	.07305	.42951
.55141	.08335	.47763
.60153	.09542	.52729
.65166	.10957	.57866
.70179	.12613	.63189
.75192	.14550	.68714
.80205	.16820	.74455
.85217	.19481	.80421
.90230	.22603	.86617
.95243	.26272	.93041
1.00256	.30587	.99678
1.05268	.35665	1.06496
1.10281	.41639	1.13436
1.15294	.48662	1.20407
1.20307	.56895	1.27269
1.25320	.67946	1.35720
1.30332	.77641	1.39769
1.35345	.90409	1.44750
1.40358	1.04825	1.48285
1.45371	1.20765	1.49814
1.50383	1.37893	1.48740
1.55396	1.55620	1.44508
1.60409	1.73094	1.36740
1.65422	1.89266	1.25370
1.70435	2.03043	1.10754
1.75447	2.13503	.93671
1.80460	2.20085	.75216
1.85473	2.22695	.56584

Table 11. Theoretical Nozzle Admittances

Chamber Mach Number = 0.08, S_{mn} = 0, γ = 1.4, θ_1 = 15°

Radii of Curvature: Throat = 0.4396, Entrance = 0.4396

.00000	.00000	.00000
.05003	.01657	.06196
.10006	.01818	.12462
.15010	.02100	.18874
.20013	.02523	.25512
.25016	.03121	.32469
.30019	.03947	.39855
.35022	.05079	.47803
.40026	.06635	.56479
.45029	.08798	.66092
.50032	.11859	.76910
.55035	.16293	.89268
.60038	.22895	1.03563
.65042	.33043	1.20177
.70045	.49162	1.39168
.75048	.75405	1.59234
.80051	1.17792	1.74711
.85054	1.79297	1.69780
.90058	2.41214	1.21261
.95061	2.58566	.38530
1.00064	2.24408	-.26297
1.05067	1.76741	-.53092
1.10070	1.37986	-.56116
1.15074	1.10824	-.49175
1.20077	.92491	-.38917
1.25080	.80226	-.27959
1.30083	.72133	-.17223
1.35086	.67025	-.06980
1.40090	.64185	.02738
1.45093	.63195	.11965
1.50096	.63843	.20733
1.55099	.66048	.29034
1.60102	.69829	.36786
1.65106	.75262	.43800
1.70109	.82430	.49743
1.75112	.91344	.54099
1.80115	1.01805	.56169
1.85118	1.13235	.55152

Table 12. Theoretical Nozzle Admittances

Chamber Mach Number = 0.08, S_{mn} = 0, γ = 1.4, θ_1 = 30°

Radii of Curvature: Throat = 0.4396, Entrance = 0.4396

.00000	.00000	.00000
.05003	.01619	.03400
.10006	.01661	.06818
.15010	.01733	.10240
.20013	.01835	.13702
.25016	.01969	.17205
.30019	.02139	.20761
.35022	.02348	.24383
.40026	.02600	.28082
.45029	.02900	.31874
.50032	.03256	.35773
.55035	.03675	.39796
.60038	.04168	.43960
.65042	.04748	.48286
.70045	.05430	.52797
.75048	.06234	.57518
.80051	.07183	.62478
.85054	.08308	.67707
.90058	.09647	.73242
.95061	.11248	.79124
1.00064	.13766	.89794
1.05067	.14786	.87444
1.10070	.18334	.99315
1.15074	.21807	1.07067
1.20077	.26094	1.15416
1.25080	.31426	1.24408
1.30083	.38109	1.34051
1.35086	.46540	1.44308
1.40090	.57236	1.55038
1.45093	.70850	1.65918
1.50096	.88149	1.76314
1.55099	1.09932	1.85100
1.60102	1.36768	1.90431
1.65106	1.68465	1.89635
1.70109	2.03235	1.79506
1.75112	2.36957	1.57478
1.80115	2.63566	1.23635
1.85118	2.77433	.82135

Table 13. Theoretical Nozzle Admittances

Chamber Mach Number = 0.08, S_{mn} = 0, γ = 1.4, θ_1 = 45°

Radii of Curvature : Throat = 0.4396, Entrance = 0.4396

.00000	.00000	.00000
.05003	$.016_12$	.02563
.10006	$.016_35$	.05131
.15010	$.016_73$	.07706
.20013	$.017_36$	.10292
.25016	$.017_96$	.12894
.30019	$.018_82$	.15515
.35022	$.019_87$	.18160
.40026	$.021_09$	.20833
.45029	$.022_52$	.23539
.50032	$.024_16$	.26281
.55035	$.026_03$	.29065
.60038	$.028_15$	.31896
.65042	$.030_55$	.34779
.70045	$.033_24$	.37720
.75048	$.036_26$	.40725
.80051	$.039_65$	.43800
.85054	$.043_44$	.46953
.90058	$.047_69$	.50191
.95061	$.052_44$	.53521
1.00064	$.057_76$	.56953
1.05067	.06372	.60495
1.10070	$.070_40$	.64157
1.15074	$.077_90$	.67951
1.20077	$.088_25$	.74202
1.25080	$.095_84$	.75974
1.30083	$.106_56$	.80243
1.35086	$.118_68$	.84687
1.40090	$.132_43$	.89332
1.45093	$.148_05$	.94191
1.50096	$.165_84$	.99285
1.55099	$.186_16$	1.04630
1.60102	$.209_44$	1.10245
1.65106	$.236_20$	1.16149
1.70109	$.267_03$	1.22360
1.75112	$.302_68$	1.28890
1.80115	$.344_03$	1.35760
1.85118	$.392_15$	1.42976

Table 14. Theoretical Nozzle Admittances

Chamber Mach Number = 0.16, S_{mn} = 0, γ = 1.4, θ_1 = 45°

Radii of Curvature: Throat = 0.4396, Entrance = 0.4396

.00000	.000$_n$0	.00000
.05013	.032$_5$4	.02535
.10026	.032$_9$4	.05074
.15038	.033$_6$1	.07618
.20051	.034$_5$5	.10171
.25064	.03577	.12735
.30077	.037$_2$8	.15313
.35089	.039$_0$8	.17909
.40102	.041$_2$0	.20525
.45115	.043$_6$5	.23165
.50128	.046$_4$4	.25831
.55141	.049$_6$0	.28527
.60153	.053$_1$4	.31256
.65166	.057$_1$0	.34021
.70179	.061$_5$1	.36825
.75192	.066$_4$0	.39673
.80205	.071$_8$0	.42568
.85217	.077$_7$6	.45512
.90230	.084$_3$3	.48511
.95243	.091$_5$6	.51568
1.00256	.099$_5$2	.54685
1.05268	.108$_2$7	.57868
1.10281	.117$_6$8	.61120
1.15294	.128$_4$4	.64445
1.20307	.140$_0$5	.67846
1.25320	.152$_8$1	.71326
1.30332	.166$_9$3	.74889
1.35345	.182$_2$6	.78537
1.40358	.199$_2$4	.82272
1.45371	.217$_9$2	.86097
1.50383	.238$_5$0	.90011
1.55396	.261$_1$8	.94013
1.60409	.286$_1$8	.98101
1.65422	.335$_3$1	1.03674
1.70435	.336$_4$0	1.04331
1.75447	.377$_7$2	1.10826
1.80460	.414$_7$4	1.15186
1.85473	.455$_5$8	1.19577

Table 15. Theoretical Nozzle Admittances

Chamber Mach Number = 0.20, S_{mn} = 0, γ = 1.4, θ_1 = 45°

Radii of Curvature: Throat = 0.4396, Entrance = 0.4396

.00000	.00000	.00000
.05020	.04096	.02519
.10040	.04143	.05041
.15060	.04222	.07568
.20080	.04334	.10101
.25100	.04478	.12644
.30120	.04656	.15199
.35140	.04869	.17767
.40160	.05119	.20353
.45180	.05405	.22957
.50200	.05731	.25582
.55220	.06099	.28232
.60240	.06510	.30907
.65259	.06967	.33611
.70279	.07473	.36347
.75299	.08031	.39115
.80319	.08645	.41920
.85339	.09318	.44763
.90359	.10055	.47647
.95379	.10861	.50574
1.00399	.11742	.53546
1.05419	.12702	.56565
1.10439	.13748	.59633
1.15459	.14889	.62752
1.20479	.16130	.65924
1.25499	.17482	.69149
1.30519	.18953	.72427
1.35539	.20554	.75760
1.40559	.22296	.79146
1.45579	.24190	.82585
1.50599	.26252	.86074
1.55619	.28494	.89610
1.60639	.30933	.93187
1.65659	.33584	.96800
1.70679	.36467	1.00441
1.75699	.39599	1.04098
1.80719	.43001	1.07758
1.85738	.46694	1.11406

Table 16. Theoretical Nozzle Admittances

Chamber Mach Number = 0.08, S_{mn} = 1.8413, $\gamma = 1.4$, $\theta_1 = 15°$

Radii of Curvature: Throat = 1.0, Entrance = 1.0

1.83539	-.08994	-.34732
1.85118	-.08901	-.33023
1.90122	-.08635	-.27569
1.95125	-.08414	-.22020
2.00128	-.08238	-.16329
2.05131	-.08111	-.10440
2.10134	-.08038	-.04285
2.15138	-.08027	.02224
2.20141	-.08089	.09198
2.25144	-.08246	.16787
2.30147	-.08527	.25201
2.35150	-.09258	.39407
2.40154	-.09694	.45840
2.45157	-.10812	.59216
2.50160	-.12624	.76049
2.55163	-.15747	.98499
2.60166	-.21707	1.30974
2.65170	-.35214	1.84003
2.70173	-.77269	2.89542
2.75176	-3.46130	5.67783
2.80179	-7.45054	-6.49983
2.85182	-.99480	-3.38172
2.90185	-.35111	-1.92857
2.95189	-.18527	-1.26046
3.00192	-.12055	-.86461
3.05195	-.03909	-.58954

Table 17. Theoretical Nozzle Admittances

Chamber Mach Number = 0.16, S_{mn} = 1.8413, γ = 1.4, θ_1 = 30°

Radii of Curvature: Throat = 1.0, Entrance = 1.0

1.81757	-.16848	-.30677
1.85473	-.16368	-.26770
1.90486	-.15765	-.21451
1.95499	-.15209	-.16045
2.00511	-.14691	-.10518
2.05524	-.14202	-.04828
2.10537	-.13730	.01072
2.15550	-.13264	.07238
2.20562	-.12784	.13739
2.25575	-.12268	.20655
2.30588	-.11684	.28069
2.35601	-.10982	.36171
2.40614	-.10094	.45063
2.45626	-.08911	.54979
2.50639	-.07172	.70757
2.55652	-.04890	.79096
2.60665	-.01337	.94166
2.65677	.04153	1.12063
2.70690	.12958	1.33608
2.75703	.27440	1.59673
2.80716	.52219	1.90567
2.85729	.95290	2.23792
2.90741	1.67827	2.47426
2.95754	2.70726	2.29605
3.00767	3.58435	1.37540
3.05780	3.65153	.12382

Table 18. Theoretical Nozzle Admittances

Chamber Mach Number = 0.08, S_{mn} = 1.8413, γ = 1.4, θ_1 = 15°

Radii of Curvature: Throat = 0.4396, Entrance = 0.4396

1.83539	-.09072	-.36134
1.85118	-.08979	-.34501
1.90122	-.08713	-.29305
1.95125	-.08487	-.24046
2.00128	-.08303	-.18686
2.05131	-.08161	-.13177
2.10134	-.08066	-.07467
2.15138	-.08022	-.01488
2.20141	-.08037	.04846
2.25144	-.08125	.11645
2.30147	-.08303	.19057
2.35150	-.08604	.27288
2.40153	-.09281	.40019
2.45157	-.09797	.47534
2.50160	-.10917	.60689
2.55163	-.12715	.77282
2.60166	-.15791	.99472
2.65169	-.21635	1.31686
2.70173	-.34858	1.84594
2.75176	-.76263	2.91138
2.80179	-3.51878	5.82775
2.85182	-6.88571	-6.82921
2.90185	-.88315	-3.28608
2.95189	-.30951	-1.86469
3.00192	-.16247	-1.21368
3.05195	-.10480	-.82796

Table 19. Theoretical Nozzle Admittances

Chamber Mach Number = 0.08, S_{mn} = 1.8413, γ = 1.4, θ_1 = 30°

Radii of Curvature: Throat = 0.4396, Entrance = 0.4396

1.83539	-.09024	-.37065
1.85118	-.08937	-.35648
1.90122	-.08684	-.31190
1.95125	-.08463	-.26763
2.00128	-.08270	-.22351
2.05131	-.08106	-.17936
2.10134	-.07969	-.13500
2.15138	-.07858	-.09023
2.20141	-.07774	-.04484
2.25144	-.07715	.00141
2.30147	-.07663	.04876
2.35150	-.07678	.09750
2.40153	-.07701	.14797
2.45157	-.07754	.20056
2.50160	-.07840	.25572
2.55163	-.08220	.37173
2.60166	-.08122	.37620
2.65170	-.08086	.39673
2.70173	-.08443	.48869
2.75176	-.08881	.59503
2.80179	-.09252	.68356
2.85182	-.09696	.78344
2.90185	-.10224	.89812
2.95189	-.10847	1.03231
3.00192	-.11571	1.19319
3.05195	-.12393	1.39175.

Table 20. Theoretical Nozzle Admittances

Chamber Mach Number = 0.08, S_{mn} = 1.8413, γ = 1.4, θ_1 = 45°

Radii of Curvature: Throat = 0.4396, Entrance = 0.4396

1.83539	-.08609	-.34806
1.85118	-.08527	-.33487
1.90122	-.08284	-.29353
1.95125	-.08067	-.25271
2.00128	-.07873	-.21230
2.05131	-.07701	-.17216
2.10134	-.07550	-.13218
2.15138	-.07417	-.09222
2.20141	-.07302	-.05216
2.25144	-.07203	-.01187
2.30147	-.07120	.02879
2.35150	-.07051	.06995
2.40153	-.06996	.11178
2.45157	-.06955	.15443
2.50160	-.06925	.19809
2.55163	-.06907	.24295
2.60166	-.06899	.28923
2.65169	-.06972	.35861
2.70173	-.06908	.38705
2.75176	-.06924	.43926
2.80179	-.06943	.49409
2.85182	-.06963	.55200
2.90185	-.06979	.61352
2.95189	-.06987	.67927
3.00192	-.06978	.75000
3.05195	-.06942	.82661

Table 21. Theoretical Nozzle Admittances

Chamber Mach Number = 0.16, S_{mn} = 1.8413, γ = 1.4, θ_1 = 45°

Radii of Curvature: Throat = 0.4396, Entrance = 0.4396

1.81757	-.13777	-.28620
1.85473	-.13273	-.25427
1.90486	-.12619	-.21154
1.95499	-.11989	-.16909
2.00511	-.11378	-.12677
2.05524	-.10778	-.08446
2.10537	-.10192	-.04203
2.15550	-.09585	.00064
2.20562	-.08978	.04371
2.25575	-.08354	.08730
2.30588	-.07704	.13155
2.35601	-.07018	.17662
2.40614	-.06287	.22268
2.45626	-.05496	.26988
2.50639	-.04633	.31841
2.55652	-.03679	.36846
2.60665	-.02614	.42024
2.65677	-.01416	.47397
2.70690	-.00054	.52989
2.75703	.01504	.58826
2.80716	.03302	.64932
2.85729	.05388	.71340
2.90741	.07825	.78071
2.95754	.10688	.85155
3.00767	.14070	.92617
3.05780	.18083	1.00473

Table 22. Theoretical Nozzle Admittances

Chamber Mach Number = 0.20, S_{mn} = 1.8413, γ = 1.4, θ_1 = 45°

Radii of Curvature: Throat = 0.4396, Entrance = 0.4396

1.80409	-.14772	-.25750
1.75699	-.15696	-.29840
1.80719	-.14713	-.25483
1.85738	-.13763	-.21171
1.90758	-.12837	-.16894
1.95778	-.11926	-.12637
2.00798	-.11021	-.08391
2.05818	-.10114	-.04145
2.10838	-.09194	.00114
2.15858	-.08254	.04396
2.20878	-.07291	.08712
2.25898	-.06265	.13073
2.30918	-.05195	.17490
2.35938	-.04056	.21973
2.40958	-.02835	.26534
2.45978	-.01514	.31184
2.50998	-.00075	.35934
2.56018	.01503	.40794
2.61038	.03246	.45774
2.66058	.05179	.50882
2.71078	.07336	.56128
2.76098	.09752	.61517
2.81118	.12470	.67052
2.86138	.17196	.77704
2.91158	.19008	.78551
2.96178	.22943	.84498

APPENDIX C

DERIVATION OF EXPLICIT EXPRESSIONS FOR α AND β

Explicit expressions for α and β can be obtained from equation (3-24), which describes the axial dependence of the pressure amplitude, and from equation (3-27) which describes the axial phase difference. To obtain values of α and β, three pressure amplitude or phase measurements must be taken at discrete axial distances along the impedance tube.

Explicit Expressions for α and β from Equation (3-24)

If the pressure amplitudes - $|p_1'|$, $|p_2'|$, $|p_3'|$ - are measured at the axial locations - z_1, z_2, z_3 -, respectively, along the tube, then equation (3-24) is used to obtain the following three equations

$$|p_1'| = A_{mn}[\cosh^2\pi\alpha - \cos^2\pi(\beta + \frac{2z_1}{\lambda})]^{\frac{1}{2}} \tag{C-1}$$

$$|p_2'| = A_{mn}[\cosh^2\pi\alpha - \cos^2\pi(\beta + \frac{2z_2}{\lambda})]^{\frac{1}{2}} \tag{C-2}$$

$$|p_3'| = A_{mn}[\cosh^2\pi\alpha - \cos^2\pi(\beta + \frac{2z_3}{\lambda})]^{\frac{1}{2}} \tag{C-3}$$

Dividing equations (C-2) and (C-3) by equation (C-1) to eliminate A_{mn} from the computations gives

$$P_{21} = \frac{\cosh^2 \pi\alpha - \cos^2 \pi(\beta + \frac{2z_2}{\lambda})}{\cosh^2 \pi\alpha - \cos^2 \pi(\beta + \frac{2z_1}{\lambda})} \qquad (C-4)$$

$$P_{31} = \frac{\cosh^2 \pi\alpha - \cos^2 \pi(\beta + \frac{2z_3}{\lambda})}{\cosh^2 \pi\alpha - \cos^2 \pi(\beta + \frac{2z_1}{\lambda})} \qquad (C-5)$$

where $P_{n1} = (p'_n/p'_1)$, $n = 2,3$. Using the identities

$$\cosh^2 x = \tfrac{1}{2}(\cosh 2x + 1)$$

$$\cos^2 x = \tfrac{1}{2}(\cos 2x + 1)$$

equations (C-4) and (C-5) become

$$P_{21} = \frac{\cosh 2\pi\alpha - \cos 2\pi(\beta + \frac{2z_2}{\lambda})}{\cosh 2\pi\alpha - \cos 2\pi(\beta + \frac{2z_1}{\lambda})} \qquad (C-6)$$

$$P_{31} = \frac{\cosh 2\pi\alpha - \cos 2\pi(\beta + \frac{2z_3}{\lambda})}{\cosh 2\pi\alpha - \cos 2\pi(\beta + \frac{2z_1}{\lambda})} \qquad (C-7)$$

Multiplying both sides of equation (C-6) and (C-7) by

$$\cosh 2\pi\alpha - \cos 2\pi(\beta + \frac{2z_1}{\lambda})$$

gives

$$(1 - P_{21})\cosh 2\pi\alpha - \cos 2\pi(\beta + \frac{2z_2}{\lambda}) + P_{21}\cos 2\pi(\beta + \frac{2z_1}{\lambda}) = 0$$

$$(1 - P_{31})\cosh 2\pi\alpha - \cos 2\pi(\beta + \frac{2z_3}{\lambda}) + P_{31}\cos 2\pi(\beta + \frac{2z_1}{\lambda}) = 0$$

Defining

$$A_{nl} = \cos \frac{4\pi z_n}{\lambda} - P_{nl} \cos \frac{4\pi z_1}{\lambda}$$

$$B_{nl} = \sin \frac{4\pi z_n}{\lambda} - P_{nl} \sin \frac{4\pi z_1}{\lambda}$$

where n = 2,3, gives

$$(1 - P_{21})\cosh 2\pi\alpha = A_{21}\cos 2\pi\beta - B_{21}\sin 2\pi\beta \qquad (C-8)$$

$$(1 - P_{31})\cosh 2\pi\alpha = A_{31}\cos 2\pi\beta - B_{31}\sin 2\pi\beta \qquad (C-9)$$

Solving equation (C-8) for $\cos 2\pi\beta$ gives

$$\cos 2\pi\beta = [B_{21}\sin 2\pi\beta + (1 - P_{21})\cosh 2\pi\alpha]/A_{21} \qquad (C-10)$$

Substituting for $\cos 2\pi\beta$ in equation (C-9) yields

$$[A_{21}(1-P_{31})-A_{31}(1-P_{21})]\cosh 2\pi\alpha = (A_{31}B_{21}-A_{21}B_{31})\sin 2\pi\beta$$

or

$$\sin 2\pi\beta = \frac{[A_{21}(1-P_{31}) - A_{31}(1-P_{21})]}{A_{31}B_{21} - A_{21}B_{31}}\cosh 2\pi\alpha \qquad (C-11)$$

Substituting equation (C-11) into equation (C-10) gives

$$\cos 2\pi\beta = \frac{[B_{21}(1-P_{31}) - B_{31}(1-P_{21})]}{A_{31}B_{21} - A_{21}B_{31}}\cosh 2\pi\alpha \qquad (C-12)$$

Dividing equation (C-11) by (C-12) to eliminate the terms involving α gives

$$\tan 2\pi\beta = \frac{A_{21}(1-P_{31}) - A_{31}(1-P_{21})}{B_{21}(1-P_{31}) - B_{31}(1-P_{21})}$$

or

$$\beta = \frac{1}{2\pi} \text{ Arctan}\left[\frac{A_{21}(1-P_{31}) - A_{31}(1-P_{21})}{B_{21}(1-P_{31}) - B_{31}(1-P_{21})}\right] \qquad (C\text{-}13)$$

Squaring both sides of equations (C-11) and (C-12) and adding gives

$$\sin^2 2\pi\beta + \cos^2 2\pi\beta = 1 =$$

$$\frac{[A_{21}(1-P_{31})-A_{31}(1-P_{21})]^2 + [B_{21}(1-P_{31})-B_{31}(1-P_{21})]^2}{(A_{31}B_{21} - A_{21}B_{31})^2} \cosh^2 2\pi\alpha$$

or

$$\cosh 2\pi\alpha = \frac{|A_{31}B_{21} - A_{21}B_{31}|}{\{[A_{21}(1-P_{31})-A_{31}(1-P_{21})]^2 + [B_{21}(1-P_{31})-B_{31}(1-P_{21})]^2\}^{\frac{1}{2}}} = X$$

Thus,

$$\alpha = \frac{1}{2\pi} \cosh^{-1}X = \frac{1}{2\pi} \ln(X + \sqrt{X^2 - 1}) \qquad (C\text{-}14)$$

A unique solution is not obtained from equation (C-13) because

β and $\beta \pm \frac{1}{2}$ both satisfy this equation. To determine the proper solution it is necessary to substitute both solutions into equation (C-4) and (C-5). The value which satisfies these two expressions is the solution which corresponds to the given physical situation.

Explicit Expressions for α and β from Equation (3-27)

Assume three phase measurements - δ_1, δ_2, δ_3 - are taken at the axial distances - z_1, z_2, z_3 -, respectively, along the tube. The following relations are obtained from equation (3-27).

$$\delta_2 - \delta_1 = a(z_2 - z_1) + \text{Arctan}\left\{\frac{\tanh\pi\alpha[\cot\pi(\beta+\frac{2z_2}{\lambda})-\cot\pi(\beta+\frac{2z_1}{\lambda})]}{1+\tanh^2\pi\alpha\cot\pi(\beta+\frac{2z_2}{\lambda})\cot\pi(\beta+\frac{2z_1}{\lambda})}\right\} \qquad (C-15)$$

$$\delta_3 - \delta_1 = a(z_3 - z_1) + \text{Arctan}\left\{\frac{\tanh\pi\alpha[\cot\pi(\beta+\frac{2z_3}{\lambda})-\cot\pi(\beta+\frac{2z_1}{\lambda})]}{1+\tanh^2\pi\alpha\cot\pi(\beta+\frac{2z_3}{\lambda})\cot\pi(\beta+\frac{2z_1}{\lambda})}\right\} \qquad (C-16)$$

Combining terms and inverting both sides of equations (C-15) and (C-16) gives

$$\cot[\delta_2-\delta_1-a(z_2-z_1)] = ct_2 = \frac{\tanh^2\pi\alpha+\tan\pi(\beta+\frac{2z_2}{\lambda})\tan\pi(\beta+\frac{2z_1}{\lambda})}{\tanh\pi\alpha[\tan\pi(\beta+\frac{2z_1}{\lambda})-\tan\pi(\beta+\frac{2z_2}{\lambda})]} \qquad (C-17)$$

$$\cot[\delta_3 - \delta_1 - a(z_3 - z_1)] = ct_3 = \frac{\tanh^2\pi\alpha + \tan\pi(\beta + \frac{2z_3}{\lambda})\tan\pi(\beta + \frac{2z_1}{\lambda})}{\tan\pi\alpha[\tan\pi(\beta + \frac{2z_1}{\lambda}) - \tan\pi(\beta + \frac{2z_3}{\lambda})]} \qquad (C-18)$$

To obtain an expression for α in terms of β, both sides of equation (C-17) are multiplied by

$$\tanh\pi\alpha[\tan\pi(\beta + \frac{2z_1}{\lambda}) - \tan\pi(\beta + \frac{2z_2}{\lambda})]$$

and both sides of equation (C-18) are multiplied by

$$\tanh\pi\alpha[\tan\pi(\beta + \frac{2z_1}{\lambda}) - \tan\pi(\beta + \frac{2z_3}{\lambda})]$$

Subtracting the resulting two expressions and solving for α gives

$$\tanh\pi\alpha = \frac{(T_3 - T_2)T_1}{ct_3(T_1 - T_3) - ct_2(T_1 - T_2)} \qquad (C-19)$$

where the shorthand notation

$$T_n = \tan\pi(\beta + \frac{2z_n}{\lambda}), \quad n = 1,2,3$$

is used. Substituting equation (C-19) into equation (C-18) and
rearranging terms yields the following result.

$$T_1(T_3-T_2) + [ct_3(T_1-T_3)T_2 - ct_2(T_1-T_2)T_3] \, x \qquad \text{(C-20)}$$

$$[ct_3(T_1-T_3) - ct_2(T_1-T_2)] = 0$$

The following trigonometric identity is now used

$$\tan\pi(\beta + \frac{2z_n}{\lambda}) = \frac{\tan\pi\beta + \tan\dfrac{2\pi z_n}{\lambda}}{1 + \tan\pi\beta\tan\dfrac{2\pi z_n}{\lambda}}, \quad n = 1,2,3$$

$$= \frac{B + Z_n}{1 + BZ_n}$$

where $B = \tan\pi\beta$ and $Z_n = \tan\dfrac{2\pi z_n}{\lambda}$. Substituting back into
equation (C-20) and multiplying through by $(1-Z_1B)^2(1-Z_2B)^2(1-Z_3B)^2$
gives

$$(B + Z_1)(1 - Z_1B)[(B + Z_3)(1 - Z_2B)-(B + Z_2)(1 - Z_3B)]^2 + \qquad (C\text{-}21)$$

$$ct_3^2 [(B + Z_1)(1 - BZ_3) - (B + Z_3)(1 - BZ_1)]^2(B + Z_2)(1 - BZ_2) +$$

$$ct_2^2 [(B + Z_1)(1 - BZ_2) - (B + Z_2)(1 = BZ_1)]^2(B + Z_3)(1 - BZ_3) -$$

$$ct_3 ct_2[(B + Z_1)(1 - BZ_3) - (B + Z_3)(1 - BZ_1)] \times$$

$$[(B+Z_1)(1-BZ_2)-(B+Z_2)(1-BZ_1)][(B+Z_2)(1-BZ_3)+(B+Z_3)(1-BZ_2)] = 0$$

Expanding equation (C-21), cancelling terms, and combining coefficients gives

$$(1 - B^2)[(Z_3 - Z_2)^2Z_1 + ct_3^2(Z_3 - Z_1)^2Z_2 + ct_2^2(Z_2 - Z_1)^2Z_3 \qquad (C\text{-}22)$$

$$- ct_2 ct_3 (Z_3 - Z_1) (Z_2 - Z_1) (Z_2 + Z_3)]$$

$$+ B [(1 - Z_1^2)(Z_2 - Z_3)^2 + (1 - Z_2^2) (Z_1 - Z_3)^2ct_3^2 +$$

$$(1-Z_3^2)(Z_1-Z_2)^2ct_2^2 - 2ct_2ct_3(Z_1-Z_2)(Z_1-Z_3)(1-Z_2Z_3)] = 0$$

Solving (C-22) for B gives

$$B = G \pm \sqrt{G^2 + 1}$$

and from the definition of B,

$$\beta = \frac{1}{\pi} \text{Arctan} \left(G \pm \sqrt{G^2 + 1} \right) \qquad \text{(C-23)}$$

where

$$G = \frac{X_z}{Y_z}$$

$$X_z = (1-Z_1^2)(Z_2-Z_3)^2 + (1-Z_2^2)(Z_1-Z_3)^2 \, ct_3^2 + (1-Z_3^2)(Z_1-Z_2)^2 \, ct_2^2$$

$$- 2ct_3 ct_2 (Z_1-Z_3)(Z_1-Z_2)(1-Z_3 Z_2)$$

$$Y_z = (Z_2 - Z_3)^2 Z_1 + ct_3^2 (Z_1-Z_3)^2 Z_2 + ct_2^2 (Z_1 - Z_2)^2 Z_3$$

$$- ct_3 ct_2 (Z_1 - Z_3)(Z_1 - Z_2)(Z_2 + Z_3)$$

Equations (C-23) and (C-19) can be used to solve for α and β explicitly. However, equation (C-23) does not give a unique solution for β. Instead, there are two solutions which differ by 1/2. To determine the solution which corresponds to the given physical situation, the solution which satisfies equations (C-17) and (C-18) is chosen.

APPENDIX D

DATA REDUCTION COMPUTER PROGRAMS

The computer programs for data reduction consist of five routines - two control routines and three subroutines. The first control routine MAIN uses pressure amplitude data to compute the nozzle admittance. The subroutines FSTAPP and BA are associated with MAIN. The second control routine MAIN1 and its corresponding subroutine AOBO can be used to determine the nozzle admittance from phase measurements. All routines are written in FORTRAN V interpretive language compatible with the UNIVAC 1108 machine language compiler. The names of the routines and their descriptions are listed in Table 23. The FORTRAN symbols used in these routines and their definitions are presented in alphabetical order in Table 24. The input data required for the calculation of the nozzle admittances are presented in Table 25. A listing of the routine MAIN and its associated subroutines are given in Table 26 and a sample output format is presented in Table 27. Routine MAIN1 and its subroutine AOBO are listed in Table 28 and a sample output format is presented in Table 29. In Figure 46 a detailed flow chart of the routine MAIN and its subroutines is presented. The flow charts for MAIN1 and AOBO are given in Figure 47.

Table 23. List of Subroutines Used in the Data Reduction
Computer Programs

Number		Subroutine Description
1	MAIN	Uses the nonlinear regression technique to determine the real and imaginary parts of the specific nozzle admittance from sound pressure level measurements
2	FSTAPP	Uses combinations of three pressure amplitude measurements to compute initial values of α, β, and A_{mn}. The set of values which gives the minimum rms error between the theoretical and experimental values of the pressure amplitudes is used as the initial set in routine MAIN
3	BA	Computes values of β and A_{mn} for values of α equal to zero
4	MAIN1	Computes values of the real and imaginary parts of the specific nozzle admittance from phase measurements using the nonlinear regression method
5	AOBO	Uses combinations of three phase measurements to compute initial values of α and β. The set of values which give the minimum rms error between the theoretical and experimental phase values is then used as the initial approximation

Table 24. Definitions of FORTRAN Variables

Variable	Routine	Definition
A	1,2,3	Integration constant A_{mn} in equation (3-24)
AA11, AA12, AA13, AA22, AA23, AA33	1	Scaled correlation coefficients used in Marquardt's algorithm discussed in Chapter III
AB	3	Parameter used for scaling purposes in Marquardt's algorithm
AB1, AB2, AB3	1,4 1,4 1	Scaled coefficients b_k^n defined after equation (3-32)
ADALP(K)	1,4	Correction to the value of α after the n-th iteration
ADAMP(K)	1	Correction to the value of A_{mn} after the n-th iteration
ADB	3	Parameter used for scaling the correlation coefficients in Marquardt's algorithm
ADBET(K)	1,4	Correction to the value of β after the n-th iteration
ABD2	3	ADB*ADB
ADN(K)	1,3,4	Determinant of the matrix of scaled correlation coefficients
ADNB, ADNB1, ADN1, ADN2	1	Parameters used in scaling the correlation coefficients of Marquardt's algorithm

Table 24. Continued

Variable	Routine	Definition
AH	1,4,5	Parameter a defined after equation (3-13)
AH2	1	AH*AH
AL(K)	1,4	Value of α after n+1 iterations
ALP	1,2,4,5	α
ALP1	2,5	Current value of α
AM	5	Value of α corresponding to a value of β computed from the expression $$\tan\pi\beta = G - \sqrt{G^2 + 1}$$
AMP(K)	1,3	Correction to the value of A_{mn} at the n-th iteration
AO	5	Current value of α
AP		Value of α corresponding to a value of β computed from the expression $$\tan\pi\beta = G + \sqrt{G^2 + 1}$$
AVALP	2	Average value of α taken over all combinations of three pressure amplitude measurements
AVAMP	2	Average value of A_{mn} taken over all combinations of three pressure amplitude measurements
AVBET	2	Average value of β taken over all combinations of three pressure amplitude measurements
A1,	2	In subroutines 1,3,4 these parameters represent
A11,	1,3,4	the unscaled coefficients in Marquardt's
A12,	1,2,3,4	algorithm. In subroutine 2 the variables A12
A13,	1,2	and A13 correspond to the parameters A_{21} and
A22,	1,3,4	A_{31} defined after equation (C-7)
A23,	1	
A33	1	

Table 24. Continued

Variable	Routine	Definition
B(K)	1,3,4	Value of β after n+1 iterations
BES	1	$J_m(S_{mn})$
BET	1,2,3,4,5	β
BET1	2,5	Current value of β
CWN	1,4	Nondimensional frequency, S
C12	2	$\cos^2\pi(\beta + \dfrac{2z_1}{\lambda})$
C2	1	C*C
C22	2	$\cos^2\pi(\beta + \dfrac{2z_2}{\lambda})$
C32	2	$\cos^2\pi(\beta + \dfrac{2z_3}{\lambda})$
D(K)	1,2,3,4,5	Axial distance from the nozzle entrance
DB12M, DB12P	2	Difference between the theoretical and predicted values of P12
DB13M, DB13P	2	Difference between the theoretical and predicted values of P13
DELP, DIF	4 5	Difference between the theoretical and experimental values of phase
DM, DP	5 5	Difference between the theoretical and experimental values of $\cot[\delta_2 - \delta_1 - a(z_2 - z_1)]$
DP(K)	1,4	Difference between the theoretical and experimental values of the pressure amplitude or phase
DPHI	4	$\delta_n - \delta_1 - a(z_n - z_1)$, n = 2,3,. . . ND

Table 24. Continued

Variable	Routine	Definition
D1, D2, D3	2,5 2,5 2,5	Distance from the nozzle entrance to the first, second, and third transducer location, respectively
ETA	1,4	$\text{Im}\left\langle \tanh_\pi(\alpha - i\beta) \right\rangle$
F	1,3,4,5	Parameter F defined by equation (3-28a)
FA	2	Numerator in equation (C-13)
FABM, FABP	2	Solutions to equation (C-13)
FB	2	Denominator in equation (C-13)
F1	2	Denominator in equations (C-11) and (C-12)
G	5	Variable defined after equation (C-23)
HEADER(K)	1,4	Test number and description
I	1,3,4,5	Integer variable used as a counter
IB(K), IBET	1,3,4	Parameters used to confine the values of β to the interval (-1,1)
IDIV	1,3,4	=1: numerical technique converged =2: numerical technique diverged
IJK	1,4	Integer variable used as a counter
ITER	1,3,4	Number of iterations
J, JJ, JJP, JP, K, M	1,2,4,5 2 2 2 1,3,4,5 1,3,4,5	Integer variables used as subscripts or counters
MACH	1,4	Chamber Mach number, $\bar{M}$

Table 24. Continued

Variable	Routine	Definition
MACH2	1,4	$\bar{M}^2$
MACH21	1,4	$1 - \bar{M}^2$
ND	1,2,3,4,5	Number of axial transducer locations
NI, NJ, NK, NL	5	Integer variables used as counters
NTESTS	1,4	Number of tests
NUM	1,2,3,4,5	Integer variable used as a counter
NWN	1,4	Number of frequency points taken during a test
P(K)	2	Experimental pressure amplitude
PA	1,4	$\pi\alpha$
PBD	1,3,4,5	$\pi(\beta + \dfrac{2z_n}{\lambda})$, $n = 1,2,\ldots$ .ND
PE(K)	1,3,4,5	Experimentally measured pressure amplitude
PHI(K)	1,3,4	Value of F after n iterations for a given value of the convergence parameter λ^n
PI	1,2,3,4,5	3.14159
PNLR(K)	1,4	Value of the pressure amplitude or phase using the values of α and β computed from the nonlinear regression method
PNORM	1,3,4	Convergence parameter. As PNORM → 0, convergence is indicated
PREF	4	δ_1

Table 24. Continued

Variable	Routine	Definition
PRMS	1,2,3,4,5	Root-mean-square deviation between the theoretical and experimental points
PRMS1	2,5	Current value of PRMS
PSI	1,4	$\text{Re}[\tanh\pi(\alpha-i\beta)]$
PT	1,3,4	Theoretical pressure amplitude or phase
PTA, PTAREF, PTALP, PTB, PTBET, PTBREF	1,3,4 4 1 4 1 4	Derivatives defined after equations (3-31) and (3-35)
P1	2,5	Experimental pressure amplitude or phase at the first transducer location
P12, P13	2	Coefficients defined after equation (C-5)
P2, P3	2,5	Experimental value of the pressure amplitude or phase at the second and third transducer locations, respectively
Q	4	Constant defined as $180/\pi$ used to convert phases from degrees to radians
R	1,4	$S_{mn}^2 \bar{M}$
RW	1	Chamber radius
R1	2	$4\pi/\lambda$
S	1	Denotes the trigonometric sine of a given argument
SC	1	$S*C$
SH	1	Denotes the hyperbolic sine of a given argument

Table 24. Continued

Variable	Routine	Definition
SI	2	Trigonometric sine of a given argument
SVN	1,4	S_{mn}
SVNR	1,4	S_{mn}/r_c
SVNR2	1,4	SVNR*SVNR
T	4,5	Trigonometric tangent of a given argument
TA	1,4	$\tanh\pi\alpha$
TB	1,4	$\tan\pi\beta$
TD1, TD2, TD3	5	Trigonometric tangent of a given argument
TEMP	1,4	Chamber temperature in $^\circ F$
TH	4	Hyperbolic tangent of a given argument
TH2	4	TH*TH
TP1, TP2, TP3, T1	5	Trigonometric tangent of a given argument
T2	4	T*T
V(K)	1,4	Convergence parameter λ^n defined after equation (3-32)
VM	1,3	Initial value of λ^n
WL	1,2,3,4,5	Wavelength, λ
WN	1,4	Wave number, k

Table 24. Concluded

Variable	Routine	Definition
WHN	1,4	Parameter $k_{mn}(1 - \bar{M}^2)$ defined after equation (3-13)
WHN2	1	WNH*WNH
WN2	1,4	WN*WN
X	2	Parameter X defined in equation (C-14)
YI	1,4	Imaginary part of the specific admittance
YM	5	Left hand side of equation (C-19) when β is determined from the equation $$\tan\pi\beta = G - \sqrt{G^2 + 1}$$
YP	5	Left hand side of equation (C-19) when β is determined from the relation $$\tan\pi\beta = G + \sqrt{G^2 + 1}$$
YR	1,4	Real part of the admittance

Table 25. Input Data

Variable	Definition
NTESTS	Number of tests to be reduced
HEADER(K)	Test number and description
NWN	Number of frequency points taken during a given test
MACH	Mach number at the nozzle entrance
SVN	Value of S_{mn}
ND	Number of transducer locations along the tube
D(K)	Axial distance from the nozzle entrance for a particular transducer
FREQ	Frequency in Hertz for a given test point
TEMP	Chamber temperature in $^{\circ}F$
PE(K)	Pressure amplitude or phase at station D(K)

Table 26. Program Listing of Routine MAIN and Its Associated Subroutines

```
1*         DIMENSION PNLR(10),DP(10),AL(2),B(2),AMP(2),ADALP(2),ADAMP(2),
2*        1          ADBET(2), ADN(2), PHI(2), V(2), IB(2)
3*        2        , HEADER(12)
4*         COMMON PI, CA, PE(10), D(10), WL, ND, BES2
5*         REAL MACH, MACH2, MACH21
6*         READ(5,1000) NTESTS
7*         DO 99 IJK = 1, NTESTS
8*         READ(5,1010) (HEADER(J), J=1,12)
9*         READ(5,1000) NWN
10*        READ(5,1020) MACH,SVN
11*        READ(5,1000) ND
12*        READ(5,1020) (D(J), J = 1, ND)
13*        PI = 3.1415926536
14*        CA = 20.0 * PI * ALOG10(EXP(1))
15*        DO 100 I = 1, NWN
16*        READ(5,1020) FREQ,TEMP
17*        READ(5,1020) (PE(J), J = 1, ND)
18*   C
19*   C THE WAVELENGTH WILL NOW BE COMPUTED FROM THE GIVEN DATA
20*                  VM = 0.01
21*                  RW = 5.6875 / 12.0
22*                  BES = 0.5819
23*                  MACH2 = MACH * MACH
24*                  MACH21 = 1 - MACH2
25*                  SVNR = SVN / RW
26*                  SVNR2 = SVNR * SVNR
27*                  R = SVNR2 * MACH
28*                  CBAR = 49.001 * SQRT(TEMP + 459.6)
29*                  WN = 2.0 * PI * FREQ / CBAR
30*                  WN2 = WN * WN
31*        IF(WN2 - SVNR2 * MACH21) 100, 100, 15
32*     15           WNH = SQRT(WN2 - SVNR2 * MACH21) / MACH21
33*                  WNH2 = WNH * WNH
34*                  WL = 2.0 * PI / WNH
35*                  AH = WN * MACH / MACH21
36*                  AH2 = AH * AH
37*                  CST = 1.0 / (WN2 + SVNR2 * MACH2)
38*                  BES2 = BES * BES
39*                  ITER = 0
40*                  CWN = WN*RW
41*        WRITE(6,2000) (HEADER(J),J=1,12),FREQ,CWN,WL,MACH
42*        DO 10 J = 1, ND
43*     10           D(J) = D(J)          / 12.0
44*   C
45*   C    THE WAVELENGTH AND OTHER NECESSARY CONSTANTS HAVE NOW BEEN DETRMINED.
46*   C THE NEWTON-RAPHSON NUMERICAL SCHEME WILL BE EMPLOYED TO FIND THE VALUES
47*   C OF ALPHA, BETA, AND A WHICH MINIMIZE THE DIFFERENCE, IN A LEAST-SQUARES
48*   C SENSE, BETWEEN THE EXPERIMENTAL AND THEORETICAL PRESSURES (IN DB). THE
49*   C FIRST APPROXIMATIONS FOR ALPHA, BETA, AND A ARE COMPUTED IN THE SUBROUT-
50*   C INE FSTAPP.
51*   C
52*        CALL FSTAPP(WL,PE,D,A,ALP,BET,NUM,ND,PRMS)
53*                  TA = TANH(PI * ALP)
54*                  TB = TAN(PI * BET)
55*                  DNM = 1.0 / (TA*TA + TB*TB)
56*                  PSI = (1.0 + TB*TB) * TA * DNM
57*                  ETA = (1.0 - TA*TA) * TB * DNM
58*                  YR = CST * (PSI * WN * WNH * MACH21 - R)
```

Table 26. Continued

```
 59*                         YI = CST * ETA * WN * WNH * MACH21
 60*                         WRITE(6,2015) ALP, BET, A, YR, YI, PRMS
 61*        20               IF(ABS(BET) - 1.0) 25, 25, 60
 62*        25               IF(ABS(PI * ALP) - 88.0) 30, 30, 80
 63*        30               PA = PI * ALP
 64*                         SH = SINH(PA)
 65*                         CH = COSH(PA)
 66*                         CH2 = CH * CH
 67*                         SC = SH * CH
 68*                         B1 = 0
 69*                         B2 = 0
 70*                         B3 = 0
 71*                         A11 = 0
 72*                         A12 = 0
 73*                         A13 = 0
 74*                         A22 = 0
 75*                         A23 = 0
 76*                         A33 = ND
 77*                         ADN1= 0
 78*                         ADN2 = 0
 79*                         ADN3 = 0
 80*                         ADNB1 = 0
 81*                         F = 0
 82*                         DO 40 J = 1, ND
 83*                         PBD = PI * (BET + 2.0 * D(J) / WL)
 84*                         C = COS(PBD)
 85*                         C2 = C * C
 86*                         S = SIN(PBD)
 87*                         DN = CH2 - C2
 88*                         PT = A + 10.0 * ALOG10(BES2 * DN)
 89*                         PTALP = CA * SC/DN
 90*                         PTBET = CA * S * C / DN
 91*                         PTA = 1.0
 92*                         F = F + (PE(J) - PT) * (PE(J) - PT)
 93*                         B1 = B1 + (PE(J) - PT) * PTALP
 94*                         B2 = B2 + (PE(J) - PT) * PTBET
 95*                         B3 = B3 + (PE(J) - PT) * PTA
 96*                         A11 = A11 + PTALP * PTALP
 97*                         A22 = A22 + PTBET * PTBET
 98*                         A12 = A12 + PTALP * PTBET
 99*                         A13 = A13 + PTALP * PTA
100*                         A23 = A23 + PTBET * PTA
101*                         ADN1= ADN1+ 1.0/DN
102*                         ADN2 = ADN2 + 1.0/(DN*DN)
103*                         ADNB = ADNB + PTBET/DN
104*                         ADNB1 = ADNB1 + (PE(J) - PT)/DN
105*        40       CONTINUE
106*                 PNORM = SQRT((B1*B1/A11 + B2*B2/A22 + B3*B3/A33)
107*         1                   / (3.0*ND))
108*        45               IF(PNORM - 0.00005) 60, 60, 50
109*        50               AA11 = 1.0
110*                         AA22 = 1.0
111*                         AA33 = 1.0
112*                         AA12 = ADNB/SQRT(ADN2*A22)
113*                         AA13 = ADN1/SQRT(ADN2*A33)
114*                         AA23 = A23 / SQRT(A22 * A33)
115*                         AB1 = ADNB1/SQRT(ADN2)
116*                         AB2 = B2 / SQRT(A22)
117*                         AB3 = B3 / SQRT(A33)
```

Table 26. Continued

```
118*    205           CONTINUE
119*                  DO 210 K = 1, 2
120*                        V(K) = VM * (10.0**(K-2))
121*                        AJN(K) = (1 + V(K)) * ((1 + V(K))**2 - AA23 * AA23)
122*      1                     - AA12 * (AA12 * (1 + V(K)) - AA13 * AA23)
123*      2                     + AA13 * (AA12 * AA23 - AA13 * (1 + V(K)))
124*                        ADALP(K) = (AB1 * ((1 + V(K))**2 - AA23 * AA23)
125*      1                     - AA12 * (AB2 * (1 + V(K)) - AB3 * AA23)
126*      2                     + AA13 * (AB2 * AA23 - AB3 * (1 + V(K))))/ADN(K)
127*                  ADBET(K) = ((1 + V(K)) * (AB2 * (1 + V(K)) - AB3 * AA23)
128*      1                     - AB1 * (AA12 * (1 + V(K)) - AA13 * AA23)
129*      2                     + AA13 * (AA12 * AB3 - AA13 * AB2)) / ADN(K)
130*                  AJAMP(K) = ((1 + V(K)) * ((1 + V(K)) * AB3 - AA23 * AB2)
131*      1                     - AA12 * (AA12 * AB3 - AA13 * AB2)
132*      2                     + AB1 * (AA12 * AA23 - AA13 * (1 + V(K))))/ADN(K)
133*                  AL(K) = ALP + ADALP(K) / SQRT(A11)
134*                  AL(K) = ABS(AL(K))
135*                  B(K) = BET + ADBET(K) / SQRT(A22)
136*                  IB(K) = B(K)
137*                  B(K) = B(K) - IB(K)
138*                  AMP(K) = A + ADAMP(K) / SQRT(A33)
139*                  PHI(K) = 0
140*                        PA = PI * AL(K)
141*                  IF(PA .GT. 88.) GO TO 80
142*                        CH = COSH(PA)
143*                        CH2 = CH * CH
144*                  IF(ABS(B(K)) .GT. 1.0) GO TO 80
145*                  DO 220 M = 1, ND
146*                        PBD = PI * (B(K) + 2.0 * D(M) / WL)
147*                        C = COS(PBD)
148*                        C2 = C * C
149*                        S = SIN(PBD)
150*                        DJ = CH2 - C2
151*                        PT = AMP(K) + 10.0 * ALOG10(BES2 * DN)
152*    220           PHI(K) = PHI(K) + (PE(M) - PT)**2
153*    210           CONTINUE
154*                  IF(F - PHI(1)) 225, 235, 235
155*    225           IF(F - PHI(2)) 230, 240, 240
156*    230           VM = VM * 10.0
157*                  IF(VM .GT. 100000000) GO TO 60
158*                  GO TO 205
159*    235           K = 1
160*                  GO TO 245
161*    240           K = 2
162*    245           VM = V(K)
163*                  PRMS = SQRT(PHI(K) / ND)
164*                  ALP = ABS(AL(K))
165*                  BET = B(K)
166*                  A = AMP(K)
167*                  IBET = BET
168*                  BET = BET - IBET
169*                  IF(ABS(BET) - 0.5) 275, 275, 260
170*    260           IF(BET) 265, 265, 270
171*    265           BET = BET + 1.0
172*                  GO TO 275
173*    270           BET = BET - 1.0
174*    275           ITER = ITER + 1
175*                  IF(ITER .GT. 200) GO TO 60
```

Table 26. Continued

```
176*                 IF(ALP - .00005) 255, 255, 250
177*      250        GO TO 20
178*      255        CALL BA(A, BET, PRMS, ITER, IDIV, PNORM)
179*                 ALP = 0
180*                 GO TO (60,80), IDIV
181*      60             TA = TANH(PI * ALP)
182*                     TB = TAN(PI * BET)
183*                     DNM = 1.0 / (TA * TA + TB * TB)
184*                     PSI = (1.0 + TB * TB) * TA * DNM
185*                     ETA = (1.0 - TA * TA) * TB * DNM
186*                     YR = CST * (PSI * WN * WNH * MACH21 - R)
187*                     YI = CST * ETA * WN * WNH * MACH21
188*                     WRITE(6,2020) ALP, BET, A,     YR,YI,PNORM,PRMS,ITER
189*                 WRITE(6,2005)
190*                     CH2 = COSH(PI*ALP) * COSH(PI*ALP)
191*                 DO 280 J = 1,ND
192*                     PBD = PI*(BET+2*D(J)/WL)
193*                     C = COS(PBD)
194*                     C2 = C*C
195*                     PNLR(J) = A + 10*ALOG10(BES2*(CH2 - C2))
196*                     D(J) =-12.0 * D(J)
197*                     DP(J) = PE(J) - PNLR(J)
198*      280            WRITE(6,2010) D(J), PE(J), PNLR(J), DP(J)
199*                     GO TO 100
200*      80             WRITE(6,2040) ITER
201*                 DO 285 J = 1,ND
202*      285            D(J) =-12.0*D(J)
203*      100 CONTINUE
204*      99  CONTINUE
205*      1000 FORMAT(2I5)
206*      1010 FORMAT(12A6)
207*      1020 FORMAT(8F10.5)
208*      2000 FORMAT(1H1, 47X, 12A6,            //, 49X, 17HFREQUENCY (HZ) = ,
209*      1         F6.1, /, 46X, 21HWAVE NUMBER        = , F7.4, /, 44X,
210*      2         24HAXIAL WAVELENGTH (FT) = , F8.4, /, 51X,
211*      3         14HMACH NUMBER = , F4.2, /)
212*      2005 FORMAT(////,18X, 17HDISTANCE FROM THE, 9X, 14HMEASURED SOUND, 9X,
213*      1         14HCOMPUTED SOUND, 9X, 10HDIFFERENCE, /, 17X,
214*      2         20HNOZZLE ENTRANCE (IN), 5X, 19HPRESSURE LEVEL (DB), 6X,
215*      3         14HPRESSURE LEVEL, 9X, 11HIN DECIBELS, /)
216*      2010 FORMAT(24X, F4.1, 20X, F6.1, 19X, F6.1, 16X, F6.1,/)
217*      2015 FORMAT(//, 53X, 14HINITIAL VALUES, /, 16X, 8HALPHA = , F7.4,
218*      1         2H, , 7HBETA = , F7.4, 2H, , 4HA = , F6.1, 2H, , 5HYR = ,
219*      2         F7.4, 2H, , 5HYI = , F7.4,2H, , 7HPRMS = , F7.4)
220*      2020 FORMAT(////, 46X, 28HNONLINEAR REGRESSION RESULTS, //,
221*      1         16X, 8HALPHA = , F6.4, 5X, 7HBETA = , F6.4, 5X, 4HA = ,
222*      1         , F6.1, 5X, 5HYR = , F8.4, 5X, 5HYI = , F8.4, //,
223*      2         27X, 8HPNORM = , F8.6, 5X, 7HPRMS = , F7.4, 5X,
224*      3         20HNO. OF ITERATIONS = , I3)
225*      2040 FORMAT(////, 45X, 15HDIVERGED AFTER , I3, 12H ITERATIONS.)
226*      2050 FORMAT(1X, 8E9.4)
227*           END
```

Table 26. Continued

```
 1*    SUBROUTINE FSTAPP(WL,P,D,A,ALP,BET,NUM,ND,PRMS)
 2*    DIMENSION P(10), D(10)
 3*    PI = 3.141592656
 4*    R1 = 4.0 * PI / WL
 5*    NUM=0
 6*    PRMS = 1000
 7*    AVALP = 0
 8*    AVBET = 0
 9*    AVAMP = 0
10*    JP = ND - 2
11*    DO 10 J = 1, JP
12*    JJ = J+1
13*    JJP = JP+1
14*    DO 20 K = JJ, JJP
15*    KK = K+1
16*    DO 30 L = KK, ND
17*    P1 = P(J)
18*    P2 = P(K)
19*    P3 = P(L)
20*    D1 = D(J)
21*    D2 = D(K)
22*    D3 = D(L)
23*    CO = COS(R1 * D1)
24*    SI = SIN(R1 * D1)
25*    P12 = 10.0**((P2 - P1) * 0.1)
26*    P13 = 10.0**((P3 - P1) * 0.1)
27*    A12 = COS(R1 * D2) - P12 * CO
28*    A13 = COS(R1 * D3) - P13 * CO
29*    B12 = SIN(R1 * D2) - P12 * SI
30*    B13 = SIN(R1 * D3) - P13 * SI
31*    F1 = A13 * B12 - A12 * B13
32*    FA = A12 * (1-P13) - A13 * (1-P12)
33*    FB = B12 * (1 - P13) - B13 * (1 - P12)
34*    DNW = SQRT(FA * FA + FB * FB)
35*    X = ABS(F1 / DNW)
36*    IF(X - 1.0) 32, 35, 35
37 32  ALP = 0.001
38     GO TO 37
39 35  ALP = (1.0 / (2.0 * PI)) * ALOG(X + SQRT(X*X - 1))
40 37  FABP = -FB/FA+SQRT((FB/FA)*(FB/FA)+1)
41     FABM = -FB/FA-SQRT((FB/FA)*(FB/FA)+1)
42     BET = (1.0/PI)*ATAN(FABP)
43     CH2 = (1.0/PI)*ATAN(FABP)
44     CH2 = COSH(PI * ALP) **2
45     C12 = COS(PI * BET + R1 * D1 / 2)**2
46     C22 = COS(PI * BET + R1 * D2 / 2)**2
47     C32 = COS(PI * BET + R1 * D3 / 2)**2
48     CC2 = (CH2 - C22) / (CH2 - C12)
49     CC3 = (CH2 - C32) / (CH2 - C12)
50     DB12P= ABS(P12 - CC2)
51     DB13P= ABS(P13 - CC3)
52     BET = (1.0 / PI ) * ATAN(FABM)
53     C12 = COS(PI * BET + R1 * D1 / 2)**2
54     C22 = COS(PI * BET + R1 * D2 / 2)**2
55     C32 = COS(PI * BET + R1 * D3 / 2)**2
56     CC2 = (CH2 - C22) / (CH2 - C12)
57     CC3 = (CH2 - C32) / (CH2 - C12)
58     DB12M= ABS(P12 - CC2)
       DB13M= ABS(P13 - CC3)
```

Table 26. Continued

```
59*                               IF(DB12P*DB13P - DB12M*DB13M) 40,40,50
60*        40                     BET = (1.0/PI)*ATAN(FABP)
61*                               C12 = COS(PI * BET + R1 * D1 / 2)**2
62*                               C22 = COS(PI * BET + R1 * D2 / 2)**2
63*                               C32 = COS(PI * BET + R1 * D3 / 2)**2
64*        50                     NUM = NUM + 1
65*                               A = (P1 - 10.0*ALOG10((0.5819**2)*(CH2-C12)) +
66*         1                          P2 - 10.0*ALOG10((0.5819**2)*(CH2-C22)) +
67*         2                          P3 - 10.0*ALOG10((0.5819**2)*(CH2-C32)))/3
68*                          AVALP = AVALP + ALP
69*                          AVBET = AVBET + BET
70*                          AVAMP = AVAMP + A
71*                          F = 0
72*                    DO 70 I = 1, ND
73*                          PBD = PI * (BET + 2.0 * D(I) / WL)
74*                          C = COS(PBD)
75*                          C2 = C * C
76*                          PT = A + 10.0 * ALOG10((0.5819**2) * (CH2 - C2))
77*        70                F = F + (P(I) - PT)**2
78*                     PRMS1= SQRT(F/ND)
79*                     IF(PRMS - PRMS1) 65, 65, 60
80*        60           PRMS = PRMS1
81*                     ALP1 = ALP
82*                     BET1 = BET
83*                     A1 = A
84*        65           CONTINUE
85*        30                  CONTINUE
86*        20           CONTINUE
87*        10 CONTINUE
88*              IF(NUM .EQ. 0) GO TO 100
89*              AVALP = AVALP / NUM
90*              AVBET = AVBET / NUM
91*              AVAMP = AVAMP / NUM
92*              F = 0
93*              DO 80 I = 1, ND
94*                    PBD = PI * (AVBET + 2.0 * D(I) / WL)
95*                    C2 = COS(PBD)**2
96*                    CH2 = COSH(PI * AVALP)**2
97*                    PT = A + 10 * ALOG10((0.5819**2) * (CH2 - C2))
98*        80          F = F + (P(I) - PT)**2
99*              PRMS1 = SQRT(F/ND)
100*             IF(PRMS - PRMS1) 90, 90, 85
101*       85    PRMS = PRMS1
102*                   ALP = AVALP
103*                   BET = AVBET
104*                   A = AVAMP
105*                   GO TO 100
106*       90          ALP = ALP1
107*                   BET = BET1
108*                   A = A1
109*       100 CONTINUE
110*             RETURN
111*             END
```

Table 26. Continued

```
 1*        SUBROUTINE BA(A, BET, PRMS, ITER, IDIV, PNORM)
 2*        COMMON PI, CA, PE(10), D(10); WL, ND; BES2
 3*        DIMENSION B(2),AMP(2),ADAMP(2),ADBET(2),ADN(2),PHI(2),V(2),IB(2)
 4*        VM = 0.01
 5*      5 IF(ABS(BET) - 1.0) 10, 10, 60
 6*     10 B1 = 0
 7*        B2 = 0
 8*        A11 = 0
 9*        A12 = 0
10*        A22 = ND
11*        ADB = 0
12*        ADB2 = 0
13*        AB = 0
14*        F = 0
15*        DO 15 I = 1,ND
16*        PBD = PI * (BET + 2.0*D(I)/WL)
17*        C = COS(PBD)
18*        S = SIN(PBD)
19*        S2 = S * S
20*        CT = C / S
21*        PT = A + 10 * ALOG10(BES2 * S2)
22*        PTA = 1.0
23*        PTBET = CA * CT
24*        ADB = ADB + CT
25*        ADB2 = ADB2 + CT * CT
26*        AB = AB + (PE(I) - PT) * CT
27*        F = F + (PE(I) -PT) * (PE(I) - PT)
28*        B1 = B1 + (PE(I) - PT) * PTBET
29*        B2 = B2 + (PE(I) - PT) * PT
30*        A11 = A11 + PTBET*PTBET
31*     15 A12 = A12 + PTBET
32*        PNORM = SQRT((B1*B1/A11 + B2*B2/A22) / (2.0*ND))
33*        IF(PNORM - 0.00005) 65, 65, 20
34*     20 A11 = 1.0
35*        A22 = 1.0
36*        A12 = ADB / SQRT(ADB2 * A22)
37*        AB1 = AB / SQRT(ADB2)
38*        AB2 = B2 / SQRT(A22)
39*     22 CONTINUE
40*        DO 25 K = 1,2
41*        V(K) = VM * (10.0**(K-2))
42*        ADN(K) = (1+V(K)) * (1+V(K)) - AA12 * AA12
43*        ADBET(K) = (AB1 * (1+V(K)) - AB2 *AA12) / ADN(K)
44*        ADAMP(K) = (AB2 * (1+V(K)) - AB1 *AA12) / ADN(K)
45*        B(K) = BET + ADBET(K) / SQRT(A11)
46*        IB(K) = B(K) - IB(K)
47*        B(K) = B(K) - IB(K)
48*        AMP(K) = A + ADAMP(K) / SQRT(A22)
49*        PHI(K) = 0
50*        IF(ABS(B(K)) .GT. 1.0) GO TO 60
51*        DO 30 M = 1,ND
52*        PBD = PI * (B(K) + 2.0*D(M)/WL)
53*        S = SIN(PBD)
54*        S2 = S * S
55*        PT = AMP(K) + 10.0*ALOG10(BES2*S2)
56*     30 PHI(K) = PHI(K) + (PE(M) - PT) * (PE(M) - PT)
57*        CONTINUE
58*     25 IF(F-PHI(1)) 35, 40, 40
```

Table 26. Concluded

```
59*        35 IF(F-PHI(2)) 45, 50, 50
60*        45    VM = VM * 10.0
61*           IF(VM .GT. 100000000) GO TO 65
62*           GO TO 22
63*        40    K = 1
64*           GO TO 55
65*        50    K = 2
66*        55    VM = V(K)
67*           PRMS = SQRT(PHI(K) / ND)
68*           A = AMP(K)
69*           BET = B(K)
70*           IBET = BET
71*           BET = BET - IBET
72*           IF(ABS(BET) - 0.5) 275, 275, 260
73*       260    IF(BET) 265, 265, 270
74*       265       BET = BET + 1.0
75*           GO TO 275
76*       270       BET = BET - 1.0
77*       275    ITER = ITER + 1
78*           IF(ITER .GT. 200) GO TO 65
79*           GO TO 5
80*        60 IDIV = 2
81*           GO TO 70
82*        65 IDIV = 1
83*        70 RETURN
84*           END
```

Table 27. Output Format

B214-55, NOZZLE NO. 15-08-2.5

FREQUENCY (HZ) = 200.0
WAVE NUMBER = .5531
AXIAL WAVELENGTH (FT) = 5.3495
MACH NUMBER = .08

INITIAL VALUES
ALPHA = .0292, BETA = .2630, A = 161.4, YR = .1678, YI = .9071, PRMS = .2759

NONLINEAR REGRESSION RESULTS

ALPHA = .0311   BETA = .2648   A = 161.2   YR = .1769   YI = .8952

PNORM = .000012   PRMS = .2478   NO. OF ITERATIONS = 2

DISTANCE FROM THE NOZZLE ENTRANCE (IN)	MEASURED SOUND PRESSURE LEVEL (DB)	COMPUTED SOUND PRESSURE LEVEL	DIFFERENCE IN DECIBELS
40.0	137.9	137.9	.0
35.0	149.1	149.1	.0
33.0	151.5	151.9	-.4
24.0	156.2	156.5	-.3
19.0	156.0	155.8	.2
17.0	155.0	154.8	.2
8.0	138.2	138.3	-.1
3.0	149.2	148.9	.3

197

Table 28. Program Listing of Routine MAIN1 and Its
Corresponding Subroutine AOBO

```
1*          DIMENSION PNLR(10), DP(18), AL(2), B(2), ADALP(2), ADBET(2),
2*         1          ADN(2), PHI(2), V(2), IB(2), HEADER(12)
3*          COMMON PI, PE(10), D(10), WL, ND, AH
4*          REAL MACH, MACH2, MACH21
5*          READ(5,1000) NTESTS
6*          PI = 3.1415926536
7*          Q = 180/PI
8*          RW = 5.6875/12.0
9*          DO 95 IJK = 1, NTESTS
10*         READ(5,1010) (HEADER(J), J = 1,12)
11*         READ(5,1000) NWN
12*         READ(5,1020) MACH, SVN
13*         READ(5,1000) ND
14*         READ(5,1020) (D(J), J = 1, ND)
15*    C
16*    C THE WAVELENGTH WILL NOW BE COMPUTED FROM THE GIVEN DATA.
17*    C
18*         D(1) = -D(1)/12
19*         MACH2 = MACH*MACH
20*         MACH21 = 1 - MACH2
21*         SVNR = SVN/RW
22*         SVNR2= SVNR * SVNR
23*         R = SVNR2 * MACH
24*         DO 100 I = 1,NWN
25*         READ(5,1020) FREQ, TEMP
26*         READ(5,1020) (PE(J), J = 1,ND)
27*         DO 5 J = 1,ND
28*    5    PE(J) = -PE(J)
29*         VM = 0.01
30*         CBAR = 49.001 * SQRT(TEMP+459.6)
31*         WN = 2.0*PI*FREQ/CBAR
32*         CWN = WN*RW
33*         WN2 = WN*WN
34*         IF(WN2-SVNR2*MACH21) 90, 90, 15
35*    15   WNH = SQRT(WN2 - SVNR2*MACH21)/MACH21
36*         WL= 2*PI/WNH
37*         AH = WN*MACH/MACH21
38*         CST = 1.0 / (WN2 + SVNR2*MACH2)
39*         ITER = 0
40*         PREF=PE(1)
41*         WRITE(6,2000) (HEADER(J), J = 1,12), FREQ, CWN, WL, MACH
42*        1          , TEMP
43*         DO 10 J = 2,ND
44*         D(J) = -D(J)/12
45*         PE(J) = PE(J) - PREF
46*         IF(ABS(PE(J)) .LT. 180) GO TO 12
47*         IF(PE(J)) 7, 7, 9
48*    7    PE(J) = PE(J) + 360
49*         GO TO 12
50*    9    PE(J) = PE(J) - 360
51*    12   DPHI = PE(J) - AH * (D(J)-D(1))*Q
52*         IF(ABS(DPHI) .LT. 90) GO TO 10
53*         IF(DPHI) 300, 300, 305
54*    300  PE(J) = PE(J) + 180
55*         DPHI = DPHI + 180
```

Table 28. Continued

```
56*                      IF(ABS(DPHI) .GT. 90) GO TO 300
57*                      GO TO 10
58*          305         DPHI = DPHI -180
59*                      PE(J) = PE(J) - 180
60*                      IF(ABS(DPHI) .GT. 90) GO TO 305
61*          10          PE(J) = PE(J) * PI / 180
62*        C
63*        C        THE WAVELENGTH AND OTHER NECESSARY CONSTANTS HAVE NOW BEEN DETERMINED.
64*        C THE NEWTON-RAPHSON NUMERICAL SCHEME WILL BE USED TO FIND THE VALUES OF
65*        C ALPHA AND BETA WHICH MINIMIZE THE DIFFERENCE, IN A LEAST-SQUARES SENSE,
66*        C BETWEEN THE EXPERIMENTAL AND THEORETICAL PHASE ANGLES(IN DEGREES). THE
67*        C FIRST APPROXIMATIONS FOR ALPHA AND BETA ARE COMPUTED IN THE SUBROUTINE
68*        C AOBO.
69*        C
70*                      CALL AOBO(ALP, BET, NUM, PRMS)
71*                      TA = TANH(PI*ALP)
72*                      TB = TAN(PI*BET)
73*                      DNM = 1.0/(TA*TA + TB*TB)
74*                      PSI = (1.0 + TB*TB) * TA * DNM
75*                      ETA = (1.0 - TA*TA) * TB * DNM
76*                      YR = CST * (PSI*WN*WNH*MACH21 - R)
77*                      YI = CST * ETA * WN * WNH * MACH21
78*                      WRITE(6,2015) ALP, BET, YR, YI, PRMS
79*          20          IF(ABS(BET) - 1.0) 25, 25, 80
80*          25          IF(ABS(PI*ALP) - 88.0) 30, 30, 80
81*          30          PA = PI*ALP
82*                      TH = TANH(PA)
83*                      TH2 = TH*TH
84*                      T = TAN(PI*(BET + 2*D(1)/WL))
85*                      PREF = AH*D(1) + ATAN(TH/T)
86*                      T2 = T*T
87*                      DNM = 1 + TH2/T2
88*                      PTAREF = PI*(1 - TH2) / (T*DNM)
89*                      PTBREF = -PI*(1 + 1/T2) * TH/DNM
90*                      B1 = 0
91*                      B2 = 0
92*                      A11 = 0
93*                      A22 = 0
94*                      A12 = 0
95*                      F = 0
96*                      DO 40 J = 2,ND
97*                          PBD = PI * (BET + 2*D(J)/WL)
98*                          T = TAN(PBD)
99*                          T2 = T*T
100*                         PT = AH*D(J) + ATAN(TH/T) - PREF
101*                         DELP = PE(J) - PT
102*                         DNM = 1 + TH2/T2
103*                         PTA = PI*(1 - TH2)/(T*DNM) - PTAREF
104*                         PTB = -PI*(1 + 1/T2)*TH/DNM - PTBREF
105*                         F = F + DELP*DELP
106*                         B1 = B1 + DELP*PTA
107*                         B2 = B2 + DELP*PTB
108*                         A11 = A11 + PTA*PTA
109*                         A22 = A22 + PTB*PTB
110*          40             A12 = A12 + PTA*PTB
111*                      PNORM = SQRT((B1*B1/A11 + B2*B2/A22)/(2.0*ND))
112*          45          IF(PNORM - 0.000005) 60, 60, 50
```

Table 28. Continued

```
113*        50      AA12 = A12/SQRT(A11*A22)
114*                AB1 = B1/SQRT(A11)
115*                AB2 = B2/SQRT(A22)
116*        205     CONTINUE
117*                DO 210 K = 1,2
118*                    V(K) = VM * (10.0**(K-2))
119*                    ADN(K) = (1 + V(K))*(1 + V(K)) - AA12*AA12
120*                    ADALP(K) = (AB1*(1 + V(K)) - AB2*AA12)/ADN(K)
121*                    ADBET(K) = (AB2*(1 + V(K)) - AB1*AA12)/ADN(K)
122*                    AL(K) = ALP + ADALP(K)/SQRT(A11)
123*                    B(K) = BET + ADBET(K)/SQRT(A22)
124*                    IB(K) = B(K)
125*                    B(K) = B(K) - IB(K)
126*                    PHI(K) = 0
127*                    PA = PI*AL(K)
128*                    IF(PA .GT. 88) GO TO 80
129*                    TH = TANH(PA)
130*                    TH2 = TH*TH
131*                    IF(ABS(B(K)) .GT. 1.0) GO TO 80
132*                T = TAN(PI*(B(K)+2*D(1)/WL))
133*                PTREF = AH*D(1) + ATAN(TH/T)
134*                    DO 220 M = 2,ND
135*                        PBD = PI*(B(K) + 2*D(M)/WL)
136*                        T = TAN(PBD)
137*                        PT = AH*D(M) + ATAN(TH/T) - PTREF
138*                        DELP = PE(M) - PT
139*        220         PHI(K) = PHI(K) + DELP*DELP
140*        210     CONTINUE
141*                IF(F - PHI(1)) 225, 235, 235
142*        225     IF(F - PHI(2)) 230, 240, 240
143*        230     VM = VM * 10.0
144*                IF(VM .GT. 100000000) GO TO 60
145*                GO TO 205
146*        235     K = 1
147*                GO TO 245
148*        240     K = 2
149*        245     VM = V(K)
150*                PRMS = SQRT(PHI(K)/ND)
151*                ALP = AL(K)
152*                BET = B(K)
153*                IBET = BET
154*                BET = BET - IBET
155*                IF(ABS(BET) - 0.5) 275, 275, 260
156*        260     IF(BET) 265, 265, 270
157*        265     BET = BET + 1.0
158*                GO TO 275
159*        270     BET = BET - 1.0
160*        275     ITER = ITER + 1
161*                IF(ITER .GT. 49) GO TO 60
162*                GO TO 20
163*        60      TA = TANH(PI*ALP)
164*                TB = TAN(PI*BET)
165*                DNM = 1.0/(TA*TA + TB*TB)
166*                PSI = (1.0 + TB*TB) * TA * DNM
167*                ETA = (1.0 - TA*TA) * TB * DNM
168*                YR = CST*(PSI*WN*WNH*MACH21 - R)
169*                YI = CST * ETA * WN * WNH * MACH21
```

Table 28. Continued

```
170*            PRMS = PRMS*Q
171*            WRITE(6,2020) ALP, BET, YR, YI, PNORM, PRMS,ITER
172*            WRITE(6,2005)
173*            T = TAN(PI*(BET + 2*D(1)/WL))
174*            PTREF = AH*D(1) + ATAN(TA/T)
175*            DO 280 J = 2,ND
176*                PBD = PI*(BET + 2*D(J)/WL)
177*                T = TAN(PBD)
178*                PNLR(J) =(AH*D(J) + ATAN(TA/T) - PTREF)*Q
179*                D(J) = -12.0 * D(J)
180*                PE(J) = PE(J) * Q
181*                DP(J) =(PE(J) - PNLR(J))
182*                WRITE(6,2010) D(J), PE(J), PNLR(J), DP(J)
183*    280     CONTINUE
184*            GO TO 90
185*    80      WRITE(6,2040) ITER
186*            DO 285 J = 2,ND
187*    285         D(J) = -12.0*D(J)
188*    90      CONTINUE
189*    100 CONTINUE
190*    95 CONTINUE
191*    1000 FORMAT(I5)
192*    1010 FORMAT(12A6)
193*    1020 FORMAT(8F10.5)
194*    2000 FORMAT(1H1, 47X, 12A6, //, 49X, 17HFREQUENCY (HZ) = , F6.1, /,
195*        1       53X, 14HWAVE NUMBER = , F7.4, /, 44X,
196*        2       24HAXIAL WAVELENGTH (FT) = , F8.4, /, 51X,
197*        3       14HMACH NUMBER = , F4.2, /, 51X, 14HTEMPERATURE = ,F5.1,/)
198*    2005 FORMAT(///,18X, 17HDISTANCE FROM THE, 9X, 14HMEASURED PHASE, 9X,
199*        1       14HCOMPUTED PHASE, 9X, 10HDIFFERENCE, /, 17X,
200*        2       20HNOZZLE ENTRANCE (IN), 5X, 19H DIFFERENCE (DEG) , 6X
201*        3       14H DIFFERENCE , 9X, 11HIN DEGREES , /)
202*    2010 FORMAT(24X, F4.1, 20X, F6.1, 19X, F6.1, 16X, F6.1, /)
203*    2015 FORMAT(///, 53X, 14HINITIAL VALUES, /, 16X, 8HALPHA = , F7.4,
204*        1       2H, , 7H3ETA = , F7.4, 2H, , 4HYR =, F7.4, 3H , , 5HYI = ,
205*        2       F7.4, 2H, , 7HPRMS = , F7.4)
206*    2020 FORMAT(///, 46X, 28HNONLINEAR REGRESSION RESULTS, //, 21X,
207*        1       8HALPHA = ,F6.4, 5X, 7HBETA = , F6.4, 5X,
208*        2       5HYR = , F8.4, 5X, 5HYI = , F8.4, //, 32X, 8HPNORM = ,
209*        3       F8.6, 5X, 7HPRMS = , F7.4, 5X, 20HNO. OF ITERATIONS = , I3)
210*    2040 FORMAT(///, 45X, 15HDIVERGED AFTER , I3, 12H ITERATIONS )
211*    2050 FORMAT(1X, 8E9.4)
212*            END
```

Table 28. Continued

```
1*        SUBROUTINE AOBO(ALP, BET, NUM, PRMS)
2*        COMMON PT, PE(10), D(10), WL, ND, AH
3*        NUM = 0
4*        PRMS = 1000
5*        NI=ND-2
6*        DO 10 I = 1,NI
7*              NJ = I+1
8*              NK = NI+1
9*              P1 = PE(I)
10*             D1 = D(I)
11*             TD1 = TAN(2*PI*D1/WL)
12*             DO 20 J = NJ,NK
13*                   NL = J+1
14*                   P2 = PE(J)
15*                   D2 = D(J)
16*                   TD2 = TAN(2*PI*D2/WL)
17*                   CT2 = 1.0/TAN(P2-P1-AH*(D2-D1))
18*                   DO 30 K = NL,ND
19*                   P3 = PE(K)
20*                   D3 = D(K)
21*                   CT3 = 1 / TAN(P3-P1-AH*(D3-D1))
22*                   TD3 = TAN(2*PI*D3/WL)
23*                   TOP = (1-TD1*TD1) * (TD2-TD3) * (TD2-TD3)
24*      1            + (1-TD2*TD2) * (TD1-TD3) * (TD1-TD3) *CT3*CT3
25*      2            + (1-TD3*TD3) * (TD1-TD2) * (TD1-TD2) *CT2*CT2
26*      3            - (1-TD2*TD3) * (TD1-TD2) * (TD1-TD3)*2*CT2*CT3
27*                   BOT = (TD2-TD3) * (TD2-TD3) * TD1
28*      1            + (TD1-TD3) * (TD1-TD3) * TD2 * CT3 * CT3
29*      2            + (TD1-TD2) * (TD1-TD2) * TD3 * CT2 * CT2
30*      3            - (TD1-TD2) * (TD1-TD3) * (TD2+TD3) *CT3*CT2
31*                   G=0.5*TOP/BOT
32*                   BP = ATAN(G + SQRT(G*G + 1))/PI
33*                   BM = ATAN(G - SQRT(G*G + 1))/PI
34*                   TP1 = TAN(PI*(BP + 2*D1/WL))
35*                   TP2 = TAN(PI*(BP + 2*D2/WL))
36*                   TP3 = TAN(PI*(BP + 2*D3/WL))
37*                   TM1 = TAN(PI*(BM + 2*D1/WL))
38*                   TM2 = TAN(PI*(BM + 2*D2/WL))
39*                   TM3 = TAN(PI*(BM + 2*D3/WL))
40*      YP = (TP3-TP2)*TP1/(CT3*(TP1-TP3) - CT2*(TP1-TP2))
41*      YM = (TM3-TM2)*TM1/(CT3*(TM1-TM3) - CT2*(TM1-TM2))
42*                   IF(ABS(YP) .GT. 1) GO TO 35
43*                   AP = ALOG((1+YP)/(1-YP))/(2*PI)
44*                   GO TO 50
45*      35           IF(YP) 40,40,45
46*      40           AP = -.2
47*                   GO TO 50
48*      45           AP = .2
49*      50           IF(ABS(YM) .GT. 1) GO TO 60
50*                   AM = ALOG((1+YM)/(1-YM))/(2*PI)
51*                   GO TO 75
52*      60           IF(YM) 65,65,70
53*      65           AM = -.2
54*                   GO TO 75
55*      70           AM = .2
56*      75           T = TANH(PI*AP )
57*                   DP = T*((1/TP2) - (1/TP1))/(1+T*T/(TP2*TP1))
```

Table 28. Concluded

58*		T = TANH(PI*AM)
59*		DM = T*((1/TM2) - (1/TM1))/(1+T*T/(TM2*TM1))
60*		T = 1/CT?
61*		DP = ABS(DP-T)
62*		DM = ABS(DM-T)
63*		IF(DP - DM) 105, 105, 110
64*	105	ALP1 = AP
65*		BET1 = BP
66*		GO TO 115
67*	110	ALP1 = AM
68*		BET1 = BM
69*	115	AO = ALP1
70*		BO = BET1
71*	145	F = 0
72*		T = TANH(PI*AO)
73*		T1 = TAN(PI*(BO + 2*D(1)/WL))
74*		DO 150 M = 2,NO
75*		PBD = PI * (BO + 2*D(M)/WL)
76*		TN = TAN(PBD)
77*		PT = AH*D(M) + ATAN(T/TN) - AH*D(1)-ATAN(T/T1)
78*		DIF =(PE(M) - PT)*180/PI
79*	150	F = F + DIF*DIF
80*		PRMS1 = SQRT(F/NO)
81*		IF(PRMS - PRMS1) 160, 160, 155
82*	155	PRMS = PPMS1
83*		ALP = AO
84*		BET = BO
85*	160	CONTINUE
86*	30	CONTINUE
87*	20	CONTINUE
88*	10	CONTINUE
89*		RETURN
90*		END

Table 29. Sample Output Format

TEST # E16-617-17, TASK II, MM-2

FREQUENCY (HZ) = 62.5
WAVE NUMBER = .1713
AXIAL WAVELENGTH (FT) = 17.3189
MACH NUMBER = .06
TEMPERATURE = 31.9

INITIAL VALUES

ALPHA = .0046, BETA = .4685, YR = .0147 , YI = .0992, PRMS = 5.6952

NONLINEAR REGRESSION RESULTS

ALPHA = .0036   BETA = .4687   YR = .0114   YI = .0988

PNORM = .000001   PRMS = .6309   NO. OF ITERATIONS = 3

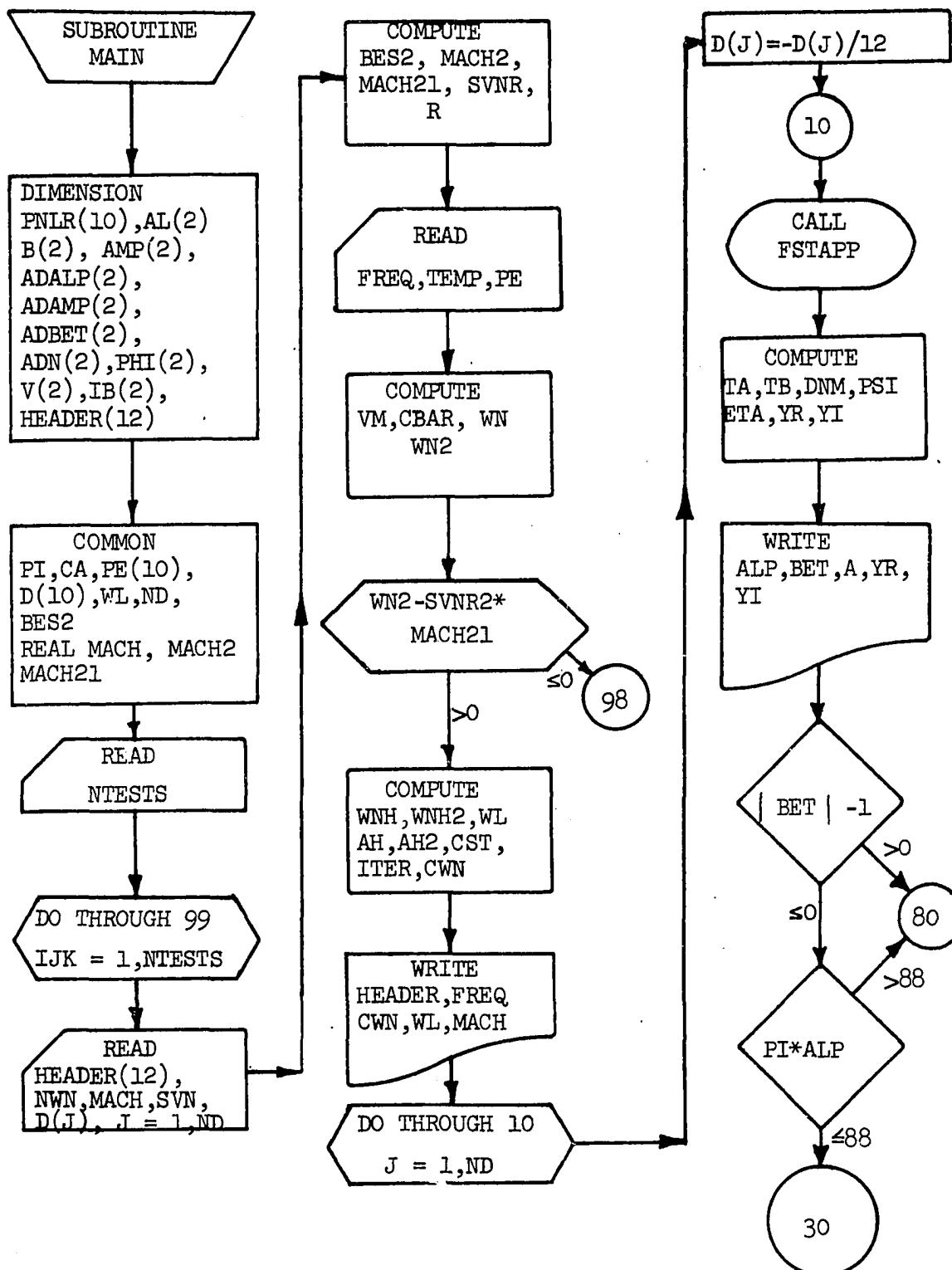| DISTANCE FROM THE NOZZLE ENTRANCE (IN)	MEASURED PHASE DIFFERENCE (DEG)	COMPUTED PHASE DIFFERENCE	DIFFERENCE IN DEGREES
45.0	57.8	57.5	.3
40.0	54.0	54.6	-.7
35.0	54.7	54.2	.5
33.0	53.2	54.2	-1.0
24.0	54.0	54.6	-.6
17.0	56.0	55.1	1.0
8.0	56.2	55.8	.4

Figure 46. Flow Chart of Program MAIN
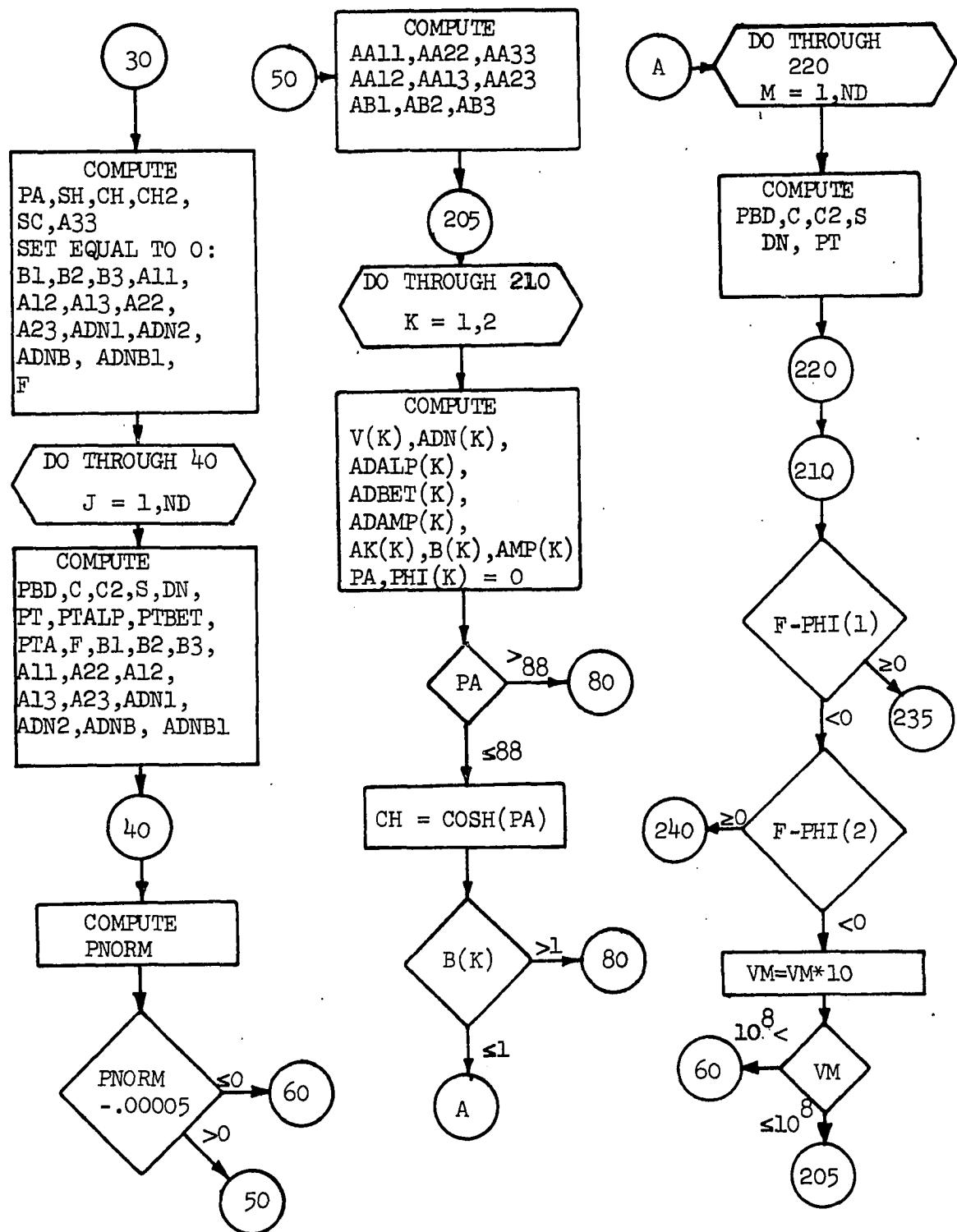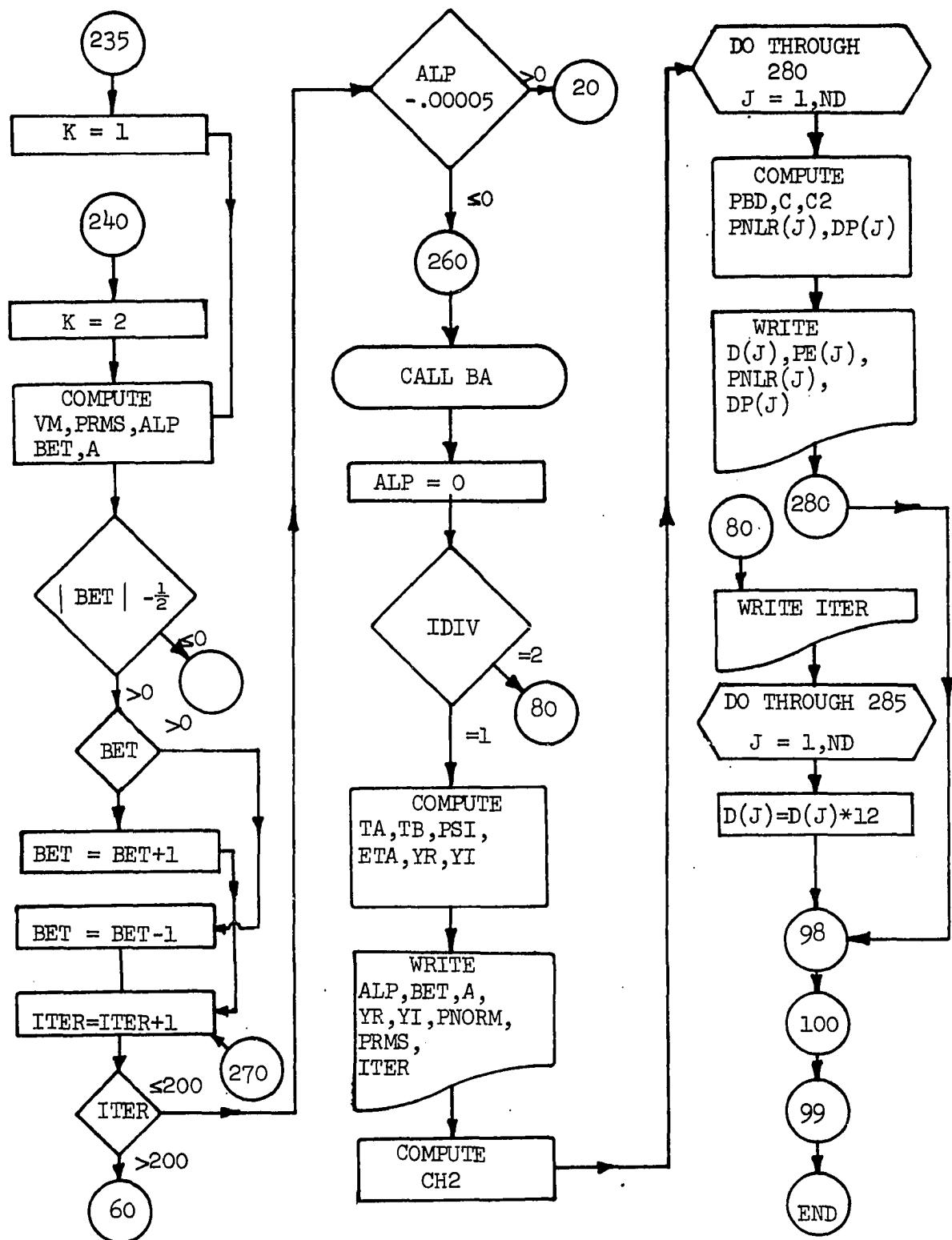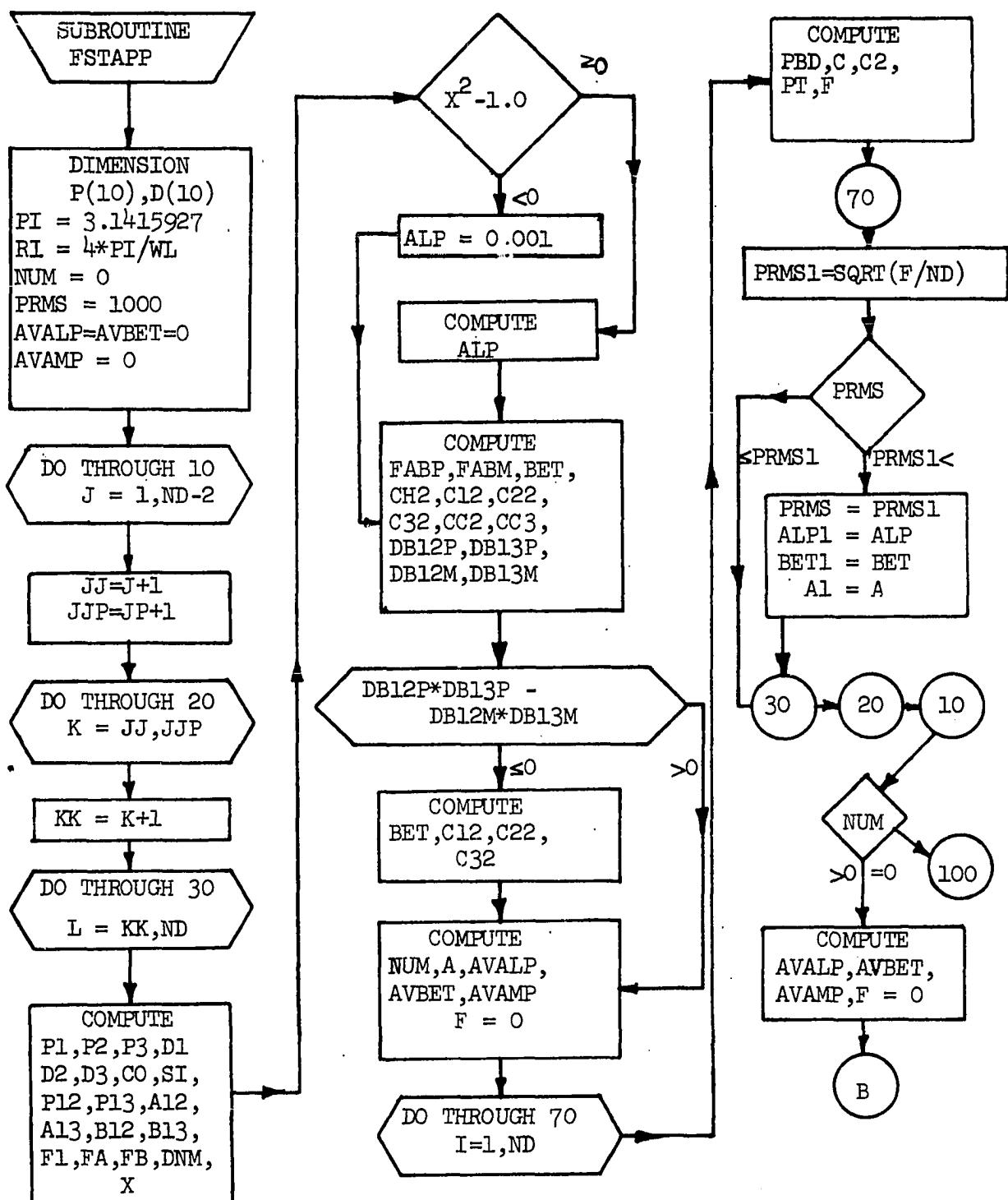
Figure 46. Continued

Figure 46.   Continued

Figure 46. Continued
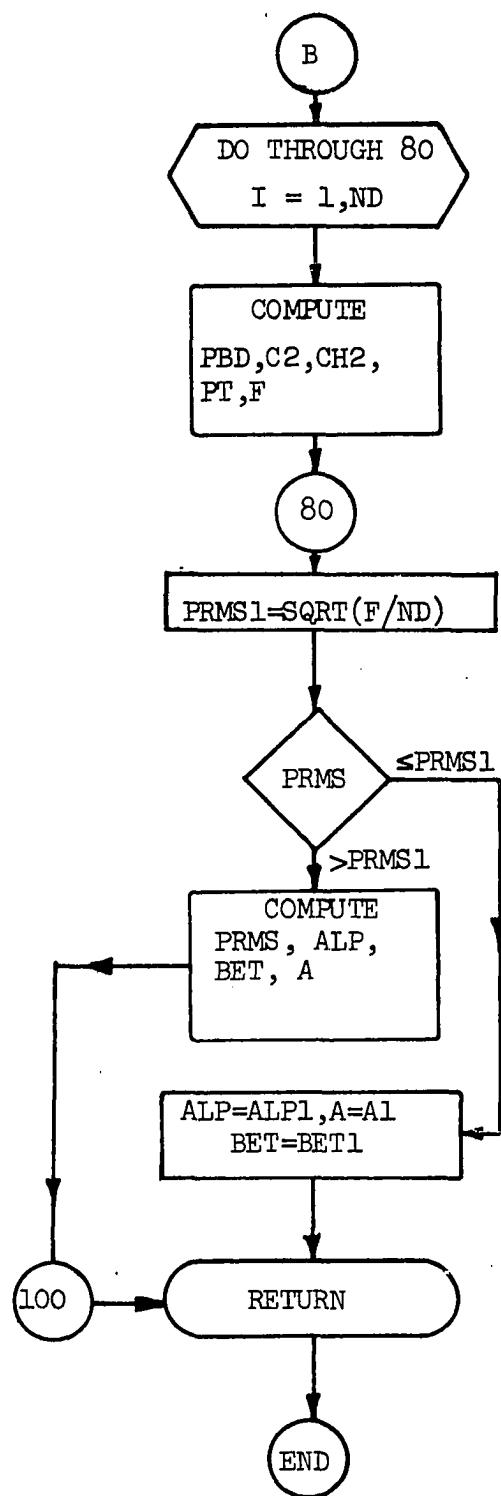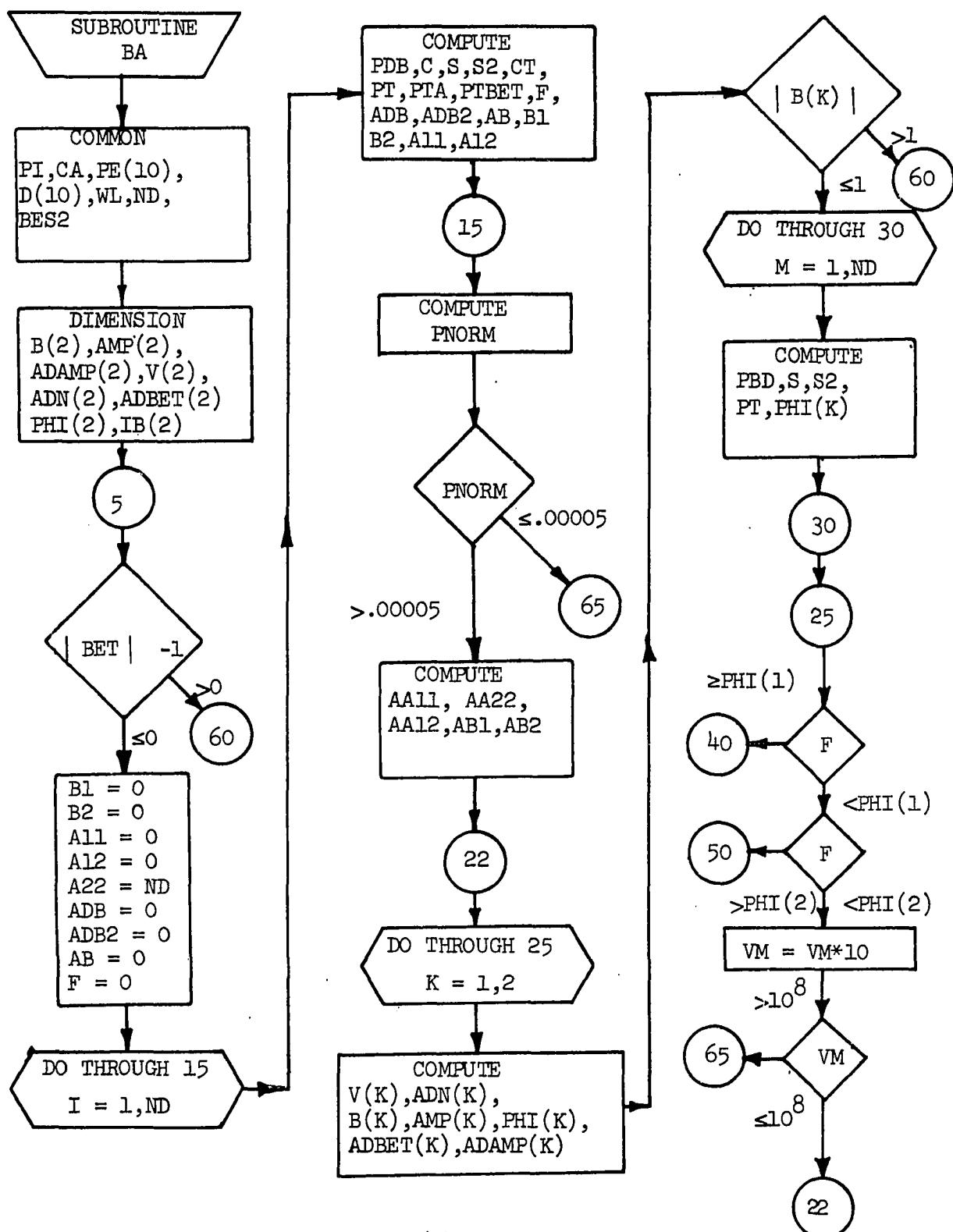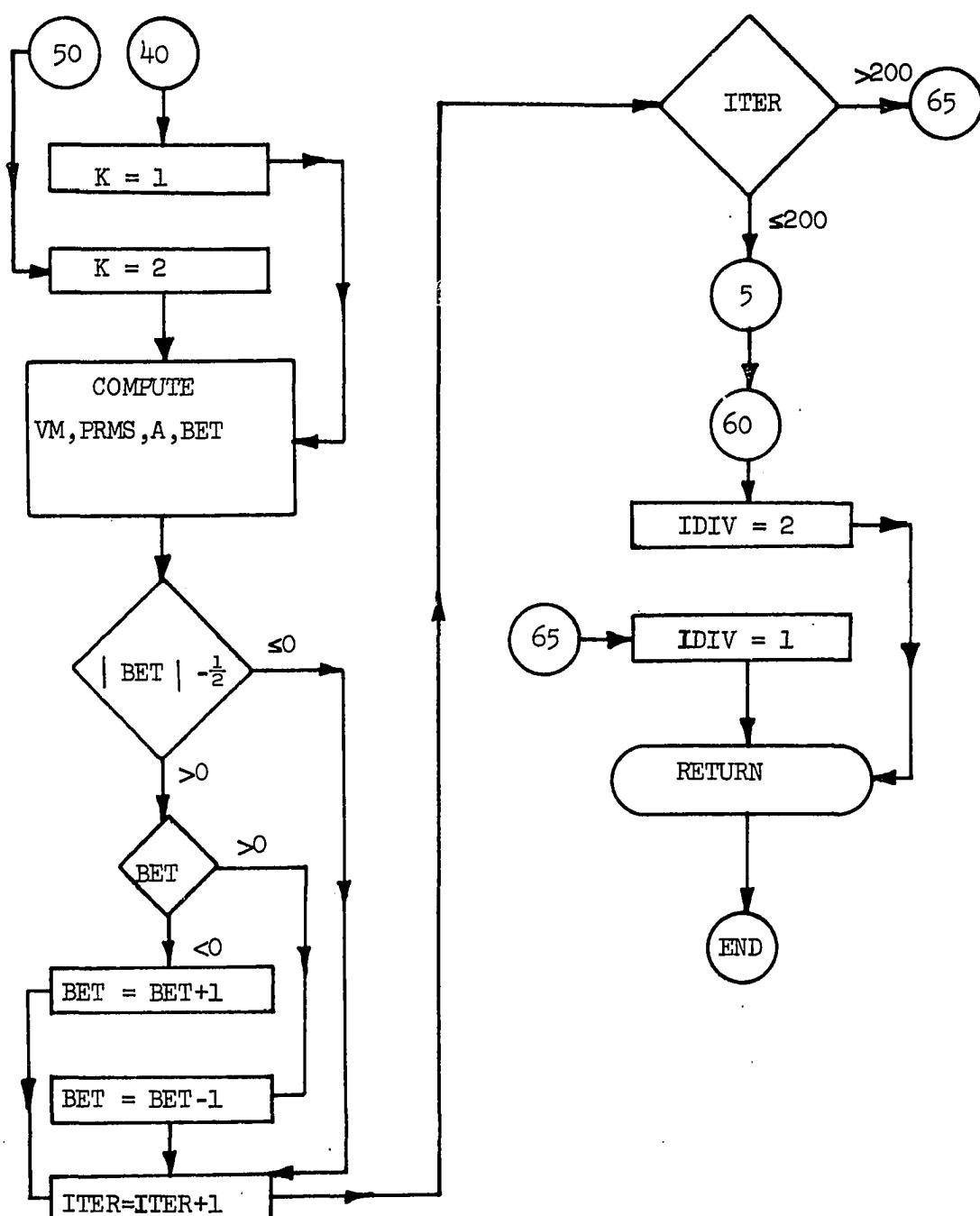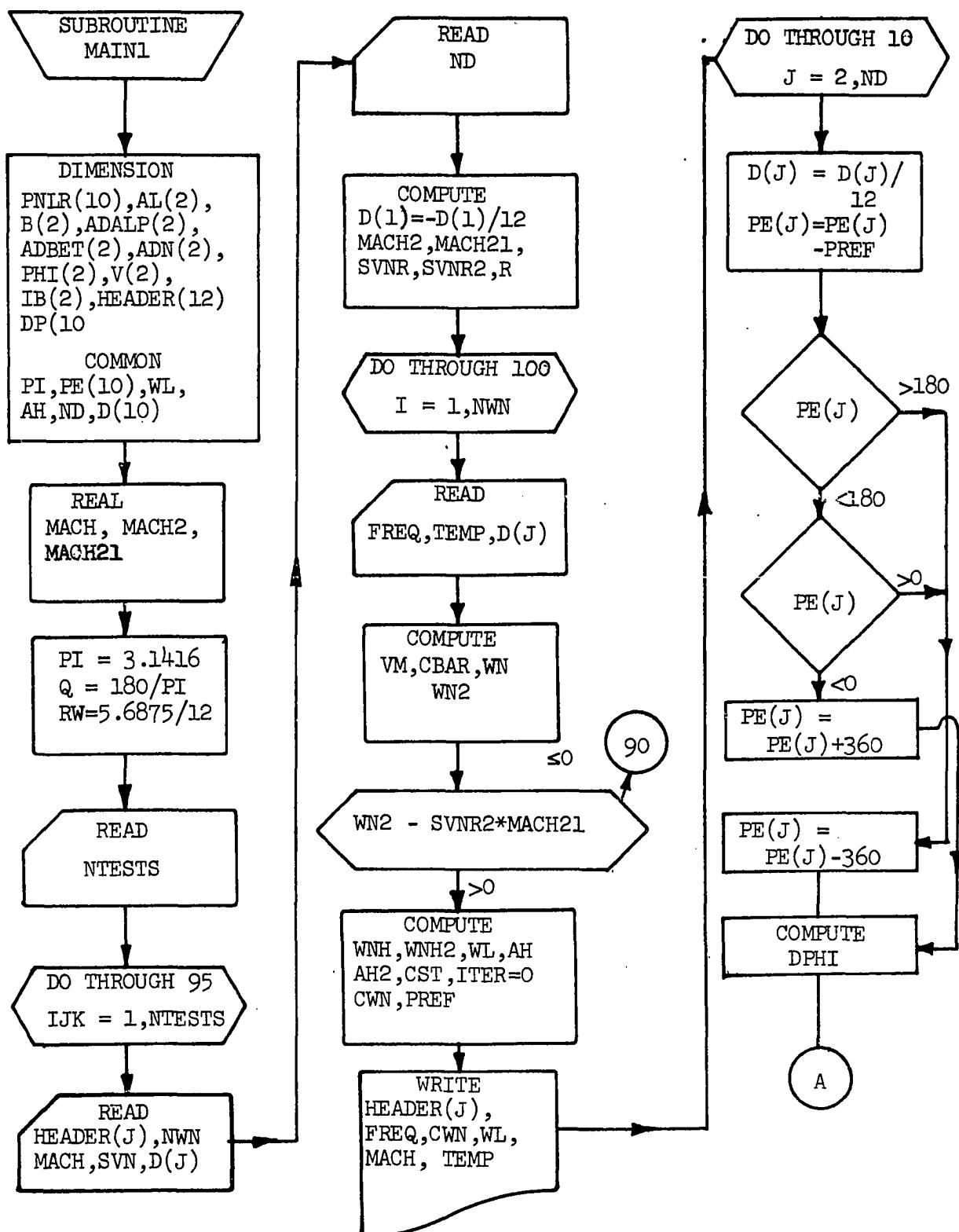
Figure 46. Continued

SUBROUTINE
BA

COMMON
PI,CA,PE(10),
D(10),WL,ND,
BES2

DIMENSION
B(2),AMP(2),
ADAMP(2),V(2),
ADN(2),ADBET(2)
PHI(2),IB(2)

5

| BET | -1

>0 → 60

≤0

B1 = 0
B2 = 0
A11 = 0
A12 = 0
A22 = ND
ADB = 0
ADB2 = 0
AB = 0
F = 0

DO THROUGH 15
I = 1,ND

COMPUTE
PDB,C,S,S2,CT,
PT,PTA,PTBET,F,
ADB,ADB2,AB,B1
B2,A11,A12

15

COMPUTE
PNORM

PNORM

≤.00005 → 65

>.00005

COMPUTE
AA11, AA22,
AA12,AB1,AB2

22

DO THROUGH 25
K = 1,2

COMPUTE
V(K),ADN(K),
B(K),AMP(K),PHI(K),
ADBET(K),ADAMP(K)

| B(K) |

>1 → 60

≤1

DO THROUGH 30
M = 1,ND

COMPUTE
PBD,S,S2,
PT,PHI(K)

30

25

≥PHI(1)

40 ← F

<PHI(1)

50 ← F

>PHI(2)   <PHI(2)

VM = VM*10

>10^8

65 ← VM

≤10^8

22

Figure 46. Continued

Figure 46. Concluded

SUBROUTINE
MAIN1

DIMENSION
PNLR(10),AL(2),
B(2),ADALP(2),
ADBET(2),ADN(2),
PHI(2),V(2),
IB(2),HEADER(12)
DP(10

COMMON
PI,PE(10),WL,
AH,ND,D(10)

REAL
MACH, MACH2,
MACH21

PI = 3.1416
Q = 180/PI
RW=5.6875/12

READ
NTESTS

DO THROUGH 95
IJK = 1,NTESTS

READ
HEADER(J),NWN
MACH,SVN,D(J)

READ
ND

COMPUTE
D(1)=-D(1)/12
MACH2,MACH21,
SVNR,SVNR2,R

DO THROUGH 100
I = 1,NWN

READ
FREQ,TEMP,D(J)

COMPUTE
VM,CBAR,WN
WN2

WN2 - SVNR2*MACH21   ≤0   90

>0

COMPUTE
WNH,WNH2,WL,AH
AH2,CST,ITER=0
CWN,PREF

WRITE
HEADER(J),
FREQ,CWN,WL,
MACH, TEMP

DO THROUGH 10
J = 2,ND

D(J) = D(J)/
12
PE(J)=PE(J)
-PREF

PE(J)   >180

<180

PE(J)   >0

<0

PE(J) =
PE(J)+360

PE(J) =
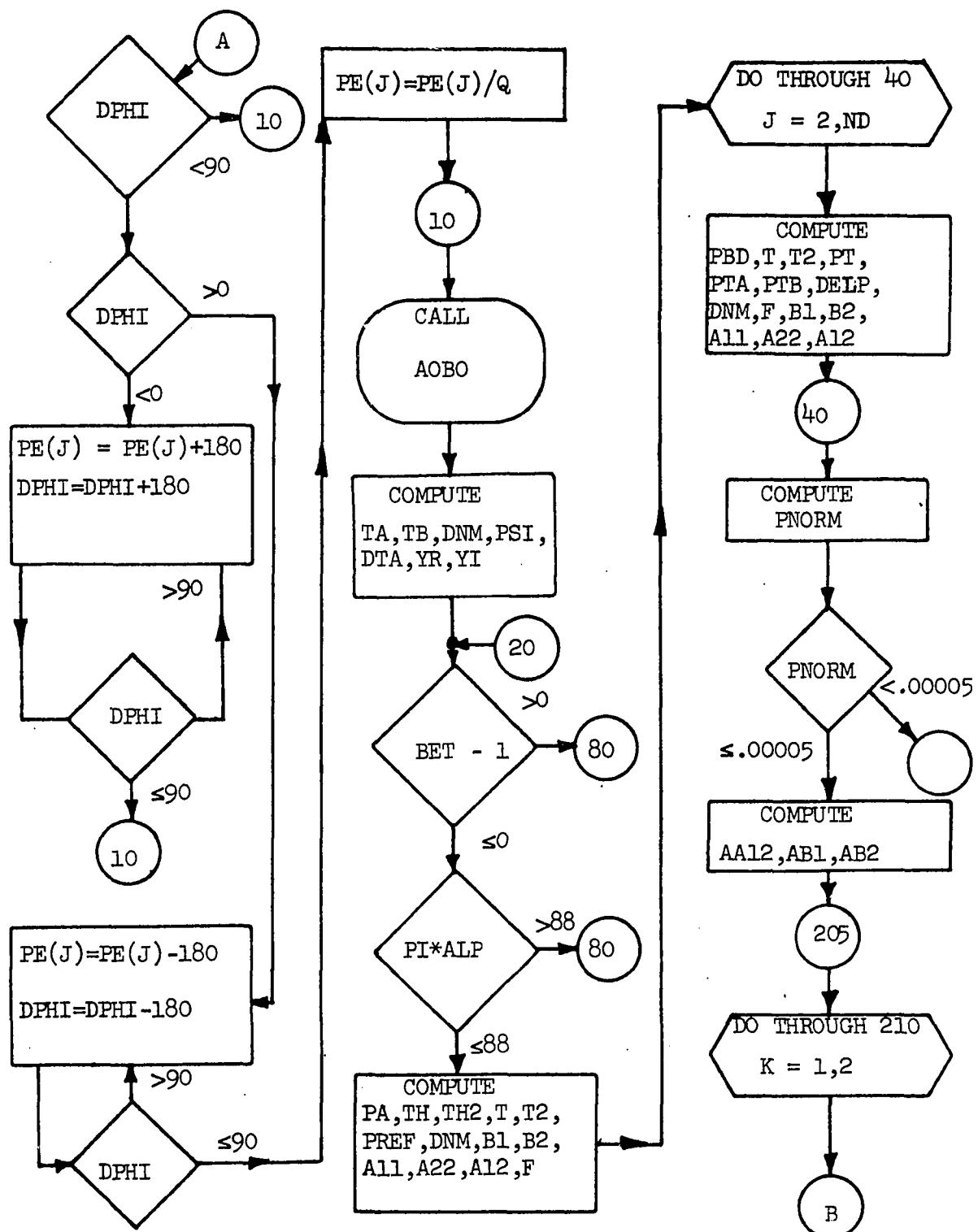PE(J)-360

COMPUTE
DPHI

A

Figure 47. Flow Chart of Program MAIN1
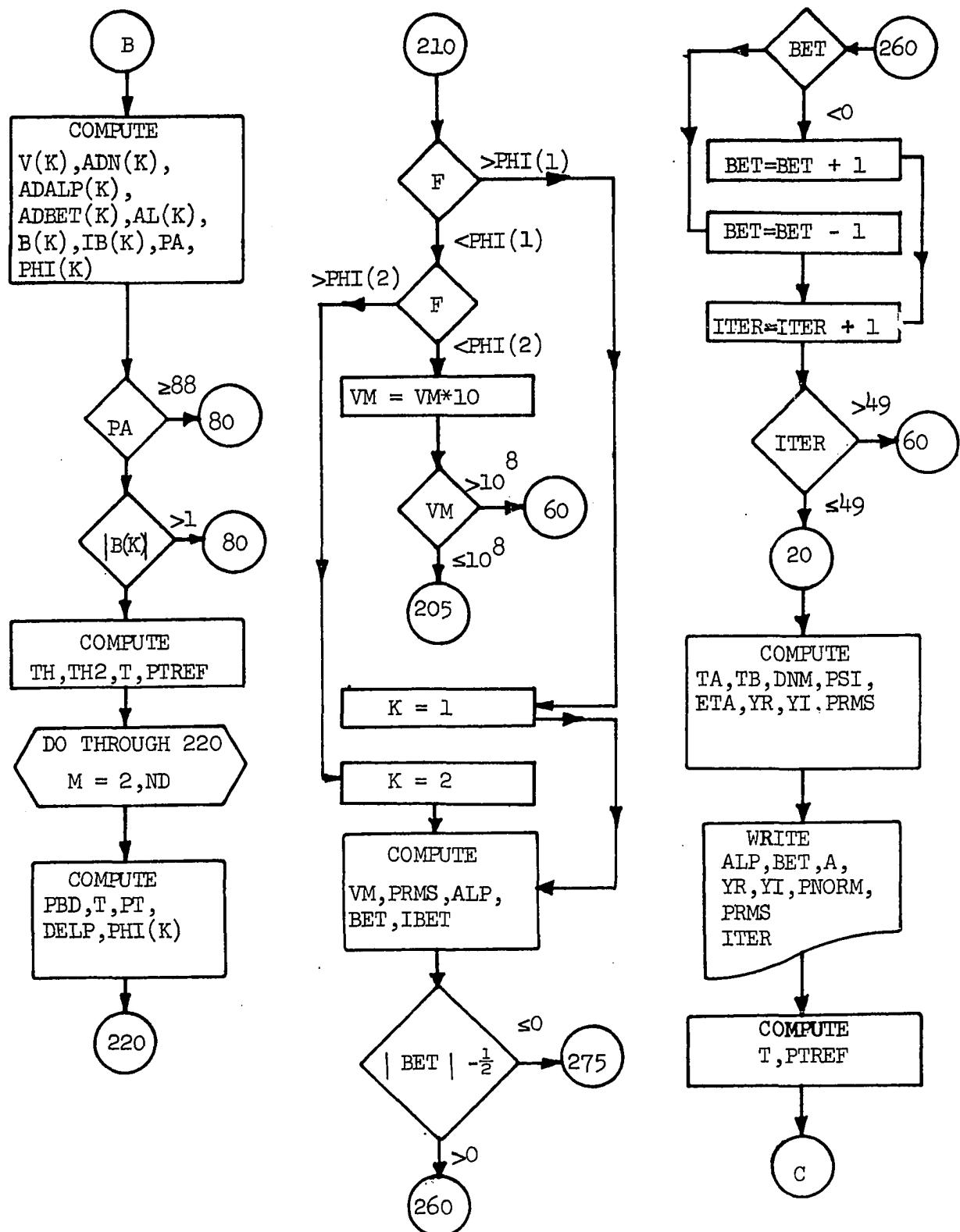
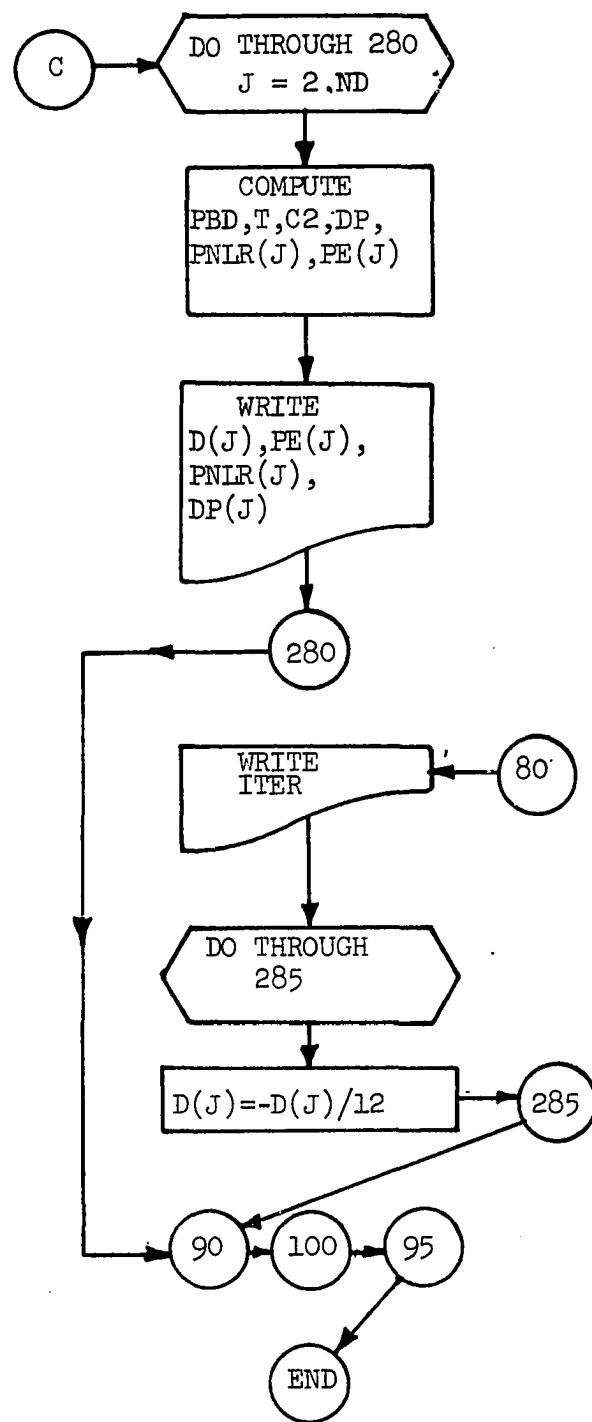Figure 47. Continued
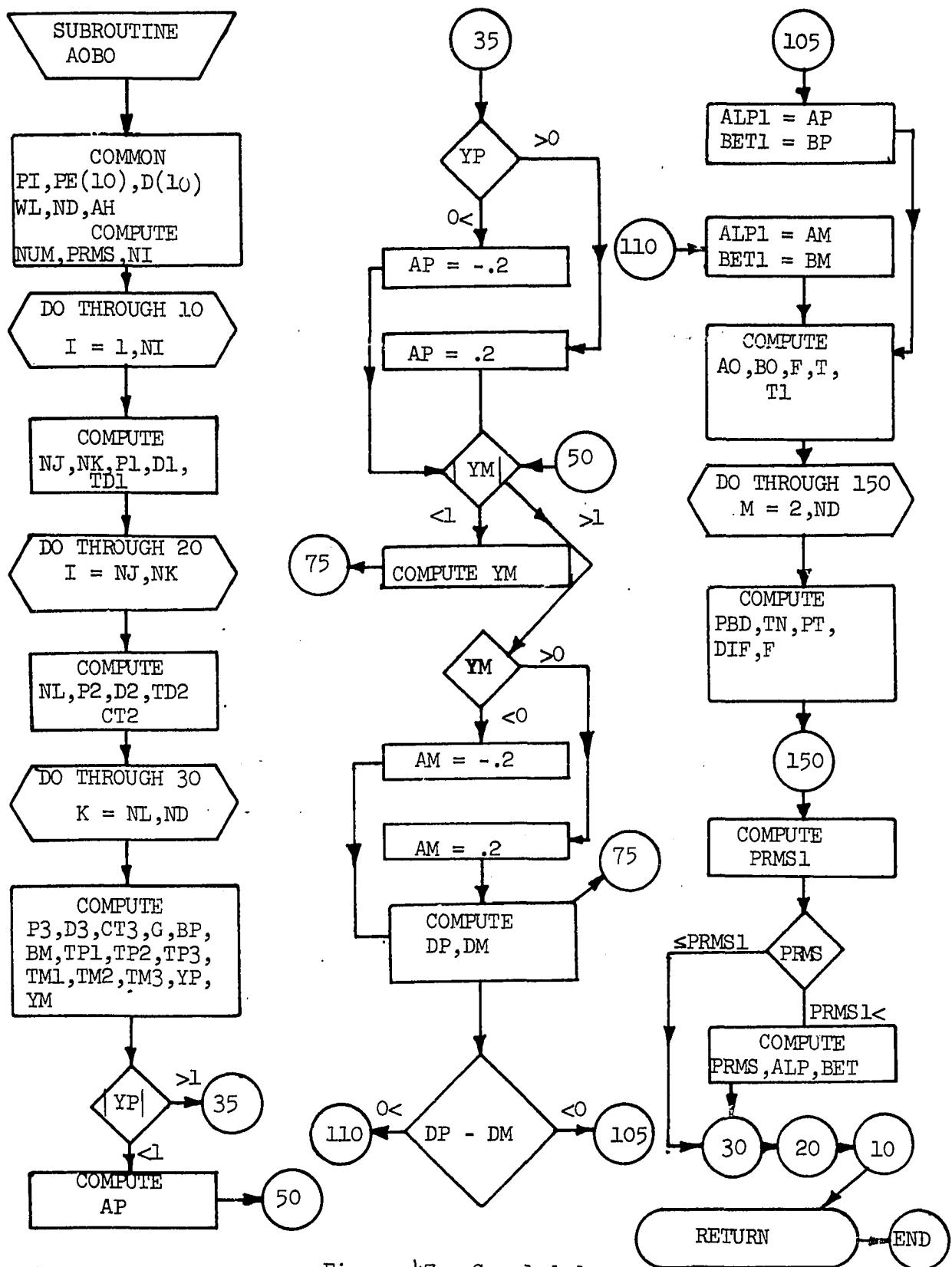
Figure 47. Continued

Figure 47. Continued

Figure 47. Concluded

REFERENCES

1. Crocco, L., and Cheng, S. I., "Theory of Combustion Instability in Liquid Propellant Rocket Motors," AGARDograph 8, Butterworth Publications Limited, 1956. (Chapter I and Appendix B).

2. Crocco, L., Grey, J., and Harrje, D., "Theory of Liquid Propellant Rocket Combustion Instability and Its Experimental Verification," ARS Journal, 30, p. 2, 1960.

3. Crocco, L., "Theoretical Studies on Liquid-Propellant Rocket Instability," Tenth Symposium (International) on Combustion, Combustion Institute, pp. 1101-1128, June, 1965.

4. Tsien, H. S., "The Transfer Function of Rocket Motors," ARS Journal, 22, p. 139, 1952.

5. Crocco, L., "Supercritical Gaseous Discharge with High Frequency Oscillations," Aerotecnica, Roma, 33, p. 46, 1953.

6. Crocco, L., and Sirignano, W. A., "Behavior of Supercritical Nozzles Under Three-Dimensional Oscillatory Conditions," AGARDograph 117, Butterworth Publications Limited, 1967.

7. Smith, A. J., Reardon, F. H., et. al., "The Sensitive Time Lag Theory and Its Application to Liquid Rocket Combustion Instability Problems," Aerojet-General Corp. Technical Report No. AFRPL-TR-67-314, Vol. I, March, 1968.

8. Crocco, L., Monti, R., and Grey, J., "Verification of Nozzle Admittance Theory by Direct Measurement of the Admittance Parameter," ARS Journal, 31, p. 771, 1961.

9. Buffum, F. G., Dehority, G. I., Slates, R. O., and Price, E. W., "Acoustic Losses of a Subscale Cold-Flow Rocket Motor for Various 'J' Values," NOTS TP 3932, 1966.

10. Culick, F. E. C., and Dehority, G. L., "An Analysis of Axial Acoustic Waves in a Cold Flow Rocket," Naval Weapons Center Report No. 4544, China Lake, California, May 1968.

11. Scott, R. A., "An Apparatus for Acoustic Measurement of the Acoustic Impedance of Sound Absorbing Materials," Proceedings of the Physical Society, 58, p. 253, 1946.

12. Lippert, W. K. R., "The Practical Representation of Standing Waves in an Acoustic Impedance Tube," *Acustica*, 3, p. 153, 1953.

13. Morse, P. M., and Ingard, K. U., *Theoretical Acoustics*, McGraw-Hill, Inc., pp. 467ff, 1968.

14. Savell, C. T., "The Evaluation of Nozzle Boundary Conditions Used in Determining Combustion Instability Limits," (Master's Special Problem), School of Aerospace Engineering, Georgia Institute of Technology, 1967.

15. Bell, W. A., "Theoretical Considerations of Impedance Tubes for Three Dimensional Oscillations," (Master's Special Problem), School of Aerospace Engineering, Georgia Institute of Technology, 1970.

16. Gately, W. S., and Cohen, R., "Methods for Evaluating the Performance of Small Acoustic Filter," *Journal of the Acoustical Society of America*, 46, p. 6, 1969.

17. Pfahl, R. C., and Mitchel, B. J., "Nonlinear Regression Methods for Simultaneous Property Measurement," *AIAA Journal*, 8, p. 1046, June, 1970.

18. Marquardt, D. W., "An Algorithm for Least-Squares Estimation of Nonlinear Parameters," *Journal of the Society for Industrial and Applied Mathematics*, 11, p. 431, June, 1963.

19. Serra, R. A., "Determination of Internal Gas Flows by a Transient Numerical Technique," *AIAA Journal*, Vol. 10, p. 603, May, 1972.

VITA

William Alvin Bell was born in Frederick, Maryland on October 17, 1944. He attended Headland High School in East Point, Georgia where he graduated in 1962. He received his higher education from the Georgia Institute of Technology where he received the degrees Bachelor of Aerospace Engineering in 1966 and Master of Science in Aerospace Engineering in 1970. He is currently employed with the Georgia Institute of Technology as a research engineer.

Mr. Bell is a member of the American Institute of Astronautics and Aeronautics, and Sigma Gamma Tau. He was elected to Who's Who Among Colleges and Universities in 1970.

He married Melody McLemore on August 8, 1970 and they are now residing in Decatur, Georgia.